The Role of 11β-Hydroxysteroid Dehydrogenase Type 1 in Wound Healing in Uraemia

Sai Krishna Duraisingham

Submitted in partial fulfilment of the requirements
of the Degree of Doctor of Philosophy

Queen Mary University of London

Statement of Originality

I, Sai Krishna Duraisingham, confirm that the research included within this thesis is my own work or that where it has been carried out in collaboration with, or supported by others, that this is duly acknowledged below and my contribution indicated. Previously published material is also acknowledged below.

I attest that I have exercised reasonable care to ensure that the work is original, and does not to the best of my knowledge break any UK law, infringe any third party's copyright or other Intellectual Property Right, or contain any confidential material.

I accept that the College has the right to use plagiarism detection software to check the electronic version of the thesis.

I confirm that this thesis has not been previously submitted for the award of a degree by this or any other university.

The copyright of this thesis rests with the author and no quotation from it or information derived from it may be published without the prior written consent of the author.

Signature: Sai Krishna Duraisingham

Date: 27th September 2019

Acknowledgments

I would like to express my gratitude to Professor Yaqoob my primary supervisor for offering me this opportunity to undertake a novel research project and his continued support both professionally and personally.

Special thanks to Steve for his boundless patience and support throughout this period as well as for a plentiful supply of baked goods.

I would like to thank my fellow team members past and present; Julius for his help with *in vivo* work to some of the best 70s and 80s tunes we could find as well as Sabrina, Samira and Damian for their advice, help, good humour and camaraderie.

I am indebted to Professor Michael Sheaff and Ismail Bulut for their help with histology, immunohistochemistry and its interpretation and to Dr Kamal Ahmed for his mentorship whilst working at The London Bridge Hospital.

Finally, but most importantly, I would like to thank my family and friends for their wise words, motivational speeches during low periods, limitless love, support and benevolence when lesser human beings would've given up on me.

I dedicate this thesis in loving memory of my father who provided the greatest support throughout my education and career. I hope you continue to be proud.

Collaboration and Publications

"Acute Wound Healing in a Rodent Model of Uremia"
Poster presentation at the Wound Healing Society meeting – Charlotte April 2018

"Impaired Cutaneous Wound Healing in a Rodent Model of Uremia"
Poster presentation at the American Society of Nephrology conference – New Orleans November 2017

Professor Michael Sheaff and Mr Ismail Bulut of Barts Health NHS Trust performed all histological slide preparation, immunohistochemistry and analysis.

Kristin Braun of The Blizzard, Queen Mary University demonstrated the *in vivo* wounding technique.

Abstract

People with Chronic Kidney Disease (CKD), advanced age and systemic cortisol excess demonstrate skin specific similarities including poor wound healing. There is accumulating evidence that patients with advanced kidney disease age prematurely. Studies have demonstrated the cortisol producing 11β-Hydroxysteroid Dehydrogenase Type 1 (11β-HSD-1) enzyme activity is increased in aged skin. We hypothesized the same should be true in the uraemic state. Skin specific 11β-HSD-1 and therefore cortisol excess may be the unifying cause for the skin phenotype and poor healing seen in CKD, advanced age and systemic cortisol excess.

The aims of this thesis were to investigate the presence of 11β-HSD-1 and 11β-HSD-2 within rodent skin with and without uraemia as well as determining the activity of 11β-HSD-1 and to elucidate the role it may play in wound healing. Finally, the efficacy of an 11β-HSD-1 inhibitor in healing was assessed as a potential future therapeutic target.

In vitro studies which included Lactate Dehydrogenase (LDH), cell viability, scratch assays and cortisol Enzyme Linked Immunosorbent Assay (ELISA) were conducted using 2 different types of primary skin cultures with the uraemic toxins Indoxyl Sulphate (IS) or *p*-Cresol (PC) or the specific 11β-HSD-1 inhibitor emodin. An *in vivo* model of skin wounding was developed in male Wistar rats rendered uraemic by an adenine supplemented diet. Healing was measured in uraemic and non-uraemic control rats at baseline, with the application of topical emodin or with systemic emodin administration. Skin samples were processed *ex vivo* to extract protein for use in immunoblotting or Ribonucleic Acid (RNA) for Polymerase Chain Reaction (PCR) and a wound healing PCR array. Immunohistochemistry was completed for selected skin samples as were corticosterone (cortisol equivalent in rats) ELISA.

The presence of 11β-HSD-1 and 11β-HSD-2 in Human Dermal Fibroblasts (HDF) and Human Epidermal Keratinocytes (HEK) was confirmed by western blotting. No differences in LDH activity, cell viability or cortisol production with the administration of IS, PC or emodin could be detected. Scratch assays utilising uraemic

toxins in isolation did not demonstrate a significant delay in wound healing. An improvement in healing using emodin in isolation could also not be demonstrated.

Contrary to the *in vitro* exposure to solitary uraemic toxins, the *in vivo* findings consistently demonstrated a delay in wound healing in uraemia and the beneficial effect of emodin on healing when administered systemically. This could not be attributed to changes in 11β-HSD-1 or 11β-HSD-2 Messenger RNA (mRNA), protein expression or enzyme activity with the techniques employed. To elucidate a definitive role of 11β-HSD-1 would require the use of radioactive isotopic activity assay and the use of a skin specific 11β-HSD-1 Knock-Out (KO) mouse model. It would be most useful to reproduce this work in human skin, comparing uraemic patients to healthy live kidney donors.

Table of Contents

List of Figures

List of Tables

Abbreviations

11β-HSD-1/2	11 Beta Hydroxysteroid Dehydrogenase Type 1 or 2
17β-HSD	17 Beta Hydroxysteroid Dehydrogenase
3β-HSD-2	3-Beta-Hydroxysteroid Dehydrogenase Type 2
5α-THF	5α-Tetrahydrocortisol
6PG	6- Phosphogluconate
ACRD	Apparent Cortisone Reductase Deficiency
ACTH	Adrenocorticotrophic Hormone
ANOVA	Analysis of Variance
β-END	β-Endorphin
B2M	Beta 2 Microglobulin
BM	Basement Membrane
BCA	Bicinchoninic Acid
cDNA	Complementary DNA
CKD	Chronic Kidney Disease
CI	Confidence Interval
CRH	Corticotrophin Releasing Hormone
CRH-R1/2	Corticotrophin Releasing Hormone Receptor 1 or 2
CO_2	Carbon Dioxide
CRD	Cortisone Reductase Deficiency
C_T	Threshold Cycle
CYP[X][Y][Z]	Cytochrome P450 Enzyme - Family: Subfamily: Member
DHOA	Dihydroxyadenine
DMEM	Dulbecco's Modified Eagle's Medium
DMSO	Dimethyl Sulphoxide
DNA	Deoxyribonucleic Acid
ECM	Extracellular Matrix
ELISA	Enzyme Linked Immunosorbent Assay
ER	Endoplasmic Reticulum
FBS	Foetal Bovine Serum
FPP	Farnesyl Pyrophosphate
G6P	Glucose-6-Phosphate

G6PT	Glucose-6-Phosphate Transporter
GAPDH	Glyceraldehyde-3-Phosphate Dehydrogenase
GC	Glucocorticoid
GR	Glucocorticoid Receptor
H6PDH	Hexose-6-Phosphate Dehydrogenase
HDF	Human Dermal Fibroblast
HEK	Human Epidermal Keratinocyte
HIF	Hypoxia Inducible Factor
HKGS	Human Keratinocyte Growth Supplement
HPA	Hypothalamic Pituitary Adrenal Axis
HRP	Horseradish Peroxidase
IgG	Immunoglobulin G
IL	Interleukin
IMM	Inner Mitochondrial Membrane
IS	Indoxyl Sulphate
KO	Knock Out
LDH	Lactate Dehydrogenase
MAPK	Mitogen Activated Protein Kinases
MC2R	Melanocortin Receptor 2
MEB	Mammalian Extraction Buffer
MGB	Minor Groove Binder
MR	Mineralocorticoid Receptor
mRNA	Messenger RNA
MTS	(3-(4,5-dimethylthiazol-2-yl)-5-(3-carboxymethoxyphenyl)-2-(4-sulphophenyl)-2H-tetrazolium)
N	Normality (of a solution)
NAD	Nicotinamide Adenine
$NADP^+$	Nicotinamide Adenine Phosphate
NADPH	Nicotinamide Adenine Dinucleotide Phosphate
NFQ	Non-Fluorescent Quencher
NO	Nitric Oxide
OAT	Organic Anion Transporter
OMM	Outer Mitochondrial Membrane
PC	*p*-Cresol

PCR	Polymerase Chain Reaction
POMC	Proopiomelanocortin
PVDF	Polyvinylidene Difluoride
RNA	Ribonucleic Acid
RO	Reverse Osmosis
siRNA	Small Interfering RNA
SNx	Subtotal Nephrectomy
StAR	Steroidogenic Acute Regulatory Protein
STARD3	StAR-Related Lipid Transfer Protein
TBS	Tris Buffered Saline
TBS-T	Tris Buffered Saline-Tween
TGF	Transforming Growth Factor
THE	Tetrahydrocortisone
THF	Tetrahydrocortisol
TNF-α	Tumour Necrosis Factor Alpha
Ucn	Urocortin
UVA	Ultraviolet Radiation 320-400 nm bandwidth
UVB	Ultraviolet Radiation 290-320 nm bandwidth
UVC	Ultraviolet Radiation 250-290 nm bandwidth
UVR	Ultraviolet Radiation
VEGF	Vascular Endothelial Growth Factor

CHAPTER 1

Introduction

1.1 Uraemia and Ageing

The uraemic syndrome is a term used to describe not only the accumulation of nitrogenous waste products in the plasma and its' concomitant symptomatology but a series of pathophysiological changes which occur in the body secondary to renal failure (1). Considerable work is ongoing in many fields to determine how these changes are mediated and whether they can be reversed without adverse consequence by restoration of normal renal function after kidney transplantation. As donor kidneys are a finite resource, reversing these changes or limiting unfavourable sequelae with alternative methods has become increasingly important.

Patients with CKD have been observed to suffer a multitude of complications, with damage occurring in multiple organs including kidneys, bone, muscles, brain, heart and vasculature (2). The most frequently encountered clinically are cardiovascular in nature including coronary artery disease, congestive heart failure, peripheral arterial disease, stroke and arrhythmia (3). Furthermore, clinicians note that patients with CKD are biologically older compared to age-matched non-uraemic controls (4). It has been postulated that uraemia accelerates the process of ageing via a multitude of processes including telomere loss (5), accumulation of advanced glycation end products and increased oxidative stress (6). Additionally, patients with CKD have been noted to be inflamed with dysregulated immunity (7) and altered autophagy (8), all of which may propagate such cardiovascular and other organ abnormalities in the CKD population.

1.2 The Structure of Mammalian Skin

Skin has numerous functions in humans including a barrier function, protecting underlying tissues and organs as well as defending against pathogens, thermoregulation, electrolyte and water content regulation, insulation and the production and inactivation of different substances such as vitamin D (9). It can be considered in 3 main layers, each of which has a different structure and cell composition. These are the epidermis, dermis and hypodermis (9).
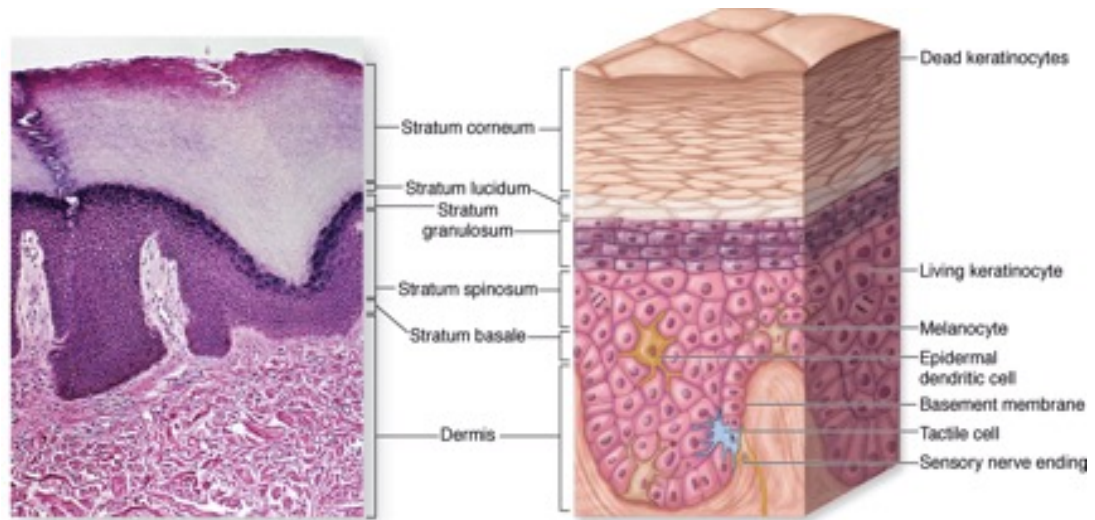
Figure 1.1 Epidermal structure. Republished with permission of McGraw-Hill Education from Junqueira's Basic Histology: Text and Atlas, 12th Edition, Mescher A, 2009 (10); permission conveyed through Copyright Clearance Center, Inc.

1.2.1 The Epidermis

The epidermal layer consists of five sublayers; stratum corneum, lucidum, granulosum, spinosum and basale (from outer surface to inner) which together provide more barrier protection than a monolayer of epidermal cells (Figure 1.1) (11). The principal cells present here are keratinocytes, the remaining are melanocytes, Merkel and Langerhans cells (11). The epidermis contains no blood vessels; instead it gains its nutrient supply from dermal diffusion (12). Obtaining oxygen via the atmosphere has also been shown to be integral to epidermal cell growth and differentiation (13). A single layer of keratinocytes in the basal layer undergo a programmed process of differentiation. After mitosis, some daughter cells migrate into the upper epidermal layers, the rest remain in the basal layer. During transition to the upper layers, the keratinocytes change morphology, for example in the spinosum layer they are spindle shaped due to the formation of desmosomes with adjacent cells, as well as initiating the synthesis of various structural and catalytic proteins (14). Above the spinosum layer is the granular layer, here keratinocytes contain keratohyalin which is needed to organise keratin filaments in the upper layers. Cells here start to lose their nuclei and cytoplasmic organelles (11). The stratum lucidum is a zone where cells transition from being live to dead and keratinized. Cell

organelles are destroyed, granules fuse with plasma membranes releasing lipids into the extracellular space (15). In the final steps of differentiation, keratinocytes are transformed into anucleated, flattened corneocytes, with aligned keratin filaments, surrounded by an inner envelope of cross-linked proteins and outer envelope of lipid thus forming an effective barrier (16).

1.2.2 The Dermis

The dermis has 2 sublayers; a papillary layer (near the epidermis) consisting of loose connective tissue with finger like projections to interdigitate with the epidermis and a reticular layer near the hypodermis with dense irregular connective tissue (collagen, elastin, reticular fibres) which confers strength and elasticity (11). The dermis contains adnexal structures such as sweat glands and sebaceous glands as well as hair follicles, nerve endings, lymphatics and blood vasculature (9, 11).

1.2.3 The Hypodermis

The hypodermis attaches the overlying skin to bone or muscle underneath. It contains its own blood vessels and nerve endings as well as loose connective tissue, elastin and adipose (to provide insulation) (9).

1.3 Skin Abnormalities in Chronic Kidney Disease

Patients with CKD develop a multitude of skin changes associated with the duration and severity of their renal failure (17). A spectrum of skin colouration has been noted in CKD; pallor secondary to anaemia of chronic disease or relative erythropoietin deficiency, yellow due to the retention of fat soluble pigments within the dermis and subcutaneous tissues, grey-brown discolouration due to haemosiderin deposition as well as hyperchromia after dialysis initiation (18). Skin is often xerotic and scaly with a tendency to decreased sweating. Shunting of blood away from cutaneous beds, likely due to autonomic neuropathy, leads to atrophy of sebaceous glands and sweat glands, resulting in reduced skin turgor (19). These changes also adversely affect the elasticity of the skin, causing it to be weak and susceptible to damage (20). Precipitation of crystals of urea on the skin surface, termed 'uraemic frost' can infrequently be seen (21). More commonly, skin is noted to bruise easily. Platelet defects in uraemia have been extensively studied in the context of systemic bleeding diatheses (22). It has been postulated that the build-up of guanidinosuccinic acid

22

inhibits adenine diphosphate induced platelet aggregation which leads to bleeding and hence ecchymoses formation (23, 24).

1.3.1 Calciphylaxis

In addition to these widespread changes, skin disorders specific (although not exclusive) to renal disease can develop. Calciphylaxis or calcific uraemic arteriolopathy mostly occurs in patients with advanced CKD treated by dialysis (25) although cases have been reported in alcoholic liver disease, malignancy and connective tissue diseases (26). Small vessel mural (predominantly medial layer) calcification, micro thrombosis and fibrointimal hyperplasia of small dermal and subcutaneous arterioles causes ischaemia and septal panniculitis (27). Painful skin lesions, with resultant skin necrosis, non-healing ulcers and gangrene can also develop (28). Risk factors for these events are thought to include Caucasian race, female gender, abnormal bone mineral metabolism (increased calcium phosphate product), hyperparathyroidism, hypoalbuminemia and the use of medications such as warfarin (29). It is associated with considerable morbidity including severe pain, infections and non-healing wounds as well as high mortality rates (29).

1.3.2 Nephrogenic Systemic Fibrosis

Nephrogenic systemic fibrosis has been associated with exposure to gadolinium based magnetic resonance imaging (30). It has been postulated that the process of transmetallation occurs, whereby cations such as calcium or zinc are substituted for the gadolinium ion (GD^{3+}) in chelates, thus releasing free GD^{3+} that can attract fibrocytes via the release of several cytokines ultimately inducing fibrosis (31). It predominantly presents as thick, hardened and indurated skin of the extremities, with the potential for contracture formation and hence reduced mobility, although internal organs such as the pleura and myocardium can also be affected (32). Susceptibility to breaks in the epidermis due to pruritus predisposes to ulcer formation and superadded bacterial infection (19). Histologically, thickened collagen bundles with mucin deposition, proliferation of dermal fibroblasts and elastic fibres, without signs of inflammation is observed (32).

1.3.3 Uraemic Pruritus

Uraemic pruritus is frequently encountered in patients with advanced CKD (33). Despite this, the pathophysiology is still not well understood (34). Two popular hypotheses currently exist; the opioid hypothesis (overexpression of opioid μ receptors and down regulation of κ receptors in dermal cells and lymphocytes) (35, 36) or the inflammatory supposition with the accumulation of chemical transmitters such as pentapeptide enkephalins, proteases, serotonin and histamine as well as undefined 'uraemic toxins' (21). The most common skin presentation of pruritus is xerosis although skin can appear normal (34). Itching leads to defects in skin integrity, such that excoriations may become ulcerated (21). Lichen simplex or prurigo nodularis may also manifest (37). Histologically, the commonest features are of a microangiopathy with endothelial cell activation and thickening and reduplication of the Basement Membrane (BM) (17).

1.3.4 Wound Healing in Uraemia

In addition, causative comorbidities such as peripheral vascular disease and diabetes mellitus directly impact on wound healing. In clinical practice, poor wound healing contributes to prolonged hospital stays, a susceptibility to infective complications and significant morbidity, including a considerable negative psychological impact (19, 38). The skin phenotype in patients with CKD are akin to those noted in the elderly population (39) further supporting theories of accelerated ageing in uraemia. This phenotype also has many similarities to patients diagnosed with Cushing's syndrome. In this condition, systemic cortisol excess has been observed to cause identical dermatological changes as seen in CKD patients, as well as hypertension, hyperglycaemia, cognitive deterioration, mood changes and chronic fatigue (40, 41). It is quite possible that, at least on the tissue specific level, hypercortisolaemia is the predominant influence in ageing, Cushing's syndrome and uraemia.

1.4 Steroid Production in the Skin
1.4.1 The Mevalonate Pathway in the Skin

It has been recognised that the skin is an important extra-adrenal steroidogenic organ, containing the apparatus necessary for producing Glucocorticoids (GC), androgens and oestrogens from systemic precursors or through the local conversion of

cholesterol to desired products (42, 43). The building block of all steroid hormones is cholesterol which is produced in eukaryotic cells from acetate by the mevalonate pathway (described in detail in Figure 1.2 (44)).

The 3-hydroxy-3-methylglutaryl-coenzyme A reductase inhibitors, commonly known as the statins, prevent the formation of mevalonate at a rate-limiting step in the cholesterol synthesis pathway (44). Although statins are prescribed predominantly to lower plasma cholesterol and modify cardiovascular risk (45) studies have also shown augmentation of wound healing when administered topically as well as systemically (46, 47). The beneficial effects have been linked to various factors such as increased angiogenesis promoted by greater Vascular Endothelial Growth Factor (VEGF) expression (48), increased Nitric Oxide (NO) concentrations (48) and lower expression of Tumour Necrosis Factor-Alpha (TNF-α) and Interleukin-1β (IL-1β) (49). In addition, improved hydroxyproline content and collagen thickness have been observed (48). At present, no published studies have correlated the enhanced healing with statin treatment to a reduction in skin cholesterol and hence reduced local steroidogenesis.

It is interesting to observe that an intermediate in the mevalonate pathway, Farnesyl Pyrophosphate (FPP), can act as an agonist for some nuclear hormone receptors (50). Vukelic *et al.* showed that FPP can act as a ligand at the Glucocorticoid Receptor (GR) *ex vivo* and *in vivo* inhibiting keratinocyte migration, epithelialization and subsequently wound healing (51). This effect was ascribed to activation of the GR rather than enhanced protein farnesylation by using an inhibitor of the farnesylation process.
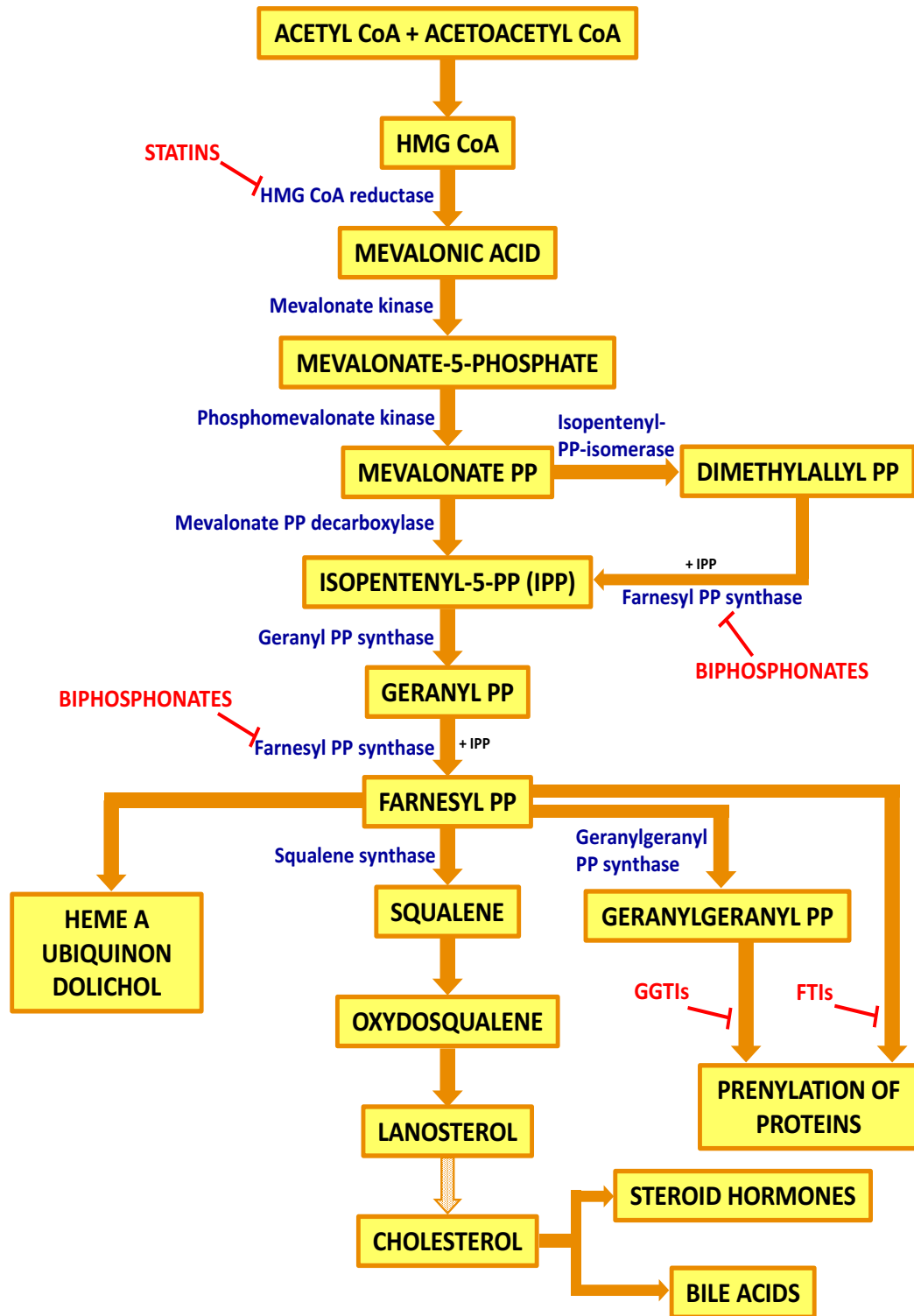
Figure 1.2 Mevalonate pathway describing the production of cholesterol from acetate. coA: co enzyme A, HMG: β-Hydroxy β-methylglutaryl, PP: pyrophosphate, IPP: isopentenyl pyrophosphate, GGTI: geranylgeranyl transferase inhibitors, FT1: farnesyl transferase inhibitors. Adapted from Buhaescu and Izzedine 2007 (44).

1.4.2 Steroid Hormones in the Skin

Skin expresses Steroidogenic Acute Regulatory Protein (StAR) and StAR-related lipid transfer protein (STARD3) (52). StAR is a 30 kDa protein that mediates the rate limiting step in steroid biosynthesis by transferring cholesterol from the Outer Mitochondrial Membrane (OMM) to the Inner Mitochondrial Membrane (IMM) (53). StAR has been detected in epidermal keratinocytes, sebocytes and outer root sheaths of hair follicles as well as regulators of StAR being identified in the epidermis (42, 43).

Synthesis of all steroid hormones proceeds with the production of pregnenolone from the cleavage of a side chain of cholesterol by the cytochrome P450 enzyme CYP11A1. Pregnenolone is successively modified by a specific series of steroidogenic enzymes to produce either mineralocorticoids, GC or sex hormones (oestrogens and androgens). This is illustrated in Figure 1.3. The enzymes expressed in human skin involved in the production of GC are CYP17A1 which converts pregnenolone to 17α-hydroxypregnenolone, followed by the actions of 3β-HSD-2 to convert this to 17α-hydroxyprogesterone. CYP21A2 then acts to form 11-deoxycortisol which is finally converted to cortisol by the enzyme CYP11B1 (42, 54-56).

Glucocorticosteroidogenic activity has been identified in epidermal keratinocytes (55, 57, 58) melanocytes (59) and dermal fibroblasts (60-62). In addition, skin cells express enzymes to locally regulate the activation or inactivation of GC (discussed in section 1.4.4).
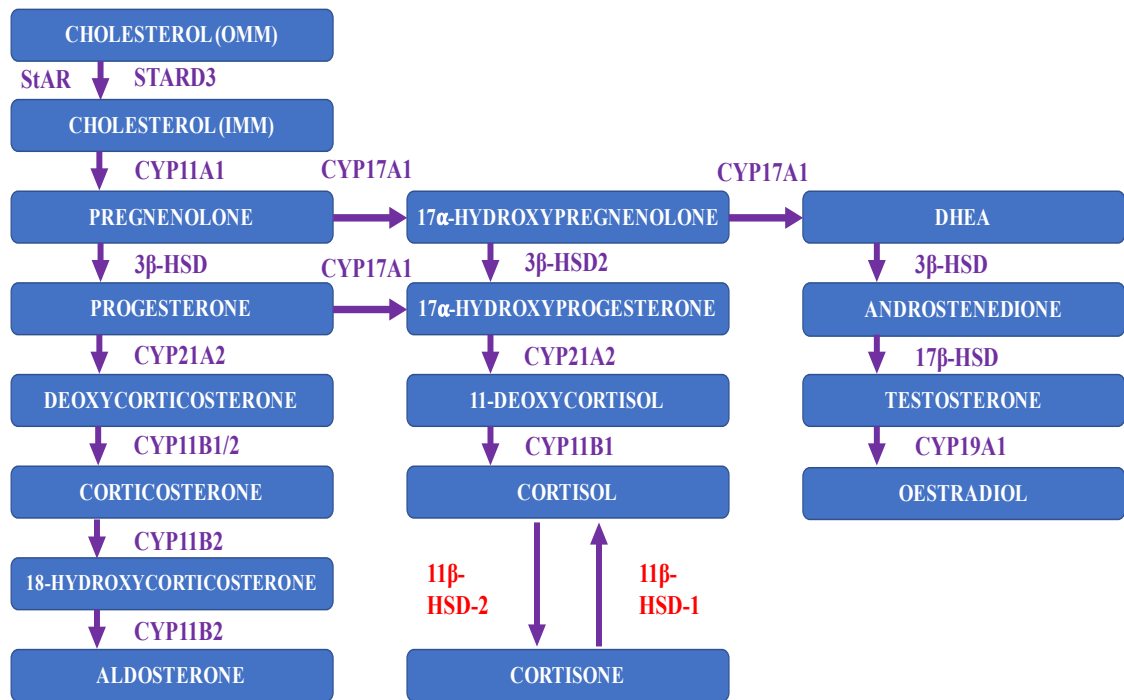
Figure 1.3 Steroidogenic pathways in human skin. Cholesterol is transferred from the OMM to IMM where it then has its side chain cleaved by CYP11A1 to produce pregnenolone which is then metabolized by steroidogenic enzymes to form mineralocorticoids, GC or sex steroids. Adapted from Slominski *et al.* 2014 (43).

1.4.3 GC Regulation in Skin

GC synthesis is systemically regulated by the Hypothalamic-Pituitary-Adrenal (HPA) axis (9, 40, 63). The hypothalamus produces and releases Corticotrophin Releasing Hormone (CRH) which stimulates CRH Receptor-1 (CRH-R1) in the anterior pituitary. Consequently, the anterior pituitary produces and releases the Proopiomelanocortin (POMC) peptides; Adrenocorticotrophic Hormone (ACTH) and β-Endorphin (β-END). Upon ACTH release into the systemic circulation, Melanocortin Receptor type 2 (MC2R) of the adrenal gland are activated resulting in the production and secretion of corticosterone (in rodents) or cortisol (in humans) (59, 64). Cortisol is 90% bound to corticosteroid binding globulin, whereas 4% is free. The remaining 6% is bound with a low affinity to albumin (40). Various factors such as infection, inflammation and trauma can affect the HPA axis at all levels of production as well as negative feedback from the produced steroid products themselves (63).

CRH, the CRH receptors CRH-R1, CRH-R2, POMC, POMC-derived peptides and associated processing machinery as well as steroidogenic enzymes have all been described within the skin itself (54, 60, 65-67). It has been shown that cell type-specific, functional regulatory loops exist with regulatory feedback pathways similar to those seen in the central HPA axis operating at a peripheral level (67). In addition, it has been postulated that local (skin) to central cross-talk can occur. Skobowiat *et al.* demonstrated that skin-only exposure to Ultraviolet B (UVB) radiation stimulated cutaneous expression of CRH, Urocortin (Ucn), POMC, ACTH, β-END, CYP11A1 and 3β-HSD peptides and *MC2R and StAR* genes with the final steroid product corticosterone being produced at significantly higher concentrations compared to animals not exposed to UVB. Moreover, hypothalamic *CRH* gene expression and peptide production was increased, as well as adrenal *MC2R* mRNA, *StAR* mRNA, *CYP11B1* mRNA and plasma CRH, Ucn, ACTH, β-END and corticosterone. Changes in plasma concentrations required an intact pituitary gland to occur (64). The mechanisms of this central activation are currently not well-defined but may include neural or humoral pathways including the promotion of cytokine production by UVB (64). The skin has a prime peripheral location with exposure to a variety of environmental stressors such that future research will be challenging.

1.4.4 The GR

GC exert their actions via the GR which is a ligand-dependent transcription factor. Although only one gene is found on chromosome 5q31-32, 10 exons codes for the GR and it is expressed as two main isoforms GRα and GRβ, due to alternate splicing of exon 9. Both isoforms are expressed in all organs and tissues including skin (68). Thus far, GRβ has not been reported to bind GC and hence is transcriptionally inactive (69). Interestingly, Oakley *et al.* noted that when culturing cells to overexpress GRβ, a dominant negative inhibitory effect on GRα mediated transactivation was observed (69). Varying expressions of the α and β isoforms have been studied in cases of GC resistance (66) and could also be implicated in regulating specific tissues' sensitivity to GC.

Lu and Cidlowski demonstrated that a single *GRα* mRNA species generated 8 N-terminal GR isoforms via alternative initiation sites (named GRα A, B, C1-3 and D1-

3). Each of these GR isoforms has unique tissue distribution patterns. They found 189 genes were regulated by all GRα isoforms, however the total number of genes regulated by individual isoforms varied, indicating each isoform regulates a unique set of genes (68). They postulated that in the same cell, the N terminal isoforms could homo-dimerize, hetero-dimerize or compete for co-regulators. They could also preferentially interact with different transcription factors or response elements on the same genes as well as undergoing post-translational modifications, thus further expanding the potential diversity in expression profiles (68).

1.4.5 Pre-Receptor Regulation - The 11β-Hydroxysteroid Dehydrogenases

The production of active GC is regulated by the 11β-hydroxysteroid dehydrogenases. These are microsomal enzymes of the short-chain alcohol dehydrogenase superfamily (70). Two isoforms 11β-HSD-1 and 11β-HSD-2 have been characterized in human tissues.

1.4.5.1 11β-HSD-1

11β-HSD-1 is a 34 kDa protein initially purified by Carl Monder's group from rodent liver in the 1980s (71). Since then it has been identified in many other organs including adipose tissue (72), skin (73), vascular smooth muscle (74), heart (75), bone (76) and placenta (77) in addition to the adrenal cortex (72). In humans, expression is absent in the first 3 post-natal months, after which expression rises in the next 9 months to adult levels (40). The gene is localized to chromosome 1q32.2 (78). 11β-HSD-1 is found anchored to the Endoplasmic Reticulum (ER) membrane orientated such that its catalytic domain is within the ER lumen (79). It is a Nicotinamide Adenine Dinucleotide Phosphate (NADPH) dependent enzyme under complex regulatory control by substances including GC, growth hormone, cytokines and stress (80).

The type 1 isoform is bi-directional; oxoreductase activity has been shown to predominate when previously studied in intact cells such as hepatocytes, fibroblasts, lung and adipose stromal cells (80). This is the conversion of inactive cortisone to active cortisol (in rodents; 11-dehydrocorticosterone to corticosterone). However, oxoreductase activity is unstable and upon tissue homogenisation can be lost,

enabling dehydrogenase activity to predominate (81). The directionality of the enzyme is thought to be determined by the position of 11β-HSD-1 within the ER lumen where Hexose-6-Phosphate Dehydrogenase (H6PDH) is located. H6PDH maintains a high enough NADPH concentration within the lumen to permit conversion of cortisone to cortisol (Figure 1.4). Clinically, loss of function mutations in the *11β-HSD-1* gene cause 'true' Cortisone Reductase Deficiency (CRD) which presents with premature adrenarche in children or polycystic ovary syndrome secondary to hyperandrogenism. In response to the reduced cortisol concentrations, the HPA axis will be activated promoting ACTH-mediated adrenal GC and androgen secretion. Urinary steroid profiles reveal elevated cortisone metabolites but low cortisol metabolites (82). Loss of function mutations in the *H6PDH* gene causes 'Apparent' CRD (ACRD). In ACRD, NADPH/NADP$^+$ ratios will be reduced, favouring the dehydrogenase activity of 11β-HSD-1, hence inactivating cortisol to cortisone (83, 84).

1.4.5.2 11β-HSD-2

11β-HSD-2 is a 44 kDa protein with the human gene located on chromosome 16q22 (78). This isoform is found largely in classical aldosterone target tissues such as the distal nephron of the kidney, colonic epithelium and salivary and sweat glands as well as adrenal cortex (85). Unlike its counterpart, it is widely expressed in the foetus and placenta from early to mid-gestation (86). It has Nicotinamide Adenine (NAD) dependent dehydrogenase activity, catalysing the opposite reaction to 11β-HSD-1 inactivating cortisol to cortisone (in rodents; corticosterone to 11-dehydrocorticosterone). It is anchored in the ER membrane with its catalytic domain orientated within the cytoplasm (in contrast to 11β-HSD-1) where it may physically interact with the cytoplasmic Mineralocorticoid Receptor (MR) (Figure 1.4) (79, 87). The type 2 isoform is unidirectional, only demonstrating dehydrogenase activity. Clinically, loss of function mutations in the *11β-HSD-2* gene results in the syndrome of apparent mineralocorticoid excess. As 11β-HSD-2 is unable to convert cortisol to cortisone, more cortisol is available to bind to not only the GR but also the MR which has a similar affinity for corticosterone, cortisol and aldosterone (78). Affected patients usually present in childhood (although few adult cases have been noted) with severe hypertension, sodium retention, hypokalaemia, metabolic alkalosis and low

plasma renin activity. Suppressing endogenous cortisol with dexamethasone was noted to reverse the features of mineralocorticoid excess (88).
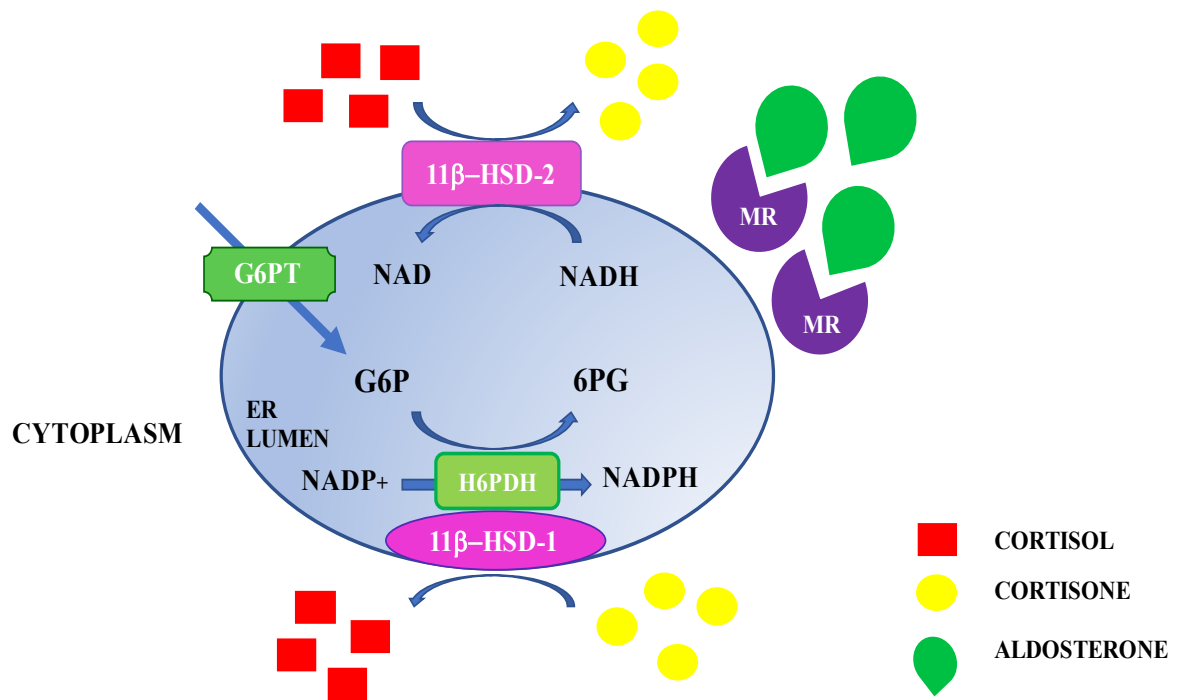
Figure 1.4 Diagrammatic representation of the reactions catalysed by 11β-HSD. G6P (Glucose-6-Phosphate) is transported from the cytoplasm into the ER lumen by a G6P transporter (G6PT) where H6PDH oxidises it to 6PG (6-Phosphogluconate) and concurrently reduces $NADP^+$ to NADPH, which is available for 11β-HSD-1 to convert cortisone to cortisol. 11β-HSD-2 catalyses the reverse reaction, inactivating cortisol to cortisone. Its presence allows only aldosterone to bind to the MR. Modified from Gathercole *et al*. 2013 (40) and Draper and Stewart 2005 (85).

1.4.5.3 11β-HSDs in Uraemia

Our group has previously shown that *11β-HSD-1* mRNA, protein and activity is upregulated in the uraemic liver with resultant elevation of intrahepatic GC concentrations, without systemic GC excess. The subsequent increase in gluconeogenesis contributes to an insulin resistant state which can be ameliorated by inhibition of this enzyme (89). The mechanism of this elevated intrahepatic 11β-HSD-1 is currently unclear. The uraemic milieu may promote similar upregulation in other tissues with a multitude of adverse effects.

N'Gankam *et al.* observed that patients treated by haemodialysis had signs and symptoms such as abnormal body fat distribution and osteopenia which could be attributed to an augmented GC response. As the kidneys are important for GC excretion and metabolism they analysed the concentrations of various GC related molecules via gas-chromatography mass spectrometry. They found that mean plasma concentrations of GC metabolites Tetrahydrocortisone (THE), Tetrahydrocortisol (THF) and 5α-Tetrahydrocortisol (5α-THF) were higher in patients before haemodialysis when compared to healthy controls. Plasma cortisone concentrations were also lower in this group, whereas there was no significant difference in cortisol concentrations for the two groups. The ratios of cortisol to cortisone and the ratio of their respective metabolites were significantly higher in the patients treated by dialysis, reflecting reduced 11β-HSD-2 activity (i.e. reduced elimination of GC) (Figure 1.5). They postulated either the presence of an inhibitory factor present in uraemic conditions or a reduced number of cells expressing 11β-HSD-2 due to lower nephron mass (90).
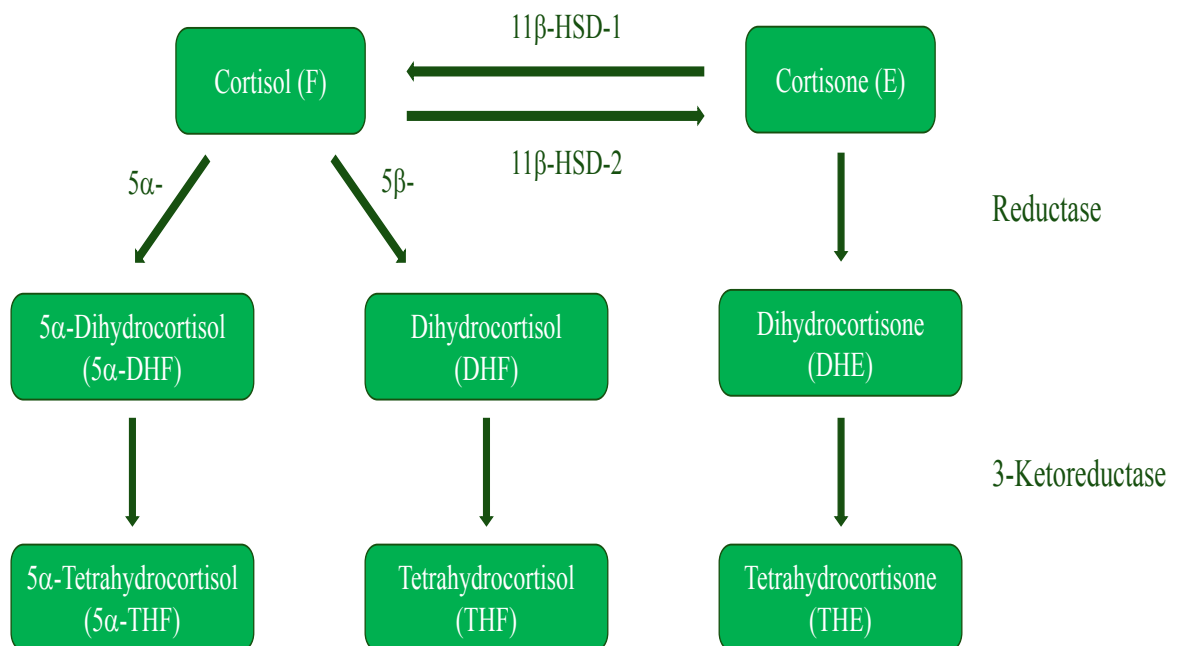
Figure 1.5 Formation of the metabolites of cortisol (F) and cortisone (E). Reduction of 11β-HSD-2 activity leads to an increase in cortisol/cortisone ratio and (5α-THF + THF)/THE. Adapted from N'Gankam *et al.* (90).

1.4.5.4 11β-HSDs in Skin

A limited number of studies have previously demonstrated the presence of 11β-HSD-1 in skin (73, 91). Paul Stewart's group have led further investigations of 11β-HSD-1 in skin and wound healing, describing the localisation of the enzyme to epidermal keratinocytes and dermal fibroblasts in both human and mouse skin as well as outer hair follicle root sheath cells in mice (92-94). In addition Lee *et al.* have observed immunoreactivity within sebaceous glands of normal skin and in inflammatory acne lesions (95).

Tiganescu *et al.* presented a trend towards increased reductase activity with increased donor age using 11β-HSD-1 activity assays performed on human skin tissue explants. They found 11β-HSD-2 activity was also present; however, this did not correlate with age. Supporting these findings, they demonstrated increased *11β-HSD-1* mRNA with donor age in primary cultures of human dermal fibroblast cells from sites exposed and protected from sunlight (lower outer versus inner upper arm). *GRα, H6PDH* and *11β-HSD-2* mRNA did not correlate with age or site. GC stimulation resulted in an upregulation of *11β-HSD-1* mRNA, although *GRα* and *11β-HSD-2* mRNA was down regulated. No regulatory effect was observed in *H6PDH* mRNA expression in response to stimulation with the same dose of cortisol (92). Using a global 11β-HSD-1 KO mouse model, they observed that aged KO mice had skin histological findings similar to young wild type controls with more organized collagen deposition and less dermal atrophy (93). These findings suggest elevated 11β-HSD-1 activity in aged skin leads to increased active cortisol production with its concomitant adverse features. In addition, the group examined the regulation of the 11β-HSDs in a mouse wound healing model. They noted a peak increase in *11β-HSD-1* gene expression and 11β-HSD-1 protein at day 2 post wounding, declining at day 4 to non-significant levels at day 8. *11β-HSD-2*, *NADPH*, *H6PDH* and *GRα* mRNA was unaffected by wound healing. 11β-HSD-1 activity was enhanced at day 2 and 4, whereas 11β-HSD-2 activity was negligible and unchanged post wounding (94). Topical 11β-HSD-1 inhibitor treatment was observed to accelerate healing of full thickness dorsal skin wounds in mice, alluding to an adverse role of the enzyme in healing (93).

1.4.5.5 Regulatory Factors of 11β-HSD-1 in Skin

1.4.5.5.1 Ultraviolet Radiation (UVR)

Different UV bandwidths have been shown to have a differing effect on the expression of 11β-HSD-1 and 11β-HSD-2 in skin. UVB and UVC increase 11β-HSD-1 protein expression and decrease GRα expression whereas UVA has no such effect. In contrast, UVA increases 11β-HSD-2 protein expression (96). Tiganescu *et al.* 2015 examined the effect of UVB radiation on 11β-HSD-1 expression in mice *in vivo* in more detail. They found mRNA expression for *11β-HSD-1* and *H6PDH* was significantly increased at day 1 post exposure to a single dose of UVB compared to control non-exposed mice. The mRNA levels remained raised at day 3 and 7; however, this was not statistically different. *GRα* mRNA expression in contrast was 30% lower in the control group at day 3, suggesting a negative feedback mechanism. 11β-HSD-1 protein expression was detected at day 3 post exposure, with a significant difference observed when compared to the control group. Histological examination of skin at day 3 post exposure noted a hyper proliferative epidermis, with 11β-HSD-1, detected by immunofluorescence, seen in the epidermis (concentrated in stratum basale layer, more diffuse in suprabasal layers and absent in stratum corneum), hair follicle outer root sheath (basal epidermal keratinocytes), with less 11β-HSD-1 detected in dermal fibroblasts. They also noted a positive correlation with 11β-HSD-1 activity and trans-epidermal water loss, suggesting disruption of skin barrier integrity (97). Hence, epidermal keratinocytes have a significant role in the regulation of 11β-HSD-1 expression and activity in response to UVR.

1.4.5.5.2 Inflammatory Cytokines

Pro-inflammatory mediators such as TNF-α and IL-1 have been shown to be inducers of 11β-HSD-1 in various cell types (preadipocytes, mesangial cells, luteinised granulomas cells, ovarian surface epithelial cells, synovial fibroblasts, bone marrow fibroblasts) promoting GC availability at the local level (91). Ito *et al*. demonstrated that IL-1β and TNF-α increased protein expression of 11β-HSD-1 in normal human keratinocyte cells as well as increasing cortisol concentrations in the culture media (63). Cells stimulated by these cytokines produced IL-6 and IL-8, an effect which was abrogated by 11β-HSD-1 Small Interfering RNA (siRNA) knock down. These findings suggested that pro-inflammatory mediators stimulate 11β-HSD-1 expression

which in turn can also stimulate production of further inflammatory cytokines. Additionally, exposure to low or high doses of cortisol had opposing effects on the production of IL-6 in keratinocytes, indicating that the influence of 11β-HSD-1 activity within cells could be crucial to the concentration of GC present and consequently whether inflammatory mediators are produced or suppressed. Vukelic *et al.* confirmed this increase in cortisol synthesis in human keratinocytes treated with IL-1β and conversely an inhibition of cortisol synthesis in cells treated with insulin-like growth factor-1. They showed correlating changes in *CYP11B1* mRNA expression but did not demonstrate its protein expression or enzyme activity in cell culture. Unfortunately, they did not concurrently investigate 11β-HSD-1 protein expression or activity to definitively delineate whether the increased cortisol concentrations were from *de novo* steroidogenesis or via the 11β-HSDs or from both pathways (98).

1.4.5.5.3 Pharmacological Inhibition

Inhibitors of the 11β-HSDs have been identified and studied extensively (99-104). In humans, the non-selective compound carbenoxolone was amongst the first to be utilised (40). Both 11β-HSD-1 and 11β-HSD-2 are inhibited by carbenoxolone thereby limiting its clinical potential due to the resultant hypokalaemia and hypertension. Selective 11β-HSD-1 inhibitors are sought to overcome these issues. Emodin (1,3,8-trihydroxy-6-methylanthraquinone) is a naturally occurring compound from the roots of *Rheum officinale* Baill, a Chinese herb (105). Emodin has been shown to have numerous pharmacological effects including antibacterial, antiviral, immunosuppressive, anti-tumour, anti-diabetic and anti-inflammatory effects (106). Tang *et al.* observed enhanced cutaneous wound healing in rats where a topical application of emodin was utilized, demonstrating increased wound contraction, angiogenesis and wound collagen content (107). They found that emodin increased *Transforming Growth Factor Beta 1* (TGF-β1) mRNA in wound tissue and identified upregulation of the intracellular proteins Smad 2 and 3 that could result in transcriptional changes of TGF-β inducible genes known to modulate the wound healing process. They also found a down-regulation of Smad 7 which acts as an inhibitor to the TGF-β1 receptor (107). Radha *et al.* observed increased fibrinolytic activity of fibroblast cells with the use of emodin, demonstrating an upregulation of

the urokinase plasminogen activator gene, protein and activity. They noted attenuated activity with ascorbic acid co-treatment, postulating the generation of reactive oxygen species as a mechanism for this upregulation. Emodin also caused an increase in cellular migration in an *in vitro* wound healing model (108). Feng *et al.* demonstrated that emodin is a potent and selective 11β-HSD-1 inhibitor in humans and mice, with no effect on 11β-HSD-2 (109). The contribution of 11β-HSD-1 inhibition by emodin in wound healing has yet to be ascertained.

1.5 Wound Healing

Wound healing after injury is a complex biological process involving diverse skin compartments as well as multitude of cellular constituents, growth factors, cytokines and is influenced by systemic factors such as the presence of diabetes mellitus, vascular disease and impaired nutritional or immunological status (110). Restoration of the functional barrier is the aim; however, failure in the process at any stage can result in chronic wound formation with its associated health and economic burden (111).

1.5.1 Phases of Healing

The normal process of healing occurs as a continuum, however to assist in further comprehending the underlying processes, it has been defined crudely into three phases; an inflammatory period followed by a proliferative and finally a remodelling period (110, 112, 113). After injury, the clotting cascade is initiated; thrombin activates fibrin formation and promotes its deposition into a mesh-like structure that can form the foundations to recruit cells including inflammatory cells such as neutrophils, macrophages and T-lymphocytes (114). Platelets are also recruited to the site of damage whereby they aggregate and degranulate releasing cytokines and chemokines that promote this process and stabilise the clot formation, achieving haemostasis (115). In parallel, the inflammatory response is propagated at the wound site with the clearance of dead or injured cells by phagocytosis (116). Additionally, bacteria are engulfed to protect against infection. In the presence of a high bacterial load, inflammatory cell influx is sustained resulting in an imbalance between inflammatory and anti-inflammatory signals, leading to delayed healing (117).

In the proliferative phase, fibroblasts and keratinocytes are recruited to the wound to begin the repair process (116, 118, 119). A sufficient blood supply is essential for all cells at the wound site as they require nutrients and oxygen to thrive. Angiogenesis is crucial for this to occur. Existing blood vessels vasodilate under the influence of histamine, prostaglandins and kinins and become more permeable, allowing leucocyte extravasation (from the intravascular to extravascular space) to promote phagocytic debridement and decontamination of the wound site (112). Macrophages can secrete endothelial chemotactic factors and growth factors as well as proteases which encourage endothelial cells to detach from the embedded endothelium (112). Endothelial cells can then divide and migrate towards the released angiogenic factors, laying down new vessels in an organised fashion (120). Sprouting of new vessels is stimulated by hypoxia and acidosis within the microenvironment (112). In turn, Hypoxia Inducible Factor (HIF) is released which can activate genes for other angiogenic factors such as VEGF (121). The endothelial cells of the new vessels mature and form new basal laminae, surrounded by a pericyte layer (122). The main aim of the proliferative phase is the formation of granulation tissue which consists of inflammatory cells, fibroblasts, neovasculature with a matrix of fibronectin, collagen, proteoglycans and glycosaminoglycans (112). Fibroblasts are an important cell type in promoting granulation tissue formation. Their migration and proliferation is stimulated by fibronectin as well as released growth factors such as fibroblast growth factor, platelet derived and TGF-β (112, 113, 123). Fibroblasts use fibrin and fibronectin deposited like a scaffold to migrate across the wound area, secreting procollagen, glycosaminoglycans, hyaluronan, chondroitin sulphate into the extracellular space thereby providing a more stable network for further fibroblast migration (113).

Keratinocytes play a key role in epithelialization. They migrate first across the wound site, then proliferate from uninjured keratinocytes at the wound edge, meeting in the middle of the wound where the process is halted by contact inhibition (112). To achieve this, desmosomal and hemi-desmosomal interactions that anchor cells to each other and the Extracellular Matrix (ECM) are disrupted (124). Intracellular actin microfilaments form to allow keratinocytes to creep over the wound surface by interacting with the matrix of fibrin crosslinked with fibronectin and collagen (124, 125). Keratinocytes must be able to dissolve the clot that has formed at the

haemostatic stage as well as interposing debris or ECM within its migration path. To assist with this, plasminogen activator is released as well as collagenases and proteases (112). Once migration has ceased, proteins can be secreted to form a new BM. The desmosomal and hemi-desmosomal interactions are re-formed to anchor cells to the BM.

Finally, wound contraction is observed where fibroblasts differentiate into myofibroblasts and contract the wound edges in a centripetal fashion. Further collagen is laid down at the same time to reinforce the wound (123).

In the final phase of wound healing, remodelling of the ECM occurs. The main feature of this is collagen remodelling under the regulation of collagenases and matrix metalloproteinases (126). Collagen type III is replaced by a greater proportion of collagen type I, which becomes more organized in structure (increased diameter of fibrils, increased inter-fibril binding, and rearrangement of fibrils). In addition, fibronectin gradually disappears, and water and proteoglycan content decreases (112, 113).

1.5.2 Wound Healing in Uraemic Skin

In the 1960s Nayman noted breakdown of abdominal wounds in the uraemic state and set out to investigate the effect of induction of acute renal failure with uranium nitrate in wound healing post-laparotomy in dogs, as well as the ability of haemodialysis to prevent wound breakdown. He reported that induction of acute renal failure within the first 6-7 days post laparotomy resulted in wound breakdown, but occurrence of renal impairment beyond this point had no effect upon the wound. Early and frequent haemodialysis abrogated this effect on wounds (127). Histological studies in mice revealed significant impairment of healing in uranium nitrate treated groups with a reduction in granulation tissue formation and inhibition of proliferation of fibroblasts and endothelial cells (128).

In the last 30-40 years, there has been a paucity of published *in vivo* studies of wound healing in CKD with no firmly established model available to examine the interactions of uraemia with healing. Seth *et al.* developed a surgical excisional wound healing murine model of CKD in 2013. They demonstrated that animals with

CKD had significantly disrupted epithelization kinetics and granulation tissue deposition rates compared to control animals. The wounds of CKD mice showed significantly less proliferating cells and a significant reduction in angiogenesis compared to their controls. Of note, uraemic mice displayed an increased inflammatory state during early stages post-wounding which was maintained to day 14 (38).

1.6 Hypothesis and Aims

We predict that the cortisol producing enzyme 11β-HSD-1, which is highly expressed in the skin, is activated in the uraemic state with resultant poor wound healing in our CKD patient population.

Aims:

- To determine the presence or absence of 11β-HSD-1 and 11β-HSD-2 in skin in uraemia
- To determine the activity of 11β-HSD-1 in skin in uraemia
- To clarify the role 11β-HSD-1 plays in wound healing in uraemia
- To investigate whether topical or systemic inhibition of skin 11β-HSD-1 can be harnessed to accelerate wound healing in uraemia

CHAPTER 2

Materials and Methods

2.1 Cell Culture Techniques

2.1.1 Cell Culture Models

Cell culture is a technique used to study the normal physiology and biochemistry of cells, outside the complexity of the whole organism. The effects of drugs and toxins can be readily analysed by manipulation of the growth environment. To simulate the uraemic milieu compounds can be added to cell culture media, which in turn is used to culture cells of interest. IS and PC are two such solutes that have been shown to be retained in the serum of patients with CKD (129). Both substances originate from bacterial fermentation of protein in the colon. Tryptophan is degraded to indole, which is then hydroxylated and sulphonated to IS in the liver (130), whereas tyrosine (and to a lesser degree phenylalanine) is fermented to PC (131).

IS was first isolated in 1911 by Obermayer and Popper where they found it to be present in high concentrations in the serum of patients with CKD (132). Since then numerous researchers have studied its role in kidney disease, toxicity and methods to reduce plasma concentrations (133). IS is a small solute with a molecular weight of 213 g/mol. It is 90% bound to proteins found in the plasma such as albumin (134). In normal functioning kidneys, it is cleared by tubular secretion. IS exists in an equilibrium between the bound and free state. As blood containing IS passes through the peritubular capillaries of the proximal tubules, unbound IS is taken up by proximal tubular cells via the Organic Anion Transporters OAT1 and OAT3 found on the basolateral surface. It then passes through apical membrane transporters into the tubular lumen. To maintain equilibrium, another molecule of IS will dissociate from the plasma proteins (135, 136). As haemodialysis cannot mimic this described tubular secretion, clearance of IS via haemodialysis is low at 25-30 mL/min compared to clearance of a water-soluble solute such as urea at 220 mL/min (134).

PC is also a small solute with a molecular weight of 108.1 g/mol. It is almost 100% bound to plasma proteins (137). Like IS, it is poorly cleared on haemodialysis due to its protein bound nature (138). PC has been shown to alter cell permeability in bacteria (139), block cell K^+ channels (140) as well as inhibit the release of platelet activating factor by peritoneal macrophages in rats (141) and decrease endothelial wound repair (129). It's concentration in the uraemic state was noted to decrease with the binding resin AST-120 (142).

2.1.2 Cell Culture Media and Buffers

For cell culture, two primary cell populations from commercial sources were utilised. HDFs (Fisher Scientific Limited, Loughborough, UK) were cultured in Dulbecco's Modified Eagle's Medium (DMEM) containing 1000 mg/L glucose, L-glutamine, sodium bicarbonate and pyridoxine supplemented with 10% Foetal Bovine Serum (FBS) and 1% penicillin/streptomycin (10000 U penicillin and 10 mg streptomycin per mL) (all from Sigma-Aldrich, Poole, UK). HEKs (Fisher Scientific Ltd) were cultured in Gibco Epilife™ medium containing 60 μM calcium supplemented with Human Keratinocyte Growth Supplement (HKGS, Fisher Scientific Ltd).

Cells were cultured in T75 flasks containing 25 mL of appropriate medium in a humidified incubator at 37^oC in a 95% air, 5% CO_2 atmosphere. On attaining 70% confluence they were passaged as required. To mitigate against trypsin related cell damage, Trypsin Neutralizing Solution (Fisher Scientific Ltd) was added in equivalent quantities after the cells had detached from the flask by using 5 mL of an alternative enzyme; TrypLE™ Express Enzyme 1X (Fisher Scientific Ltd). The 10 mL suspension was centrifuged at 650 g for 5 min. The cell pellet was re-suspended in 1 mL of the appropriate growth media, which was then added to the desired volume of filtered media for subsequent culture.

To perform experiments, the cell pellets were suspended into a total volume of media such that 5 mL could be seeded into T25 flasks. Cells were incubated in complete media until they had achieved 70% confluence. Thereafter the media was removed and replaced with 5 mL media without supplements or antibiotics for 24 h prior to experimentation. Serum starvation was employed to bring all cells in to the same phase of the cell cycle and to control for the multitude of effects that the serum components may have on the outcomes being measured (143, 144).

2.1.3 Simulation of Uraemia using Uraemic Toxins

To simulate the uraemic milieu, two different solutes previously shown to accumulate in patients with CKD were investigated. These are IS and PC. Cultured cells were treated at a range of concentrations of uraemic toxins, including dilutions greater and less than those found in patients with CKD (IS 10 μg/mL and PC 25 μg/mL).

IS (Sigma-Aldrich, Poole, Dorset, UK) was dissolved in double pass reverse osmosis purified water (RO) to make a stock solution of 10 mg/mL. Calculated volumes of IS stock were added to supplement-free cell culture media to achieve final concentrations of 25, 50 and 100 μg/mL. RO grade water was utilised as vehicle. Media from T25 flasks was aspirated, discarded and replaced with 3 mL IS experimental solution and incubated over a range of 1 - 48 h before the cells were lysed.

PC was solubilised in Dimethyl Sulphoxide (DMSO) (both from Sigma-Aldrich) to make a stock solution of 10 mg/mL. Calculated volumes of PC stock were added to supplement-free cell culture media to achieve final concentrations of 10, 25 and 50 μg/mL. DMSO was utilised as vehicle. Media from T25 flasks was aspirated, discarded and replaced with 3 mL PC experimental solution and incubated over a range of 1 - 48 h before the cells were lysed.

2.1.4 Inhibition of 11β-HSD-1 by Emodin

Emodin (Sigma-Aldrich) was solubilised in DMSO to make a stock solution of 10 mM. Calculated volumes of emodin stock were added to supplement-free cell culture media to achieve final concentrations of 20, 50 and 100 μM. DMSO was utilised as the vehicle control. Media from T25 flasks was aspirated, discarded and replaced with 3 mL emodin experimental solution and incubated over a range of 1 - 48 h.

2.1.5 LDH Assay

Prior to cell lysis, 1 mL of the cell culture media was removed from each T25 flask and transferred to a 1.5 mL Eppendorf tube (Fisher Scientific Ltd). The media was briefly centrifuged at 600 g for 3 min to remove any cell debris before performing a LDH cytotoxicity assay (Roche Diagnostics Limited, distributed by Sigma-Aldrich). 100 μL supernatant was added to a clear bottomed 96-well plate before adding 100 μL of reaction mixture (catalyst (diaphorase/NAD^+ mixture) and dye solution (iodotetraxolium chloride and sodium lactate) in a ratio of 45:1). The plate was then protected from light for 5 min. A Dynex Technologies MRX TC II Microplate Absorbance Reader was used to measure absorbance at 490 nm after this period.

This colorimetric assay quantitates cytotoxicity based on the measurement of LDH activity released from the cytoplasm of damaged cells. Released LDH reduces NAD^+ to $NADH^+$ and H^+ by oxidation of lactate to pyruvate. In the coupled enzymatic reaction, $2 H^+$ are transferred from the $NADH^+ H^+$ to the yellow tetrazolium salt (2-[4-iodophenyl]-3-[4-nitrophenyl]-5-phenyltetrazolium chloride by the catalyst formulating a formazan product with an orange colour which can then be measured.

2.1.6 Cell Lysis and Protein Extraction

After media removal, the cells were washed in 3 mL ice-cold calcium and magnesium free phosphate buffered saline solution (Severn Biotech Limited, Kidderminster, UK) which was then aspirated and discarded. Prior to harvesting the cells with a plastic cell lifter (Fisher Scientific Ltd), 300 µL of Mammalian Protein Extraction Buffer (MEB) (GE Healthcare, distributed by VWR International Limited) supplemented with 1% of Calbiochem protease and phosphatase inhibitors (Merck, Watford, UK) was added to each T25 flask. The lysed products were collected into an Eppendorf tube for centrifugation at 16,000 g at 4^oC for 15 min. The supernatant was collected for use in future work and stored at -80^oC.

2.1.7 Cell Viability Assay

Cells were suspended in appropriate media before 100 µL was dispensed into 72 wells of a 96-well plate. The remaining 24 wells were left empty to use as negative controls. After 24 h, this media was aspirated and discarded before every well was replaced with 100 µL of either IS (0, 25, 50, 100 µg/mL), PC (0, 10, 25, 50 µg/mL) or emodin (0, 20, 50, 100 µM) experimental solutions in either complete or supplement-free media. To determine cell viability, the CellTiter 96® AQueous One Solution Cell Proliferation Assay (Promega, Southampton, UK) was performed. 20 µL of the kit reagent was added to each well prior to incubation at 37^oC in a 95% air, 5% CO_2 atmosphere for 1 hour. A Dynex Technologies MRX TC II Microplate Absorbance Reader was then used to measure absorbance at 490 nm.

This assay employs the principle that viable cells can generate products such as NADPH that can reduce the tetrazolium compound, MTS (3-(4,5-dimethylthiazol-2-yl)-5-(3-carboxymethoxyphenyl)-2-(4-sulphophenyl)-2H-tetrazolium)   in   the

presence of an electron coupling reagent such as phenazine ethosulphate, into a soluble formazan product with a detectable colour. Upon cell death, the ability to reduce MTS is lost and less formazan product is formed. Hence, the number of viable cells is taken to be directly proportional to the production of the coloured formazan product which can be quantified by absorbance measurements.

2.1.8 Scratch Assays with the JuLI[TM] Stage Cell Imager

Cells were suspended in appropriate media before 1mL was dispersed into each well of a 12-well plate. The plate was cultured in a humidified incubator at $37^{o}C$ in a 95% air, 5% CO_2 atmosphere. Upon attaining 70% confluence, 3 parallel vertical scratches were made in the middle of each well with a 20 μL graduated pipette tip. The media was aspirated and discarded before being replaced with 1mL of designated experimental solutions that had been pre-warmed to $37^{o}C$ either IS (0, 25, 50 or 100 μg/mL), PC (0, 10, 25, 50 μg/mL) or emodin (0, 20, 50, 100 μM). The plate was placed on the JuLI[TM] Stage cell imager and the most uniform scratch in each well was selected for serial imaging over 24 hours at 1 hour intervals. The inbuilt software uses image capture and time lapse recording to generate growth curves for each well by calculating the percentage healing across the scratch in each well at each time interval. The experiments were repeated using media without supplements or antibiotics for 24 hours prior to scratching and to make up the IS, PC and emodin experimental solutions.

2.2 *In vivo* and *ex vivo* Methods

All *in vivo* work was carried out under Home Office Project License number PPL 70/8350 with ethical approval from Queen Mary University of London. The principles of the 3Rs (replacement, reduction and refinement) were employed in the execution of all experiments.

2.2.1 Adenine Diet Model

Yokozawa *et al*. first showed in 1986 that feeding adenine to rats produced metabolic abnormalities like those found in patients with CKD (145). The formation of 2, 8-Dihydroxyadenine (DHOA) by xanthine oxidase occurs secondary to the saturation of the enzyme adenine phosphoribosyltransferase by excess adenine. Instead of the

formation of adenosine monophosphate and subsequently allantoin 25, DHOA is formed which is poorly water soluble and hence precipitates out of urine. DHOA has been shown to cause a crystal nephropathy as well as renal stones, with the potential to cause obstruction and subsequent hydronephrosis (146). Histologically, needle shaped crystals are deposited within the lumen of the renal tubule causing pathological expansion of the tubule. Although there is a predisposition for the proximal tubule, crystals can be found along the entire length of the tubule both in the renal cortex and the medulla. Interstitial oedema and fibrosis can result. Granulomas composed of histiocytes and multinucleate giant cells are observed around these crystals causing a granulomatous interstitial nephritis and subsequent renal function impairment. The glomerulus itself is spared in this process (147).

By altering the concentration of adenine within the diet as well as the duration it is given to animals, renal failure of varying severity can be studied. Okada *et al.* showed that rats fed 0.75% adenine for 2 weeks developed reversible, partially recoverable renal failure as compared to those fed for 4 weeks that developed non-progressive, irreversible damage and those at 6 weeks that had progressive, irreversible renal failure. At 6 weeks, a rise in serum sodium, potassium, hypoproteinaemia, leukopenia and a higher mortality rate were noted prompting the authors to conclude that to generate a favourable experimental model, 4-5 weeks of 0.75% adenine feed in rats was sufficient (147).

2.2.2 Subtotal Nephrectomy (SNx) Model

An alternative model used by our research group is that of SNx whereby 5/6th of renal mass is removed in a 2-stage procedure. Initially, a left flank incision is made under general anaesthesia. Underlying musculature is blunt dissected to the parietal peritoneum. A further incision is made through which the kidney is carefully externalised. After removal of the perinephric fat and renal capsule, an arterial clamp is placed across the hilum. Approximately 2/3rds of the renal parenchyma is removed from the upper and lower renal poles as well as the lateral surface. The arterial clamp is then removed and haemostasis achieved by applying manual pressure to the cut surfaces. The kidney is returned to the abdomen. 1 mL of sterile saline is instilled into the abdominal cavity to compensate for surgical fluid losses. The musculature is sutured and the skin incision stapled closed. Subcutaneous analgesia is then

administered. 2 weeks after recovery from the first operative stage, the animals are anaesthetized and a contralateral right flank incision made. The kidney is externalised. After applying the arterial clamp, the renal artery and vein are ligated. The whole kidney is excised distal to the ties. Sterile saline is instilled, and the incisions closed as before. After recovery, animals are given 4 weeks to recover during which they develop a uraemic state. Sham operated animals undergo the same anaesthetic, incisions, externalisation of kidneys, decapsulation and arterial clamping. However, no renal tissue is excised. These animals form suitable controls for experimental work (148). The SNx model generates a more restrained increase in serum urea and creatinine which is sustained from 3 weeks post-surgery (149).

2.2.3 Rat Uraemic Model

6-week old male Wistar Rats (Charles River Laboratories, Kent, UK) were housed in a temperature controlled facility. 12 h light and dark cycles were maintained as was free access to water and standard chow (Rat and Mouse No. 1 Maintenance, SDS Diets, Essex, UK). Following a 1-week acclimatization period, the animals were randomly assigned to 2 groups: standard chow supplemented with 0.75% adenine (SDS Diets) to develop a uraemic phenotype or standard chow alone (control animals). Over the subsequent 3 weeks, survival, growth rate and general well-being were closely monitored.

2.2.3.1 Rat Wound Healing Model

Animals were weighed and examined for general health before undergoing wounding. Under 5 L/min IsoFlo 100% v/v (isoflurane, Zoetis, London, UK) inhaled anaesthesia, the dorsum was shaved with electric clippers. Chlorhexidine (Fisher Scientific Ltd) was used to clean the skin. Under 1.5 L/min isoflurane anaesthesia, 30 µL Vetergesic (buprenorphine, Ceva Animal Health Limited, Amersham, UK) was injected subcutaneously. The dorsal skin was drawn together in a fold. One 5 mm Stiefel punch biopsy tool (Schuco, Watford, UK) was employed to make 2 wounds through the skin with one punch; entrance wound A and exit wound B (Figure 2.1). The punched-out skin was bisected; half was snap frozen in liquid nitrogen (later stored at -80°C) and the remaining half mounted onto Polyvinylidene Difluoride (PVDF) 0.45 µm membrane (Fisher Scientific Ltd), stored in 10% neutral buffered formalin solution

(Sigma-Aldrich) and then transferred to 70% ethanol (VWR International Ltd) 24 h later. Animals were observed to recover from anaesthesia before returning to cages.

2.2.3.2 Topical Emodin in Rat Wound Healing Model

Emodin (Fluorochem Limited, Glossop, UK) was solubilised into 2% Carbopol®934 (Enzo Lifesciences (UK) Limited, Exeter, UK) using triethylamine (Sigma-Aldrich) to form a gel with a final concentration of 500 µg/mL or 1000 µg/mL. 0.5 mL of drug or 2% Carbopol®934 as vehicle was massaged into each wound once daily from day 0 - 4 after wound healing. Animals were culled at day 7.

A)

B)

C)
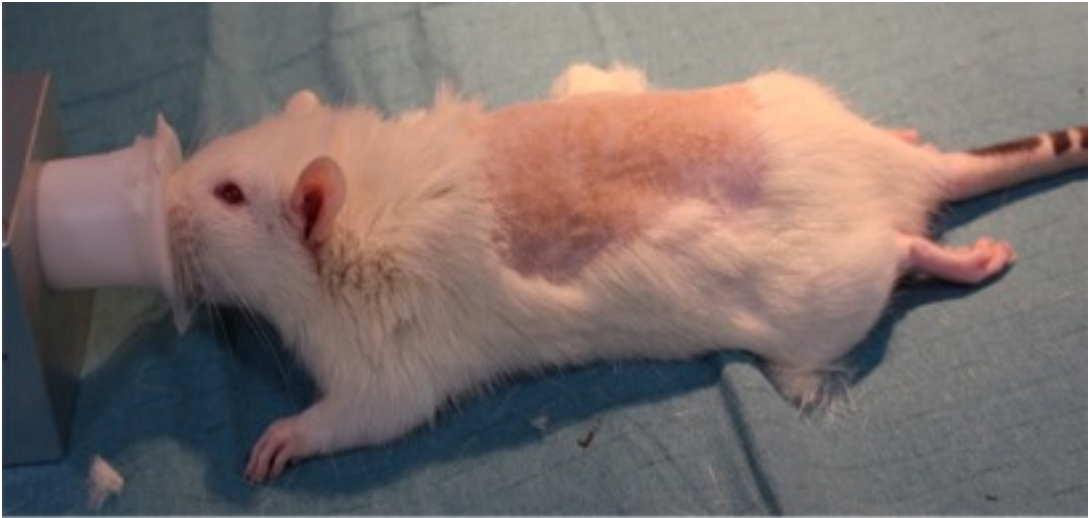
D)

Figure 2.1 Images of rat wound healing procedure. A) skin preparation, B & C) anaesthesia administration and D) wounding with punch tool.

2.2.3.3 Systemic Emodin in Rat Wound Healing Model

Emodin (Fluorochem Limited) 100 mg/kg or vehicle 10% ethanol (VWR International Ltd) was administered once daily to animals by oral gavage from day 0-2. Animals were then culled at day 3. For a secondary experiment, emodin 100mg/kg or vehicle 10% ethanol was administered once daily from day 0-4 after wound healing with animals being culled at day 7.

2.2.4 Tissue Retrieval

All animals were culled in accordance with Home Office (Animals Scientific Procedures Act 1986) Schedule 1 regulations. After weighing animals, a terminal dose of thiopentone (Archimedes Pharma, Reading, UK) was administered intraperitoneally. Blood was obtained by cardiac puncture in a heparin sodium (Wockhardt Limited, Wrexham, UK) coated 2 mL syringe. 1 sample was left to clot at room temperature for 2 h before centrifugation for 20 min at 2000 g. Serum was transferred to a clean Eppendorf and stored at -20°C for corticosterone measurement. A second sample was stored at 4°C, centrifuged at 7000 g for 3 min. The serum obtained was sent to IDEXX BioResearch Laboratories, Ludwigsburg, Germany for biochemical analysis.

The dimensions of wounds A and B were measured. The wounds and a small surrounding area of skin were excised and bisected; half was snap frozen in liquid nitrogen and the remaining half mounted onto PVDF membrane (Fisher Scientific Ltd), stored in 10% neutral buffered formalin solution (Sigma-Aldrich) and then transferred to 70% ethanol (VWR International Ltd) 24 h later. Organs of interest including liver and non-wounded skin were concurrently snap frozen in liquid nitrogen and then stored at -80°C.

2.2.5 Tissue Homogenisation for Protein Isolation

Tissues retrieved from -80°C were stored on the bench in liquid nitrogen until ready for use. Skin samples were dissected with scalpel and forceps to remove subcutaneous adipose and muscular tissue. After cutting into small pieces, the sample was re-frozen in liquid nitrogen. A ceramic pestle and mortar with rough surfaces was cooled with liquid nitrogen before adding the sample and manually grinding until a powder formed. Liquid nitrogen was replenished as required until this had been

achieved. 1 mL of MEB (GE Healthcare) with 1% Calbiochem protease and phosphatase inhibitors was added to the powder before transferring to an Eppendorf and returning to liquid nitrogen. All samples were thawed together at room temperature before centrifugation at 16000 g for 15 min at 4°C. The supernatant was preserved, aliquoted and stored at -80°C until ready for use for protein quantification or western blotting.

2.2.6 Tissue Homogenisation for RNA Isolation

All equipment and laboratory surfaces were cleaned with RNase Away (Molecular BioProducts, Fisher Scientific Ltd). Care was taken to minimize the introduction of RNases by using autoclaved laboratory consumables and regularly changing gloves. Tissue retrieved from -80°C was stored in liquid nitrogen until ready for use. Skin samples were dissected with scalpel and forceps to remove subcutaneous adipose and muscular tissue. After cutting into small pieces, the sample was re-frozen in liquid nitrogen. A ceramic pestle and mortar with rough surfaces was cooled with liquid nitrogen, before adding the sample and manually grinding until a powder formed. Liquid nitrogen was continuously replenished until this had been achieved. 300 μL Buffer RLT (Qiagen RNeasy$^{®}$ Fibrous Tissue Mini Kit, Manchester, UK) with 10 μL/mL β-mercaptoethanol (Sigma-Aldrich) was added to approximately 30 mg of tissue. Lysates were stored at -80°C until ready for use.

2.3 Western Blotting

2.3.1 Protein Quantification

Protein concentration was determined using a bicinchoninic acid (BCA) assay (Pierce™ BCA Protein Assay Kit, Fisher Scientific Ltd). Bovine serum albumin (Sigma-Aldrich) diluted with RO grade water was used to create calibrants of known concentrations (0 – 2000 μg/mL) against which cell lysate or tissue homogenate protein concentration could be measured. 25 μL of standards or samples was added to a clear bottomed 96-well plate. 200 μL of working reagent (50:1 reagent A to reagent B) was then added to each well before mixing and then incubating the plate for 30 min at 37°C. A Dynex Technologies MRX TC II Microplate Absorbance Reader was used to measure absorbance at 550 nm after this time.

This assay allows for the colorimetric detection and quantitation of protein in samples. Cu^{2+} is reduced to Cu^{1+} by protein in an alkaline medium (the biuret reaction). Two molecules of BCA then chelate with one cuprous cation, forming a purple coloured product which can be measured spectrophoretically.

2.3.2 Sample Preparation

30 µL sample and 10 µL NuPage® Sample Loading Buffer 4X (Fisher Scientific Ltd) were heated in a water bath at 75°C for 15 min to denature and reduce disulphide bonds. A standardized concentration of protein was used for each western blot (in the range of 30 to 60 µg protein per well).

2.3.3 Gel Electrophoresis

The XCell SureLock™ Mini-Cell (Fisher Scientific Ltd) apparatus was assembled for electrophoresis. Pre-cast 4-12% Bis-Tris gels (NuPage™ Novex™ Fisher Scientific Ltd) with the appropriate number of wells (10, 12 or 15) were chosen according to the number of samples to be run. Gels were removed from packaging, discarding the preservative solution within. Combs inset to form loading wells were carefully removed and rinsed with MOPS solution (50 mL NuPage® MOPS SDS Running Buffer 20X, Fisher Scientific Ltd and 950 mL RO grade water). Gels were placed in the apparatus and clamped *in situ*. MOPS solution was used to fill the space between gels to ensure no leakage (upper buffer chamber). Samples were loaded alongside a marker (Cruz Marker™ Molecular Weight Standards: sc-2035, Insight Biotechnology, Wembley, UK). The remaining MOPS solution was used to fill the Mini-Cell before running at 200 V for 1 h.

2.3.4 Protein Transfer

Transfer buffer was made to transfer 2 membranes simultaneously as follows: 200 mL methanol (VWR International Ltd), 50 mL transfer buffer (NuPage® Transfer Buffer 20X, Thermo Fisher Scientific) and 750 mL RO grade water. This was used to soak blotting pads and 2.5 mm thick filter paper. PVDF 0.45 µm membrane (Thermo Fisher Scientific) was cut to size and pre-soaked in 100% methanol (VWR International Ltd) for 2 min. The pre-cast gels were opened, PVDF membrane placed on top, ensuring no air bubbles were present, and both incorporated into the transfer

'sandwich' made with blotting pads and filter paper. This was inserted into the Mini-Cell and the clamp applied. Transfer buffer was used to fill the upper buffer chamber and RO water used to fill the lower buffer chamber. Protein transfer was performed over 2 h at 30 V.

2.3.5 Blocking and Detection

Non-specific protein binding was blocked by incubating the membranes in a commercial blocking buffer (Starting Block™(TBS) Blocking Buffer, Thermo Fisher Scientific) for 30 min. The membranes were then incubated with either anti-rabbit 11β-HSD-1 antibody or anti-rabbit 11β-HSD-2 (OABF01282 and OABB00330 both Aviva Systems Biology, Insight Biotechnology) diluted to an optimized concentration of 1:1000 in blocking buffer overnight, with shaking, at 4^oC. The membranes were then washed three times in Tris Buffered Saline (TBS 10X) (Severn Biotech Limited) plus 0.05% Tween-20 (Fisher Scientific Ltd) for 10 min before incubating with goat derived anti-rabbit Immunoglobulin G (IgG) conjugated to Horseradish Peroxidase (HRP) (sc-2030, Santa Cruz Biotechnology, obtained from Insight Biotechnology) diluted to 1:4000 for 1 h at room temperature. After three further 10 min washes in TBS-T, protein bands were detected using the Pierce^{TM} ECL Western Blotting Substrate Kit (Fisher Scientific Ltd) and Amersham Hyperfilm ECL (GE Healthcare).

To confirm accurate protein loading, membranes were agitated in Restore™ PLUS Western Blot Stripping Buffer (Fisher Scientific Ltd) for 20 min, washed in TBS-T and then incubated for 15 min at room temperature with anti-rabbit Glyceraldehyde 3-Phosphate Dehydrogenase (GAPDH) (G9545, Sigma-Aldrich) at a concentration of 1:5000. Following three 5 min TBS-T washes, the membranes were incubated with anti-rabbit IgG-HRP (Santa Cruz Biotechnology) at a concentration of 1:10000 for 15 min at room temperature, before being washed thrice in TBS-T. Protein bands were detected using the aforementioned ECL kit and film.

2.3.6 Western Blot Analysis

Image J software (imagej.nih.gov) was utilised to measure protein band intensity from western blot images. 11β-HSD-1 and 11β-HSD-2 expression was normalised to that of GAPDH.

2.4 ELISA

Commercially provided competitive enzyme immunoassays for cortisol and corticosterone were utilized (Bio-Techne, Abingdon, UK). Using these assays, corticosterone concentrations can be measured within the range of 0.012 - 0.047 ng/mL and cortisol within the range of 0.030 – 0.111 ng/mL. Cortisol or corticosterone in samples competes with a fixed amount of HRP-conjugated cortisol/corticosterone which is added alongside an antibody specific to the steroid to a microplate coated with a complementary IgG antibody. After washing steps to remove excess unbound sample, HRP-conjugate and antibody, a substrate solution is added to the wells to determine bound HRP activity. The reaction is terminated with a stop solution after 30 min. The absorbance is read at 490 nm on Dynex Technologies MRX TC II Microplate Absorbance Reader. The intensity of the colour generated is inversely proportional to the concentration of steroid in the sample. A standard curve is generated from a stock calibrator provided with the kit by which the concentration of cortisol or corticosterone in the test samples can be determined. These assays will measure *de novo* (as well as residual) steroidogenesis in the skin or cell culture sample from the collected media.

2.4.1 Cortisol ELISA

Cortisol measurements were determined from cell culture media aspirated from T25 flasks used for IS, PC and emodin experiments. Media was stored at -20°C until ready for use. The manufacturer's protocol was followed as directed.

2.4.2 Serum Corticosterone ELISA

Serum corticosterone concentrations were quantified in blood collected from animals at the time of culling. After centrifugation for 20 min at 2000 g, serum was stored at -20°C until ready for use. To remove possible contaminating proteins and protein bound corticosterone, 150 µL of sample was added to 150 µL of Pre-Treatment E (provided by the kit consisting of 0.6 N trichloracetic acid) in a microfuge tube, mixed and incubated at room temperature for 15 min. After centrifugation at 12000 g for 4 min, the supernatant was used in the assay as per the manufacturer's protocol.

2.4.3 Skin Corticosterone ELISA

Skin samples from *in vivo* studies (2.2.3.1 Wound Healing, 2.2.3.2 Topical Emodin in Rodent Wound Healing and 2.2.3.3 Systemic Emodin in Rodent Wound Healing) were retrieved from storage at $-80^{\circ}C$. After removing subcutaneous adipose and muscle, a small section was cut. These sections were weighed and placed at the air: liquid interface of a 24 well plate prepared with 1 mL serum-free DMEM added per well. The plate was incubated in a humidified incubator at $37^{\circ}C$ in a 95% air, 5% CO_2 atmosphere for 24 h. The media was aspirated, centrifuged at 16000 g for 15 min and then assayed as per the manufacturer's protocol.

2.5 PCR

2.5.1 RNA Extraction

RNA was extracted from tissue homogenates using the RNeasy® Fibrous Tissue Mini Kit (Qiagen Ltd, Manchester, UK). Samples were lysed in a buffer containing guanidine thiocyanate (RLT) before dilution with RNase-free water. Proteinase K was added to assist with removal of contractile proteins, connective tissue and collagen and the samples were then heated to $55^{\circ}C$ for 10 min to optimize this reaction. After centrifugation, the debris that had pelleted was discarded. The supernatants were mixed with ethanol and centrifuged through the RNeasy spin columns contained in the kit. (RNA binds to the silica membrane therein). To eliminate contaminating DNA that may have also been present, DNase I (Qiagen) was incorporated for on-column elimination. Addition of further buffers contained within the kit (RW1 and RPE) followed by centrifugation was employed to wash away contaminants, before RNA was eluted in RNase-free water. RNA was stored at $-80^{\circ}C$ until ready for use.

2.5.2 Estimation of RNA Purity and Quantity

RNA integrity and quantity was ascertained using a Nanodrop (Thermo Scientific Nanodrop 2000c Spectrophotometer). An A260/280 ratio of >2.0 was deemed sufficient to proceed.

2.5.3 Reverse Transcription

250 ng of the extracted RNA from each sample and from Rat XpressRef Universal Total RNA (Qiagen) were reverse transcribed using the Maxima First Strand cDNA

Synthesis Kit (Fisher Scientific). 20 μL 5X Reaction Mix plus 10 μL Maxima Enzyme Mix was added to the RNA in a microfuge tube and nuclease free water used to make up a total reaction volume of 100 μL. After gentle mixing, the following conditions were run in a G-Storm^{TM} GSI thermal cycler: 10 min at 25°C, 15 min at 50°C followed by reaction termination by heating to 85°C for 5 min. Products were stored at -80°C until ready for use.

2.5.4 PCR of Complementary DNA (cDNA)

Quantitative PCR of cDNA was performed on skin samples for 11β-HSD-1 and 11β-HSD-2. Concurrently, the same skin samples were processed to assay the housekeeping gene Beta 2 Microglobulin (B2M). TaqMan$^®$ Gene Expression assays (Thermo Fisher Scientific) were utilised. Each assay contains a pair of unlabelled primers as well as a TaqMan$^®$ probe with a FAM^{TM} dye label on the 5' end and a Minor Groove Binder (MGB) and Non-Fluorescent Quencher (NFQ) on the 3' end. The first step of cycling involves a temperature rise which denatures the double stranded cDNA. At this stage, the signal from the FAM^{TM} dye at the 5' end is quenched by the NFQ on the 3' end. As the reaction temperature is then lowered, the primers and probe anneal to their target sequences. *Taq*DNA polymerase synthesizes new strands of DNA using the available primers and template. When the enzyme reaches a TaqMan$^®$ probe, its 5' nuclease activity cleaves the probe separating the FAM^{TM} dye from the NFQ. As each cycle of PCR proceeds, more dye molecules are released and unquenched. The increase in fluorescence is proportional to the amount of target synthesized and can be measured with a compatible cycler (Figure 2.2).
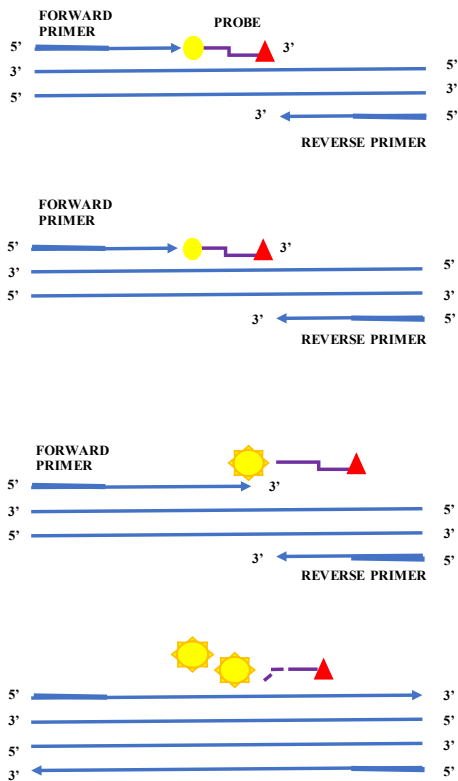
A Taqman® probe has a fluorescent reporter dye at its 5' end and a quencher at its 3' end. When the Taqman® probe is intact, the fluorescent dye emission is quenched.

If the target sequence is present, The Taqman® probe anneals downstream from one of the primer sites.

The probe is cleaved by the 5' nuclease activity of *Taq* Polymerase. Cleavage of the probe separates the reporter dye from the quencher, increasing the reporter dye signal. The probe is also removed from the target strand allowing primer extension to continue to the end of the template strand.

Additional reporter dye molecules are cleaved with each cycle, resulting in an increase in fluorescence proportional to the amount of amplicon produced.

Figure 2.2 Overview of TaqMan® based PCR reactions. Adapted from www.thermofisher.com (150).

DNA standards of 5 known concentrations were made for each gene of interest by a 1 in 10 serial dilution of the cDNA transcribed from the Rat XpressRef Universal Total RNA (2, 0.2, 0.02, 0.002 and 0.0002 ng/µL). 1 µL 20X TaqMan® Gene Expression Assay (11β-HSD-1 Rn00567167_m1 or 11β-HSD-2 Rn04341420_g1/Rn00492539_m1 or B2M Rn03928990_g1) plus 10 µL 2X Maxima probe/ROX qPCR Master Mix (Thermo Fisher Scientific) was added to 2 µL sample cDNA, DNA standard or RNase-free water for a no template control. RNase-free water was added to make the total reaction volume 20 µL. Each sample was run in duplicate in a Rotor-Disc 100 ring. The ring was then sealed with Rotor-Disc Heat-Sealing Film (Qiagen) and the Rotor-Disc Heat Sealer (Qiagen). A Corbett Rotor Gene 6000 Real Time PCR machine was used to run the samples under the following conditions: 1 cycle 10 min at 95°C, 40 cycles 15 s at 95°C and 50 cycles 60 s at 60°C.

Gene of Interest	Sequence
11β-HSD-1	TCTCCTCCATGGCTGGGAAAATGAC
11β-HSD-2	CTGCTTCAAGACAGAGGCAGTGACT or CGCGGTGCTCATCACCGGTTGTGAC
B2M	TACTTGGATAACTGTGGTAATTCTA

Table 2.1 TaqMan® Gene Expression Assay primer sequences.

2.5.5 Rat Wound Healing PCR Array

2.5.5.1 Reverse Transcription

100 ng of the extracted RNA was reverse transcribed using the RT^2 First Strand Kit (Qiagen). 2 µL of Buffer GE was added to the RNA, followed by RNase-free water to make a total reaction volume of 10 µL. The samples were incubated at 42^oC for 5 min and placed on ice for 1 min. This reaction was performed to eliminate genomic DNA contamination. 10 µL of reverse transcription mix (5X Buffer BCS 4 µL, Control P2 1 µL, RE3 RT Mix 2 µL and RNase-free water 3 µL) was added to the samples. After gentle mixing, the following conditions were run in a G-Storm™ GSI thermal cycler: 42^oC for 15 min followed by 95^oC for 5 min. 91 µL RNase-free water was added, the samples were mixed by pipetting and placed on ice.

2.5.5.2 RT^2 RNA Quality Control PCR Array

The quality of 12 RNA samples was simultaneously assessed using 6 µL of the final product of the reverse transcription reaction (2.5.5.1) in the RT^2 RNA Quality Control PCR Array (Qiagen). 3 separate PCR component mixes for each RNA sample were prepared in a microcentrifuge tube as follows:

Mix 1: 2X RT^2 SYBR Green Mastermix (Qiagen) 75 µL, cDNA 6 µL and RNase-free water 69 µL

Mix 2: 2X RT^2 SYBR Green Mastermix 13 µL, 1/100 dilution of total input RNA 1µL and RNase-free water 13 µL

Mix 3: 2X RT^2 SYBR Green Mastermix 30 µL and RNase-free water 30 µL

The 3 mixes for each RNA sample were dispensed into the Rotor-Disc 100 ring provided as follows:

Well	Mastermix	Control Type
1 - 12	1	Beta Actin: Housekeeping Gene
13 - 24	1	Hypoxanthine phosphoribosyltransferase 1: Housekeeping Gene
25 - 36	1	Reverse transcription control
37 - 48	1	Positive PCR control
49 - 60	1	Rat genomic DNA contamination control
61 - 72	2	No reverse transcription control
73 - 84	3	Positive PCR control
85 - 96	3	No template control
97 - 100	Water	Nil

Table 2.2 Rotor-Disc 100 RT2 RNA quality control PCR array layout.
Adapted from Qiagen product information (151).

The ring was then sealed with Rotor-Disc Heat-Sealing Film and the Rotor-Disc Heat Sealer. A Corbett Rotor Gene 6000 Real Time PCR machine was used to run the samples under the following conditions: 1 cycle 10 min at 95°C, 40 cycles 10 s at 95°C and 40 cycles 30 s at 60°C.

2.5.5.3 RT^2 Profiler Wound Healing Array

A mastermix for each sample was prepared in a 5 mL tube as follows: 2X RT^2 SYBR Green ROX FAST Mastermix (Qiagen) 1150 µL, cDNA from reverse transcription synthesis reaction 102 µL and RNase-free water 1048 µL. 20 µL was loaded into each

well of the array Rotor-Disc 100 rings provided. These are ready prepared with primer assays for 84 wound healing focused genes and 5 housekeeping genes. 7 wells contain a genomic DNA control, reverse transcription controls and a positive PCR control. The remaining 4 wells are empty, however mastermix is still loaded into these to ensure the ring is balanced. The arrays were then sealed with Rotor-Disc Heat-Sealing Film and the Rotor-Disc Heat Sealer. A Corbett Rotor Gene 6000 Real Time PCR machine was used to run the samples under the following conditions: 1 cycle 10 min at 95°C, 40 cycles 15 s at 95°C and 40 cycles 30 s at 60°C.

2.5.6 Data Analysis

Rotor-Gene Q Software Version 2.3 was used to analyze the PCR results (2.5.4 and 2.5.5) and determine threshold cycle (C_T) values for each well. The standard curve method for relative quantification of gene expression was utilized (152).

$$\text{Relative quantification} \quad = \quad \frac{(\text{Efficiency Gene of interest})^{\Delta CT(\text{Gene of Interest})}}{(\text{Efficiency Reference Gene})^{\Delta CT(\text{Reference Gene})}}$$

To analyse the RT^2 Profiler Wound Healing Array, the C_T values for each primer assay for each sample were compiled in one Microsoft Excel file. Samples were assigned to either control or test groups. This was uploaded to Qiagen's data analysis centre https://www.qiagen.com/gb/shop/genes-and-pathways/data-analysis-center-overview-page/?akamai-feo=off. This web based portal calculates fold change/regulation using the $\Delta\Delta C_T$ method (ΔC_T is calculated between the gene of interest and an average of the selected reference genes, followed by $\Delta\Delta C_T$ calculations (ΔC_T (Test Group) – ΔC_T (Control Group)). Fold change is then calculated using the $2^{-\Delta\Delta CT}$ formula.

Housekeeping genes manually selected were B2M, hypoxanthine phosphoribosyltransferase 1, LDH A and ribosomal protein lateral stalk subunit P1. The fold regulation cut off was set to 2 (fold regulation represents fold-change in a biologically relevant way such that values greater than one indicate an upregulation and values less than one indicate a downregulation). A *p* value cut off was set at 0.05

(calculated within the portal based on a Student's t-test of the replicate $2^{-\Delta CT}$ values for each gene in the control group and treatment groups).

2.6 Histology and Immunohistochemistry

Tissues from wound healing experiments were stored in 70% ethanol (VWR International Ltd) and processed by Professor Michael Sheaff and Ismail Bulut of Barts Health National Health Service Trust. The tissues were embedded in paraffin overnight using the Tissue-Tek VIP 6 AI Vacuum Infiltration Processor, Sakura, The Netherlands and 3 μm sections cut on a rotary microtome (Lecia RM2235, Leica Biosystems, Milton Keynes UK). Sections were then de-waxed, rehydrated and stained with Hematoxylin and Eosin (Vector Laboratories. Peterborough, UK).

Immunohistochemistry was performed using the Vectastain®Elite®ABC HRP Kit, (Peroxidase, Universal), R.T.U (Ready to Use) as well as DAB Peroxidase (HRP) Substrate Kit (with Nickel), 3,3'-diaminobenzidine and counterstained with Hematoxylin (all from Vector Laboratories). 11β-HSD-1 antibody (Aviva Systems Biology) was used in 1:100 dilution with a 1 hour incubation period. Slides were then dehydrated, cleared and mounted using the Tissue-Tek Film Automated Cover Slipper (Sakura).

A second set of prepared slides were incubated with Picro-sirius red (Sigma Aldrich) for 1 hour after staining cell nuclei with Weigert's Hematoxylin (Sigma Aldrich) for 8 minutes. After washing in acidified water and drying, slides were dehydrated, cleared and mounted as above.

Professor Sheaff used the Aperio ImageScope Pathology Slide Viewing Software (Leica Biosystems) to review and analyse the slides prepared.

2.7 Statistical Analysis

Statistical analysis was completed using GraphPad Prism 8.0 software (San Diego, California, USA). Data is presented as median with 95% Confidence Interval (CI) for non-parametric unpaired data. If comparisons were made between only 2 groups the Mann-Whitney U test was employed. If more than 2 groups were analysed

together the Kruskal Wallis test with Dunn's multiple comparison test (between predefined groups) was performed. Two-way Analysis of Variance (ANOVA) was utilized to determine whether there was an interaction between the two independent variables on the dependent variable (for example the effect of drug concentration and time on final cortisol concentration). An extension of this, when one of the variables was a repeated measure was employed for analysing scratch assay data (mixed effects model with Geisser-Greenhouse correction and Dunnett's multiple comparison test). A p value of < 0.05 was considered statistically significant.

CHAPTER 3

In vitro Models of Wound Healing in Uraemia

3.1 Introduction

Skin is a major extra-adrenal organ for steroid production (43, 67, 153, 154). Several steroidogenic enzymes and regulators have already been described within the skin including the GC regulators 11β-HSD-1 and 11β-HSD-2 (54, 60, 65-67, 73, 91). The localisation and activity of these GC regulators have also been described in aged skin (92, 93). As the uraemic state has been postulated as a state of accelerated ageing (6, 155), we studied these enzymes in uraemic skin to ascertain whether similarities exist.

To investigate the changes of expression or activity of 11β-HSD-1 and 11β-HSD-2 in skin in renal failure, 2 cell types found in the dermis and epidermis (HDFs and HEKs) were studied. Due to inherent differences in function as well as localisation, each type could behave differently in response to stimulation. In this study, both were cultured separately in monolayers to investigate the effect of two uraemic toxins, IS and PC (Sigma-Aldrich) on cell survival and growth as well as looking at changes in expression of our enzymes of interest. A surrogate measure for 11β-HSD-1 reductase activity, cortisol production was measured via ELISA (Bio-Techne).

Emodin (Sigma-Aldrich), a compound which has previously been shown to be a specific inhibitor of 11β-HSD-1 (105-109) was also studied in these cell types to ascertain whether a beneficial effect in healing could be observed.

The scratch wound assay is felt to be a simple, reproducible and cost effective assay to study wound healing *in vitro* by analysing cell migration across a wound as well as cell-cell interactions (156-158). This model has been successfully used in healing studies in various cell types for over 25 years (158, 159). Anderson *et al.* employed scratch assays in confluent monolayers of two renal tubular epithelial cell lines to study mechanisms of recovery from mechanical injury. They studied different growth platforms such as fibronectin and collagen as well as the effects addition of EGF, TGF-β1 or various interleukins to wounds would have (159). On this basis, an *in vitro* scratch assay was employed to study the effects of IS, PC and emodin on healing. Utilising the JuLI^{TM} Stage real time automated cell imager system (from Cambridge Bioscience, Cambridge UK) enabled the visualisation of cell migration across the

wounded area over a defined period. Images were acquired at the start and at regular intervals to calculate the rate of cell migration.

3.2 Results

HDFs or HEKs (Fisher Scientific) were cultured in T25 flasks until 70% confluent as described in section 2.1.2 and then serum starved overnight. To investigate the possible effect of the uraemic toxins IS and PC on 11β-HSD-1 and 11β-HSD-2 protein expression, either IS or PC were added to cultures in a range of concentrations for 1, 3, 16 or 48 h (section 2.1.3). Cells were lysed (section 2.1.6) to extract protein, which was semi-quantified and resolved on western blots (section 2.3).

To investigate the inhibitory effect of emodin on 11β-HSD-1 protein expression, emodin was added to cultures at a range of concentrations for 1, 3, 16 or 48 h (section 2.1.4) before cells were lysed to extract protein, which was semi-quantified and resolved on western blots.

3.2.1 Western Blotting
3.2.1.1 Western Blots of Protein Extracts from HDFs

Figures 3.1 and 3.2 demonstrate that HDFs do express both 11β-HSD-1 and 11β-HSD-2 proteins, however there is no discernible change in either enzyme's protein expression in response to the concentrations of IS or PC used at the time points investigated.
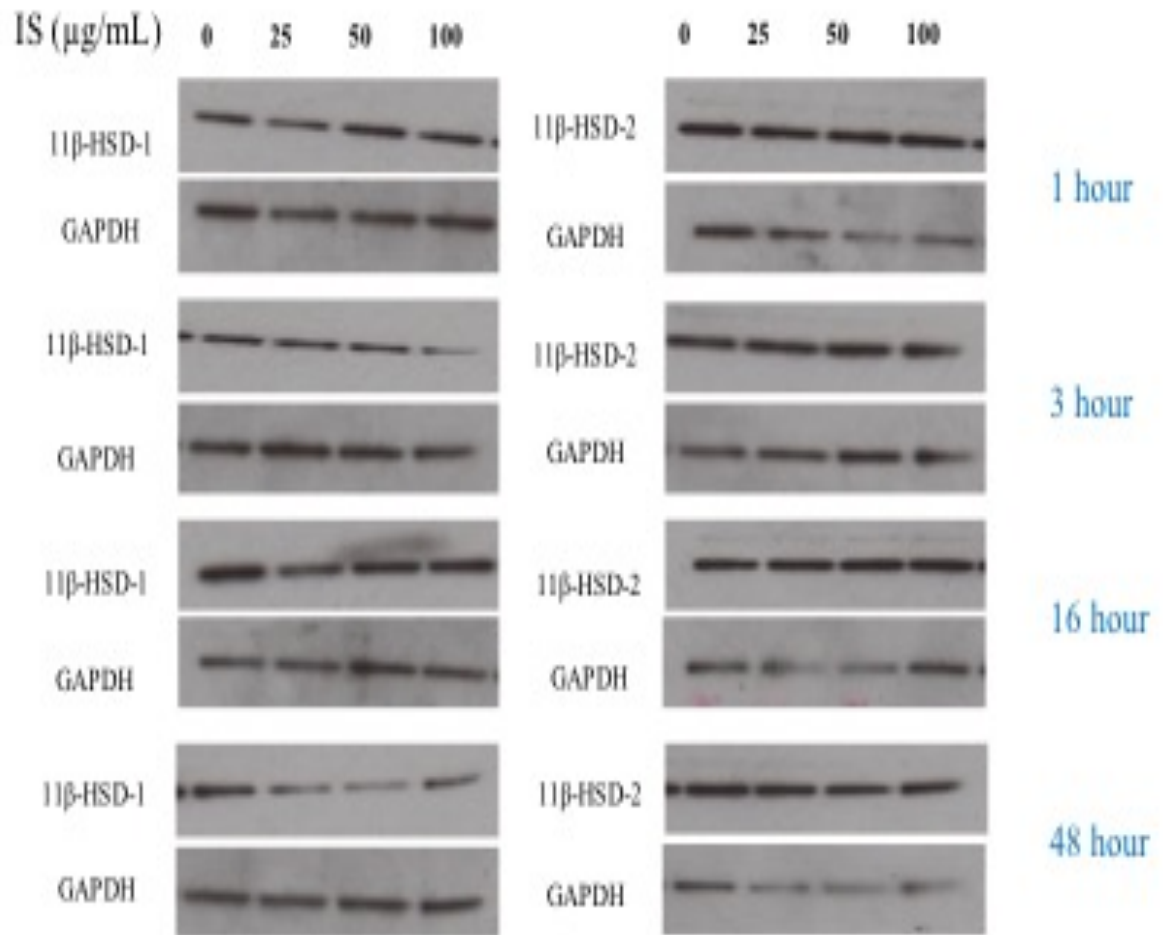
Figure 3.1 Expression of 11β-HSD-1 and 11β-HSD-2 in HDFs cultured with IS.
HDF cells were grown to 70% confluency in T25 flasks, with IS added to achieve
concentrations of 0, 25, 50 or 100 μg/mL for 1, 3, 16 or 48 h. Protein bands from cell
lysates were resolved by western blotting. Bands immunoreactive to antibodies for
11β-HSD-1 at 32 kDa, 11β-HSD-2 at 44 kDa and GAPDH at 36 kDa are shown.
Images representative of n = 3 per each western blot.
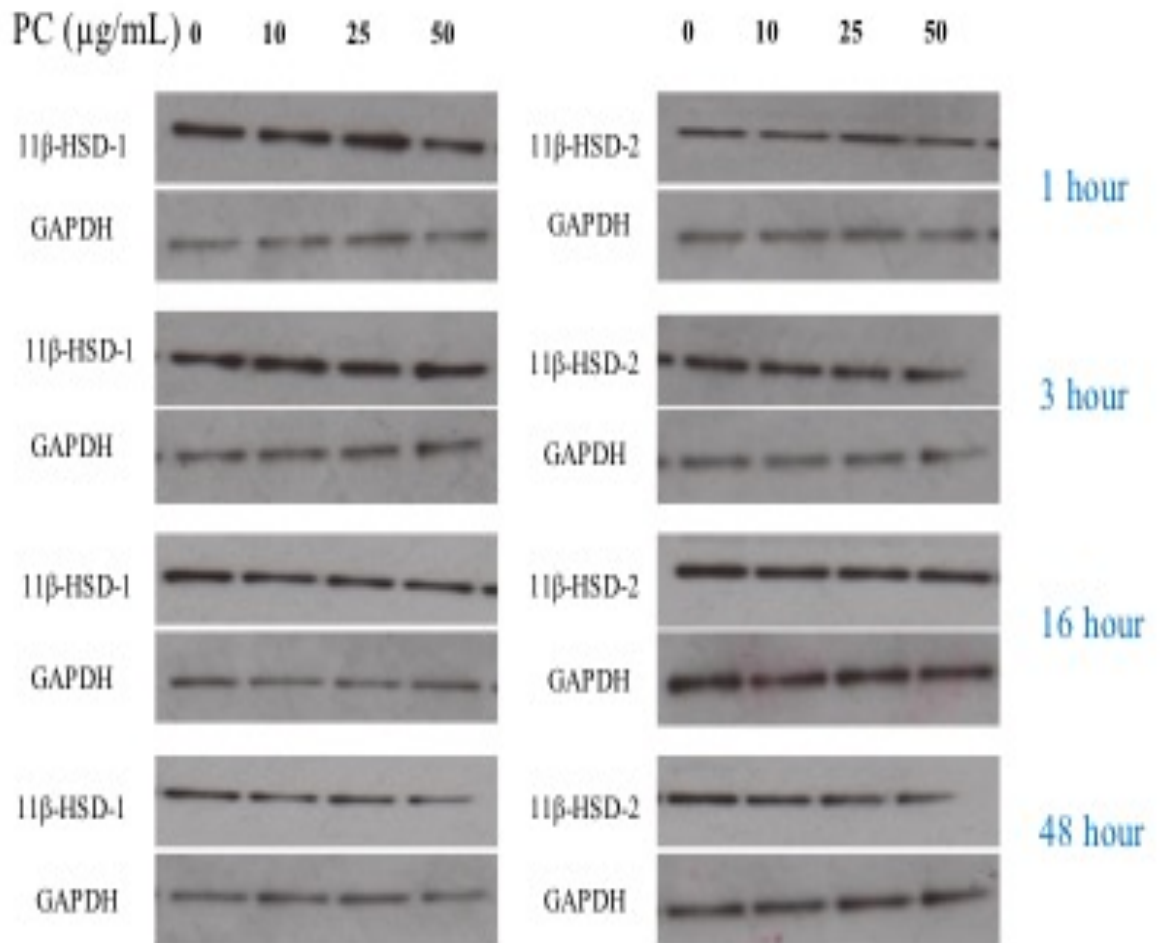
Figure 3.2 Expression of 11β-HSD-1 or 11β-HSD-2 in HDFs cultured with PC.
HDF cells were grown to 70% confluency in T25 flasks with PC added to achieve
concentrations of 0, 10, 25 or 50 μg/mL for 1, 3, 16 or 48 h. Protein bands from cell
lysates were resolved by western blotting. Bands immunoreactive to antibodies for
11β-HSD-1 at 32 kDa, 11β-HSD-2 at 44 kDa and GAPDH at 36 kDa are shown.
Images representative of n = 3 per each western blot.

Figure 3.3 demonstrates that HDF cultures demonstrate no change in either 11β-HSD-1 or 11β-HSD-2 protein expression in response to the concentrations of emodin used at the time points investigated.
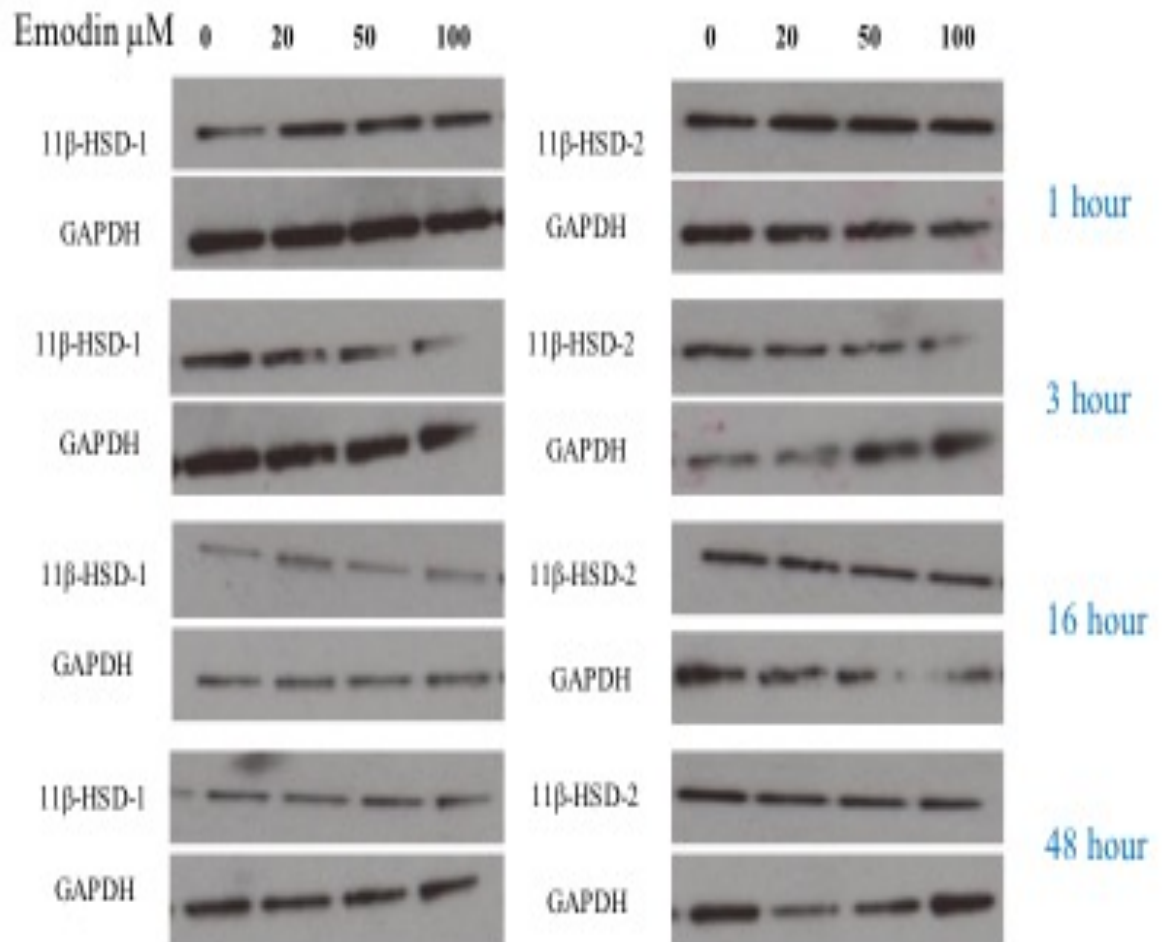
Figure 3.3 Expression of 11β-HSD-1 or 11β-HSD-2 in HDFs cultured with emodin. HDF cells were grown to 70% confluency in T25 flasks, with emodin added to achieve concentrations of 0, 20, 50 or 100 μM for 1, 3, 16 or 48 h. Protein bands from cell lysates were resolved by western blotting. Bands immunoreactive to antibodies for 11β-HSD-1 at 32 kDa, 11β-HSD-2 at 44 kDa and GAPDH at 36 kDa are shown. Images representative of n = 3 per each western blot.

3.2.1.2 Western Blots of Protein Extracts from HEKs

Figures 3.4 and 3.5 demonstrate that HEKs do express both 11β-HSD-1 and 11β-HSD-2 proteins, however there is no change in either enzyme's protein expression in response to the concentrations of IS or PC used at the time points investigated. A second band was detected (at approximately 46 kDa) only on western blots incubated with 11β-HSD-2 of IS experiments at 1 and 3 h as well as all 4 time points of PC experiments. Thurston *et al.* also demonstrated two bands on western blots differing by 2 kDa, postulating that the larger detected protein was a form of 11β-HSD-2 that had been post-translationally modified (160). This would be a feasible explanation for the two bands seen in these blots as well. Only one band was detected when membranes were re-probed for GAPDH.
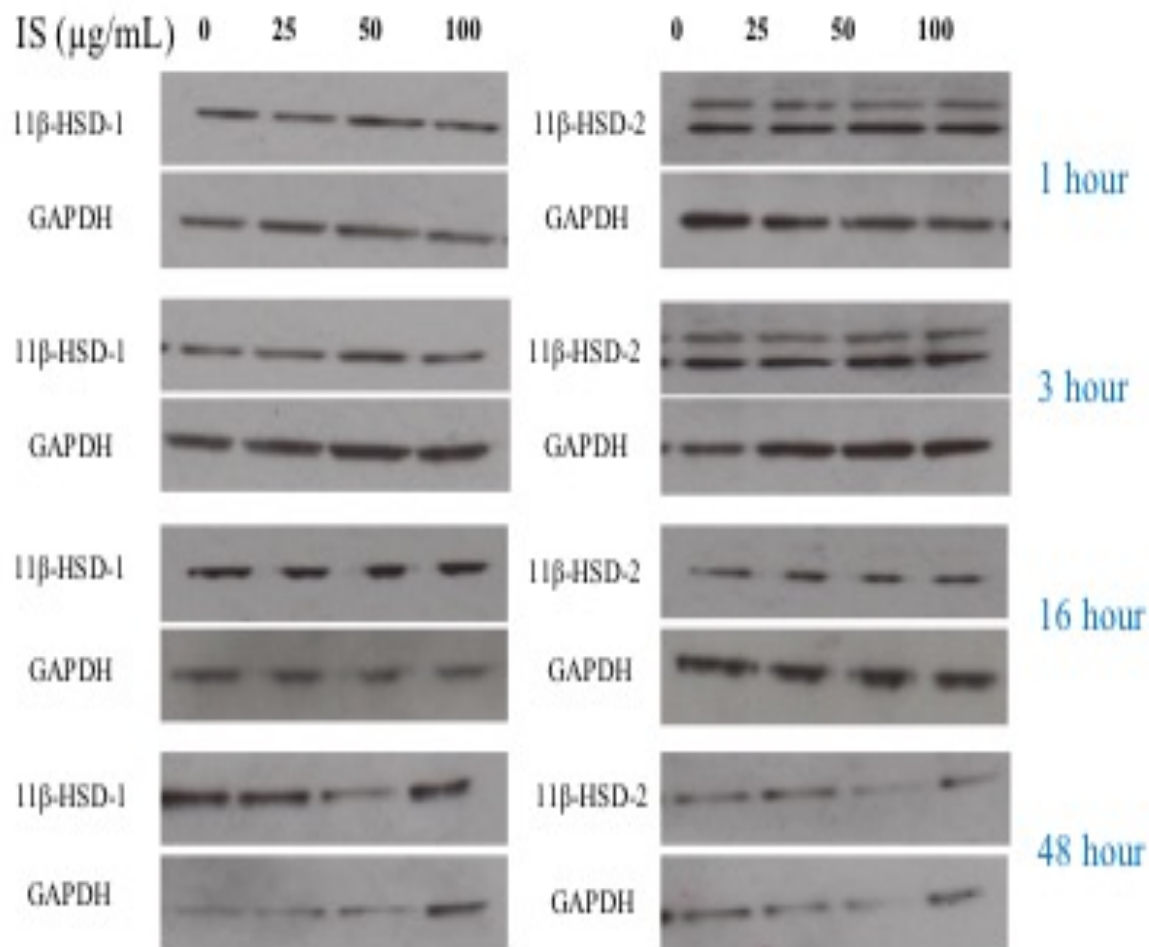
Figure 3.4 Expression of 11β-HSD-1 or 11β-HSD-2 in HEKs cultured with IS.
HEK cells were grown to 70% confluency in T25 flasks, with IS added to achieve concentrations of 0, 25, 50 or 100 μg/mL for 1, 3, 16 or 48 h. Protein bands from cell lysates were resolved by western blotting. Bands immunoreactive to antibodies for 11β-HSD-1 at 32 kDa, 11β-HSD-2 at 44 kDa and GAPDH at 36 kDa are shown. Images representative of n = 3 per each western blot.
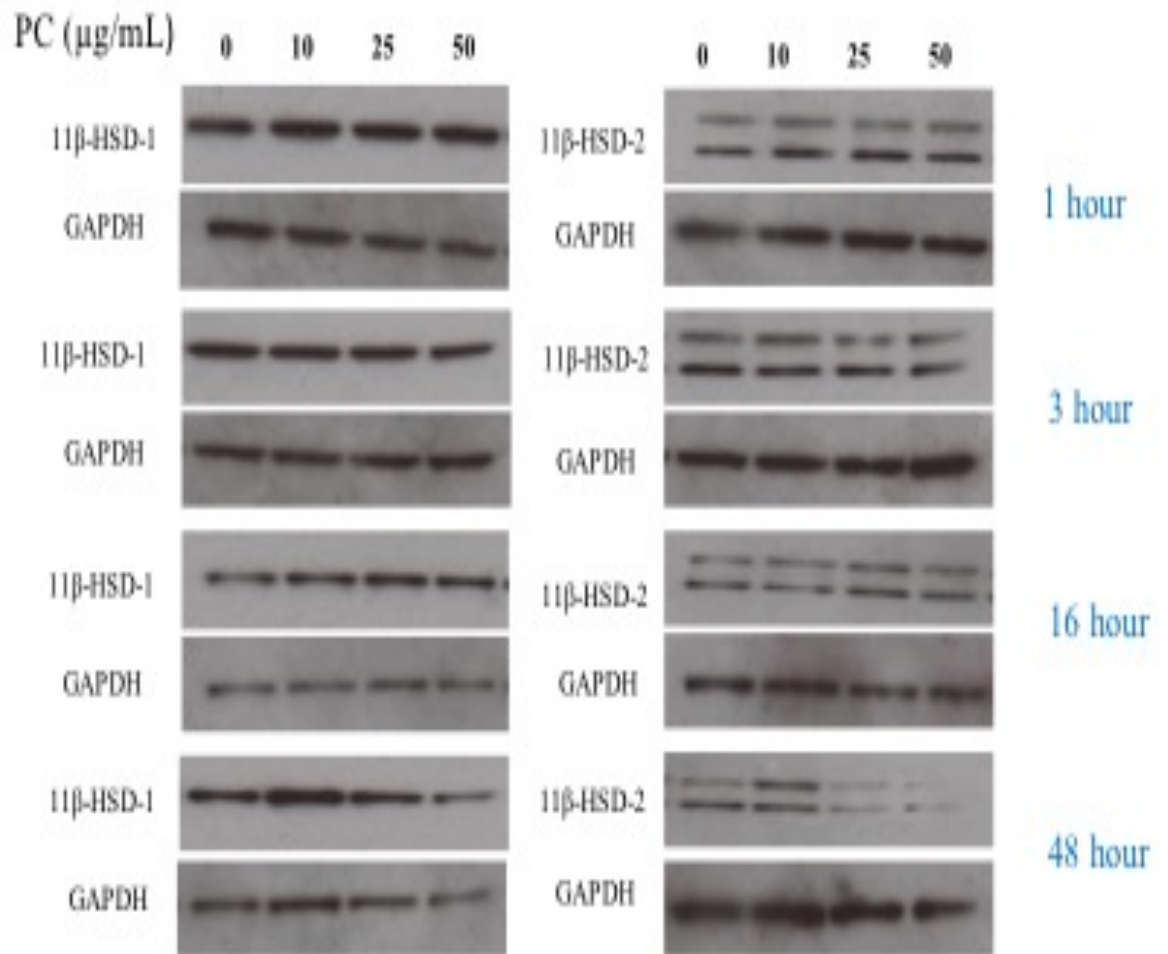
Figure 3.5 Expression of 11β-HSD-1 or 11β-HSD-2 in HEKs cultured with PC.
HEK cells were grown to 70% confluency in T25 flasks, with PC added to achieve concentrations of 0, 10, 25 or 50 μg/mL for 1, 3, 16 or 48 h. Protein bands from cell lysates were resolved by western blotting. Bands immunoreactive to antibodies for 11β-HSD-1 at 32 kDa, 11β-HSD-2 at 44 kDa and GAPDH at 36 kDa are shown. Images representative of n = 3 per each western blot.

Figure 3.6 demonstrates that HEK cultures demonstrate no change in either 11β-HSD-1 or 11β-HSD-2 protein expression in response to the concentrations of emodin used at the time points investigated. At 1 and 3 h a double band is again noted on western blots incubated with 11β-HSD-2, this time at lower molecular weight than expected, most likely due to degraded samples. The second band was not detected when re-probed for GAPDH.
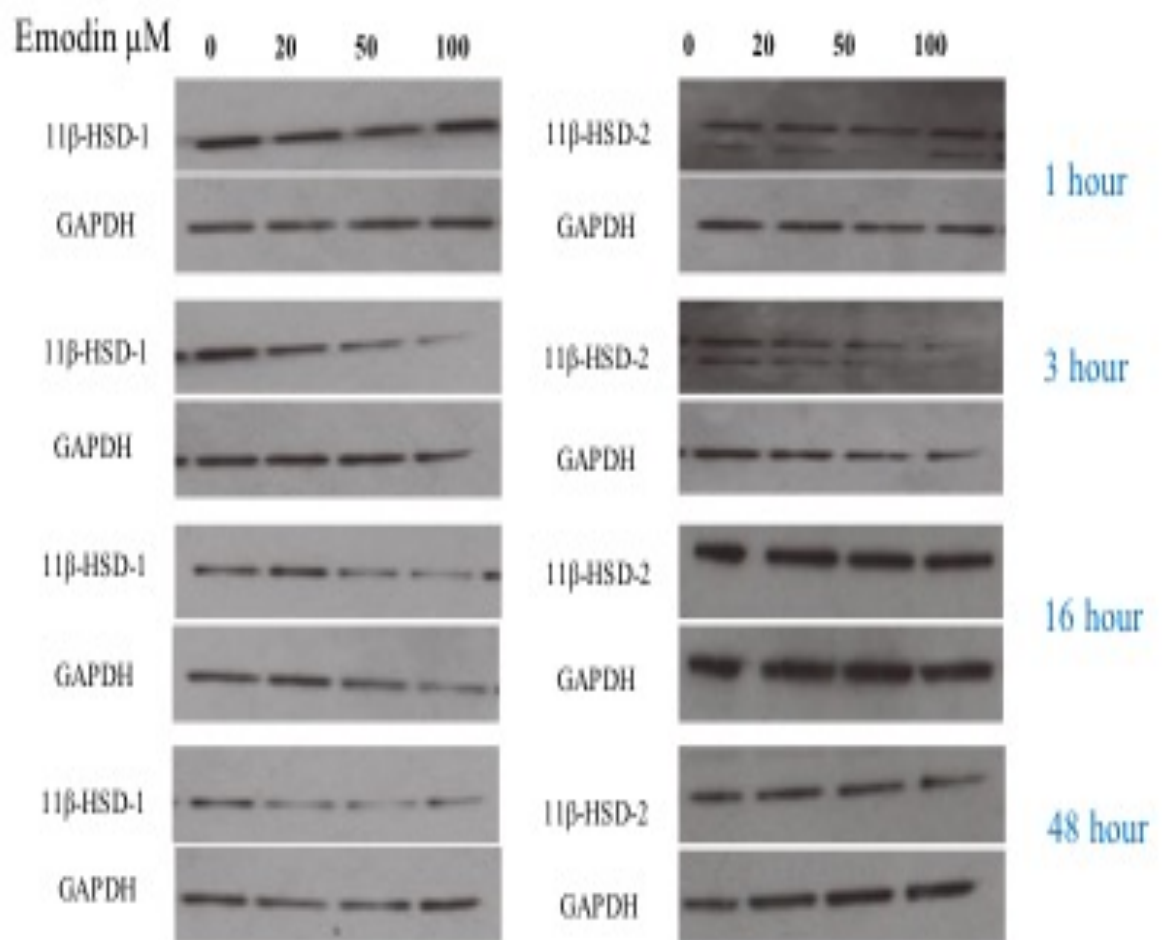
Figure 3.6 Expression of 11β-HSD-1 or 11β-HSD-2 in HEKs cultured with emodin. HEK cells were grown to 70% confluency in T25 flasks, with emodin added to achieve concentrations of 0, 20, 50 or 100 μM for 1, 3, 16 or 48 h. Protein bands from cell lysates were resolved by western blotting. Bands immunoreactive to antibodies for 11β-HSD-1 at 32 kDa, 11β-HSD-2 at 44 kDa and GAPDH at 36 kDa are shown. Images representative of n = 3 per each western blot.

3.2.2 LDH Assays

LDH assays (Roche Diagnostics Limited) were performed on media removed from T25 flasks of all HDF and HEK experiments with IS, PC and emodin at 1, 3, 16 and 48 h as described in section 2.1.5. The cell culture media used for both cell lines contained pyruvate, which is known to interfere with LDH activity (in an inhibitory fashion). Minimal activity could be detected that could not reliably be attributed to the compounds being investigated, hence this data has been excluded. In addition, the formazan product measured in this assay has an orange colour. Likewise, the formulation of emodin used in these experiments had orange colouration which interfered with the accurate detection of true LDH activity (data not shown).

3.2.3 Cortisol ELISA

Cortisol ELISA (Bio-Techne) was performed on 100 µL media removed from T25 flasks of all HDF and HEK experiments conducted with IS, PC and emodin at 1, 3, 16 and 48 h as described in section 2.4. Cortisol concentrations were corrected for total protein concentration of the cell lysates from the flask, as ascertained by a BCA assay (Fisher Scientific Ltd). Cortisol concentrations from HDF experiments were not reliably detectable within the range of this ELISA (concentrations were too low) even when media samples obtained from T25 flasks were pooled (data not shown).
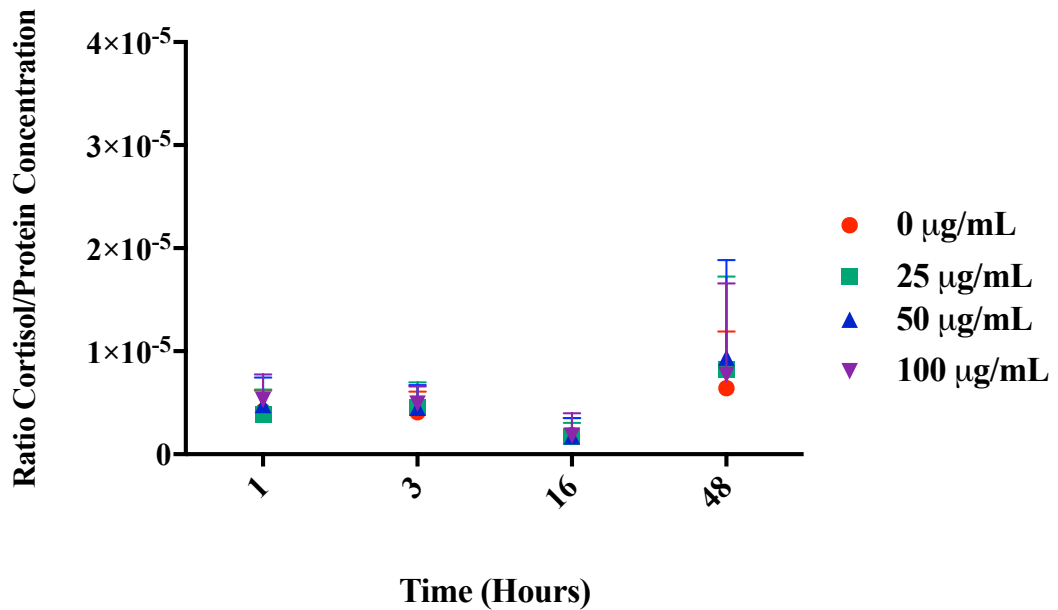
Figure 3.7 Cortisol concentration of HEKs cultured with IS. HEK cells were grown to 70% confluency in T25 flasks with IS added to achieve concentrations of 0, 25, 50 and 100 μg/mL for 1, 3, 16 or 48 h. 100 μL of the culture medium was used in a cortisol ELISA. The detected cortisol concentration was corrected to the protein concentration of the cell lysates as determined by a BCA assay, n = 3 per IS concentration at each time point. Data shown as median + 95% CI analysed by 2-way ANOVA.

A two-way ANOVA was conducted that examined the effect of IS concentration and time on cortisol concentrations. There was no statistically significant interaction between the effects of IS concentration and time $F(9,32) = 0.063$, p > 0.999.
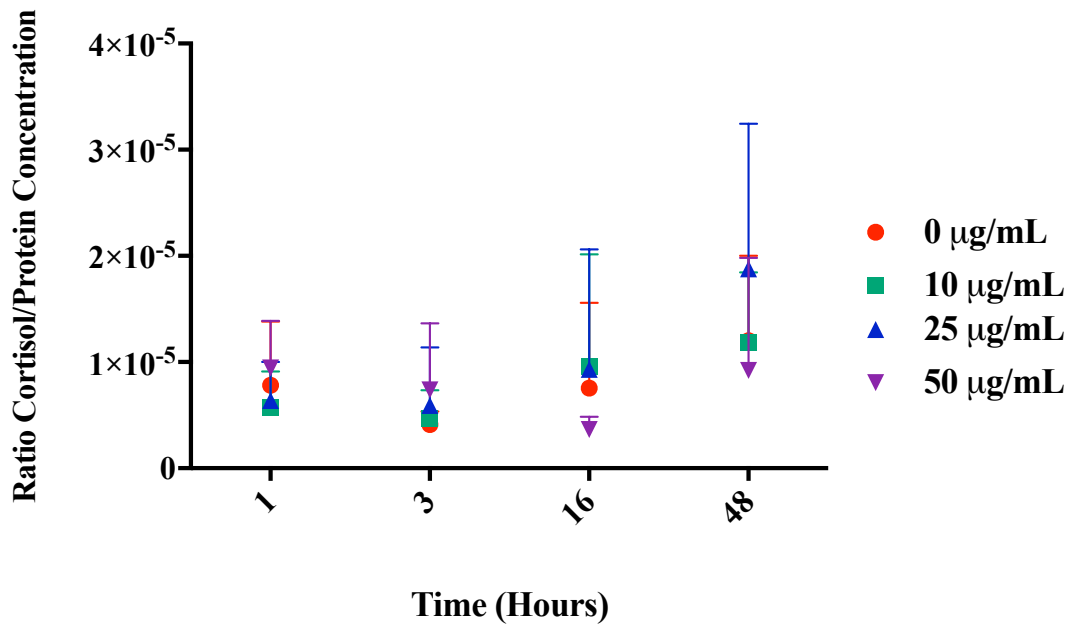
Figure 3.8 Cortisol concentration of HEKs cultured with PC. HEK cells were grown to 70% confluency in T25 flasks with PC added to achieve concentrations of 0, 10, 25 and 50 µg/mL for 1, 3, 16 or 48 h. 100 µL of the culture medium was used in a cortisol ELISA. The detected cortisol concentration was corrected to the protein concentration of the cell lysates as determined by a BCA assay, n = 3 per PC concentration at each time point. Data shown as median + 95% CI analysed by 2-way ANOVA.

A two-way ANOVA was conducted that examined the effect of PC concentration and time on cortisol concentrations produced by HEK cells. There was no statistically significant interaction between the effects of PC concentration and time $F(9,36) = 0.44$, p = 0.907.
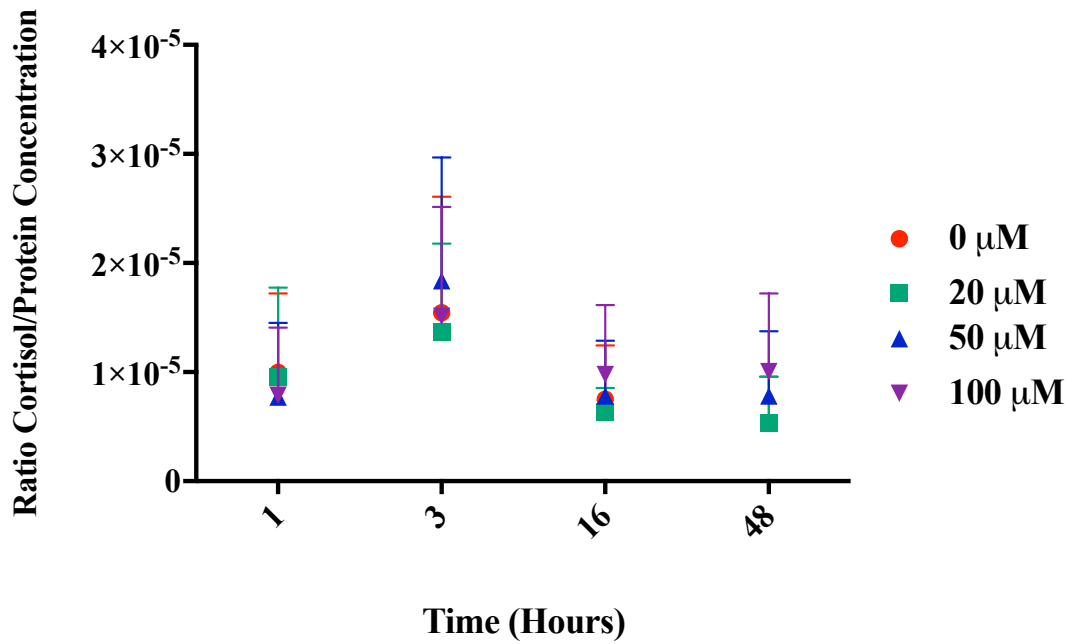
Figure 3.9 Cortisol concentration of HEKs cultured with emodin. HEK cells were grown to 70% confluency in T25 flasks with emodin added to achieve concentrations of 0, 20, 50 and 100 μM for 1, 3, 16 or 48 h. 100 μL of the culture medium was used in a cortisol ELISA. The detected cortisol concentration was corrected to the protein concentration of the cell lysates as determined by a BCA assay, n = 3 per emodin concentration at each time point. Data shown as median + 95% CI analysed by 2-way ANOVA.

A two-way ANOVA was conducted that examined the effect of emodin concentration and time on cortisol concentrations produced by HEK cells. There was no statistically significant interaction between the effects of emodin concentration and time $F(9,32)$ = 0.18, p = 0.995.

3.2.4 MTS Assays

HDFs or HEKs were cultured in 96 well plates prior to the addition of IS, PC or emodin over the range of concentrations used in experiments conducted in T25 flasks (section 2.1.3 and 2.1.4). After 48 h of incubation, a MTS assay (Promega) was completed as described in 2.1.7. These experiments were also carried out in cells that had been serum starved overnight prior to the addition of IS, PC or emodin as

components of undefined FBS could interact with the MTS assay (causing increased production of the formazan product) (161).

3.2.4.1 MTS Assays in HDFs

Upon addition of 100 μg/mL of IS, a significantly reduced absorbance at 490nm and hence reduced MTS activity was noted as compared to control cells. This difference was noted whether the HDFs were serum starved or not (Figure 3.10 A and B). In addition, when HDFs were serum starved with 50 μg/mL of IS, significantly reduced MTS activity was also observed.
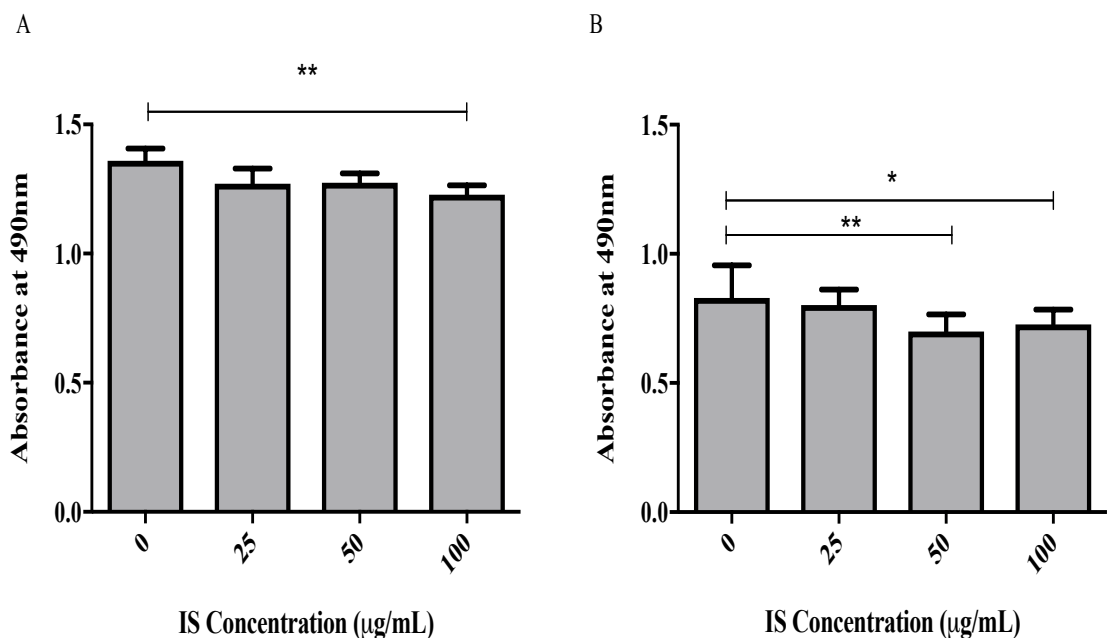
Figure 3.10 MTS activity of HDFs cultured with IS; with FBS (A) or serum starved overnight (B). HDF cells were cultured in 96 well plates with IS added to achieve concentrations of 0, 25, 50 and 100 μg/mL. After 48 hours, a MTS assay was performed. N = 20 per IS concentration, n = 4 per negative control (no cells). Data represented as median + 95% CI analysed by Kruskal-Wallis with Dunn's multiple comparisons test. * denotes significance level $p < 0.05$ and ** $p < 0.01$.

No significant differences in MTS activity were noted when PC was added to HDFs in the fed state (Figure 3.11 A). However, when HDFs were serum starved, treatment with 10, 25 or 50 µg/mL of PC seemed to significantly increase MTS activity (Figure 3.11 B). These results are likely artefactual as the PC 0 µg/mL MTS activity is lower than expected.
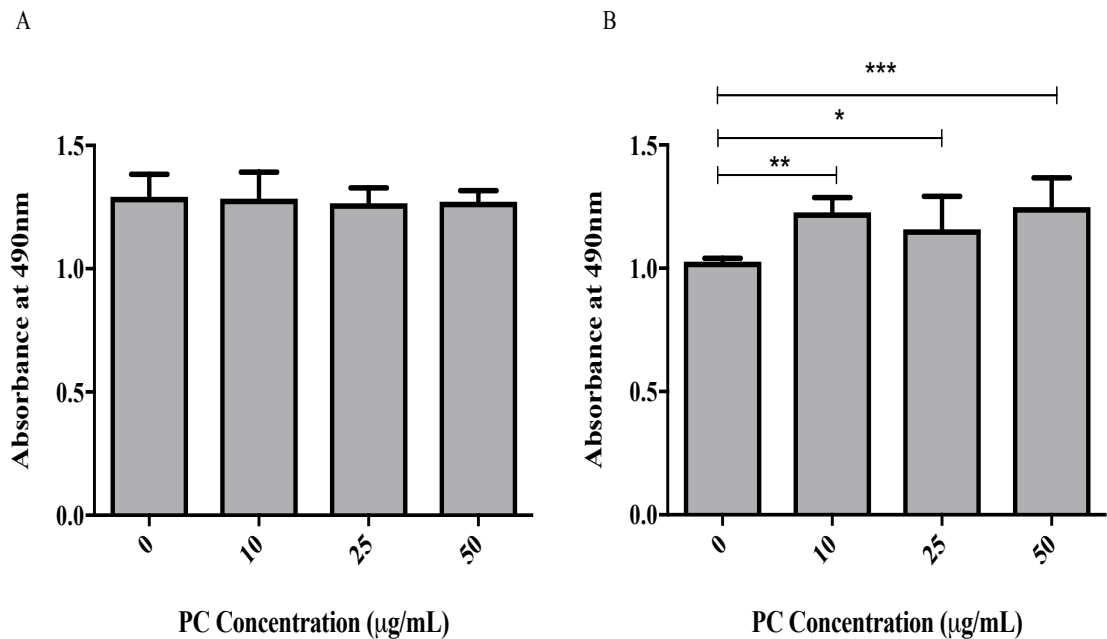
Figure 3.11 MTS activity of HDFs cultured with PC; with FBS (A) or serum starved overnight (B). HDF cells were cultured in 96 well plates with PC added to achieve concentrations of 0, 10, 25 and 50 µg/mL. After 48 hours, a MTS assay was performed. N = 20 per PC concentration, n = 4 per negative control (no cells). Data represented as median + 95% CI analysed by Kruskal-Wallis with Dunn's multiple comparisons test. * denotes significance level $p < 0.05$ ** $p < 0.01$ and *** $p < 0.001$.

When treating HDFs in the serum starved and fed state with emodin, significantly reduced MTS activity was seen at all concentrations (Figures 3.12 A and B)
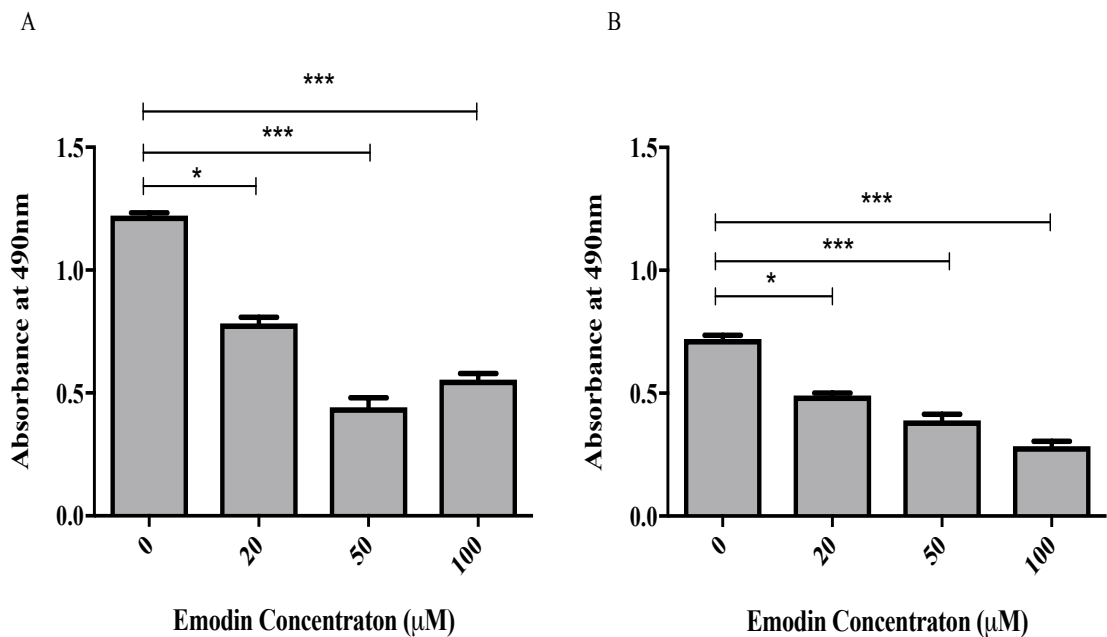
Figure 3.12 MTS activity of HDFs cultured with emodin; with FBS (A) or serum starved overnight (B). HDF cells were cultured in 96 well plates with emodin added to achieve concentrations of 0, 20, 50 and 100 μM. After 48 h, a MTS assay was performed. N = 20 per emodin concentration, n = 4 per negative control (no cells). Data represented as median + 95% CI analysed by Kruskal-Wallis with Dunn's multiple comparisons test. * denotes significance level $p < 0.05$ and *** $p < 0.001$.

3.2.4.2 MTS Assays in HEKs

Upon addition of 100 μg/mL of IS, a significantly reduced absorbance at 490nm and hence reduced MTS activity was noted as compared to control cells (Figure 3.13 A). This difference did not retain significance when the cells were serum starved (Figure 3.13 B).
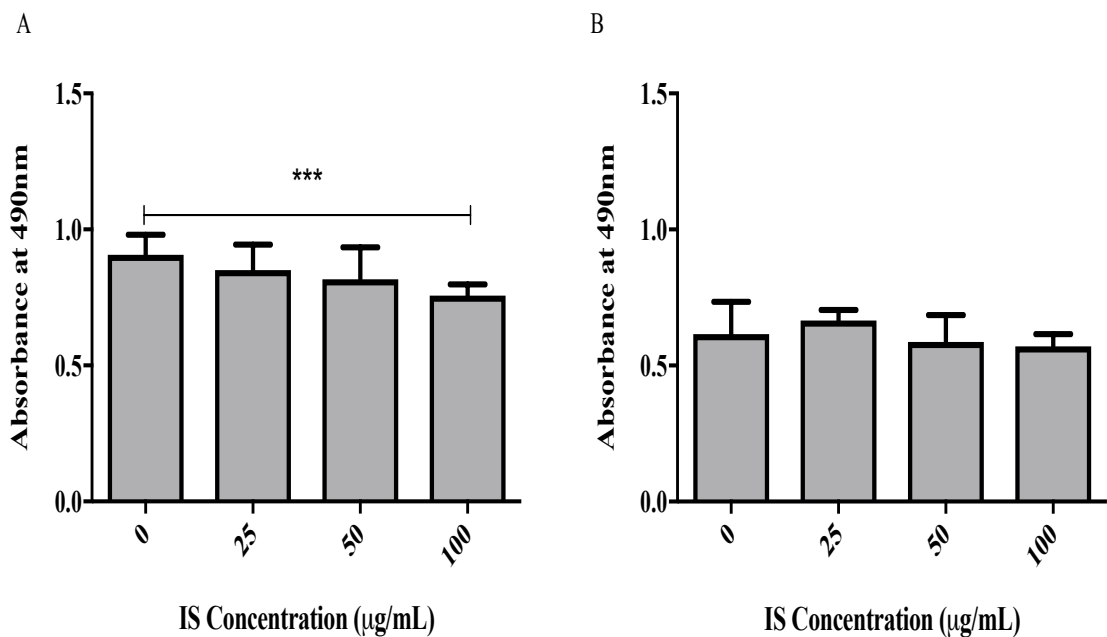
Figure 3.13 MTS activity of HEKs cultured with IS; with FBS (A) or serum starved overnight (B). HEK cells were cultured in 96 well plates with IS added to achieve concentrations of 0, 25, 50 and 100 μg/mL. After 48 hours, a MTS assay was performed. N = 20 per IS concentration, n = 4 per negative control (no cells). Data represented as median + 95% CI analysed by Kruskal-Wallis with Dunn's multiple comparisons test. *** denotes significance level $p < 0.001$.

Upon addition of 25 or 50 µg/mL PC to HEKs in the fed state, significantly greater MTS activity was detected. No significant differences in MTS activity were noted when PC was added to HEKs in the serum starved state (Figure 3.14 B).
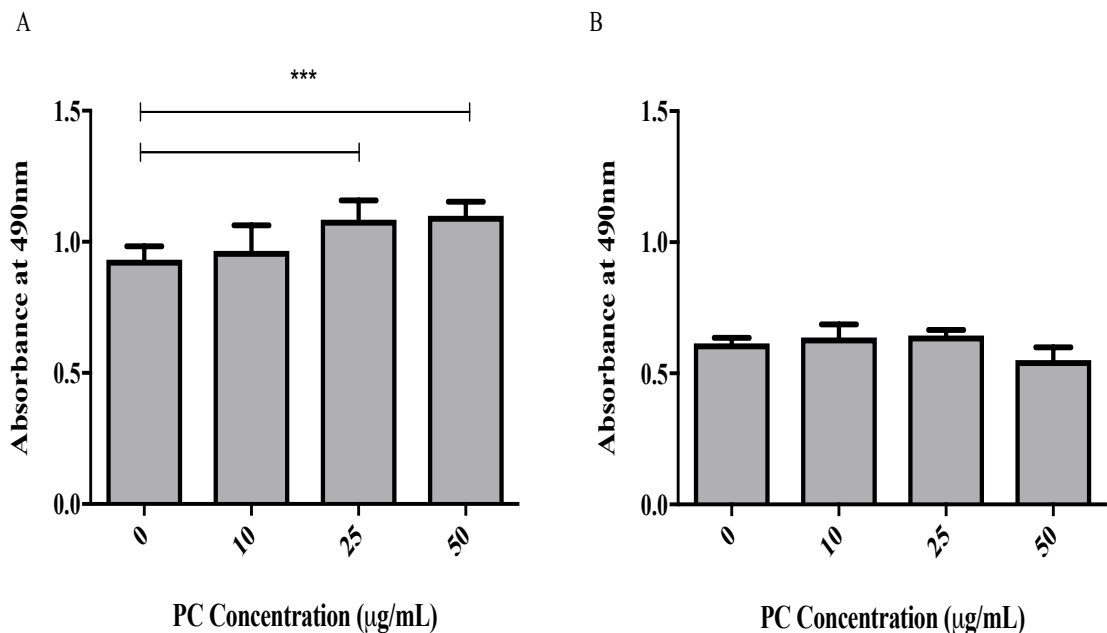
Figure 3.14 MTS activity of HEKs cultured with PC; with FBS (A) or serum starved overnight (B). HEK cells were cultured in 96 well plates with PC added to achieve concentrations of 0, 10, 25 and 50 µM. After 48 hours, a MTS assay was performed. N = 20 per PC concentration, n = 4 per negative control (no cells). Data represented as median + 95% CI analysed by Kruskal-Wallis with Dunn's multiple comparisons test. *** denotes significance level p < 0.001.

When treating HEKs in the serum starved and fed state with emodin, significantly reduced MTS activity was seen at all concentrations (Figures 3.15 A and B).
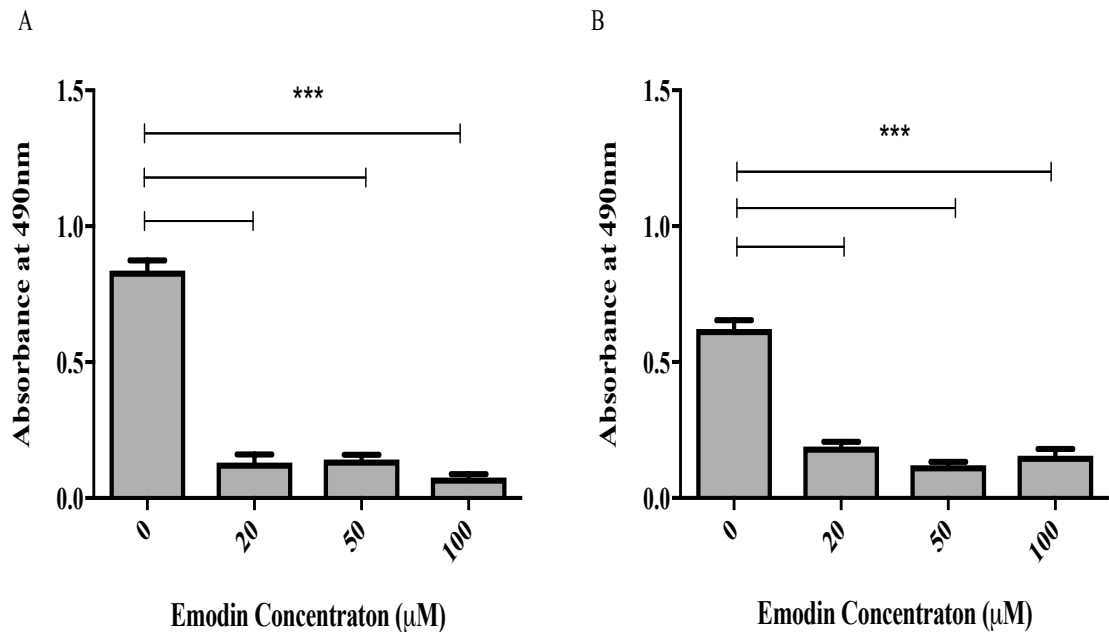
Figure 3.15 MTS activity of HEKs cultured with emodin; with FBS (A) or serum starved overnight (B). HEK cells were cultured in 96 well plates with emodin added to achieve concentrations of 0, 20, 50 and 100 μM. After 48 hours, a MTS assay was performed. N = 20 per emodin concentration, n = 4 per negative control (no cells). Data represented as median + 95% CI analysed by Kruskal-Wallis with Dunn's multiple comparisons test. *** denotes significance level $p < 0.001$.

3.2.5 Scratch Wound Healing Assays

HDFs or HEKs were cultured to 70% confluency in 12 well non-coated plates. A scratch was made across the well with a 20 μL sterile pipette tip before the old culture media was removed and replaced with solutions of IS, PC or emodin across the range of concentrations used in T25 flask experiments (section 2.1.3 and 2.1.4). Healing of the scratch wound was measured by the JuLI™ Stage cell imager over a predefined period. Experiments were also carried out in cells that had been serum starved overnight before scratching and addition of experimental solutions (see section 2.1.8).

3.2.5.1 Scratch Assays in HDFs
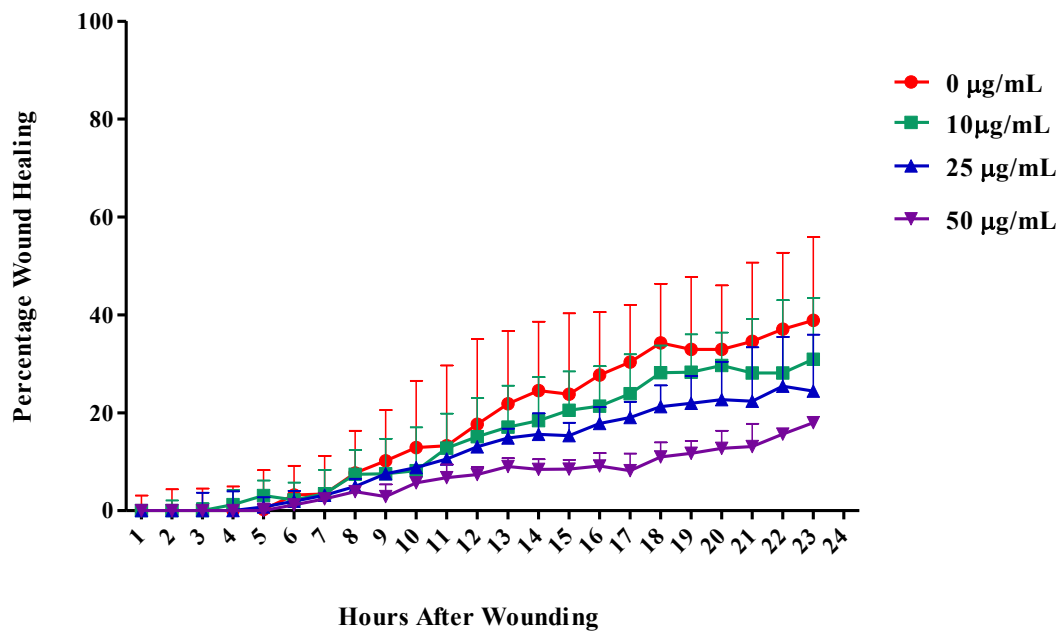
Figure 3.16 Scratch assay in HDFs cultured with PC. HDF cells were grown to 70% confluency in 12 well plates. After a scratch was made with a 20 μL pipette tip, PC was added to achieve concentrations of 0, 10, 25 and 50 μg/mL. Wound healing over 24 h was measured by the JuLI^{TM} Stage cell imager, n = 3 per PC concentration. Data represented as median + 95% CI analysed by mixed effects model with Geisser-Greenhouse correction and Dunnett's multiple comparison test.

A mixed effects model with Greenhouse-Geisser correction showed a statistically significant interaction between PC concentration and time of wound healing in HDFs, $F(66,176) = 5.597$, p <0.001. There was a significant main effect of time $F(1.618, 12.94) = 140.7$, p <0.001 suggesting that time is the influential factor (Figure 3.16).
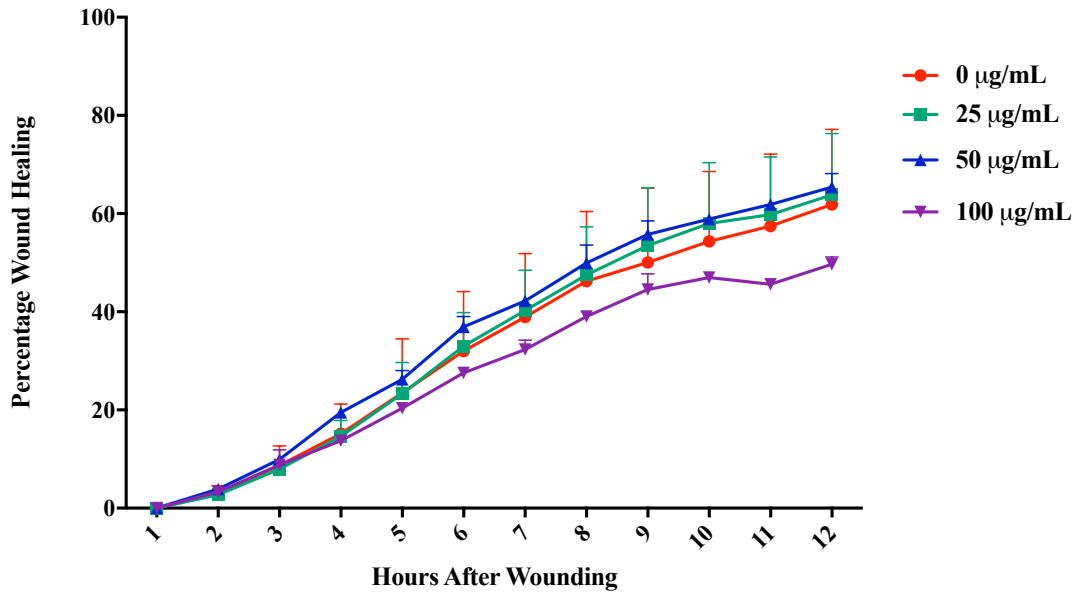
Figure 3.17 Scratch assay in serum starved HDFs cultured with IS. HDF cells were grown to 70% confluency in 12 well plates before being serum starved overnight. After a scratch was made with a 20 μL pipette tip, IS was added to culture medium containing no FCS or antibiotics to achieve concentrations of 0, 25, 50 and 100 μg/mL. Wound healing over 24 hours was measured by the JuLI™ Stage cell imager, n = 2 per IS concentration. Data represented as median + 95% CI analysed by mixed effects model with Geisser-Greenhouse correction and Dunnett's multiple comparison test.

A mixed effects model with Greenhouse-Geisser correction showed no statistically significant interaction between IS concentration and time of wound healing in serum starved HDFs, $F(33,44) = 0.488$, p = 0.983 (Figure 3.17).

3.2.5.2 Scratch Assays in HEKs
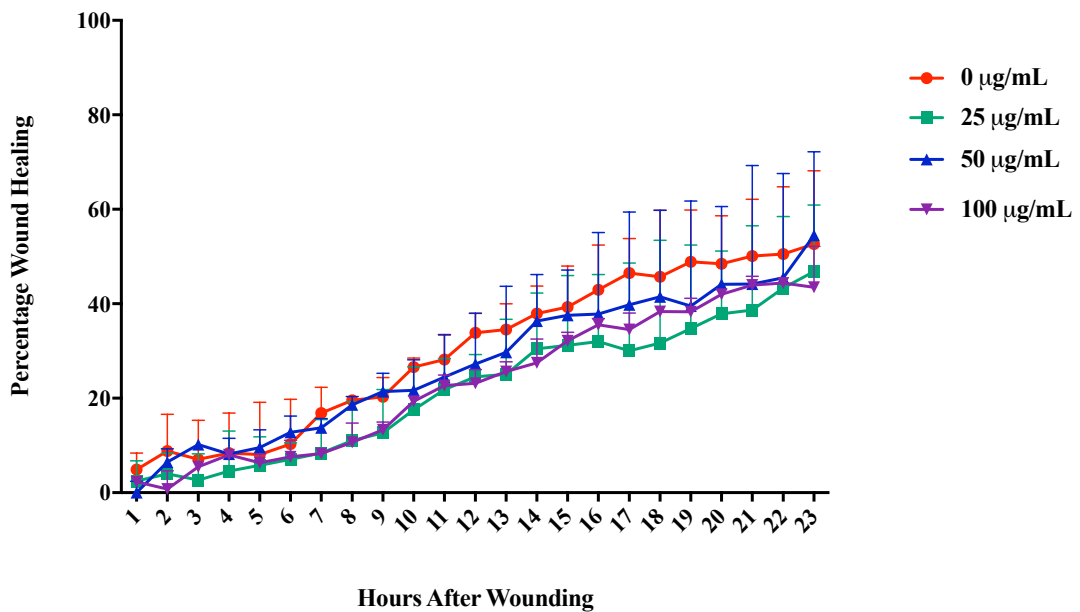
Figure 3.18 Scratch assay in HEKs cultured with IS. HEK cells were grown to 70% confluency in 12 well plates. After a scratch was made with a 20 µL pipette tip, IS was added to achieve concentrations of 0, 25, 50 and 100 µg/mL. Wound healing over 24 hours was measured by the JuLI^{TM} Stage cell imager, n = 3 per IS concentration. Data represented as median + 95% CI analysed by mixed effects model with Geisser-Greenhouse correction and Dunnett's multiple comparison test.

A mixed effects model with Greenhouse-Geisser correction showed no statistically significant interaction between IS concentration and time of wound healing in HEKs, $F(66,176) = 0.824$, p = 0.817 (Figure 3.18).
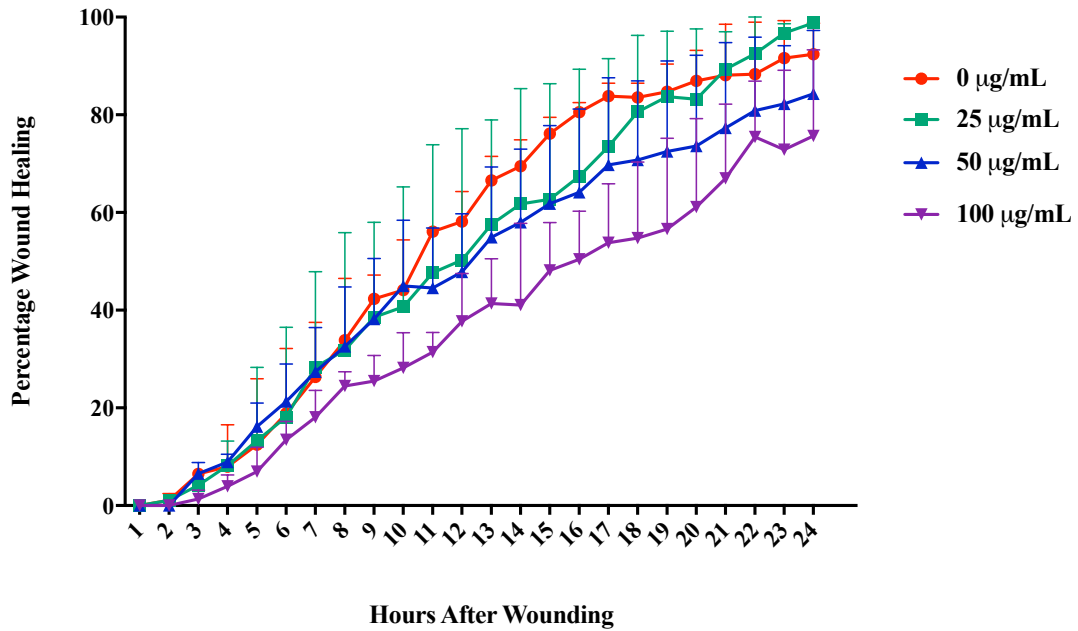
Figure 3.19 Scratch assay in serum starved HEKs cultured with IS. HEK cells were grown to 70% confluency in 12 well plates before being serum starved overnight. After a scratch was made with a 20 µL pipette tip, IS was added to culture medium containing no FCS or antibiotics to achieve concentrations of 0, 25, 50 and 100 µg/mL. Wound healing over 24 hours was measured by the JuLI[TM] Stage cell imager, n = 3 per IS concentrations except n = 2 for 50 µg/mL. Data represented as median + 95% CI analysed by mixed effects model with Geisser-Greenhouse correction and Dunnett's multiple comparison test.

A mixed effects model with Greenhouse-Geissser correction showed a statistically significant interaction between IS concentration and time on wound healing in serum starved HEKs, $F(69,161) = 1.657$, p = 0.005. There was a significant main effect of time $F(2.009, 14.07) = 3.139$, p <0.001 suggesting that time was the influential factor (Figure 3.19). Within Dunnett's multiple comparison test, at 3 h there was a significant difference in healing between control cells and those exposed to 25 µg/mL and 100µg/mL. This difference was no longer significant by the 4th hour. At 11 h, 15 h and 16 h post wounding there was a significant difference in healing between those cells exposed to 100 µg/mL of IS and control cells which had disappeared by 17 h (Figure 3.19).
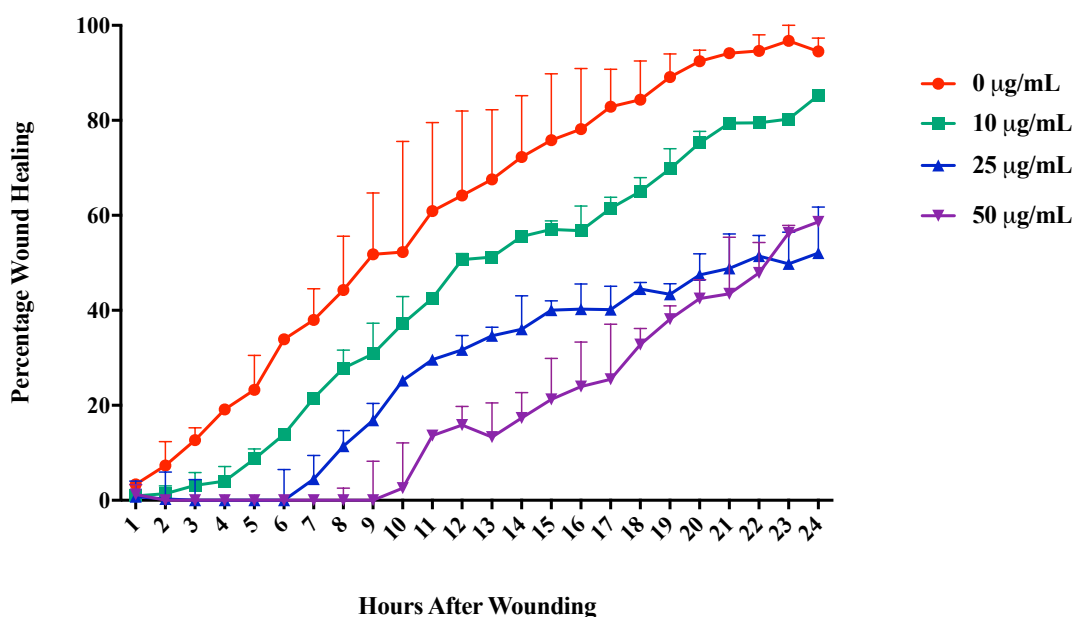
Figure 3.20 Scratch assay in HEKs cultured with PC. HEK cells were grown to 70% confluency in 12 well plates. After a scratch was made with a 20 μL pipette tip, PC was added to achieve concentrations of 0, 10, 25 and 50 μg/mL. Wound healing over 24 h was measured by the JuLI^{TM} Stage cell imager, n = 3 per PC concentration. Data represented as median + 95% CI analysed by mixed effects model with Geisser-Greenhouse correction and Dunnett's multiple comparison test.

A mixed effects model with Greenhouse-Geisser correction showed a statistically significant interaction between PC concentration and time on wound healing in HEKs, $F(69,182) = 11.570$, p <0.001. There was a significant main effect of time $F(3.307,26.17) = 411.3$, p <0.001 and a significant main effect of PC concentration $F(3,8) = 72.50$, p < 0.001 (Figure 3.20). Within Dunnett's multiple comparison test, increasing PC concentration had a significant effect on percentage wound healing in HEK cells when compared to control cells between 3 and 7 hours for all PC experimental concentrations (10, 25 and 50 μg/mL) and inexplicably at 15, 17 and 21 h. HEK cells cultured with 50 μg/mL PC demonstrated consistent significant differences in healing when compared to control cells from 3 through to 24 h (Figure 3.20). Further investigation of the effect of PC on wound healing in HEKs would be indicated.
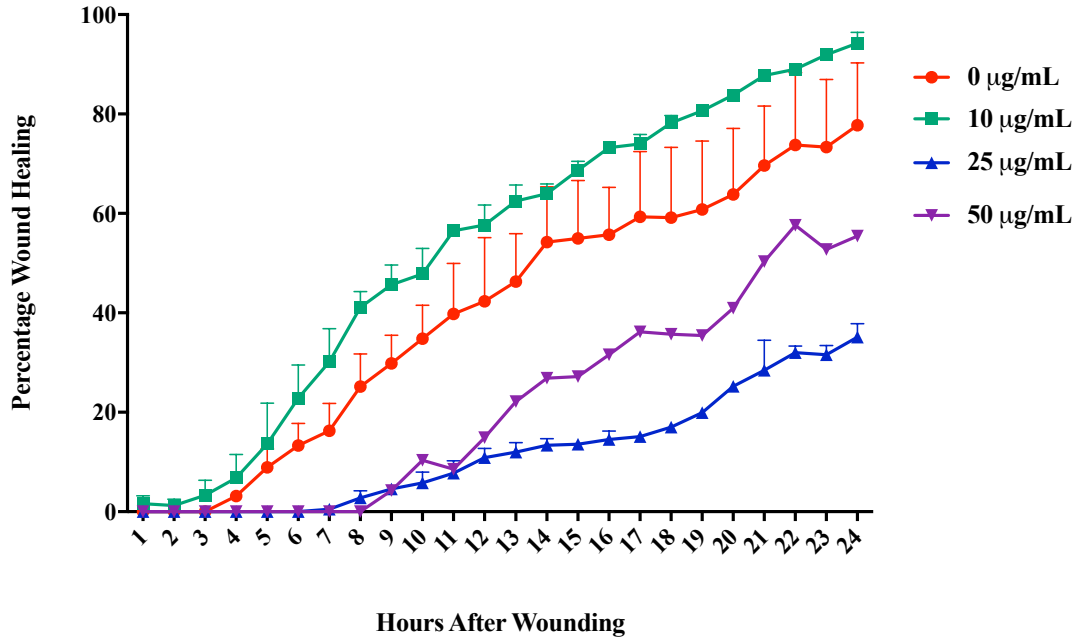
Figure 3.21 Scratch assay in serum starved HEKs cultured with PC. HEK cells were grown to 70% confluency in 12 well plates before being serum starved overnight. After a scratch was made with a 20 µL pipette tip, PC was added to culture medium containing no FCS or antibiotics to achieve concentrations of 0, 10, 25 and 50 µg/mL. Wound healing over 24 h was measured by the JuLI^{TM} Stage cell imager, n = 2 per PC concentration except n =1 for 50 µg/mL. Data represented as median + 95% CI analysed by mixed effects model with Geisser-Greenhouse correction and Dunnett's multiple comparison test.

A mixed effects model with Greenhouse-Geisser correction showed a statistically significant interaction between PC concentration and time of wound healing in serum starved HEKs, $F(69,69) = 7.699$, $p < 0.001$. There was a significant main effect of time $F(1.552, 4.655) = 132.2$, $p < 0.001$ and a significant main effect of PC concentration $F(3,3) = 12.24$, $p = 0.034$ (Figure 3.21). Further studies are warranted given the small numbers investigated.
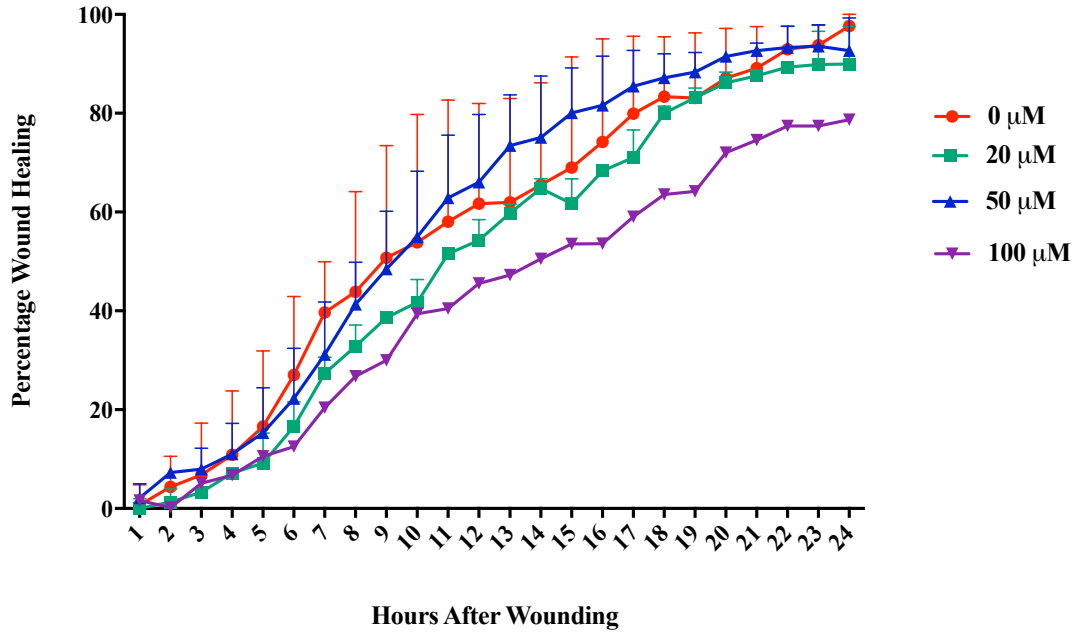
Figure 3.22 Scratch assay in HEKs cultured with emodin. HEK cells were grown to 70% confluency in 12 well plates. After a scratch was made with a 20 μL pipette tip, emodin was added to achieve concentrations of 0, 20, 50 and 100 μM. Wound healing over 24 h was measured by the JuLI^{TM} Stage cell imager, n = 3 per emodin concentration except n = 1 for 100 μM. Data represented as median + 95% CI analysed by mixed effects model with Geisser-Greenhouse correction and Dunnett's multiple comparison test.

A mixed effects model with Greenhouse-Geisser correction showed no statistically significant interaction between emodin concentration and time on wound healing in HEKs, $F(69,138) = 0.716$, p = 0.938 (Figure 3.22).

Figure 3.23 Scratch assay in serum starved HEKs cultured with emodin. HEK cells were grown to 70% confluency in 12 well plates before being serum starved overnight. After a scratch was made with a 20 μL pipette tip, emodin was added to culture medium containing no FCS or antibiotics to achieve concentrations of 0, 20, 50 and 100 μM. Wound healing over 24 h was measured by the JuLI^{TM} Stage cell imager, n = 3 per emodin concentration. Data represented as median + 95% CI analysed by mixed effects model with Geisser-Greenhouse correction and Dunnett's multiple comparison test.

A mixed effects model with Greenhouse-Geisser correction showed a statistically significant interaction between emodin concentration and time on wound healing in serum starved HEKs, $F(69,184) = 2.002$, p < 0.001. There was a significant main effect of time $F(1.353, 10.82) = 113.3$, p <0.001 (Figure 3.23).

Scratch assays were also performed with concentrations of IS that were much greater than used thus far (100, 200 and 400 μg/mL) to determine whether healing would be adversely affected (Figure 3.24 and 3.25).
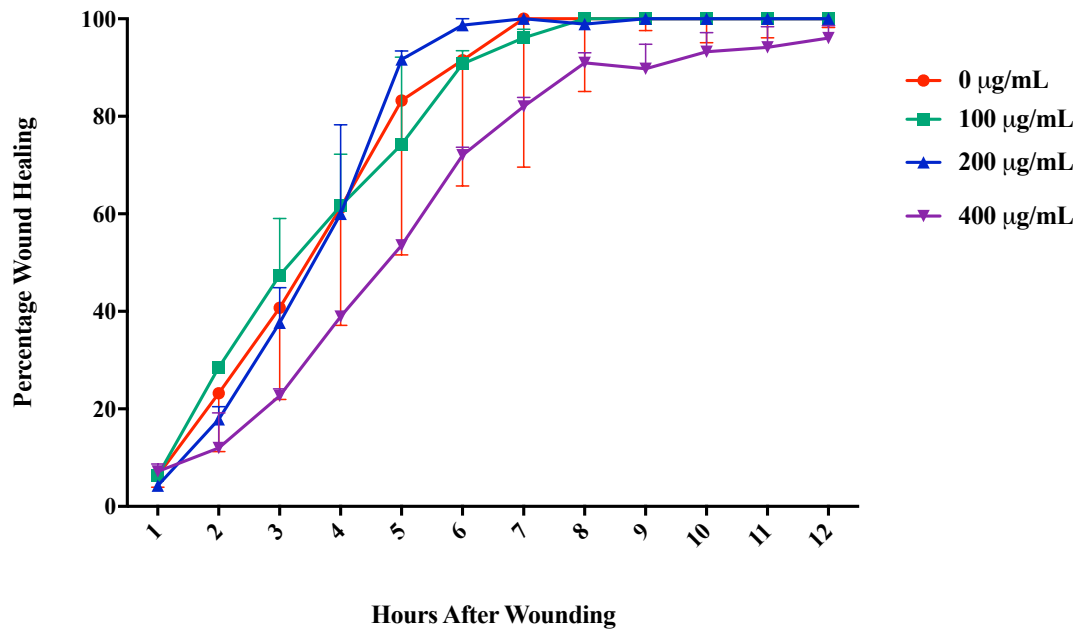
Figure 3.24 Scratch assay in HEKs cultured with high concentration IS. HEK cells were grown to 70% confluency in 12 well plates. After a scratch was made with a 20 μL pipette tip, IS was added to achieve concentrations of 0, 100, 200 and 400 μg/mL. Wound healing over 12 h was measured by the JuLI^{TM} Stage cell imager, n = 3 per IS concentration. Data represented as median + 95% CI analysed by mixed effects model with Geisser-Greenhouse correction and Dunnett's multiple comparison test.

A mixed effects model with Greenhouse-Geisser correction showed no statistically significant interaction between higher IS concentration and time on wound healing in HEKs, $F_{(33,88)} = 1.137$, p = 0.312 (Figure 3.24).
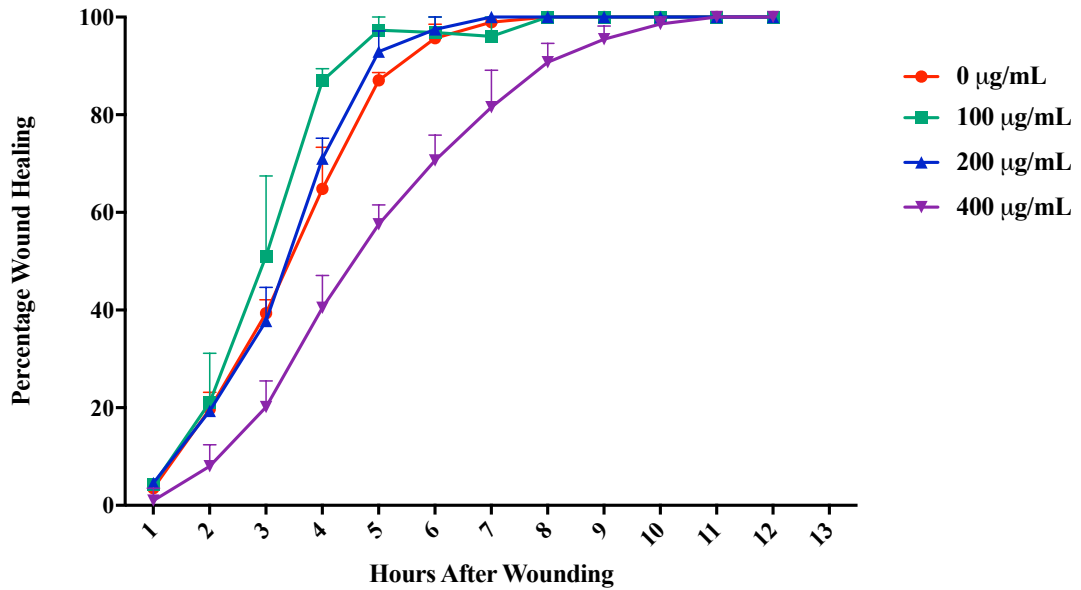
Figure 3.25 Scratch assay in serum starved HEKs cultured with high concentration IS. HEK cells were grown to 70% confluency in 12 well plates before being serum starved overnight. After a scratch was made with a 20 μL pipette tip, IS was added to culture medium containing no FCS or antibiotics to achieve concentrations of 0, 100, 200 and 400 μg/mL. Wound healing over 12 hours was measured by the JuLI^{TM} Stage cell imager, n = 3 per IS concentration. Data represented as median + 95% CI analysed by mixed effects model with Geisser-Greenhouse correction and Dunnett's multiple comparison test.

A mixed effects model with Greenhouse-Geisser correction showed a statistically significant interaction between higher IS concentration and time of wound healing in serum starved HEKs, $F(33,88) = 2.028$, p = 0.005. There was a significant main effect of time $F(1.376, 11.0) = 289.7$, p <0.001 (Figure 3.25).
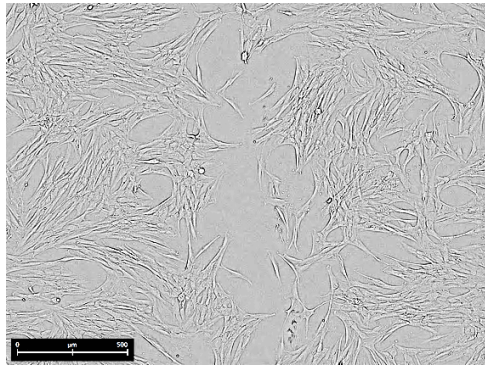
Control – 0 hours
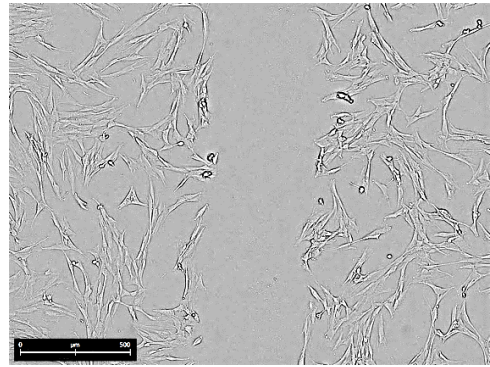
Treated – 0 hours
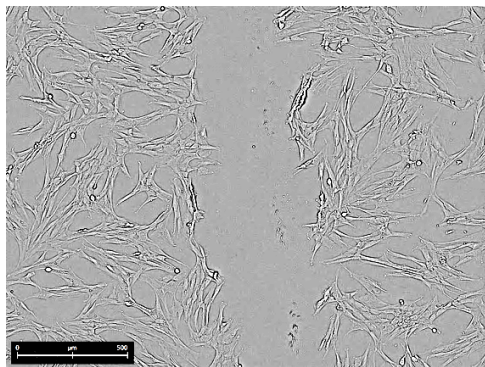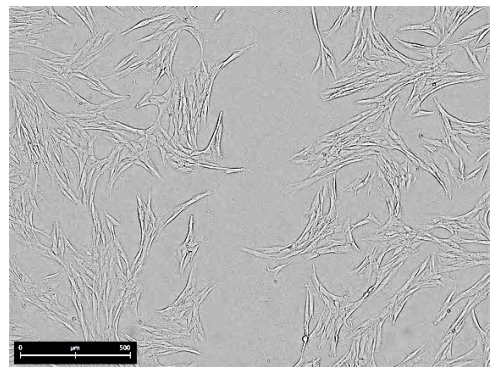
Control – 12 hours
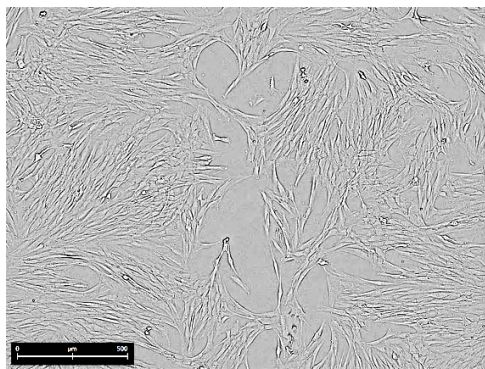
Treated – 12 hours
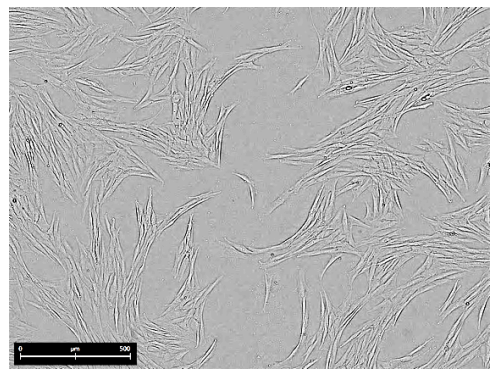
Control – 24 hours

Treated – 24 hours

Figure 3.26 In vitro wound healing in HDFs. Representative images shown for control and 1 treatment concentration at 0, 12 and 24 h after wounding.
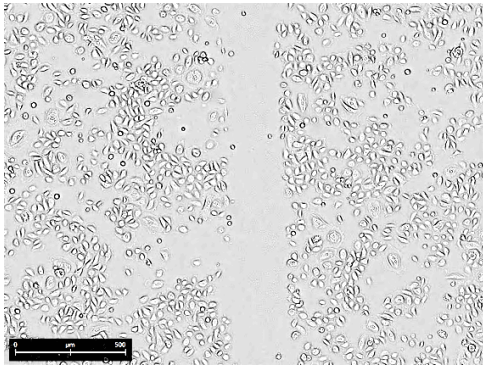
Control – 0 hours
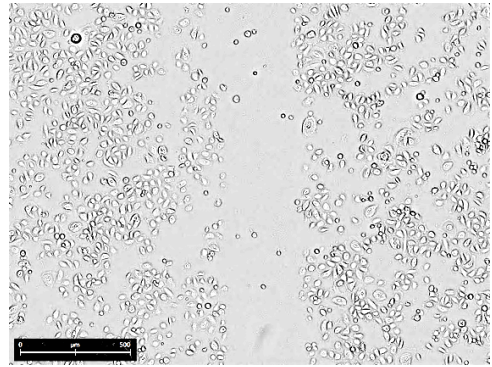
Treated – 0 hours
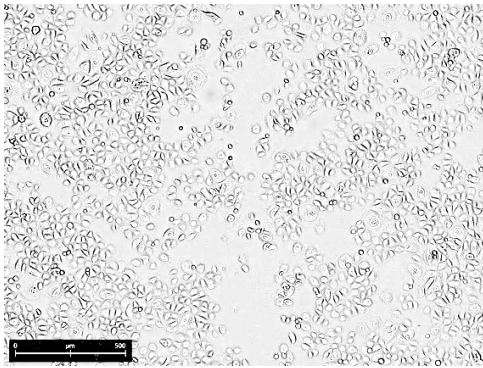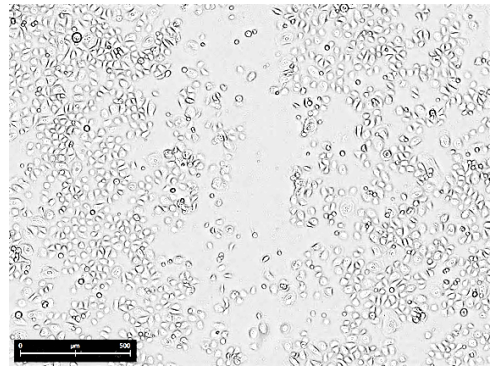
Control – 12 hours

Treated – 12 hours
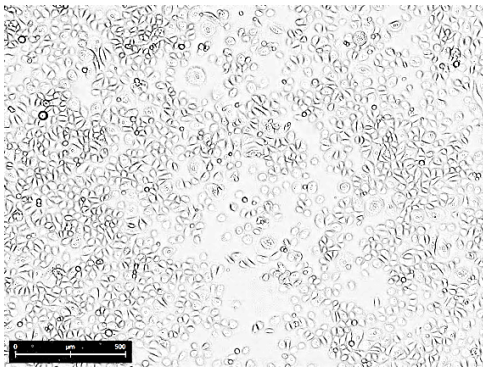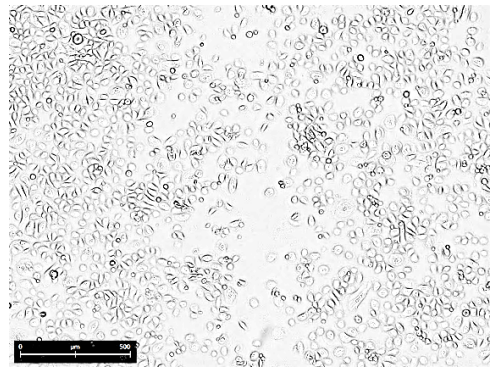
Control – 24 hours

Treated – 24 hours

Figure 3.27 In vitro wound healing in HEKs. Representative images shown for control and 1 treatment concentration at 0, 12 and 24 hours after wounding.

3.3 Discussion

Whilst culturing HDF and HEK cells for experiments, several difficulties were encountered. The cells were found to be sensitive to Trypsin-EDTA (Sigma-Aldrich) even after the briefest exposure to minimal volumes needed for successful passaging. The cells would recover and grow poorly after this contact. Initially, Trypsin Neutralizing Solution (Fisher Scientific Ltd) was used in equivalent quantities to Trypsin-EDTA after cells had detached from the flask to mitigate against this with some improvement. Ultimately, TrypLE™ Express Enzyme 1X (Fisher Scientific Ltd) was used to detach cells followed by Trypsin Neutralizing Solution in equal quantities.

Specific culture media was required for each cell type. At the outset, Human Fibroblast Basal Medium with antibiotic and Human Fibroblast Growth Supplement (all from Cellworks, supplied by Caltag Medsystems, Buckingham, UK) was used with HDFs and Keratinocyte Medium with antibiotic and Keratinocyte Growth Supplement (all from ScienCell, supplied by Caltag Medsystems, Buckingham, UK) used for HEKs. Both media were found to be photosensitive and heat labile in our hands which affected cell proliferation. After this discovery, the use of water baths was avoided and media bottles were left to equilibrate to room temperature, protected from light by a cover prior to use. After an initial set of experiments had been completed, I recognized that the composition of complete media was unknown and may contain steroid hormones that could affect the expression or activity of 11β-HSD-1 and 11β-HSD-2. The manufacturers were contacted to try to define the constituents. Cellworks reported this information was proprietary and they could not assist us whilst ScienCell confirmed the presence of hydrocortisone 0.5 µg/mL and bovine pituitary extract which was undefined. Experiments were thus repeated using openly defined media; DMEM with FBS and antibiotics (Sigma-Aldrich) and Gibco Epilife™ medium with 60 µM calcium (Fisher Scientific Ltd) and provided supplement Human Keratinocyte Growth Supplement (HKGS). Prior to performing experiments with toxins or inhibitors of interest, the cells were starved of the supplements overnight (FBS, antibiotics for HDFs and HKGS for HEKs) and experiments conducted in non-supplemented media. This was done to bring all cells into the same phase of the cell cycle and to control for the multitude of both protective

or destructive effects the various constituents of undefined FBS/supplements could have on 11β-HSD-1 and 11β-HSD-2 expression and activity. As IS and PC are both protein bound compounds, the true effect of the toxins may not have been seen in serum starved conditions with the concentrations of toxins used here. In retrospect, all experiments would have been conducted firstly with the addition of toxin in conditions with and without serum. If a difference was detected, experiments could've been repeated with increasing concentrations of serum and titrated doses of toxin.

Western blotting demonstrates that HDFs and HEKs do express both 11β-HSD-1 and 11β-HSD-2 proteins. In response to uraemic toxins in isolation, the expression of neither enzyme changes at the doses used or in the time frame studied. Although these doses are in the range found in patients with CKD (129) the published concentrations in CKD were ascertained from serum not skin samples. Thus far, it is unclear whether IS or PC have a direct pathogenic effect in skin or indeed whether their metabolism or toxicity is diminished as the skin is considered a peripheral organ. Studying cells in a monolayer may be artificial in comparison to *in vivo*, where in the epidermis cells are stacked, interacting closely with each other (14). Epidermal cells undergo a gradated differentiation response (16) which may alter the cells' responsiveness to an insult from IS or PC and indeed may alter their ability to express 11β-HSD-1 and 11β-HSD-2.

No firm conclusions can be drawn with regards to 11β-HSD-1 activity in response to IS, PC or emodin over the period studied from the associated cortisol ELISA performed. Detecting cortisol from cell culture supernatants via ELISA was challenging. Experiments with IS, PC or emodin were initially conducted in 6-well plates with 100 μL of the total 1.5 mL media used in the ELISA. However, cortisol concentrations were undetectable with this method. Aliquots of supernatants from several 6-well experiments were pooled and the ELISA repeated, to no avail. All experiments were repeated in T25 flasks to increase the ratio of cells to media. Cortisol concentrations were finally measurable (range of assay 0.030 -0.111 ng/mL) consistently for HEK cells but unfortunately not for HDFs. 11β-HSD-1 is known to possess bidirectional properties (70, 80). Although oxoreductase activity (converting cortisone to cortisol) has previously been shown to predominate in certain intact cell

systems (80) it is unclear whether reductase or dehydrogenase activity prevails in HDF and HEK cultures at baseline and whether IS, PC or emodin influence the directionality of the enzyme. To ascertain this information, cortisone and cortisol concentrations would need to be assayed simultaneously. The use of tritiated tracers has been shown to be useful in similar situations (162, 163). Unfortunately, this was not available to our laboratory during this study. In retrospect, the use of a positive control in these experiments (a promoter of cortisol synthesis such as ACTH or CYP11B1 and a plentiful supply of NADPH) may have assisted in teasing out this information.

The aim of using LDH and MTS assays was to ascertain whether HDF and HEK cells were viable over the course of experiments with IS, PC and emodin. As previously described, LDH assays were non-contributory as cell culture media contained pyruvate, which is known to interfere with LDH activity (164). Low levels of LDH activity were unreliably detected, which could not fully exclude this confounding factor.

The MTS assays performed for 48 h did not provide consistent data. HDF and HEK cells treated with 100 µg/mL IS in complete media demonstrated significantly reduced absorbance measurements at 490nm and hence MTS activity. This remained true for serum starved HDFs treated with 50 and 100 µg/mL IS but not serum starved HEKs. Astonishingly, PC at all concentrations in serum starved HDFs and at 25 and 50 µg/mL in HEKs in complete media seemed to have a positive effect on MTS activity. These results need to be treated with caution due to the limitations of the assay; interactions with any compound with inherent reductive properties could alter the amount of formazan product made (165) as can composites of the culture medium such as the pH and glucose concentration (166, 167). Additionally, the confluence of cells within the plate may alter the results obtained as contact inhibition of cells can change metabolic activity in a fashion that is non-linear to the number of cells present (thus altering absorbance in a non-predictable manner) (168). It is likely the orange colouration of emodin interfered with the colorimetric measurements obtained with HDFs and HEKs in both the LDH and MTS assays, hence cannot be relied upon to draw firm conclusions. Specific 11β-HSD-1 inhibitors that were inexpensive and

opaque were not available. Furthermore, although cells may be viable the MTS assay does not enlighten us as to whether the cell phenotype has changed in response to the toxin exposure.

Similarly, with scratch assays analysed by the JuLI™ Stage cell imager no robust conclusions with regards to the effects of IS, PC or emodin on wound healing can be drawn (n = 3) although the results of HEK cells treated with PC show promise for further investigation as do higher concentrations of IS. Despite solubilisation in DMSO prior to addition to culture medium, emodin was observed to precipitate out in 12-well plates over time causing a foggy appearance that clouded the scratches made. It is doubtful that the programme software could have accurately corrected for this effect when reporting percentage wound healing. A known inhibitor of keratinocyte migration and subsequent wound healing called zaragozic acid A, a squalene synthetase inhibitor known to increase FPP concentrations or indeed FPP itself could be employed as a positive control in future scratch assays (51).

Unfortunately, time was limited to fully utilise the inbuilt functions of the JuLI™ Stage cell imager. Rates of healing are likely to differ for cells of different passages and at non-standardized confluency as well as in different sized vessels (for example a 24-well plate versus a 6-well plate). Plates coated with growth matrices such as collagen or fibronectin would provide a more true-to-life base to study wound healing as would co-culturing skin cells and performing scratch assays thereafter, although teasing apart contributions from each contributory cell culture may be arduous.

CHAPTER 4

In vivo Wound Healing in a Rat Model of Uraemia

4.1 Introduction

As observed in Chapter 3, HDF and HEK cells do express 11β-HSD-1 and 11β-HSD-2, although their expression did not alter *in vitro* in response to simulated uraemia. The uraemic milieu is complex, although numerous compounds have been isolated and extensively studied (1, 169, 170), there are thought to be other toxins which have not yet been identified or their pathogenic effects fully described. Similarly, skin as an organ is a complex multi-layered structure incorporating several cell types which interact with each other and respond to noxious stimuli (11, 12, 15, 171). These interactions cannot be sufficiently replicated in a monolayer cell culture.

Rodents have been successfully used to study wound healing (38, 93, 94, 128, 172). Mouse skin has a paucity of eccrine sweat glands that express 11β-HSD-2 (except in paw pad skin) unlike human skin where these glands are commonly found (92). Tiganescu *et al.* did not detect 11β-HSD dehydrogenase activity in wild type mouse skin explants following incubation with corticosterone but did detect dehydrogenase activity in human skin explants (92). As the findings from these experiments would ultimately be used to benefit human patients, mice were not the animal of choice in these studies. We have previously demonstrated the successful induction of renal impairment in two rat models (148). The adenine diet model has been chosen for these *in vivo* studies. The induction of renal impairment is rapid, reliable and reproducible. This model eliminates the inter and intra-operative variability associated with the SNx procedure as well as requiring no surgical skill or training to employ. Additionally, post-operatively SNx rodents will be inflamed which will add a confounding factor to wound healing studies. In keeping with our laboratory group's published success employing the adenine diet model in rats (148) and the 3R principles, the number of animals per group was intentionally kept as low as possible to enable sufficient sample collection for all the proposed experiments. No premature mortality was observed in these experiments.

A specific inhibitor of 11β-HSD-1 (108, 109) was required which was non-toxic and cost effective in the quantities required. Carbenoxolone could not be used as it is known to inhibit both 11β-HSD-1 and 11β-HSD-2 (173, 174). Therefore, any differences seen in healing could not be clearly attributed to 11β-HSD-1. For these

reasons, emodin (Fluorochem Limited) was utilised in the *in vivo* experiments. Topical application was the preferred method of drug dosing to investigate a skin specific effect. Systemic dosing was also employed to guarantee dose delivery. Two different time points after wounding were chosen to see when potential wound healing effects would be found (day 3 and day 7). Tiganescu *et al.* demonstrated 10-fold greater 11β-HSD-1 mRNA expression at day 2 compared to unwounded control skin, which had reduced to 3-fold greater expression by day 4, returning to levels similar to those found in unwounded skin by day 8. Similar patterns were seen with 11β-HSD-1 protein expression (94).

Variables measured included serum and skin corticosterone concentrations (to determine the product of 11β-HSD-1 reductase enzyme activity and to find whether the results observed could be attributed solely to tissue specific or systemic 11β-HSD-1 activity), percentage area of wound healing and rat weight. Western blotting was performed on skin tissue homogenates to ascertain the presence or absence of 11β-HSD-1 and 11β-HSD-2. Following on from this, RNA extracted from tissue homogenates was utilised in PCR reactions to quantify the 11β-HSD-1 mRNA present. As additional molecules and pathways could be implicated in wound healing in uraemia, a wound healing array (Qiagen) was performed with the RNA samples to identify targets for further research.

4.2 Results
4.2.1 Rat Wound Healing
20 male Wistar rats were used for initial experiments. 10 rats had uraemia induced by feeding a 0.75% adenine supplemented normal diet (SDS Diets) and the remaining 10 rats were fed normal chow over 3 weeks and acted as controls. Each animal underwent wounding as described on day 0 (section 2.2.3.1). After 3 days 5 uraemic and 5 control animals were culled. After 7 days, the remaining 5 uraemic and 5 control animals were culled.

Figure 4.1 demonstrates serum urea and creatinine concentrations in all groups of animals, with significant differences observed between the uraemic and control groups at both day 3 and day 7.

A
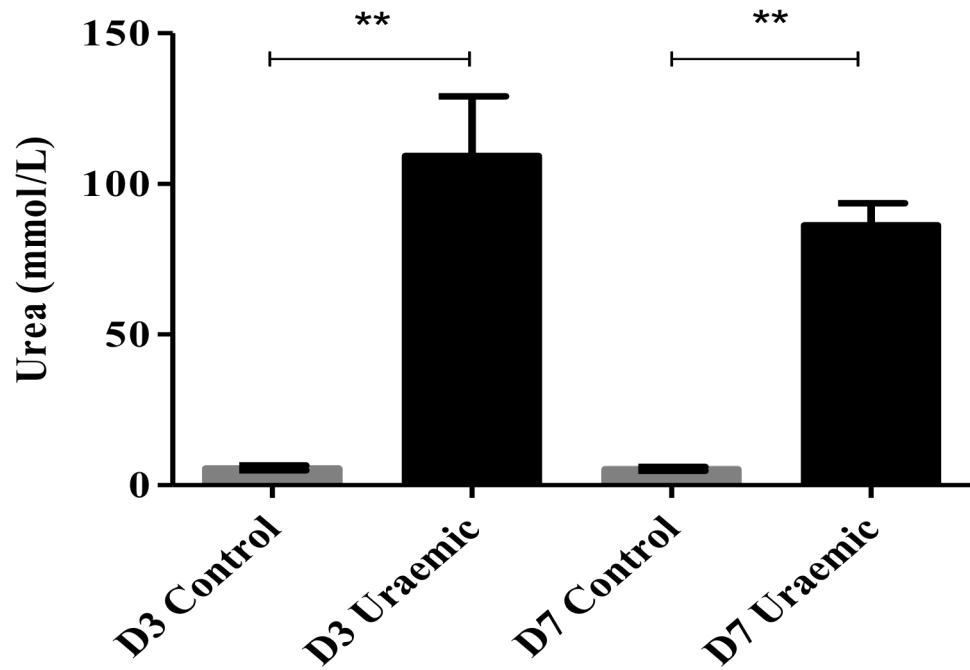
B
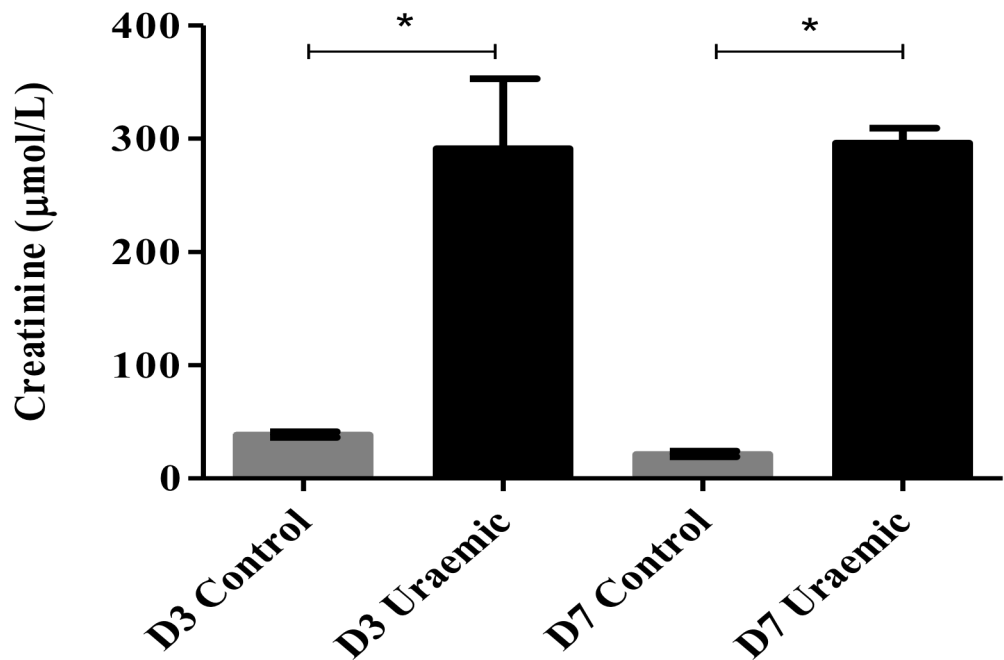
Figure 4.1 Serum urea (A) and creatinine (B). Serum obtained from rats at time of culling at day 3 or day 7 demonstrated significant differences between control and uraemic groups in urea and creatinine. n = 5 per group. Data represented as median + 95% CI analysed by Mann-Whitney U test; * denotes significance level $p < 0.05$ and ** denotes $p < 0.01$.

Figure 4.2 illustrates serum corticosterone concentrations as determined by ELISA (Bio-Techne). At day 3 and day 7 there was no significant difference between uraemic and control groups. There were no significant differences seen between the day 3 and day 7 control animals or between the day 3 and day 7 uraemic animals' serum corticosterone concentrations.
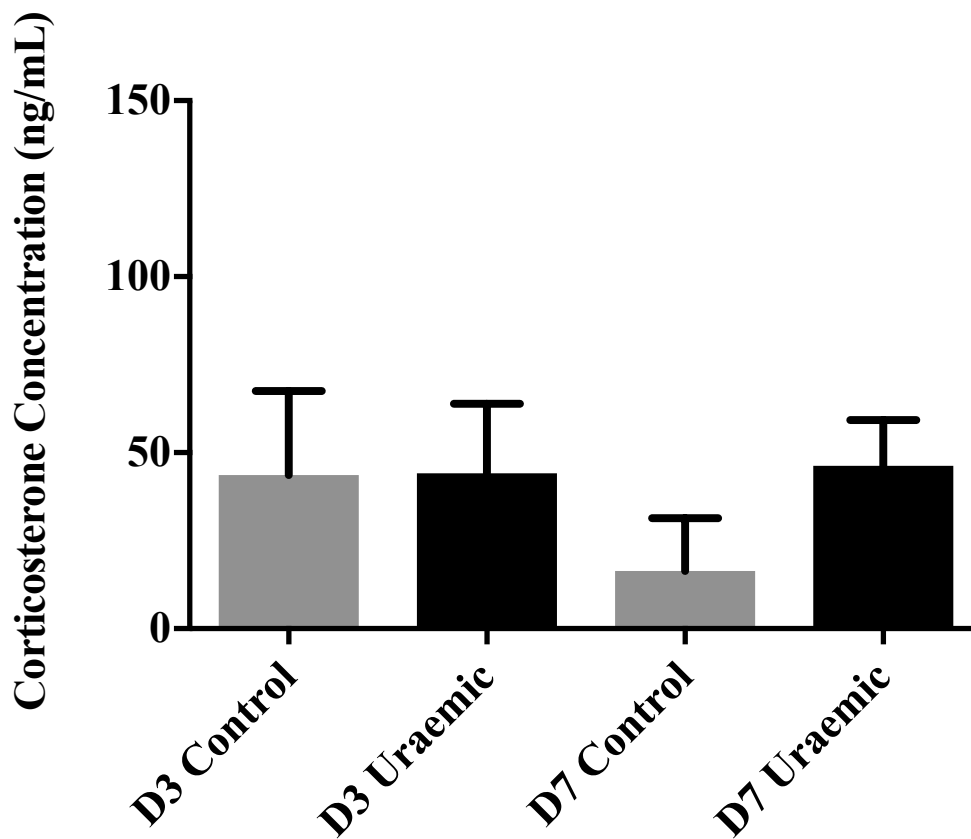
Figure 4.2 Serum corticosterone concentrations as determined by ELISA. Serum obtained from rats at time of culling demonstrated no difference between control and uraemic groups at day 3 or day 7, n = 5 per group. Data represented as median + 95% CI analysed by Kruskal-Wallis with Dunn's multiple comparisons test.

With respect to the wounds themselves, uraemic animals showed a significant reduction in area of wounds healed compared to the control animals at day 7 (Figure 4.3). This difference was not seen at day 3. In the control animals, healing was significantly greater at day 7 than day 3. Although this trend in area of wound healed being diminished was similar in uraemic animals from day 3 to day 7, this difference was not statistically significant (p = 0.065).
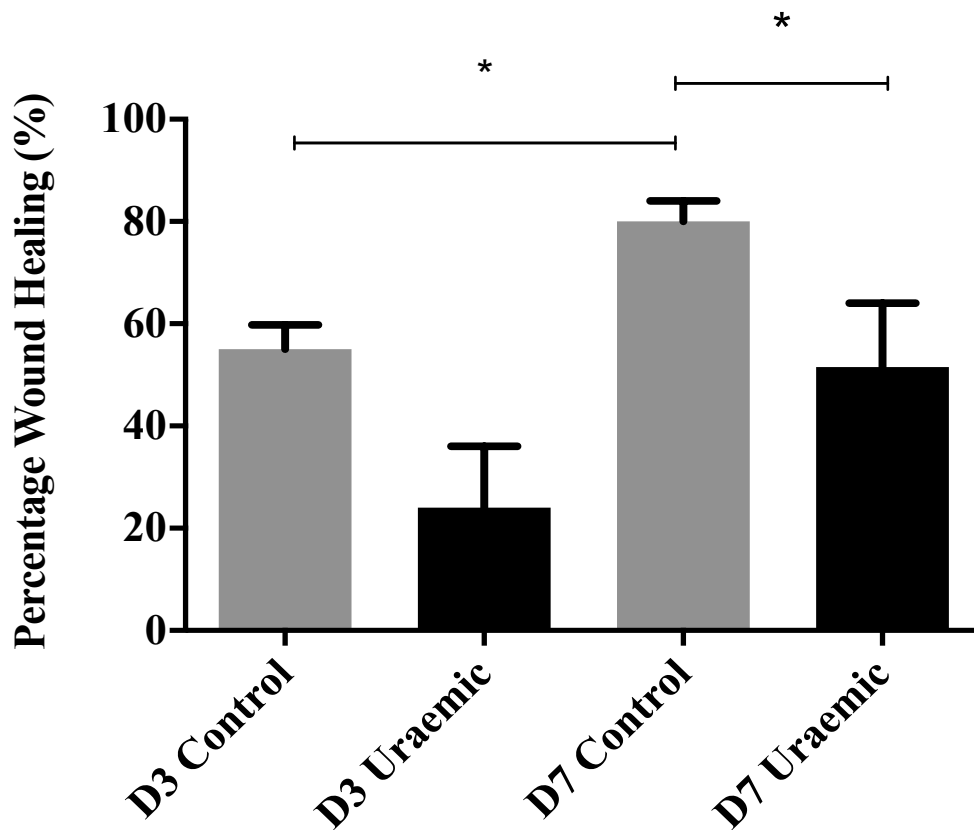
Figure 4.3 Area of wound healed. Percentage area of wound healed as compared to wound made on day 0 was significantly greater in control versus uraemic groups at day 7. n = 10 per group. Data represented as median + 95% CI analysed by Kruskal-Wallis with Dunn's multiple comparisons test. * denotes significance level p < 0.05.

From day 0 until the day of culling at day 7 the uraemic animals were noted to lose a significant amount of weight in contrast to the control animals that gained weight. There was no significant difference between the weights of the uraemic and control groups at day 3 (Figure 4.4). There were no significant differences between the day 3 and day 7 control animal weights or the day 3 and day 7 uraemic animal weights.
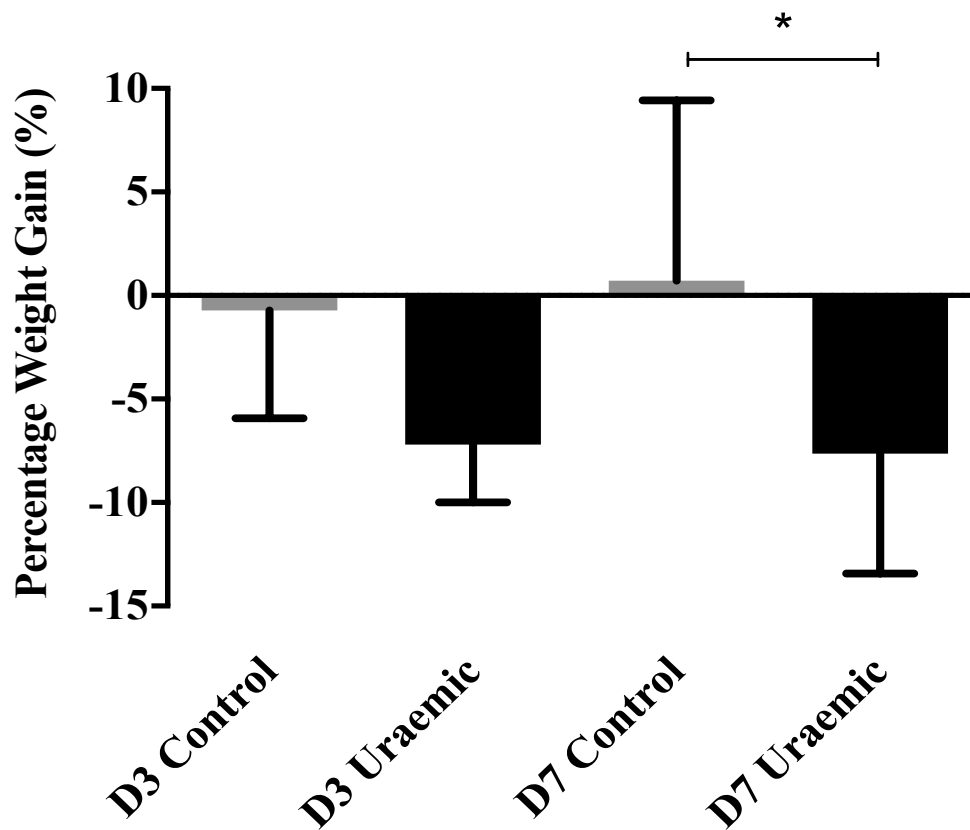
Figure 4.4 Percentage weight gain. Percentage weight gain as compared to day 0 was significant in the control compared to the uraemic group culled at day 7. n = 5 per group. Data represented as median + 95% CI analysed by Kruskal-Wallis with Dunn's multiple comparisons test. * denotes significance level $p < 0.05$.

Skin corticosterone concentrations were determined after incubating a section of skin in DMEM (Sigma-Aldrich) without FBS or antibiotics overnight. The media was retrieved and utilized in an ELISA. These results were used as a surrogate marker of 11β-HSD-1 activity. No differences were observed between control and uraemic animals' skin corticosterone concentrations at day 3. Although the uraemic group of animals appeared to have greater corticosterone concentrations than their respective controls at day 7, these results did not achieve statistical significance (Figure 4.5). There were no significant differences between the day 3 and day 7 control animals' skin corticosterone concentrations or the day 3 and day 7 uraemic animal skin corticosterone concentrations.
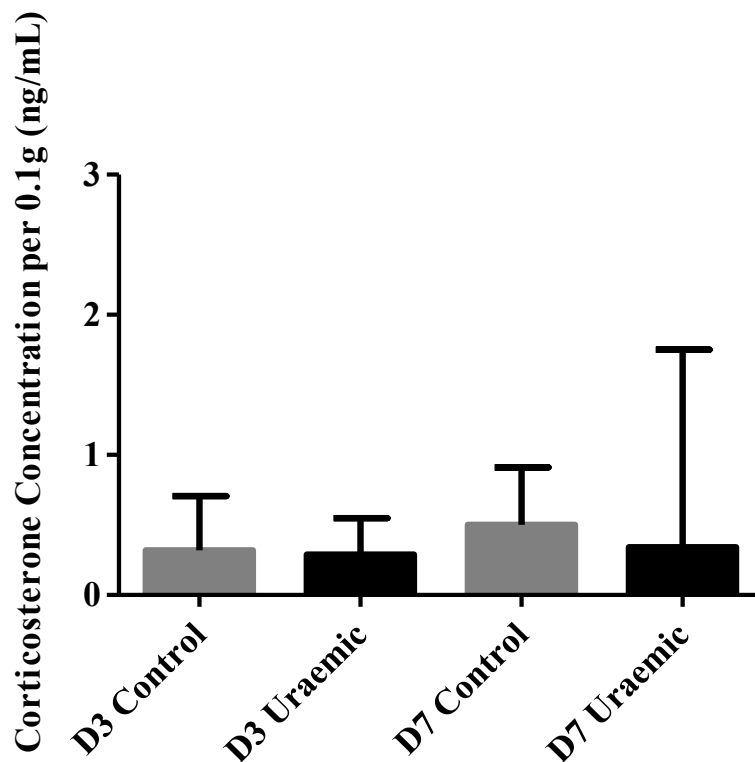
Figure 4.5 Skin corticosterone concentrations as determined by ELISA. After removal of subcutaneous fat and muscle, skin sections were incubated for 24 h in 1 mL DMEM without FBS or antibiotics. Corticosterone concentrations assayed by ELISA from the media demonstrated no significant differences between control and uraemic groups at day 3 or 7. n = 5 per group. Data represented as median + 95% CI analysed by Kruskal-Wallis with Dunn's multiple comparisons test.
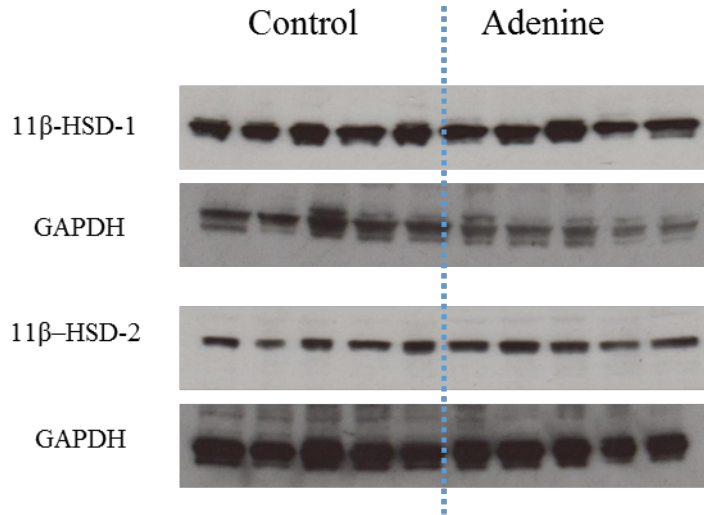
Figure 4.6 Western blots of skin homogenates at day 3 post wounding. Protein bands from tissue homogenates were resolved by western blotting. Bands immunoreactive to antibodies for 11β-HSD-1 at 32 kDa, 11β-HSD-2 at 44 kDa and GAPDH at 36 kDa are shown.
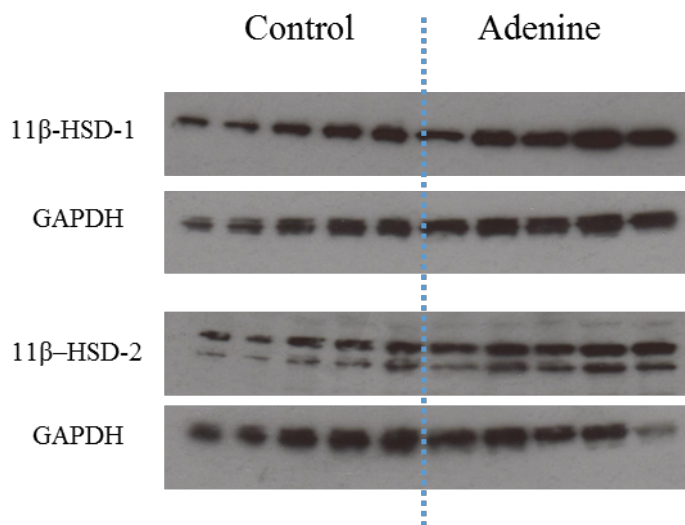
Figure 4.7 Western blots of skin homogenates at day 7 post wounding. Protein bands from tissue homogenates were resolved by western blotting. Bands immunoreactive to antibodies for 11β-HSD-1 at 32 kDa, 11β-HSD-2 at 44 kDa and GAPDH at 36 kDa are shown.

Skin samples from animals were homogenized to extract protein to be assessed by western blotting. Densitometry was performed using Image J software (version 1.4.3.67) to semi-quantify the band density of 11β-HSD-1 or 11β-HSD-2 protein relative to GAPDH. A double band was seen at a lower molecular weight than 44 kDa on the western blot for 11β-HSD-2 at day 7. The most likely reason for this is due to sample degradation as homogenates were stored at -80°C, defrosted for protein quantification and frozen again at -20°C after preparation for western blotting. The length of time samples were frozen at both temperatures did vary, as did time to final use for western blotting. At day 3 and day 7, skin homogenates of the uraemic animals demonstrated more 11β-HSD-1 and 11β-HSD-2 protein expression compared to control animals although these results were not statistically significant (Figures 4.6, 4.7 and 4.8).
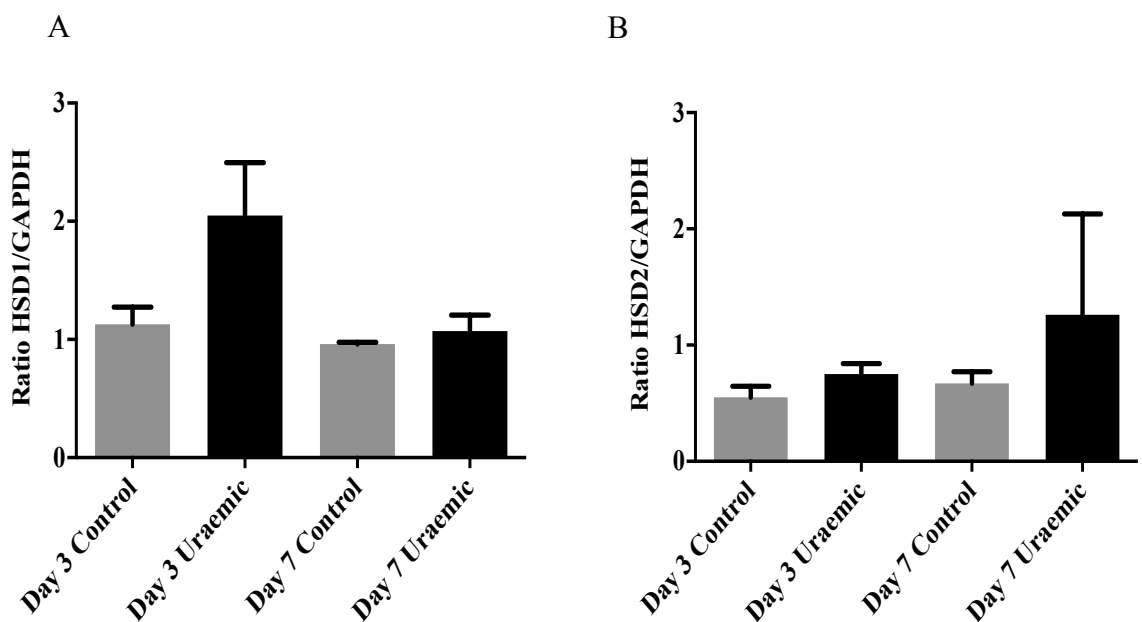
Figure 4.8 Densitometry; ratios of 11β-HSD-1 (A) and 11β-HSD-2 (B) relative to GAPDH. Performed on western blots of Figures 4.6 and 4.7. Data represented as median + 95% CI analysed by Kruskal-Wallis with Dunn's multiple comparisons test.

4.2.2 Topical Emodin in Rat Wound Healing

24 male Wistar rats were used for this experiment. 12 rats had uraemia induced by feeding a 0.75% adenine supplemented normal diet and the remaining 12 rats were fed normal chow and served as controls. Each animal underwent wounding as described on day 0 (section 2.2.3.1). Emodin was prepared in 2% Carbopol®934 (Enzo Lifesciences) to form a gel that could be easily applied. On days 0 to 4, 0.5 mL of either emodin at 500 μg/mL or 1000 μg/mL was applied to each wound of 3 uraemic and 3 control animals. Plain 2% Carbopol®934 (as the vehicle) was applied to each wound of 6 uraemic and 3 control animals. No treatment (henceforth denoted as 'none') was applied to 3 control animals (section 2.2.3.2). All animals were culled on day 7.

Figure 4.9 demonstrates serum urea and creatinine concentrations in all 7 groups of animals. Differences observed between the uraemic and control groups did not reach statistical significance, likely due to small group sizes.

A

B
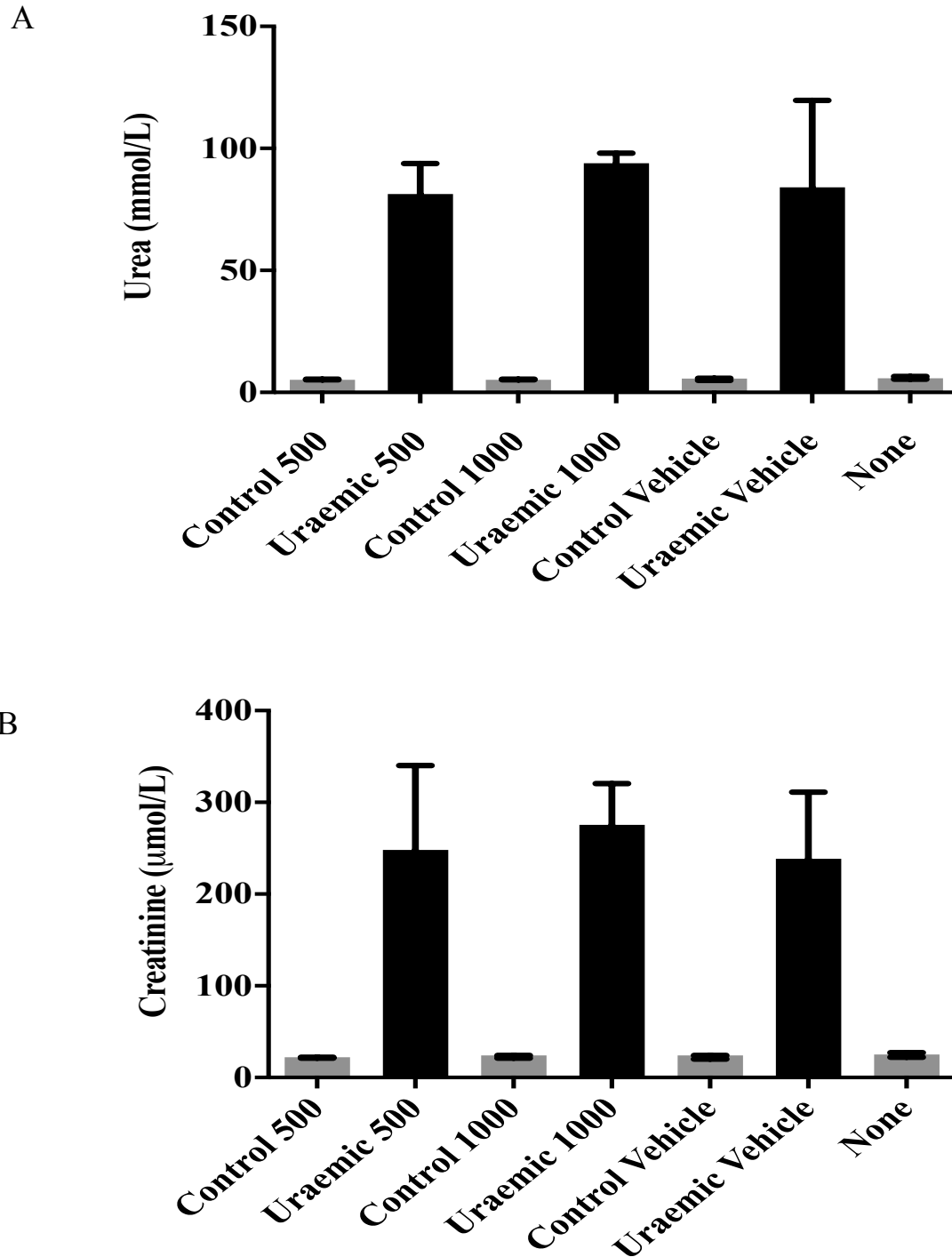
Figure 4.9 Serum urea (A) and creatinine (B). Serum obtained from rats at time of culling at day 7 demonstrated no statistically significant differences in urea and creatinine between control and uraemic groups with emodin 500 μg/mL, emodin 1000 μg/mL or vehicle applied topically. n = 3 per group n = 6 per uraemic vehicle group. Data represented as median + 95% CI analysed by Mann-Whitney U test.

Figure 4.10 demonstrates serum corticosterone concentrations as determined by ELISA in each group, with no statistically significant results seen between control and uraemic groups for any treatment received.
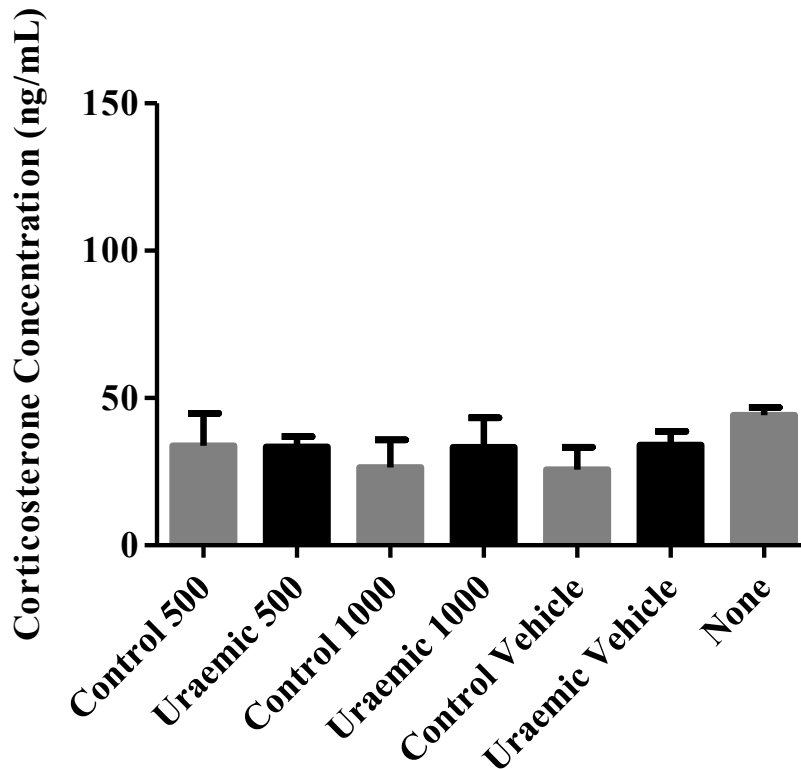
Figure 4.10 Serum corticosterone concentrations as determined by ELISA. Serum obtained from rats at time of culling at day 7 demonstrated no significant difference between control and uraemic groups with vehicle, emodin 500 μg/mL or emodin 1000 μg/mL applied topically. n = 3 per group except n = 6 per uraemic vehicle group. Data represented as median + 95% CI analysed by Kruskal-Wallis with Dunn's multiple comparisons test.

With respect to the wounds themselves, there was minimal difference in percentage area of wound healing between all control animal groups. Although not statistically significant, uraemic animals treated with vehicle did have wounds that healed less than either emodin treatment uraemic groups. There were no differences noted in healing between control and uraemic animals when either concentration of emodin was applied. Of note, there was still a statistically significant difference between the uraemic vehicle and control vehicle groups as well as between the uraemic vehicle and no treatment (none) group (Figure 4.11) demonstrating a delay in healing in uraemia at the baseline state.
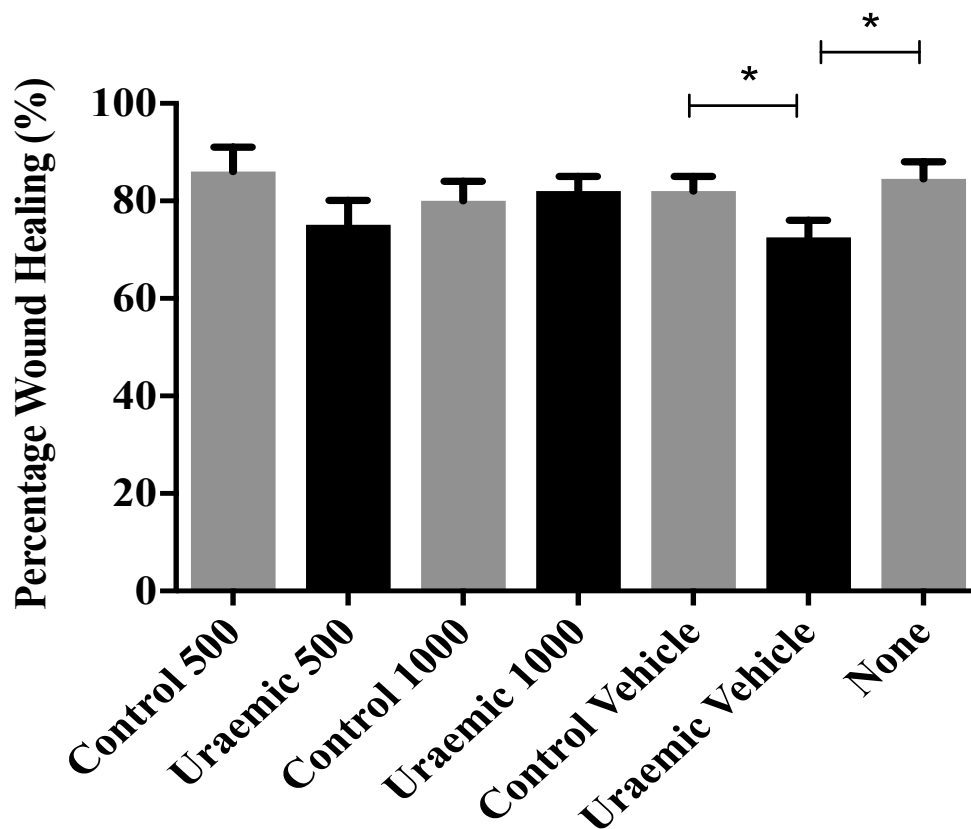
Figure 4.11 Area of wound healed. Percentage area of wound healed by day 7 as compared to wound made on day 0 was only significant between the control vehicle versus uraemic vehicle groups and the uraemic vehicle versus no treatment applied group. n = 6 per group except n = 12 uraemic vehicle group. Data represented as median + 95% CI analysed by Kruskal-Wallis with Dunn's multiple comparisons test. * denotes significance level $p < 0.05$.

From day 0 to day 7 the uraemic animals were noted to lose weight in contrast to their respective control animals that gained weight. These differences were not statistically significant (Figure 4.12).
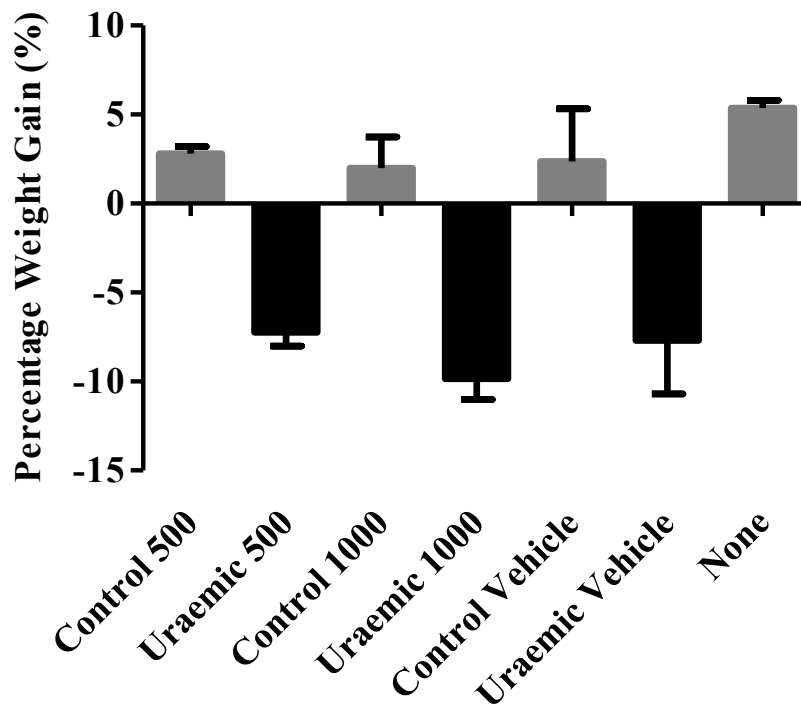
Figure 4.12 Percentage weight gain. Percentage weight gain as compared to day 0 was not significant between control and uraemic groups with vehicle, emodin 500 μg/mL or emodin 1000 μg/mL applied topically. n = 3 per group except n = 6 uraemic vehicle group. Data represented as median + 95% CI analysed by Kruskal-Wallis with Dunn's multiple comparisons test.

Skin corticosterone concentrations were determined after incubating a section of skin in DMEM without FBS or antibiotics overnight (Figure 4.13). The media was retrieved and utilized by ELISA. No significant differences were found in corticosterone concentrations in the skin of uraemic animals treated with drug or vehicle compared to their respective control animals.
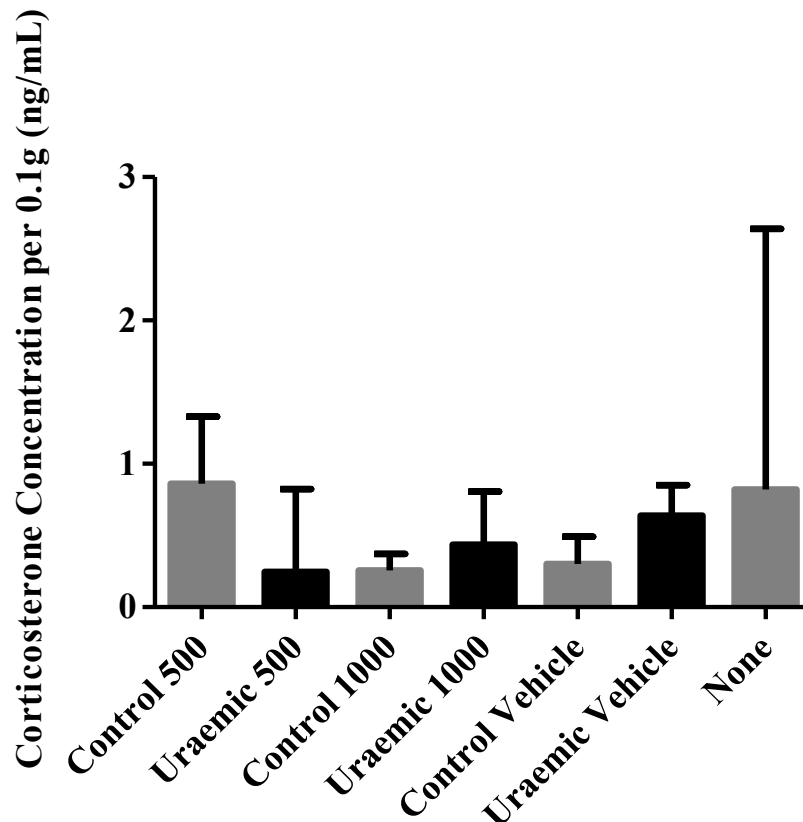
Figure 4.13 Skin corticosterone concentrations as determined by ELISA. After removal of subcutaneous fat and muscle, skin sections were incubated for 24 h in 1 mL DMEM without FBS or antibiotics. Corticosterone concentrations assayed by ELISA from the media demonstrated no significant differences between control and uraemic groups with vehicle, emodin 500 µg/mL or emodin 1000 µg/mL applied topically. n = 3 per group except n = 6 per uraemic vehicle group. Data represented as median + 95% CI analysed by Kruskal-Wallis with Dunn's multiple comparisons test.
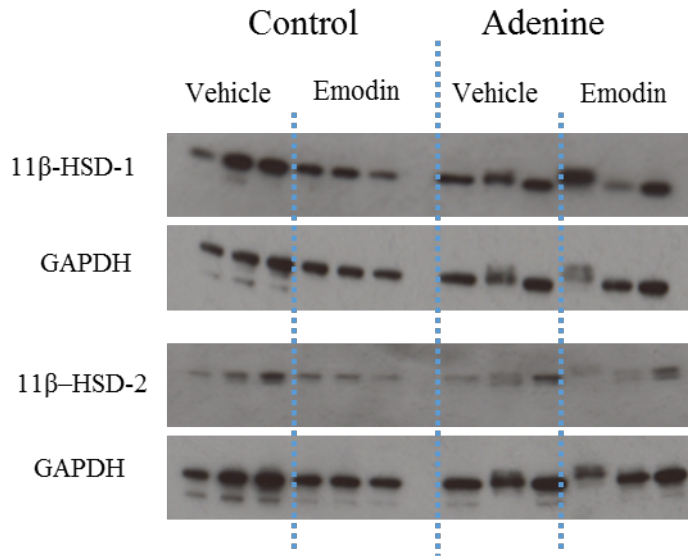
Figure 4.14 Western blots of skin homogenates at day 7 post wounding, emodin 500 µg/mL or vehicle administered. Protein bands from tissue homogenates were resolved by western blotting. Bands immunoreactive to antibodies for 11β-HSD-1 at 32 kDa, 11β-HSD-2 at 44 kDa and GAPDH at 36 kDa are shown.
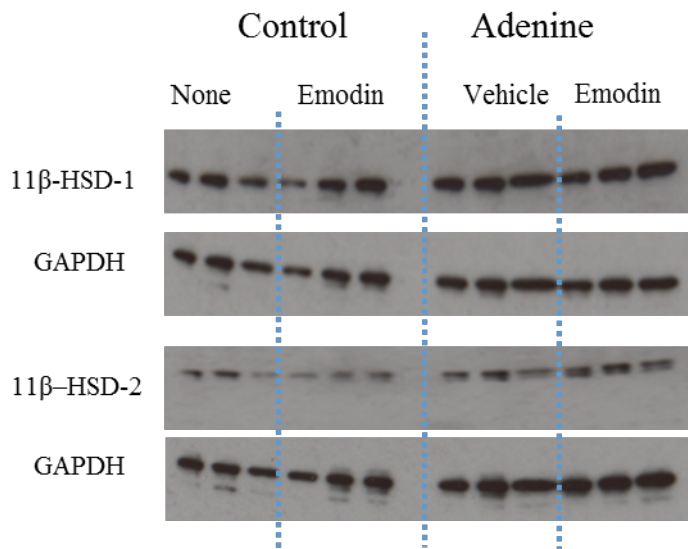
Figure 4.15 Western blots of skin homogenates at day 7 post wounding, emodin 1000 µg/mL, vehicle or no treatment administered. Protein from tissue homogenates was resolved by western blotting. Bands immunoreactive to antibodies for 11β-HSD-1 at 32 kDa, 11β-HSD-2 at 44 kDa and GAPDH at 36 kDa are shown.

Skin samples from animals were homogenized to extract protein to be assessed by western blotting. Densitometry was performed using Image J software (version 1.4.3.67) to semi-quantify the band intensity of 11β-HSD-1 or 11β-HSD-2 protein relative to GAPDH. In skin homogenates of animals treated with emodin at 500 µg/mL or 1000 µg/mL there were no appreciable differences in 11β-HSD-1 or 11β-HSD-2 protein expression when compared to respective controls by western blotting (Figure 4.14, 4.15 and 4.16).

A   B
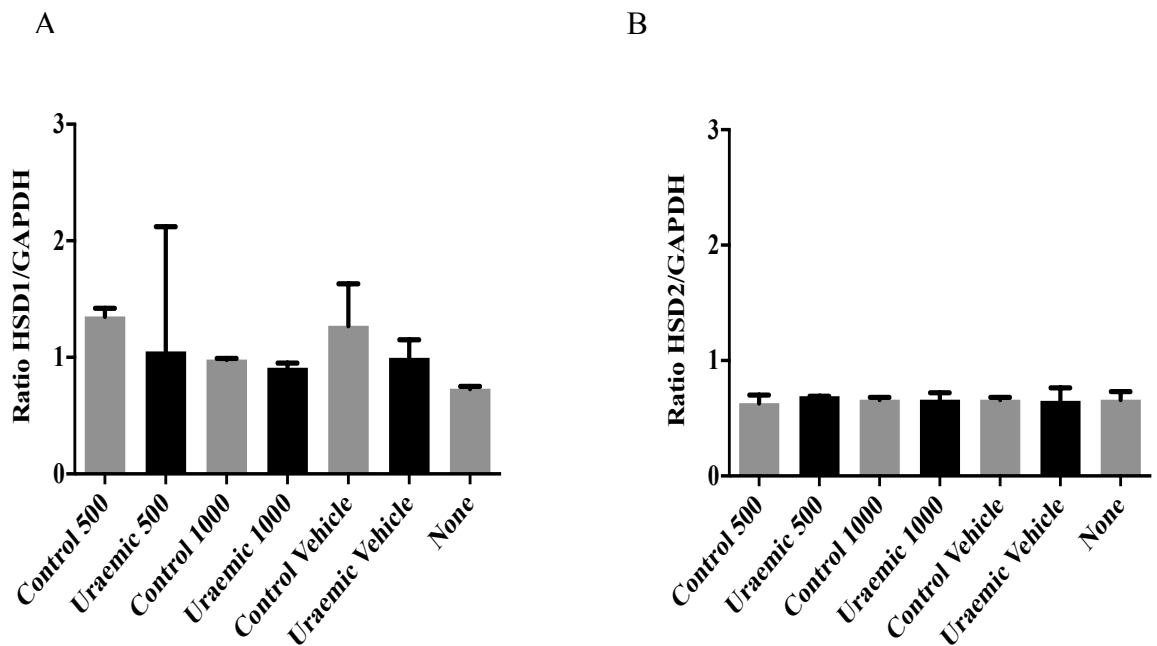
Figure 4.16 Densitometry; ratios of 11β-HSD-1 (A) and 11β-HSD-2 (B) relative to GAPDH. Performed on western blots of Figures 4.14 and 4.15. Data represented as median + 95% CI analysed by Kruskal-Wallis with Dunn's multiple comparisons test.

4.2.3 Systemic Emodin in Rat Wound Healing at Day 3

24 male Wistar rats were used for these experiments. 12 rats had uraemia induced by feeding a 0.75% adenine supplemented diet and the remaining 12 rats were fed normal chow and acted as controls. Each animal underwent wounding as described on day 0 (section 2.2.3.1). 12 uraemic and control animals received emodin 100 mg/kg by oral gavage on days 0 to 2, the remaining 12 uraemic and control animals received 10% ethanol (VWR International Ltd) as vehicle. All animals were culled on day 3 (section 2.2.3.3).

Figure 4.17 demonstrates serum urea and creatinine concentrations in all groups of animals, with significant differences found between the uraemic and control groups treated with drug and between the uraemic and control groups treated with vehicle.

A

B
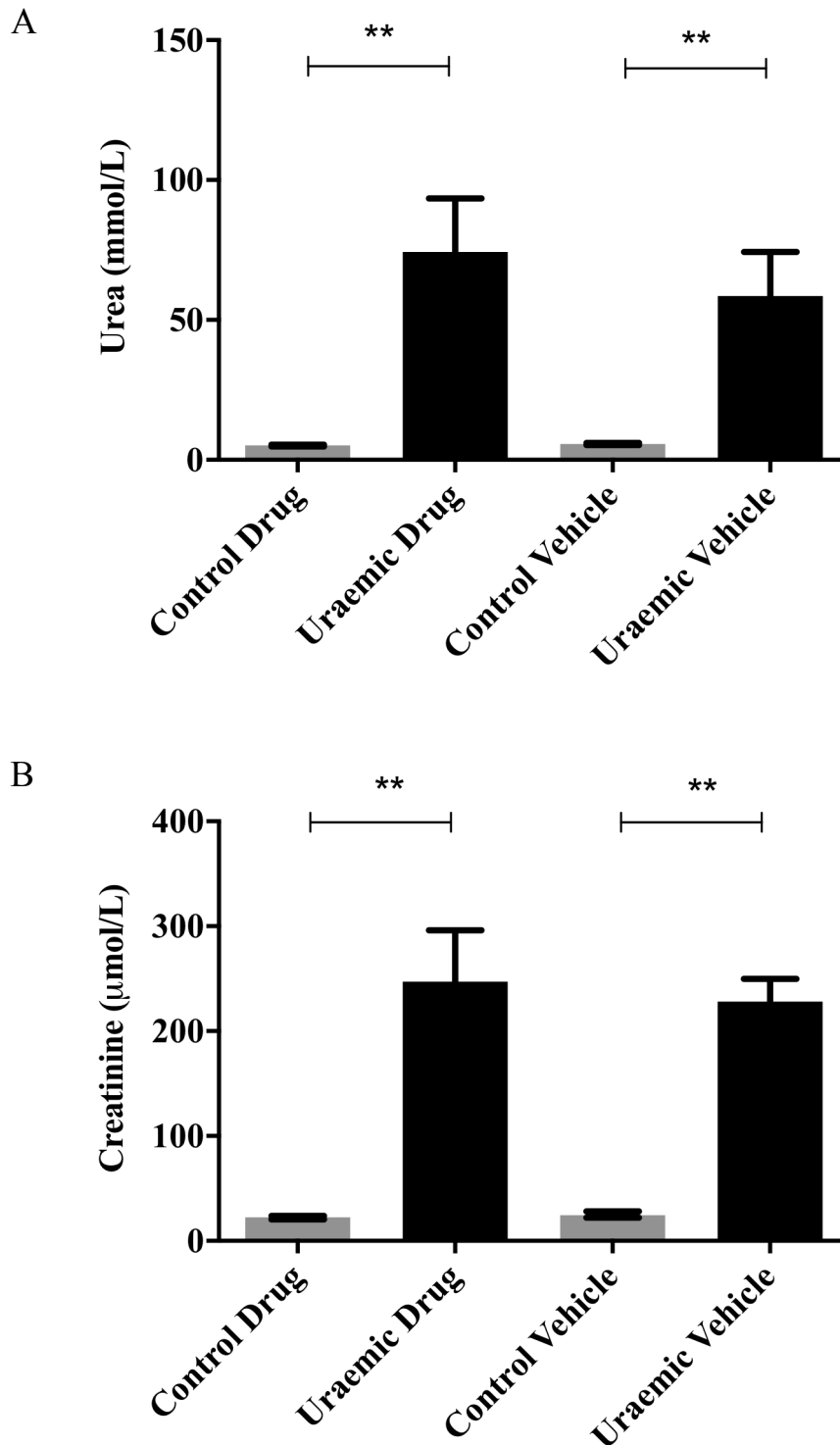
Figure 4.17 Serum urea (A) and creatinine (B). Serum obtained from rats at time of culling at day 3 demonstrated significant differences in urea and creatinine between control and uraemic groups whether systemic emodin or vehicle was administered. n = 6 per group. Data represented as median + 95% CI analysed by Mann-Whitney U test; ** denotes significance level $p < 0.01$.

Figure 4.18 demonstrates serum corticosterone concentrations as determined by ELISA. Despite the control vehicle animals yielding an almost 2-fold greater serum corticosterone concentration than the uraemic vehicle treated animals, this difference did not achieve statistical significance (p = 0.110). There was no significant difference in serum corticosterone concentrations between either the control drug treated and uraemic drug treated animals (p > 0.999) nor between the 2 control groups or 2 uraemic groups.
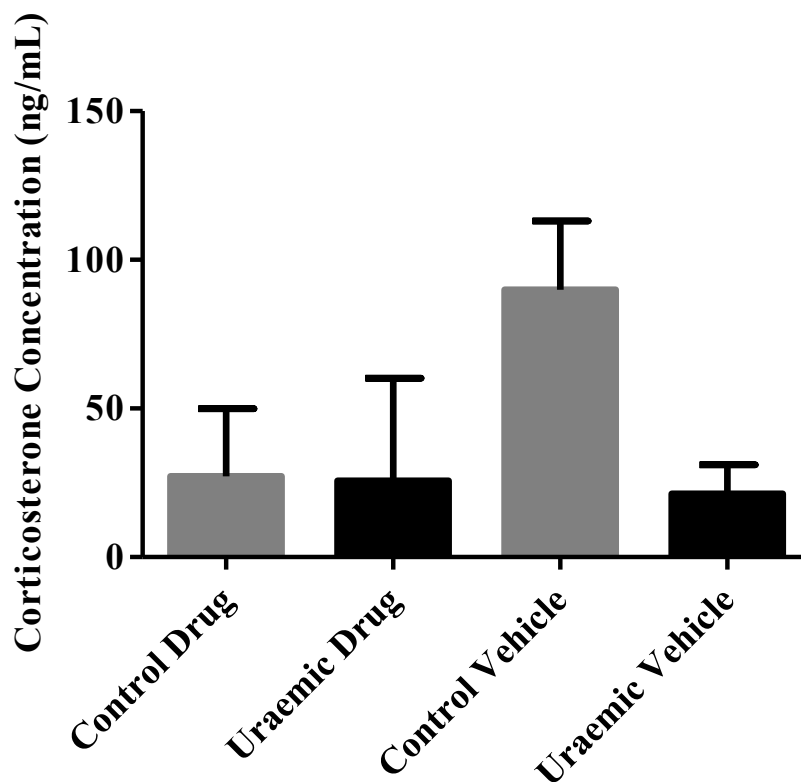
Figure 4.18 Serum corticosterone concentrations as determined by ELISA. Serum obtained from rats at time of culling at day 3 demonstrated no significant difference between the control and uraemic groups either with systemic emodin or vehicle administration. n = 6 per group. Data represented as median + 95% CI analysed by Kruskal-Wallis with Dunn's multiple comparisons test.

With respect to the wounds themselves, uraemic drug treated animals demonstrated similar wound healing to control drug treated animals, with no significant difference observed between the percentage area of the wound healed ($p > 0.999$). However, this was also the case between the control vehicle treated and uraemic vehicle treated animals ($p = 0.490$) (Figure 4.19).
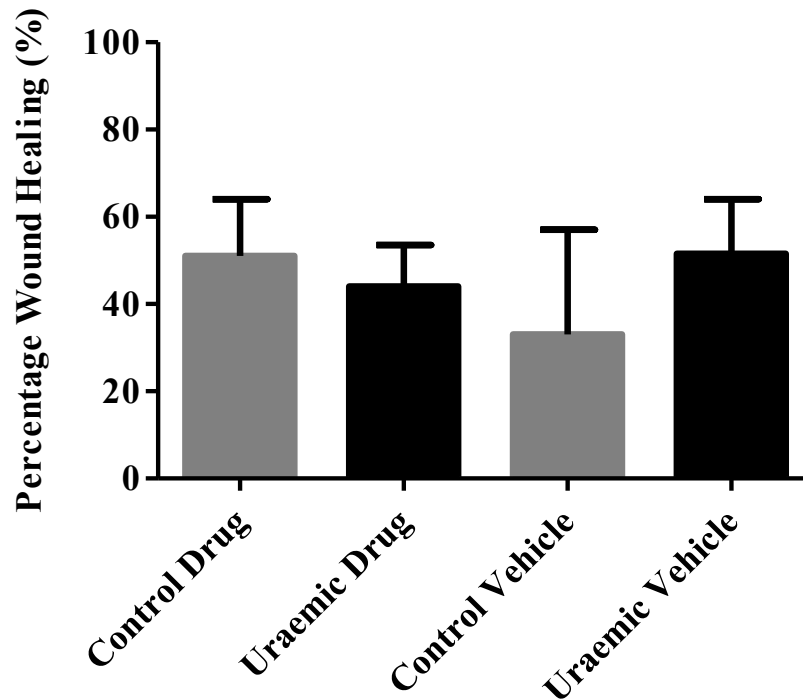
Figure 4.19 Area of wound healed. Percentage area of wound healed on day 3 as compared to wound made on day 0 was not significant between the control and uraemic groups with systemic emodin or vehicle administration. n = 12 per group. Data represented as median + 95% CI analysed by Kruskal-Wallis with Dunn's multiple comparisons test.

From day 0 to day 3 the uraemic animals, irrespective of treatment received, had a lower weight in comparison to their respective control animals (not statistically significant) (Figure 4.20). In addition, the animals in each drug treated group had lower weights than their vehicle treated counterparts (not statistically significant).
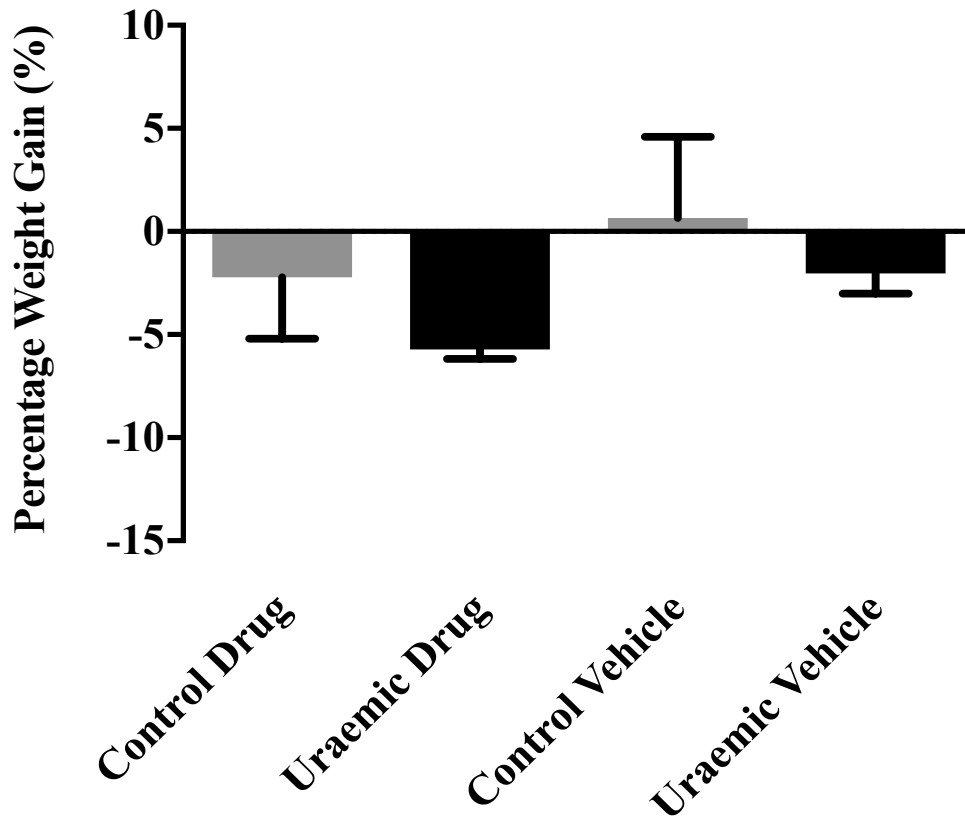
Figure 4.20 Percentage weight gain. Percentage weight gain as compared to day 0 was not significant between control and uraemic groups with systemic emodin or vehicle administration in animals culled at day 3. n = 6 per group. Data represented as median + 95% CI analysed by Kruskal-Wallis with Dunn's multiple comparisons test.

Skin corticosterone concentrations were determined after incubating a section of skin in DMEM without FBS or antibiotics overnight. The media was retrieved and utilized in the ELISA. The uraemic vehicle treated group had greater skin corticosterone concentrations compared to the uraemic emodin treated group (not statistically significant). In addition, the control vehicle treated group had greater skin corticosterone concentrations compared to the control emodin treated group although this did not reach statistical significance. There were no significant differences in corticosterone skin concentrations between the 2 drug treated groups or between the 2 vehicle treated groups (Figure 4.21). The skin corticosterone concentrations seem to mirror the serum corticosterone concentrations measured.
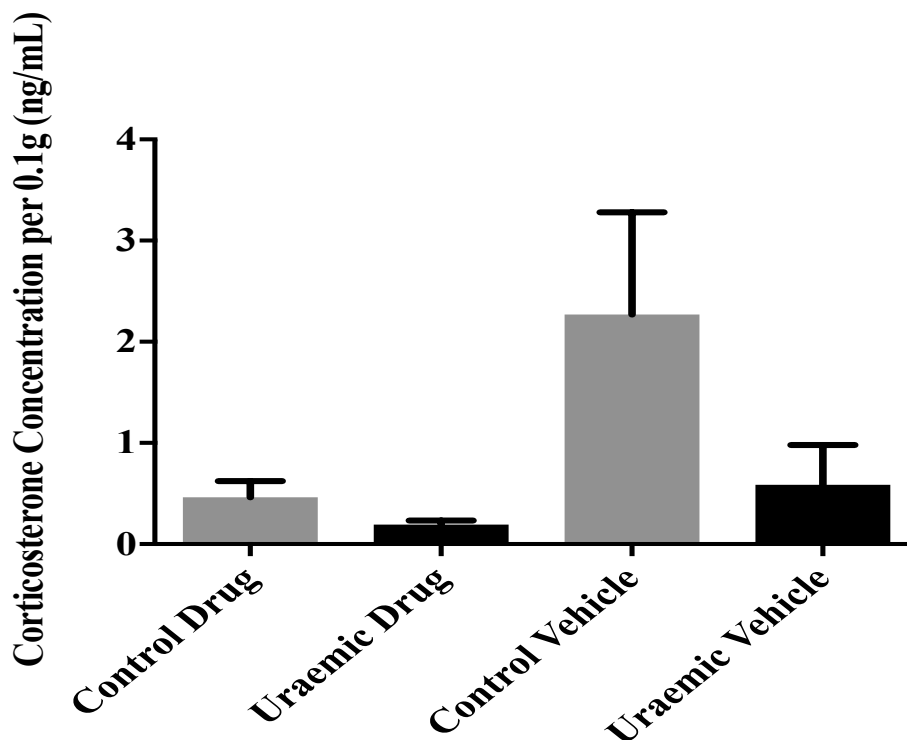
Figure 4.21 Skin corticosterone concentrations as determined by ELISA. After removal of subcutaneous fat and muscle, skin sections were incubated for 24 h in 1 mL DMEM without FBS or antibiotics. Corticosterone concentrations assayed by ELISA from the media demonstrated no significant differences between control and uraemic groups with systemic emodin or vehicle administration. n = 6 per group. Data represented as median + 95% CI analysed by Kruskal-Wallis with Dunn's multiple comparisons test.
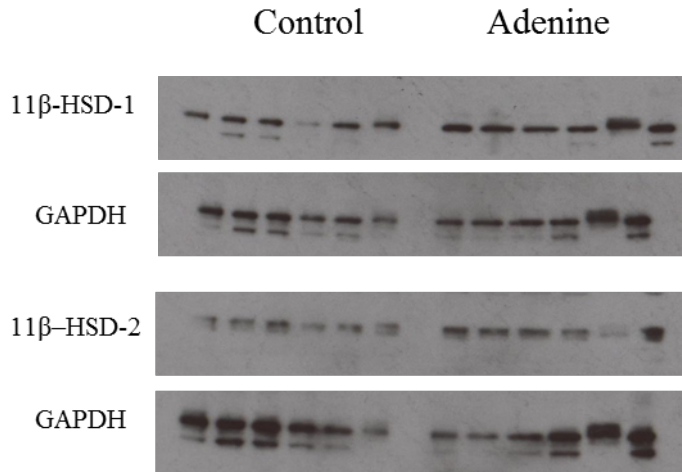
Figure 4.22 Western blots of skin homogenates at day 3 post wounding, emodin 100 mg/kg systemically administered. Protein bands from tissue homogenates were resolved by western blotting. Bands immunoreactive to antibodies for 11β-HSD-1 at 32 kDa, 11β-HSD-2 at 44 kDa and GAPDH at 36 kDa are shown.
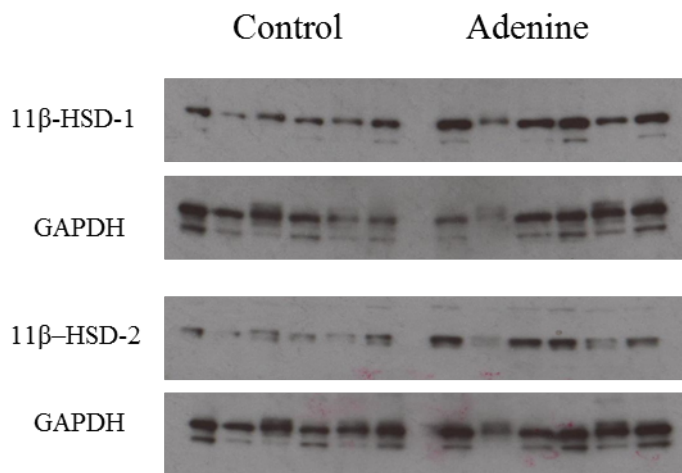
Figure 4.23 Western blots of skin homogenates at day 3 post wounding, vehicle 10% ethanol administered. Protein from tissue homogenates was resolved by western blotting. Bands immunoreactive to antibodies for 11β-HSD-1 at 32 kDa, 11β-HSD-2 at 44 kDa and GAPDH at 36 kDa are shown.

Skin samples from animals were homogenized to extract protein to be assessed by western blotting. Densitometry was performed using Image J software (version 1.4.3.67) to semi-quantify the amount of 11β-HSD-1 or 11β-HSD-2 protein relative to GAPDH. A double band was seen at a lower molecular weight than 32 kDa for some 11β-HSD-1 samples and lower than 36 kDa on all western blots for GAPDH, likely due to sample degradation. In skin homogenates of animals, uraemic or control, treated with emodin or vehicle there were no appreciable differences in 11β-HSD-1 or 11β-HSD-2 protein expression by western blotting. (Figure 4.22, 4.23 and 4.24).

A

B
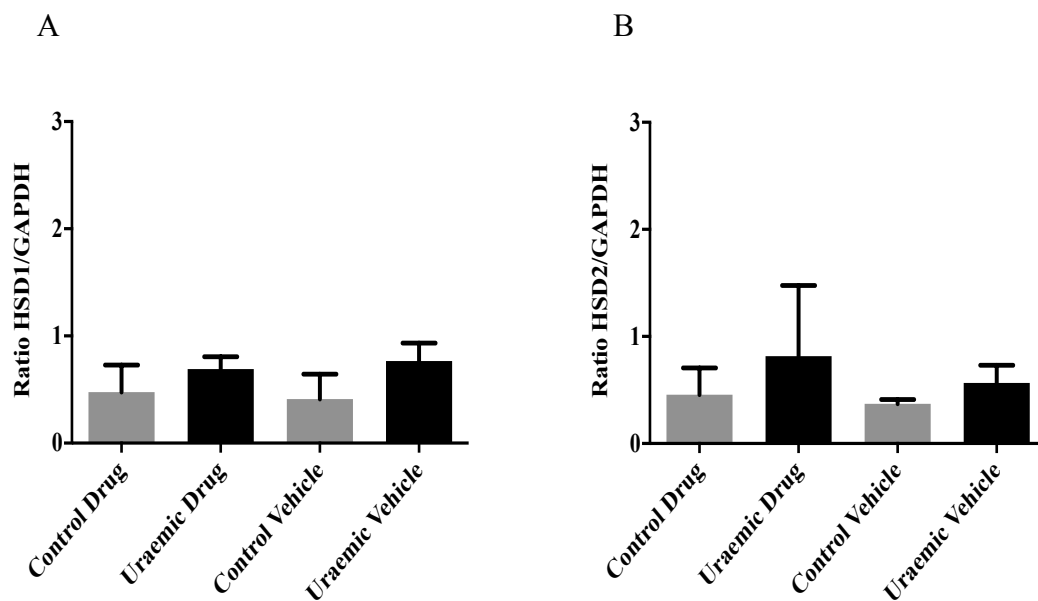
Figure 4.24 Densitometry; ratios of 11β-HSD-1 (A) and 11β-HSD-2 (B) relative to GAPDH. Derived from day 3 post wounding western blots of Figures 4.22 and 4.23. Data represented as median + 95% CI analysed by Kruskal-Wallis with Dunn's multiple comparisons test.

4.2.4 Systemic Emodin in Rat Wound Healing at Day 7

64 male Wistar rats were used for these experiments. 32 rats had uraemia induced by feeding a 0.75% adenine supplemented normal diet and the remaining 32 rats were fed normal chow and acted as controls. Each animal underwent wounding as described on day 0 (section 2.2.3.1). 16 uraemic and control animals received emodin 100 mg/kg by oral gavage on days 0 to 4, the remaining 16 uraemic and control animals received 10% ethanol as vehicle. All animals were culled on day 7 (section 2.2.3.3).

Figure 4.25 demonstrates serum urea and creatinine concentrations in all groups of animals, with significant differences observed between the uraemic and control groups treated with drug and between the uraemic and control groups treated with vehicle.
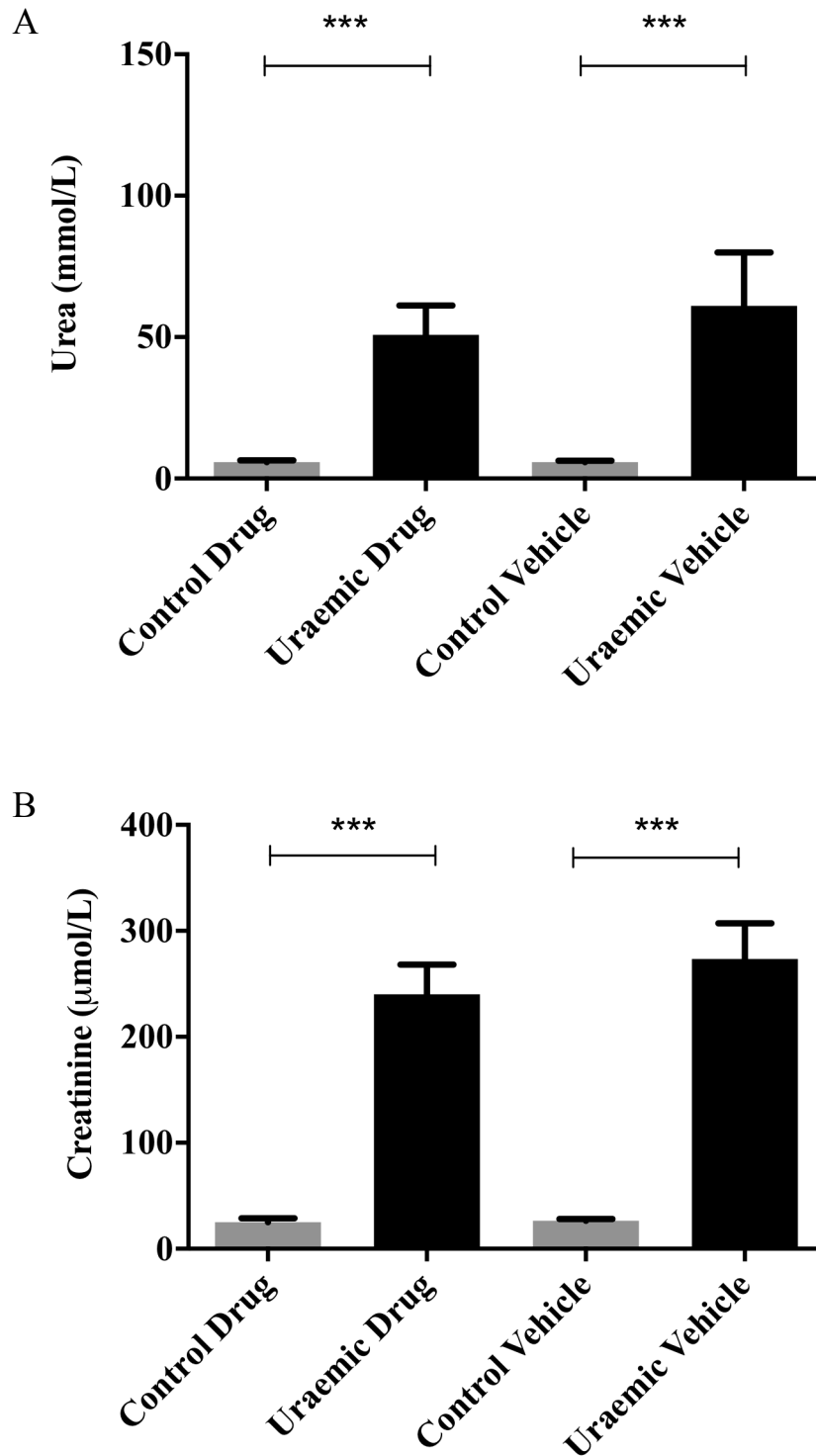
Figure 4.25 Serum urea (A) and creatinine (B). Serum obtained from rats at time of culling at day 7 demonstrated significant differences between control and uraemic groups in urea and creatinine whether systemic emodin or vehicle was administered. n = 16 per group. Data represented as median + 95% CI analysed by Mann-Whitney U test; *** denotes significance level p < 0.001.

Figure 4.26 demonstrates serum corticosterone concentrations as determined by ELISA. There were no significant differences in serum corticosterone concentrations between either the control drug and uraemic drug treated animals or between the control vehicle and uraemic vehicle treated groups of animals.
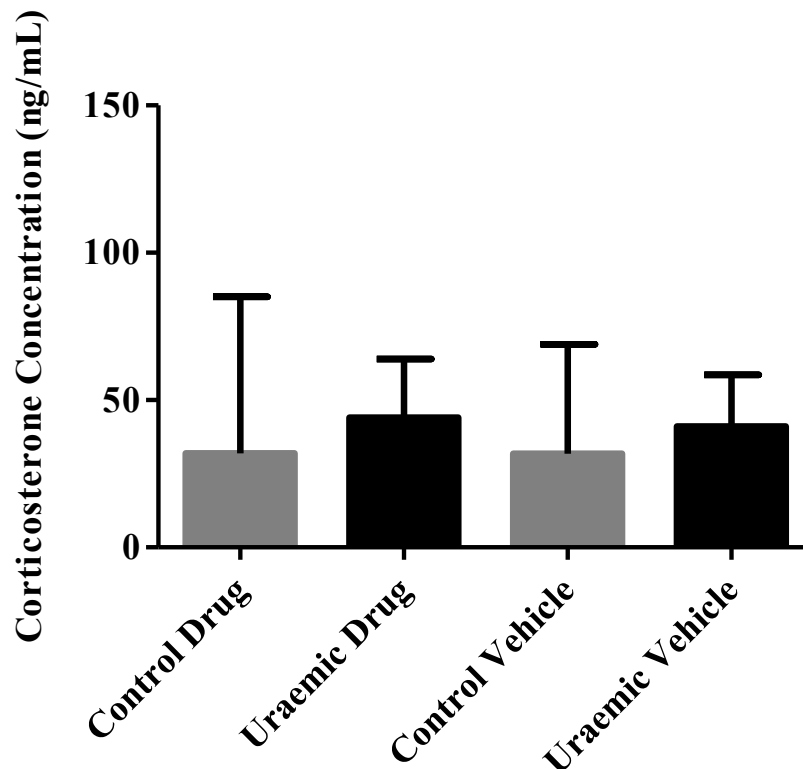
Figure 4.26 Serum corticosterone concentrations as determined by ELISA. Serum obtained from rats at time of culling at day 7 demonstrated no significant difference between control and uraemic groups either with systemic emodin or vehicle administration. n = 16 per group. Data represented as median + 95% CI analysed by Kruskal-Wallis with Dunn's multiple comparisons test.

With respect to the wounds themselves uraemic vehicle treated animals demonstrated significantly less wound healing compared to control vehicle treated animals as before. This difference disappeared under the influence of emodin, indicative of restoration of wound healing to the same extent as healthy controls. When comparing uraemic emodin treated animals with uraemic untreated animals a beneficial effect of emodin was clearly demonstrated. (Figure 4.27). This was not true when comparing healing in the control drug treated group with the control vehicle group, suggesting emodin has a predilection for working in the uraemic setting only possibly due to increased enzyme activity in uraemia.
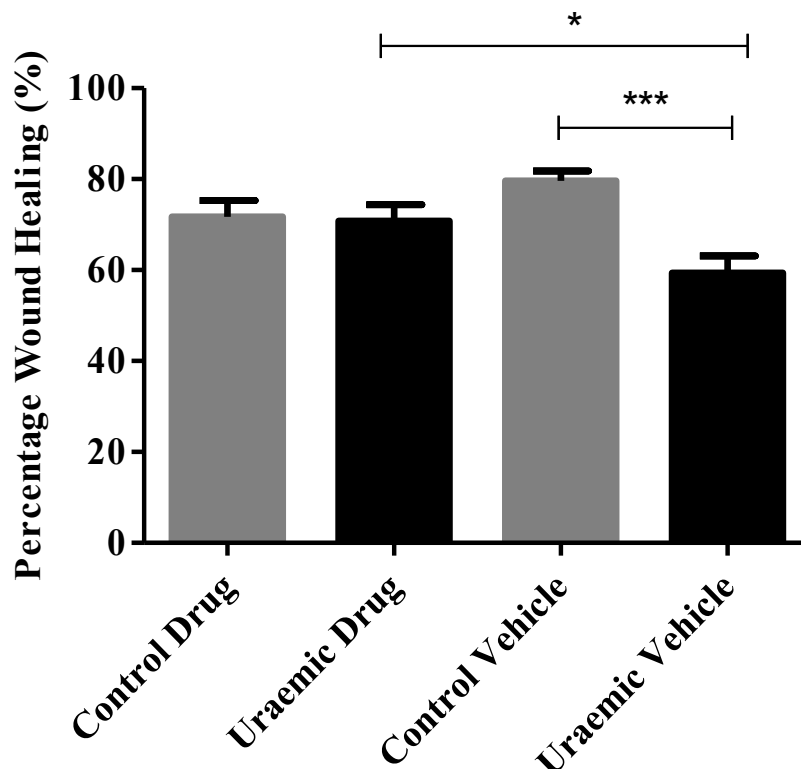
Figure 4.27 Area of wound healed. Percentage area of wound healed on day 7 as compared to wound made on day 0 was significant between the uraemic drug and uraemic vehicle groups as well as between the control vehicle and uraemic vehicle groups n = 32 per group. Data represented as mean + 95% CI analysed by Kruskal-Wallis with Dunn's multiple comparisons test. * denotes significance level $p < 0.05$, *** denotes significance level $p < 0.001$.

From day 0 to day 7 the uraemic animals were noted to lose weight in contrast to the control animals that gained weight. The uraemic vehicle treated animals had a significant lower weight in comparison to the respective control vehicle treated animals (Figure 4.28). Although the uraemic drug treated animals had a lower weight than the control drug treated animals, this was not a statistically significant difference ($p = 0.200$).
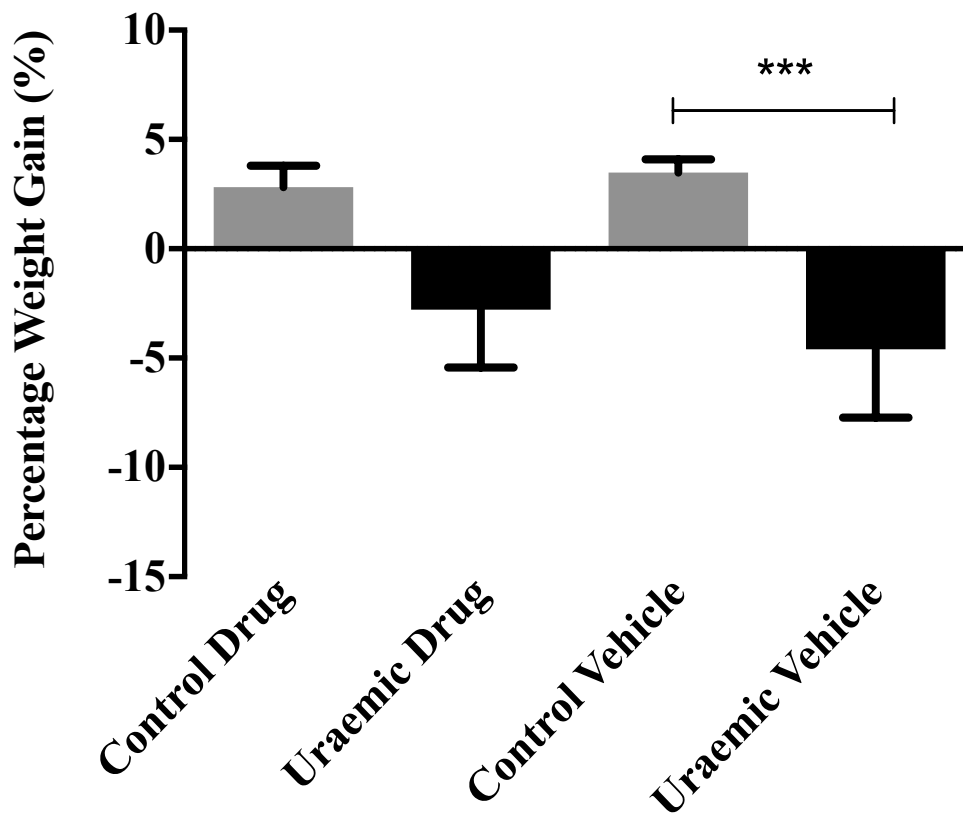
Figure 4.28 Percentage weight gain. Percentage weight gain as compared to day 0 was significant in the control versus uraemic groups treated with vehicle. n = 16 per group. Data represented as median + 95% CI analysed by Kruskal-Wallis with Dunn's multiple comparisons test. *** denotes significance level $p < 0.001$.

Skin corticosterone concentrations were determined after incubating a section of skin in DMEM without FBS or antibiotics overnight. The media was retrieved and utilized in the ELISA. The uraemic emodin treated group had lower skin corticosterone concentrations compared to the uraemic vehicle treated group, although this result was not statistically significant. In addition, the control vehicle treated group had lower skin corticosterone concentrations compared to the uraemic vehicle treated group although this also did not reach statistical significance (Figure 4.29).
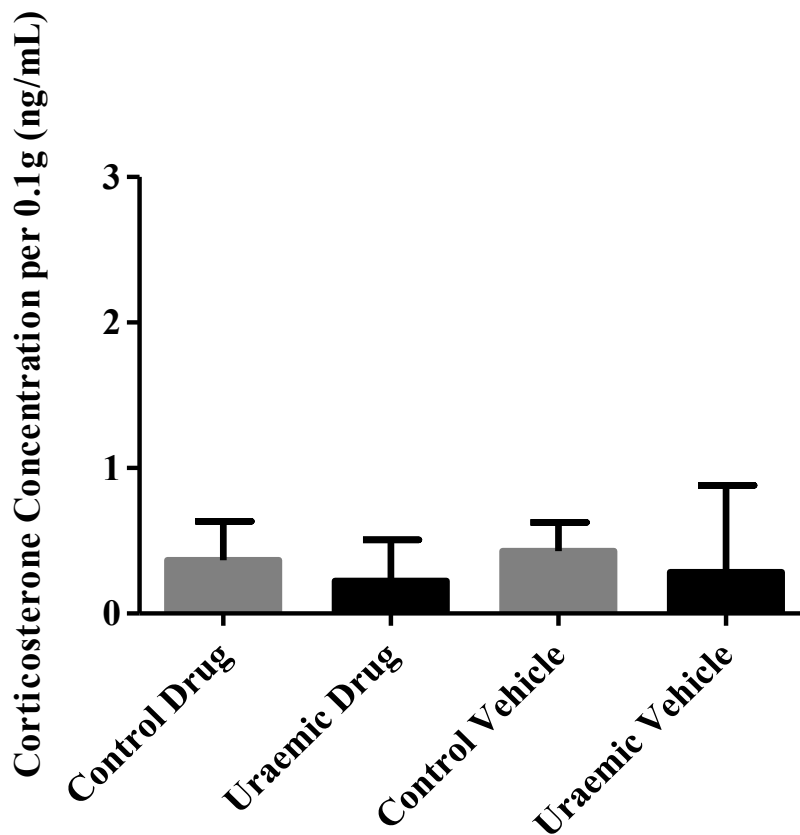
Figure 4.29 Skin corticosterone concentrations as determined by ELISA. After removal of subcutaneous fat and muscle, skin sections were incubated for 24 h in 1 mL DMEM without FBS or antibiotics. Corticosterone concentrations assayed by ELISA from the media demonstrated no significant differences between control and uraemic groups whether systemic emodin or vehicle was administered. n = 16 per group. Data represented as median + 95% CI analysed by Kruskal-Wallis with Dunn's multiple comparisons test.
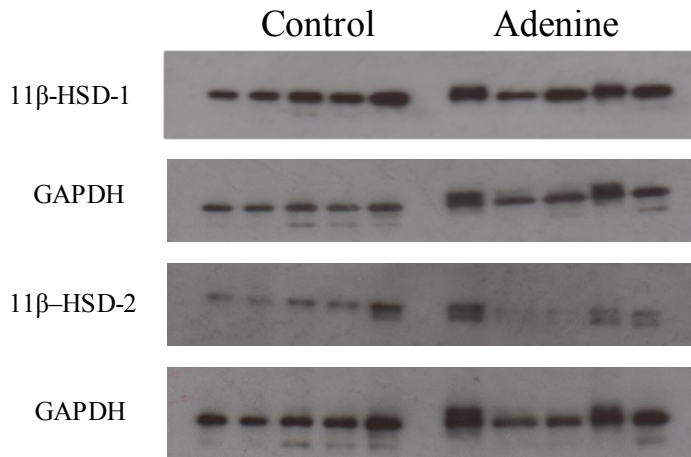
Figure 4.30 Representative western blots of skin homogenates at day 7 post wounding, emodin 100mg/kg systemically administered. Protein bands from tissue homogenates were resolved by western blotting. Bands immunoreactive to antibodies for 11β-HSD-1 at 32 kDa, 11β-HSD-2 at 44 kDa and GAPDH at 36 kDa are shown. Blot representative of total n = 16 per group.
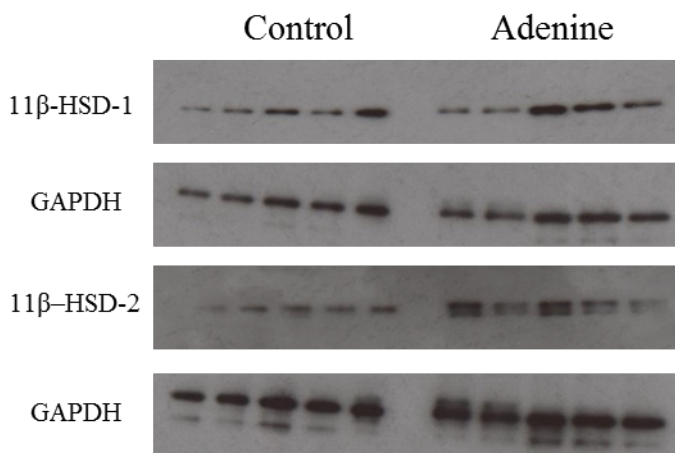
Figure 4.31 Representative western blots of skin homogenates at day 7 post wounding, vehicle 10% ethanol administered. Protein from tissue homogenates was resolved by western blotting. Bands immunoreactive to antibodies for 11β-HSD-1 at 32 kDa, 11β-HSD-2 at 44 kDa and GAPDH at 36 kDa are shown. Blot representative of total n = 16 per group.

Skin samples from animals were homogenized to extract protein to be assessed by western blotting. Densitometry was performed using Image J software (version 1.4.3.67) to semi-quantify the band density of 11β-HSD-1 or 11β-HSD-2 protein relative to GAPDH. (Double bands seen at a lower than expected molecular weight are likely due to sample degradation). In skin homogenates of animals treated with emodin there was greater 11β-HSD-1 protein expression than vehicle treated counterparts. This was applicable for uraemic as well as control animals, although the results were not statistically significant. No significant differences in 11β-HSD-2 protein expression were found (Figure 4.30, 4.31 and 4.32).

A   B
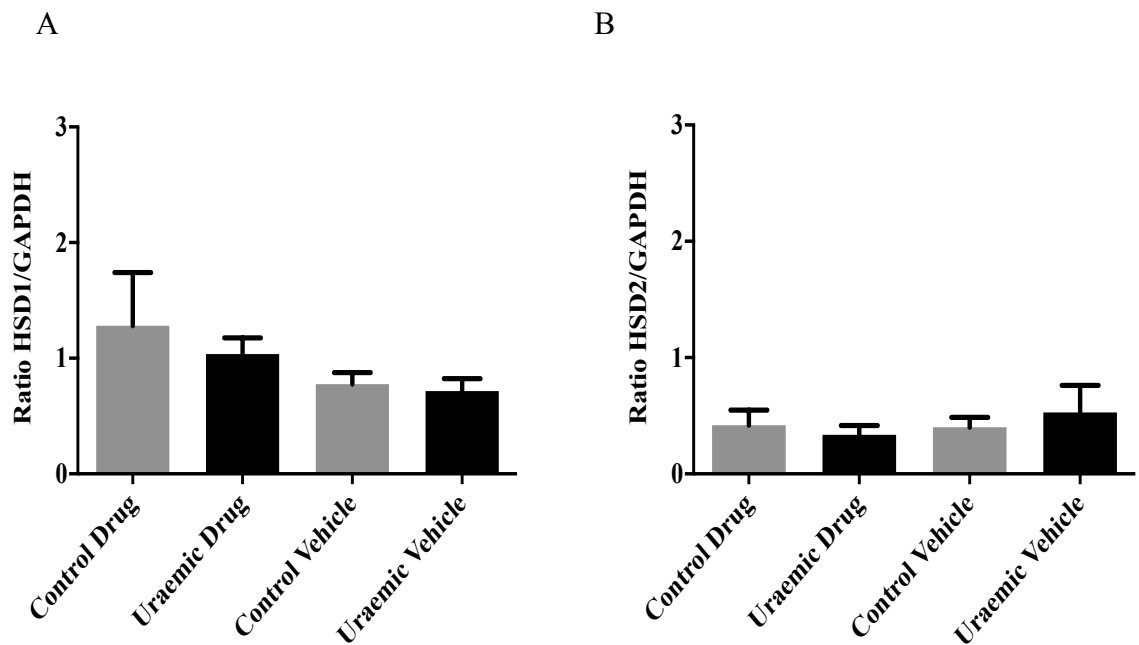
Figure 4.32 Densitometry; ratios of 11β-HSD-1 (A) and 11β-HSD-2 (B) relative to GAPDH. Performed on all western blots from skin homogenates at day 7 post wounding including Figures 4.30 and 4.31. Data represented as median + 95% CI analysed by Kruskal-Wallis with Dunn's multiple comparisons test.

4.2.4.1 The Effect of Systemic 11β-HSD-1 Inhibition on Liver
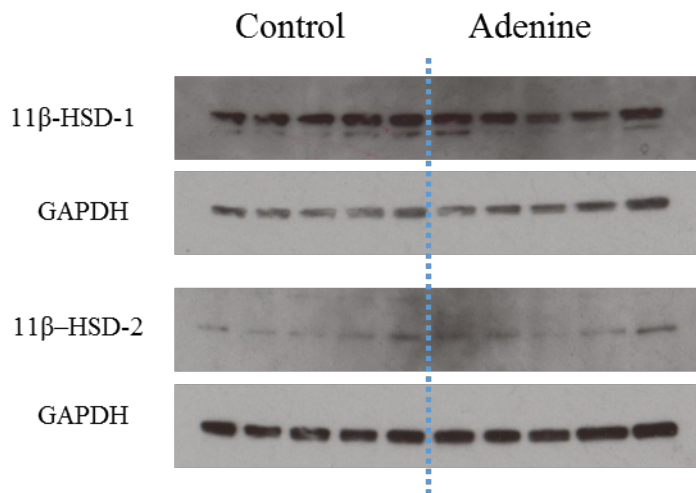
Figure 4.33 Western blots of liver homogenates at day 7 post wounding, emodin 100 mg/kg systemically administered. Protein bands from tissue homogenates were resolved by western blotting. Bands immunoreactive to antibodies for 11β-HSD-1 at 32 kDa, 11β-HSD-2 at 44 kDa and GAPDH at 36 kDa are shown.
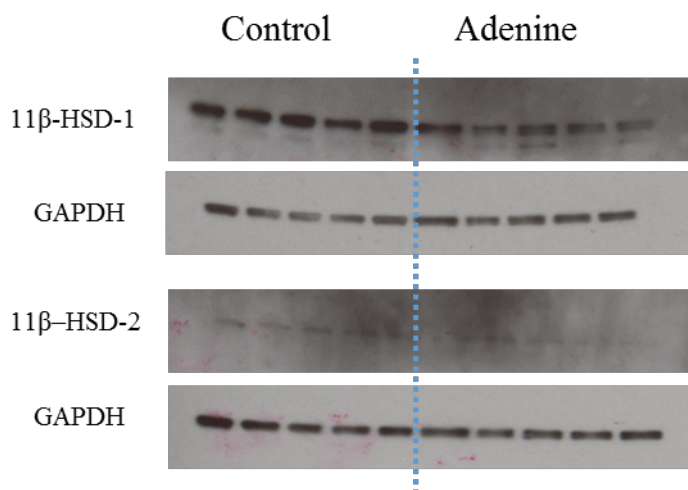
Figure 4.34 Western blots of liver homogenates at day 7 post wounding, vehicle 10% ethanol administered. Protein from tissue homogenates was resolved by western blotting. Bands immunoreactive to antibodies for 11β-HSD-1 at 32 kDa, 11β-HSD-2 at 44 kDa and GAPDH at 36 kDa are shown.

Densitometry was performed using Image J software (version 1.4.3.67) to semi-quantify the band density of 11β-HSD-1 or 11β-HSD-2 protein relative to GAPDH. In liver homogenates of animals treated with emodin there was greater 11β-HSD-1 protein expression than vehicle treated animals. This was applicable for uraemic as well as control animals, although the results were not statistically significant. There were no significant differences in 11β-HSD-2 protein expression (Figure 4.33, 4.34 and 4.35). These results parallel the 1β-HSD-1 and 11β-HSD-2 protein expression results seen for skin homogenates (Figure 4.32).
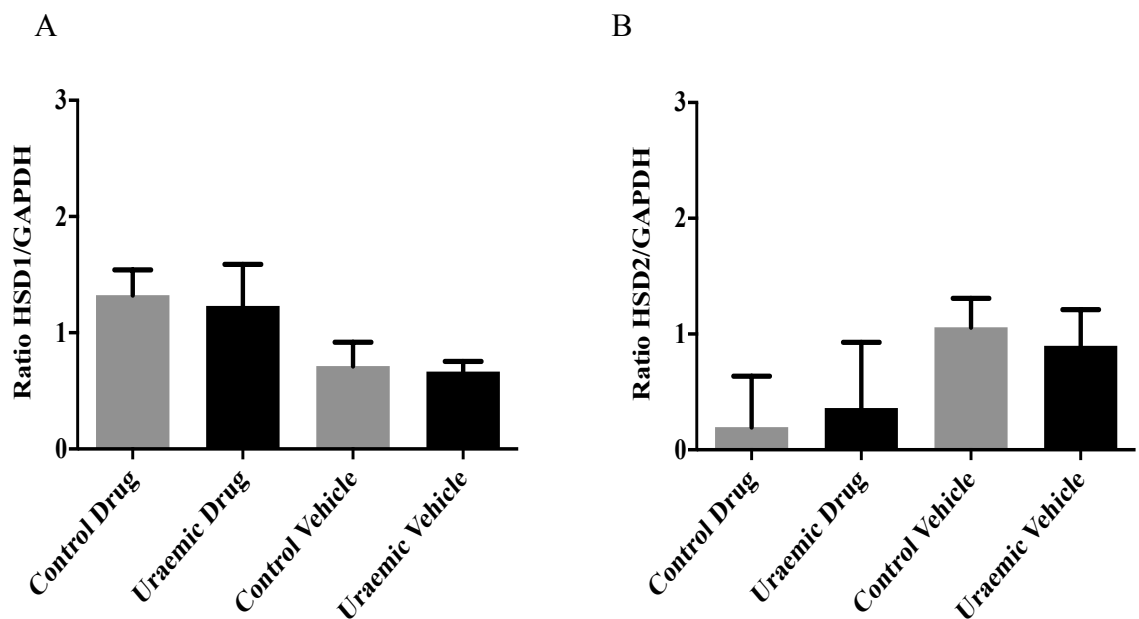
Figure 4.35 Densitometry; ratios of 11β-HSD-1 (A) and 11β-HSD-2 (B) relative to GAPDH. Performed on western blots of Figures 4.33 and 4.34 Data represented as median + 95% CI analysed by Kruskal-Wallis with Dunn's multiple comparisons test.

4.2.5 Summary of *in vivo* Results

In all experiments, the concentrations of serum urea and creatinine were consistently greater in the uraemic compared to the control groups. Statistically the results were not significant in the topical emodin experiment, even though serum results were

comparable to other experiments. This is likely due to the small numbers of animals per group rather than failure in the induction of experimental uraemia *per se*.

Serum corticosterone concentrations were not statistically significantly different between uraemic and control groups at day 3 or day 7 whether no treatment, topical or systemic emodin or the corresponding vehicle only was administered.

When measuring skin corticosterone concentrations by ELISA, no statistically significant results were obtained in any experiment. In animals administered systemic emodin and culled at day 3, there was a trend towards greater skin corticosterone concentrations in vehicle treated rather than emodin treated animals (whether they were control or uraemic animals), which was not seen at day 7 after systemic emodin administration.

From the initial wound healing experiment, it was evident that uraemic animals healed less well compared to control animals at day 7. Predictably, more healing was evident at day 7 compared to day 3 in both uraemic and control groups although this was only statistically significant for the control groups. This suggests the rate of healing is delayed in uraemic rats. In the topical emodin experiment, significantly reduced percentage of area of wound healed in the uraemic vehicle treated group compared to control vehicle or no treatment groups was demonstrated in keeping with the baseline experiment. No differences in healing were found between the topical emodin treated control and uraemic animals, suggesting that topical emodin improves healing in uraemic animals to a similar extent of healing in control emodin treated animals. It is prudent to treat this result with caution as the apparent effect may simply be due to small group numbers. When systemic emodin was administered, no differences in wound healing were demonstrated at day 3. However, by day 7, significantly less healing was seen in the uraemic vehicle treated group compared to the control vehicle treated group in keeping with previous findings of delayed healing in uraemia. Conversely, percentage wound healing was similar in the control and uraemic emodin treated groups suggesting systemic emodin in uraemic animals improves wound healing to that of control emodin treated animals. In support of this, significantly more

healing was noted in the uraemic emodin treated group compared to the uraemic vehicle treated group but not between the two control groups.

The significant differences in wound healing between uraemic and control animals treated with emodin at day 7 do not correlate with changes in serum or skin corticosterone concentrations, suggesting that either the methods employed here are not suitably designed to measure changes in 11β-HSD-1 activity or that alternate pathways are implicated in poor wound healing in uraemia. As systemic emodin treatment seems to improve healing in uraemic animals to the same degree as control animals, more studies should be performed to define the mechanism of action of emodin in the uraemic state. Delineating the pharmacokinetics and pharmacodynamics of emodin and comparing this within other organs, in both the uraemic and non uraemic state would be informative. Studying other specific 11β-HSD-1 inhibitors would also add strength to the use of such drugs in aiding wound healing in future.

Due to the small numbers of animals in each group, with considerable variability in weights it is difficult to draw firm conclusions about animal weights across all 4 *in vivo* experiments. In initial experiments at day 3, control and uraemic animals lost weight to a similar extent. At day 3, after systemic emodin or vehicle administration no statistically significant differences in animal weight were established. In initial experiments at day 7, control animals gained significantly more weight than uraemic animals that lost weight. This pattern remained significant in animals culled at day 7 after systemic vehicle administration. Although a similar pattern was noted for the animals treated with systemic emodin in the same experiment this result did not attain statistical significance. A similar trend was seen in the topical emodin experiment, with uraemic animals losing weight and control animals gaining weight irrespective of treatment, although these results were not statistically significantly different. Animals could not be caged individually due to spatial logistics in the biological services unit. Although each cage had a plentiful supply of drinking water and feed, it is likely each cage had more dominant animals that influenced feeding within the group. To tease out whether weight has a direct impact on wound healing would require more detailed studies into mass of chow consumed per single caged animal as

well as further measurements such as trans-epidermal water loss of skin and tensile strength.

11β-HSD-1 protein expression appeared greater in uraemic animals than control animals at day 3 and day 7 of the baseline experiment, although this did not attain statistical significance. Robust conclusions cannot be drawn about 11β-HSD-1 protein expression after topical emodin or vehicle administration due to the small sample sizes (n = 3) used. Furthermore, the rats were found to have removed the dressings applied after wounding and topical emodin or vehicle administration during vigorous grooming. It was not possible to ensure each animal received the proposed topical dose as a result, or to exclude accidental systemic dosing after licking their wounds. To ensure the dressings remained intact, the animals would have to be subjected to prolonged general anaesthesia or the dressings sutured *in situ* which would be impractical for repeated dosing, not to mention beyond the remit of our Home Office project license.

After 3 days of systemic emodin or vehicle administration, no differences in 11β-HSD-1 expression were observed. At day 7, although both control and uraemic emodin treated animals' skin appeared to express more 11β-HSD-1 than their vehicle counterparts this was not statistically significant when densitometry was performed. No significant differences in 11β-HSD-1 expression were seen between the drug treated animals or between the vehicle treated animals either. Likewise, 11β-HSD-1 expression in liver homogenates mimicked this pattern with no significant differences found between the drug treated animals or between the vehicle treated animals but both control and uraemic emodin treated animals' liver again appeared to express more 11β-HSD-1 than their vehicle counterparts (not statistically significant by densitometry).

With regards to 11β-HSD-2 protein expression from skin homogenates, it appeared as though greater 11β-HSD-2 protein expression was observed at both day 3 and day 7 in uraemic animals compared to their respective controls (not statistically significant). No significant differences were demonstrated in the experiments utilizing topical or systemic emodin although a trend to increased 11β-HSD-2 protein

139

expression was observed in the uraemic vehicle treated animals compared to the control vehicle treated animals in the systemic emodin experiments. No significant differences in 11β-HSD-2 protein expression were observed in western blots of liver homogenates from the systemic emodin experiment.

4.2.6 PCR

4.2.6.1 Reverse Transcription PCR for 11β-HSD-1 and B2M

Skin samples from 24 of the male Wistar rats of experiment described in section 2.2.3.3 were used for these experiments. 12 rats had uraemia induced by feeding a 0.75% adenine supplemented normal diet and the remaining 12 rats were fed normal chow and acted as controls. Each animal underwent wounding as described (section 2.2.3.1) on day 0. 6 uraemic and control animals received emodin 100 mg/kg by oral gavage on days 0 to 4, the remaining 6 uraemic and control animals received 10% ethanol as vehicle. All animals were culled on day 7.

Skin samples were initially snap frozen in liquid nitrogen and stored at -80°C until ready for use. These samples were homogenized in a ceramic pestle and mortar with liquid nitrogen until a powder was formed, then transferred to a RNase free Eppendorf (Fisher Scientific Ltd). After addition of 300 μL Buffer RLT (Qiagen) they were stored at -80°C until ready to extract RNA utilizing the RNeasy® Fibrous Tissue Mini Kit (Qiagen).

The samples were analysed with a Nanodrop (Thermo Scientific Nanodrop 2000c Spectrophotometer) for RNA quantity and integrity. An A_{260}/A_{280} ratio of 2.0 was accepted as being sufficiently pure to proceed with further experimentation. A_{260}/A_{230} ratios were also analysed for additional information regarding RNA contamination. An A_{260}/A_{230} in the range of 2.0-2.2 is ordinarily the aim. 21 of the 24 RNA samples had A_{260}/A_{280} ratios of greater than 2.0. The remaining 3 samples had ratios above 1.9 so were still utilized for further experiments with caution (Table 4.1). All 24 samples had very low A_{260}/A_{230} ratios, this may be due to a contaminant absorbing at 230nm or less which has been seen in guanidine contamination (175) (used in column based kits such as the RNeasy® Fibrous Tissue Mini Kit).

After reverse transcription, all samples were run in the PCR reaction with TaqMan$^{®}$ probes for 11β-HSD-1, 11β-HSD-2 and B2M (described in 2.5.4 from Thermo Fisher Scientific). To calculate C_T values, the threshold was manually set to be the same across all runs within the Rotor-Gene Q software. C_T values of sample replicates were excluded if > 0.3 C_T difference was noted and samples were then run again in a subsequent PCR reaction. Inbuilt analysis via the 2-standard curve method was employed to obtain relative gene expression for each sample.

Despite multiple attempts with 2 different TaqMan$^{®}$ probes for 11β-HSD-2, reproducible results could not be obtained for half the samples and hence further analysis did not proceed. These inaccuracies were also noted for the DNA standards used with these probes (data not shown).

Sample ID	ng/ μL	A_{260}	A_{280}	A_{260}/A_{280}	A_{260}/A_{230}
1	27.3	0.682	0.318	2.14	0.51
2	7.1	0.178	0.069	2.57	0.12
3	38.0	0.950	0.477	*1.99	1.24
4	4.2	0.105	0.042	2.53	0.48
5	17.8	0.445	0.209	2.13	1.67
6	33.2	0.829	0.387	2.14	1.08
7	30.8	0.770	0.371	2.08	0.64
8	10.9	0.272	0.117	2.33	0.06
9	39.6	0.990	0.478	2.07	1.39
10	11.7	0.291	0.125	2.33	0.58
11	36.2	0.906	0.432	2.10	0.33
12	19.6	0.491	0.234	2.10	1.82
13	105.7	2.642	1.293	2.04	0.76
14	83.1	2.079	1.025	2.03	0.73
15	26.6	0.666	0.325	2.05	0.78
16	83.3	2.084	1.021	2.04	1.19
17	48.2	1.206	0.581	2.07	1.35
18	101.7	2.543	1.242	2.05	1.56
19	63.6	1.589	0.819	*1.94	0.59
20	61.2	1.531	0.756	2.03	0.80
21	11.7	0.292	0.151	*1.93	0.10
22	26.2	0.654	0.319	2.05	0.54
23	48.8	1.220	0.572	2.13	1.17
24	39.6	0.990	0.490	2.02	0.51

Table 4.1 Nanodrop results for RNA extracted from skin samples.

* denotes A260/A280 ratios under 2.0.
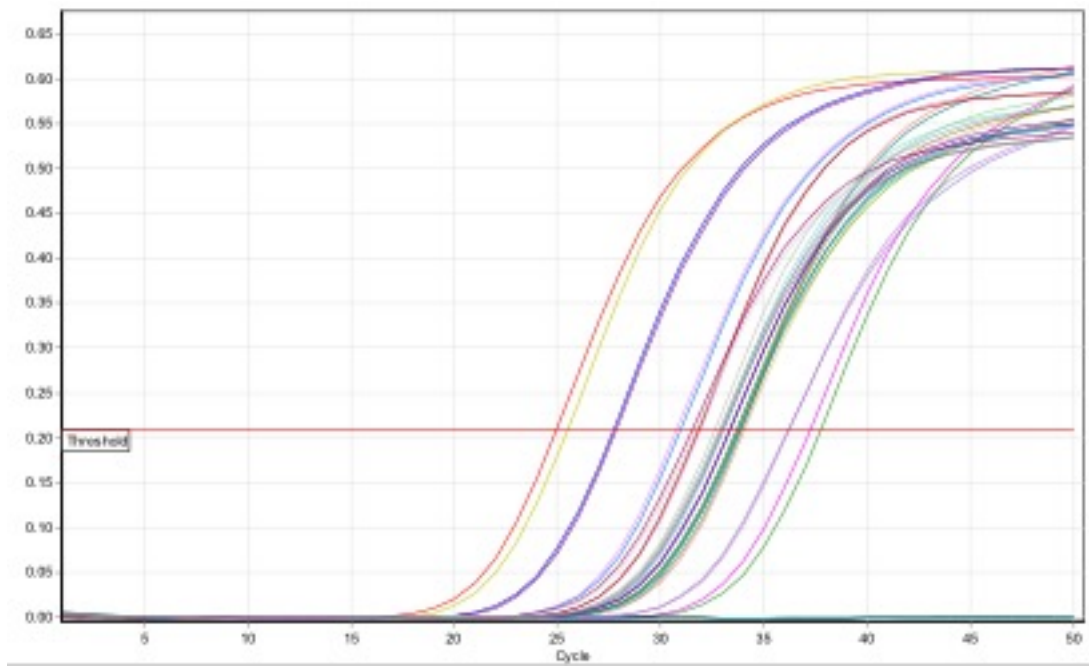
Figure 4.36 Representative amplification curves of gene of interest 11β-HSD-1.
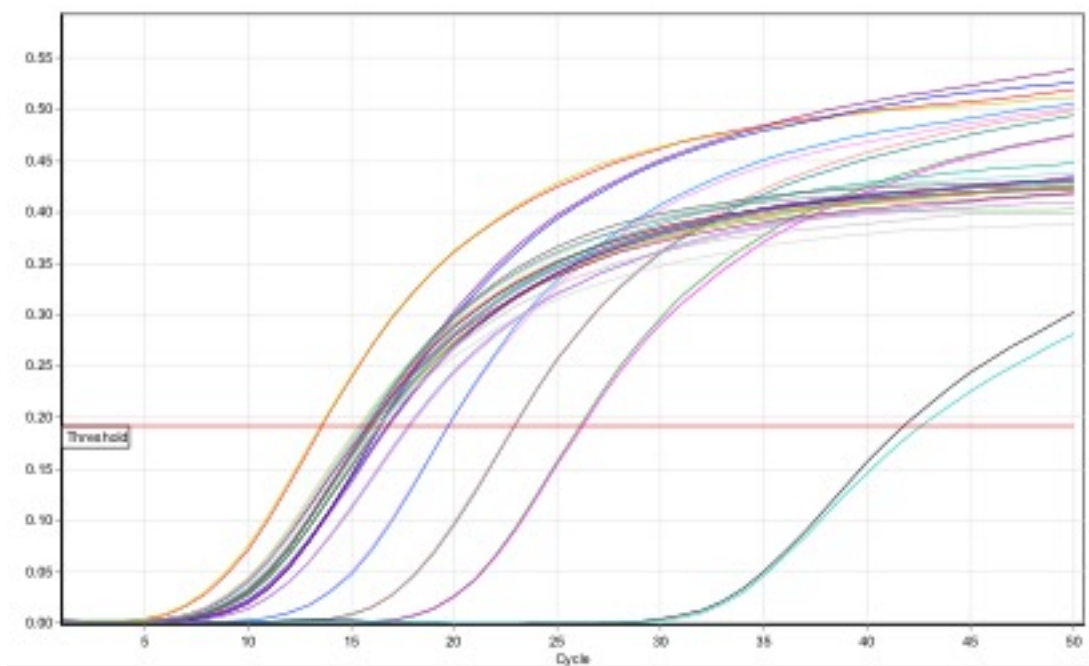
Figure 4.37 Representative amplification curves of housekeeping gene B2M.
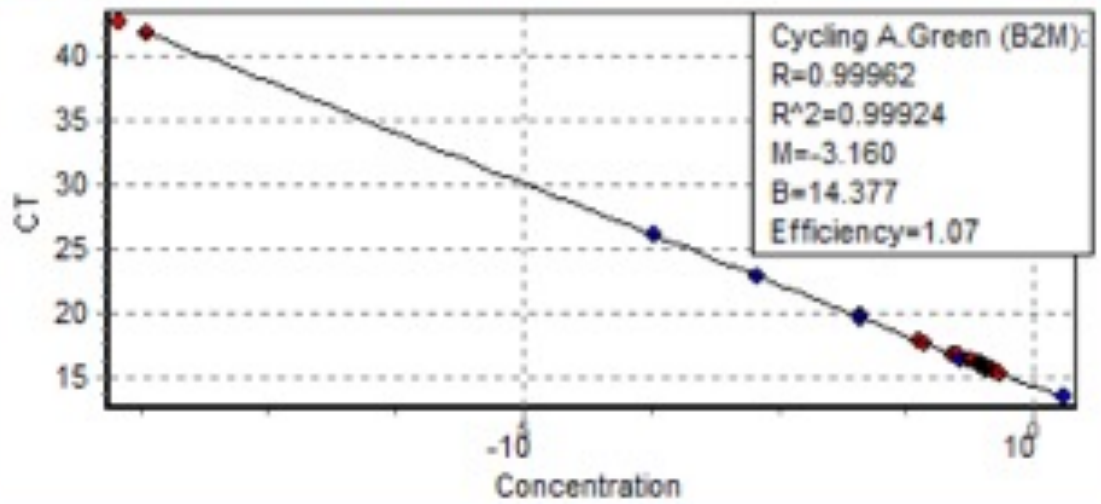
Figure 4.38 Representative standard curve from PCR analysis. Standard curve replicates demonstrated in blue, unknown samples and No Template Controls demonstrated in red.

Sample	11β-HSD-1 Concentration ng/μL	B2M Concentration ng/μL	Relative Concentration
1	0.0028	0.7216	0.0040
2	0.0055	0.5418	0.0090
3	0.0005	0.1111	0.0040
4	0.0001	0.0475	0.0030
5	0.0650	0.7100	0.1040
6	0.0696	0.6568	0.1200
7	0.0121	0.4168	0.0260
8	0.0030	0.2714	0.0100
9	0.0030	0.2838	0.0100
10	0.0242	0.3670	0.0750
11	0.0268	0.2101	0.1450
12	0.0194	0.2831	0.0780
13	0.0040	0.1928	0.0190
14	0.0214	0.6388	0.0330
15	0.0650	0.2288	0.3230
16	0.1071	0.1246	0.9780
17	0.0123	0.9699	0.0120
18	0.0155	0.5487	0.0280
19	0.0062	0.3319	0.0170
20	0.0052	0.4256	0.0110
21	0.0074	0.1969	0.0370
22	0.0298	0.0200	1.6950
23	0.0177	0.6067	0.0290
24	0.0066	0.3573	0.0180

Table 4.2 11β-HSD-1 Expression Relative to B2M expression.
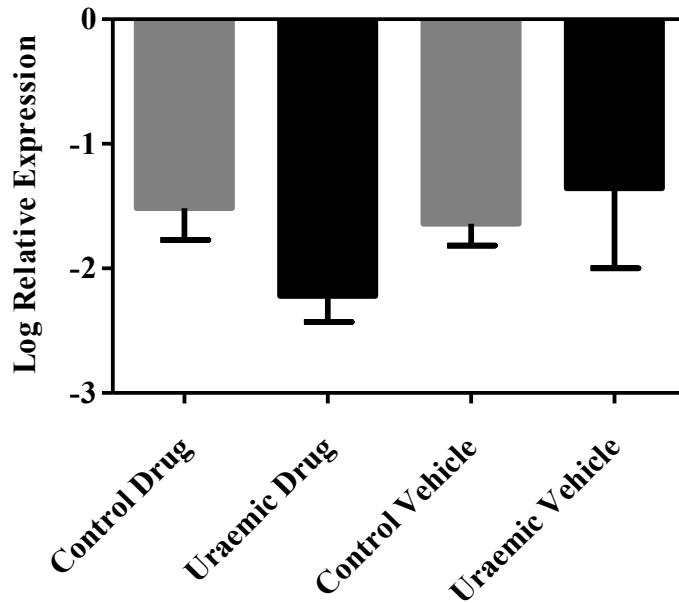
Figure 4.39 Relative expression of 11β-HSD-1 normalised to B2M. n= 6 per group. Data represented as median + 95% CI, analysed by Kruskal Wallis with Dunn's multiple comparison test.

No significant differences in 11β-HSD-1 mRNA expression were noted between the drug treated groups or the vehicle treated groups. In addition, there were no significant differences noted between each uraemic group and its respective control (Figure 4.39).

4.2.6.2 Wound Healing PCR Array

12 of the RNA samples extracted to use for PCR were also reverse transcribed using the RT[2] First Strand Kit for use in a Rat Wound Healing PCR Array (both Qiagen). This commercially available array is ready prepared with primer assays for 84 wound healing focused genes and 5 housekeeping genes as well as PCR controls. Using one RNA sample per array, the expression of key genes involved in all aspects of the wound healing response can be acquired. This profile can then be compared across differing experimental conditions to ascertain those genes with altered expression under said conditions. In these experiments, 3 samples were utilised per treatment group; control emodin treated, uraemic emodin treated, control vehicle treated and uraemic vehicle treated.

4.2.6.2.1 Quality Control PCR Array

All 12 cDNA samples were first run in a Quality Control array (Qiagen) to ensure they were suitable for use in further experiments. Reverse transcription controls are included to check for impurities in the RNA sample that can affect the reverse transcription step of the array, whereas the Positive PCR control checks for impurities in the sample that could inhibit the PCR amplification of the positive PCR control and hence also the mRNA of interest. The Genomic DNA control is included to ascertain whether the sample has been contaminated with genomic DNA. The No Reverse Transcription Control is an additional control to assess the amount of DNA contamination in the sample as the reverse transcriptase enzyme is absent. Finally, a No Template Control does not contain DNA or RNA template, hence serves as a control for any nucleic acid contamination. The pass/fail considerations and results obtained are demonstrated in Table 4.3 and 4.4 respectively. The 12 chosen samples fulfilled all the necessary requirements to proceed

	Pass	Fail
Reverse Transcription Control (RTC)	$C_T^{25\ to\ 36} - C_T^{73\ to\ 84}$ value < 5	$C_T^{25\ to\ 36} - C_T^{73\ to\ 84}$ value > 5
Positive PCR Control (PPC)	$C_T^{37\ to\ 48} - C_T^{73\ to\ 84} < 3$	$C_T^{37\ to\ 48} - C_T^{73\ to\ 84} > 3$
Genomic DNA Contamination Control (GDC)	$C_T^{49-60} > 33$	$C_T^{49-60} < 33$
No Reverse Transcription Control (NRT)	$C_T^{61\ to\ 72}$ value ≥ 33 or NA	$C_T^{61\ to\ 72}$ value < 33 or NA
No Template Control (NTC)	$C_T^{85\ to\ 96}$ value ≥ 33 or NA	$C_T^{85\ to\ 96}$ value < 33 or NA

Table 4.3 Quality control parameters to ascertain whether RNA samples are suitable to proceed with further experimentation.

Numbers in superscript denote well position on RotorDisc-100. Adapted from Qiagen (151)

Sample	RTC	PPC	GDC	NRT	NTC
1	2.57	0.26	> 35	36.26	> 35
2	2.69	0.39	> 35	> 35	> 35
3	2.30	0.35	> 35	> 35	> 35
4	2.06	0.31	> 35	> 35	> 35
5	2.03	0.31	35.76	> 35	> 35
6	2.20	0.33	> 35	> 35	> 35
7	3.03	0.50	> 35	> 35	> 35
8	2.75	0.41	33.48	> 35	> 35
9	2.12	0.13	36.97	38.36	> 35
10	2.51	0.44	> 35	> 35	> 35
11	2.91	0.27	> 35	> 35	> 35
12	2.36	0.26	34.48	34.6	> 35

Table 4.4 Quality control PCR array results for RNA samples.

4.2.6.2.2 Rat Wound Healing PCR Array

Each RNA sample was run in a separate Rat Wound Healing PCR array Rotor-disc 100 ring (Qiagen) under identical run conditions to obtain C_T values per gene of interest. The C_T values were collated in one Microsoft Excel file and analysed using Qiagen's data analysis centre. The following volcano plots were obtained for the data analysed.
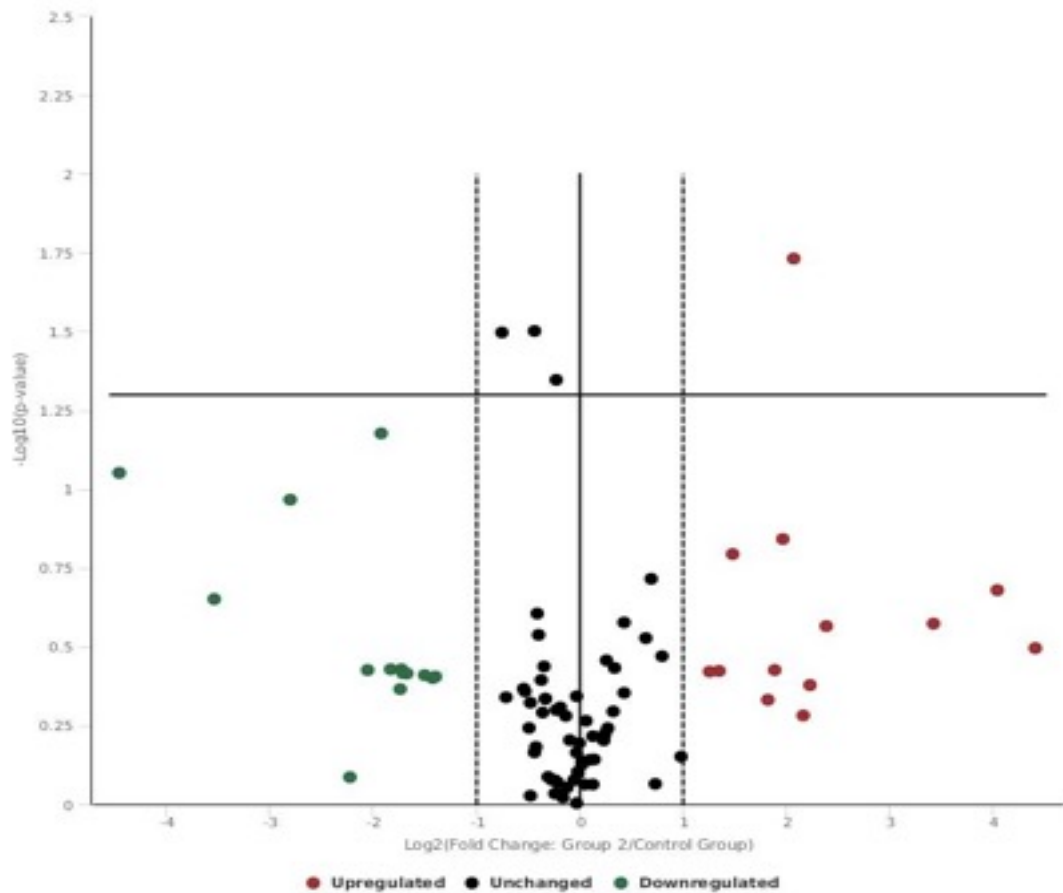
Figure 4.40 Volcano plot for gene expression when comparing uraemic vehicle treated animals with control vehicle treated animals. This plot displays statistical significance of $p < 0.05$ (y-axis) against fold change of 2 (x-axis). Genes above the horizontal black line are statistically significant as per the Student's t-test.

Genes Over Expressed	Fold Change	*p* Value
Itga5	4.21	0.0186

Table 4.5 Genes over expressed with greater 2 fold difference when comparing uraemic vehicle treated animals with control vehicle treated animals.
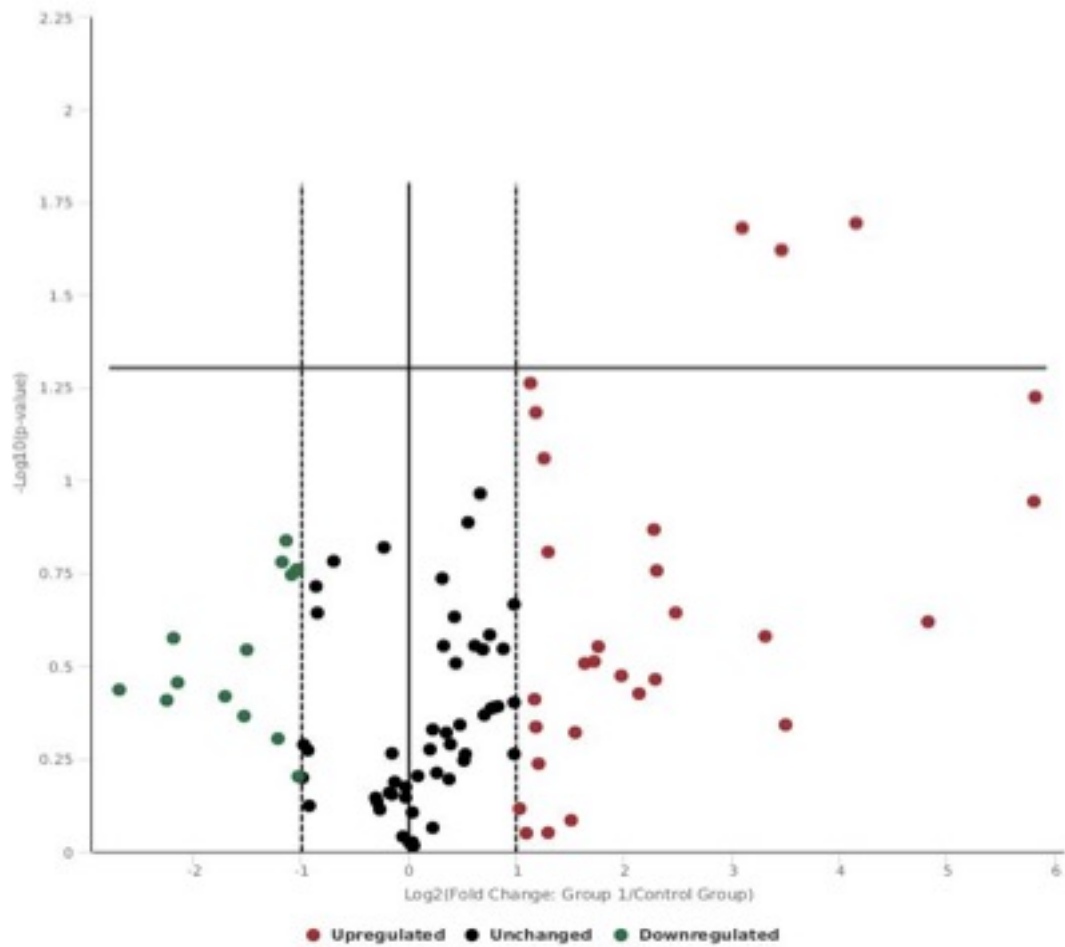
Figure 4.41 Volcano plot for gene expression when comparing control emodin treated animals with control vehicle treated animals. This plot displays statistical significance of $p < 0.05$ (y-axis) against fold change of 2 (x-axis). Genes above the horizontal black line are statistically significant as per the Student's t-test.

Genes Over Expressed	Fold Change	*p* Value
Cxcl3	17.78	0.0203
Col4a1	11.07	0.0239
Wnt5a	8.55	0.0209

Table 4.6 Genes over expressed with greater than 2 fold difference when comparing control emodin treated animals with control vehicle treated animals.
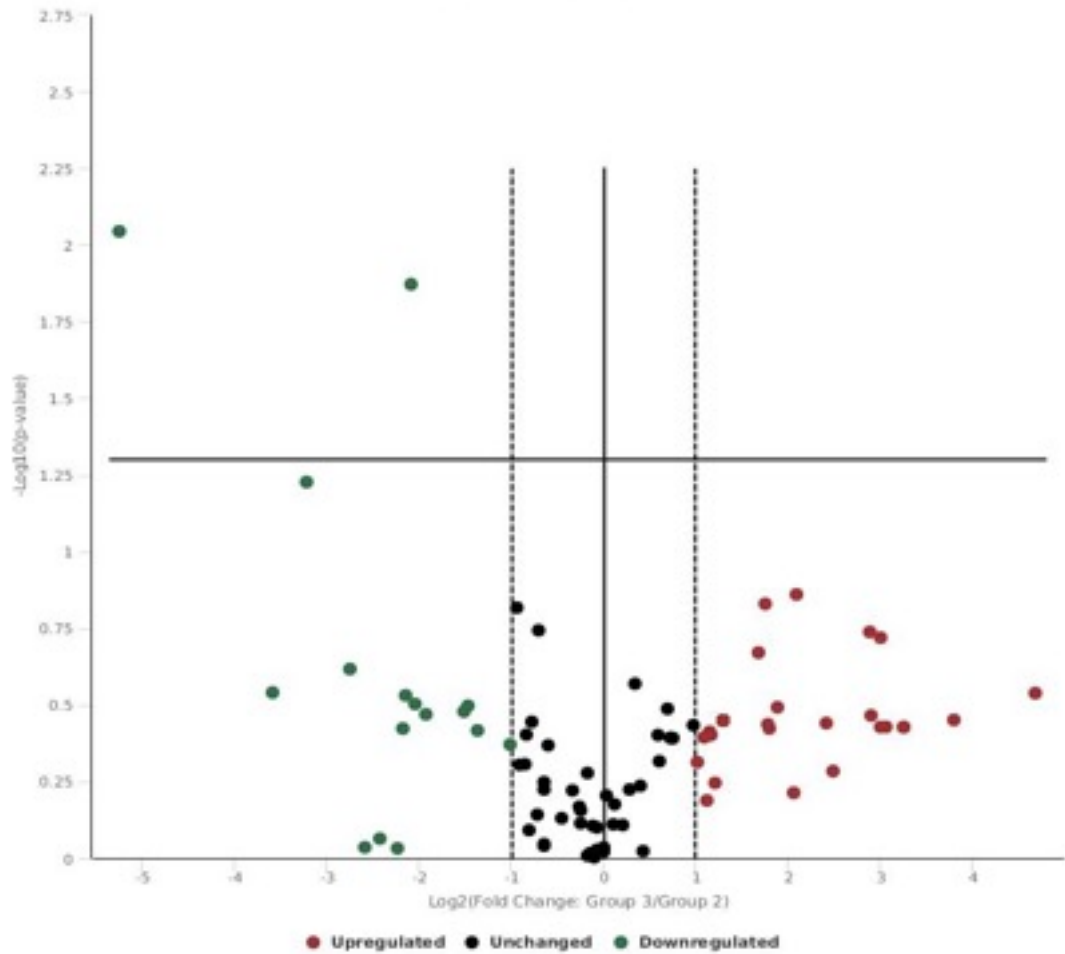
Figure 4.42 Volcano plot for gene expression when comparing uraemic emodin treated animals with uraemic vehicle treated animals. This plot displays statistical significance of p < 0.05 (y-axis) against fold change of 2 (x-axis). Genes above the horizontal black line are statistically significant as per the Student's t-test.

Genes Under Expressed	Fold Change	*p* Value
Plat	-37.87	0.0090
Itga5	-4.24	0.0134

Table 4.7 Genes under expressed with greater than 2 fold difference when comparing uraemic emodin treated animals with uraemic vehicle treated animals.

4.2.6.2.3 Interpretation of Wound Healing Arrays

4.2.6.2.3.1 The Effect of Uraemia on Wound Healing Related Gene Transcription

When comparing uraemic vehicle treated versus control vehicle treated groups, infererences can be made with regards to wound healing gene transcription that could be altered by the uraemic state. Only one gene showed a greater than 2 fold difference in expression with a significance of $p < 0.005$. (See appendix for gene expression that may be altered but did not reach statistical significance).

Itga5 was expressed 4.21 fold greater in uraemic animals than control animals ($p = 0.0186$). The integrin family of heterodimeric transmembrane receptors are important in mediating cell attachments to extracellular matrix molecules and adjacent cells. They are composed of an alpha chain and a beta chain (176). Integrin 5 alpha is one such protein which undergoes post-translational cleavage, binding with a beta 1 chain to form a fibronectin receptor. During wound healing, migrating keratinocytes at the leading edge of the wound have been shown to express $\alpha_5\beta_1$ thought to allow keratinocyte attachment and migration over the wound matrix (177, 178). Integrins also have a role in cell-surface mediated signalling (176).

4.2.6.2.3.2 The Effect of Emodin on Wound Healing Related Gene Transcription in Control Animals

When comparing control emodin treated versus control vehicle treated groups, inferences can be made with regards to wound healing gene transcription that could be mediated by emodin. Three genes showed a greater than 2 fold difference in expression with a significance of $p < 0.005$. (See appendix for gene expression that may be altered but did not reach statistical significance).

Cxcl3 was expressed 17.78 fold greater in emodin treated control animals than control vehicle treated animals ($p = 0.0203$). Chemokines are chemoattractive proteins implicated in cell to cell communication as well as directing migration of structural cells (179). Chemokine ligand 3 is a cytokine involved in the acute inflammatory response. It has a role in recruiting and activating polymorphonuclear leukocytes as well as bearing pro angiogenic properties (180).

Col4a1 was expressed 11.07 fold greater in emodin treated control animals than control vehicle treated animals (p = 0.0239). Collagen type IV alpha 1 is a subunit of type IV collagen, a major structural component of the BM (181). The non collagenous domain or NC1 domain has been shown to possess antiangiogenic properties *in vivo*. NCI binds to $\alpha 1\beta 1$ integrin, inhibiting signalling pathways in vascular epithelial cells (182). It has also been found to regulate HIF-1α and VEGF by inhibiting the Mitogen-Activated Protein Kinases (MAPK) signaling cascade (182, 183).

Wnt5a was expressed 8.55 fold greater in emodin treated control animals than control vehicle treated animals (p = 0.0209). Wnts are lipid modified secreted glycoproteins that have roles in the regulation of development, cell proliferation and differentiation (184). Wnt5a has been shown to have an important role in hair follicle morphogenesis (185). In addition, it is expressed in human primary endothelial cells as well as murine vasculature and has been shown to promote angiogenesis, induce endothelial cell proliferation and enhance cell survival. Wnt5a expression has also been shown to enhance capillary network formation (186).

4.2.6.2.3.3 The Effect of Emodin on Wound Healing Related Gene Transcription in Uraemic Animals

When comparing uraemic emodin treated versus uraemic vehicle treated groups, inferences can be made with regards to wound healing gene transcription that could be mediated by emodin but altered by the uraemic state. Two genes showed a greater than 2 fold difference in expression with a significance of p < 0.005. (See appendix for gene expression that may be altered but did not reach statistical significance).

Plat was expressed 37.87 fold less in uraemic emodin treated animals compared to uraemic vehicle treated animals (p = 0.009). Tissue plasminogen activator is a serine protease found on endothelial cells and histiocytes (187). It catalyzes the conversion of plasminogen to plasmin. Plasmin is an enzyme involved in the break down of blood clots (188, 189). Studies have shown wound closure is delayed in plasminogen deficient mice (190). Sulnite *et al.* demonstrated plasminogen transport to the wound by inflammatory cells and that in plasminogen deficient mice, excess fibrin and neutrophil deposition was observed in the wound after re-epethelialisation had

occurred, representing chronic inflammation. They postulated that fibroblast function was impaired in the absence of plasminogen contributing to a delay in granulation tissue formation. Hence, as well as being an activator of the inflammatory phase of healing, plasminogen is also required to terminate the inflammatory phase appropriately (191).

Itga5 was expressed 4.24 fold less in uraemic emodin treated animals compared to uraemic vehicle treated animals (p = 0.0134). Intrestingly this was downregulated with emodin treatment in uraemia where as the gene was significantly upregulated in uraemic vehicle animals compared to control vehicle treated animals (section 4.2.6.2.3.1).

4.2.7 Histology

Wounds and surrounding skin sections obtained as 24 animals were culled on day 7 after either emodin or vehicle administration (see section 2.2.3.3 and 2.2.4) were excised, bisected, mounted on PVDF membrane (Fisher Scientific Ltd) and placed in 10% neutral buffered formalin solution (Sigma-Aldrich). A small portion of the liver was retrieved to use as a positive control. After 24 hours, these were transferred and stored in 70% ethanol (VWR International Ltd) before processing by Ismail Bulut at Barts Health NHS Trust. After paraffin embedding, sections obtained were stained with haematoxylin and eosin (not shown), 11β-HSD-1 (Aviva Systems Biology) and Picro-sirius red (Sigma-Aldrich) (Figures 4.43. 4.44 and 4.45).

Professor Sheaff at Barts Health NHS Trust, who was blinded to the animals' treatment groups, reviewed all slides, allocating each animal a weighted score based on the intensity of 11β-HSD-1 staining in the sections. Figure 4.46 demonstrates the median score by each treatment group. No significant differences were noted between the drug treated groups or the vehicle treated groups. There were also no significant differences in the intensity of 11β-HSD-1 staining between the two control groups or between the two uraemic groups. 11β-HSD-1 was reported to be present in keratinocytes, fibroblasts, endothelial cells as well as inflammatory cells, with no predominance for a single cell type. Additionally, 11β-HSD-1 staining was observed in subcutaneous muscle as expected.

Picro-sirius red staining was performed as a difference in collagen presence in uraemic versus control animals could be pertinent in wound healing. Although formal histological analysis has not yet been performed, there appears to be no difference in distribution or density of collagen whether the sections are from uraemic animals or drug treated animals.

A
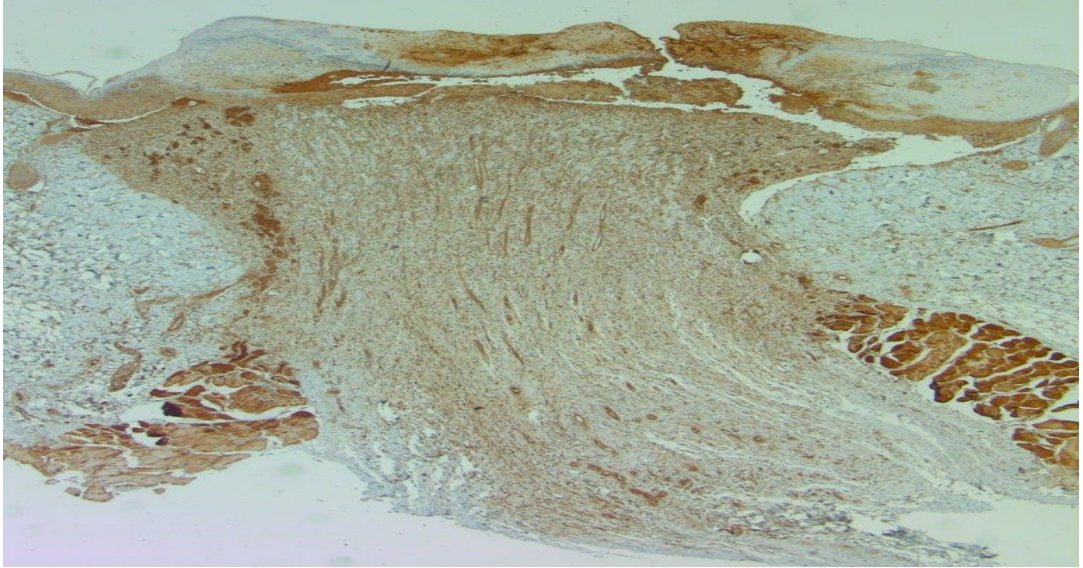
B
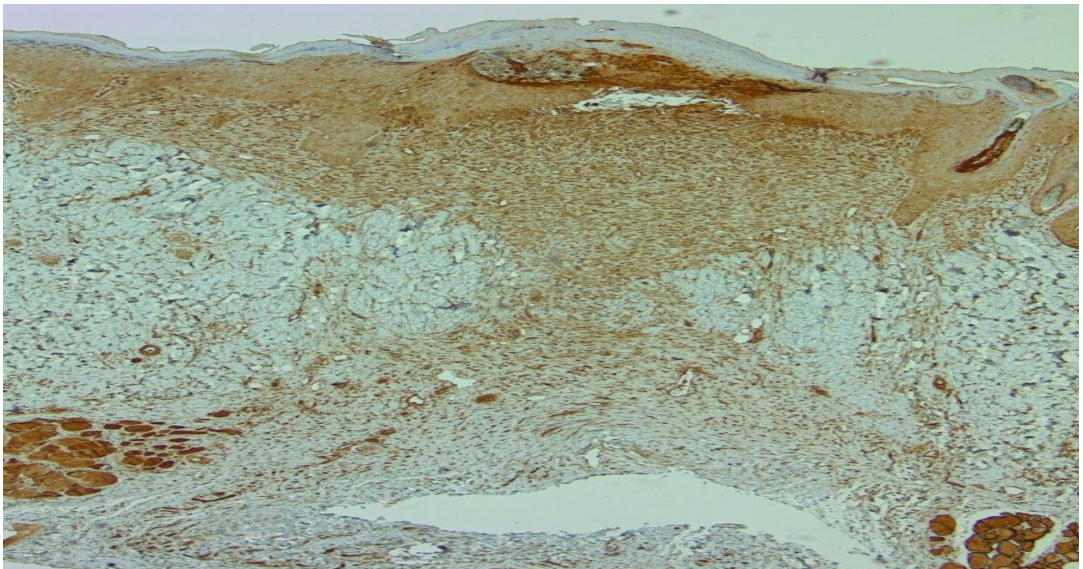
Figure 4.43 Immunohistochemistry for 11β-HSD-1 on representative skin sections. 40X magnification. A) control vehicle treated, B) control drug treated, C) uraemic drug treated and D) uraemic vehicle treated (C & D overleaf). Wounds and surrounding skin retrieved from rats at time of culling at day 7 after systemic emodin or vehicle administration.

C
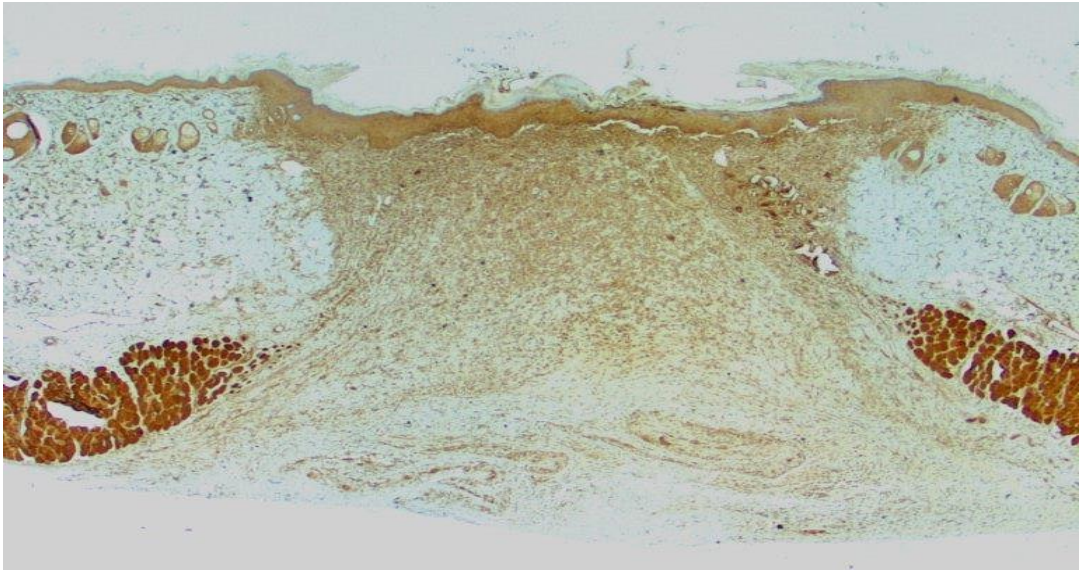
D
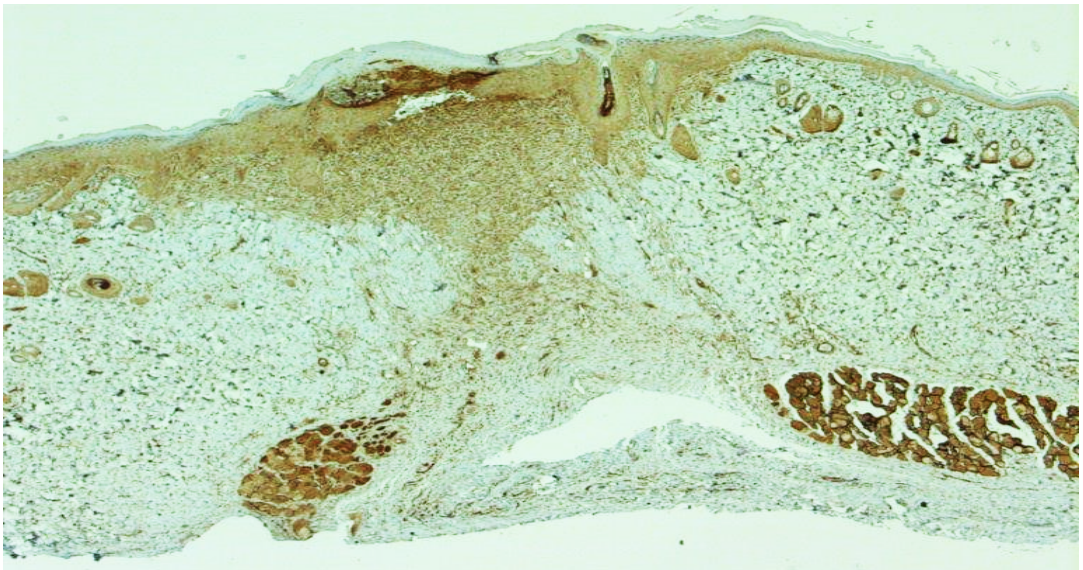
A
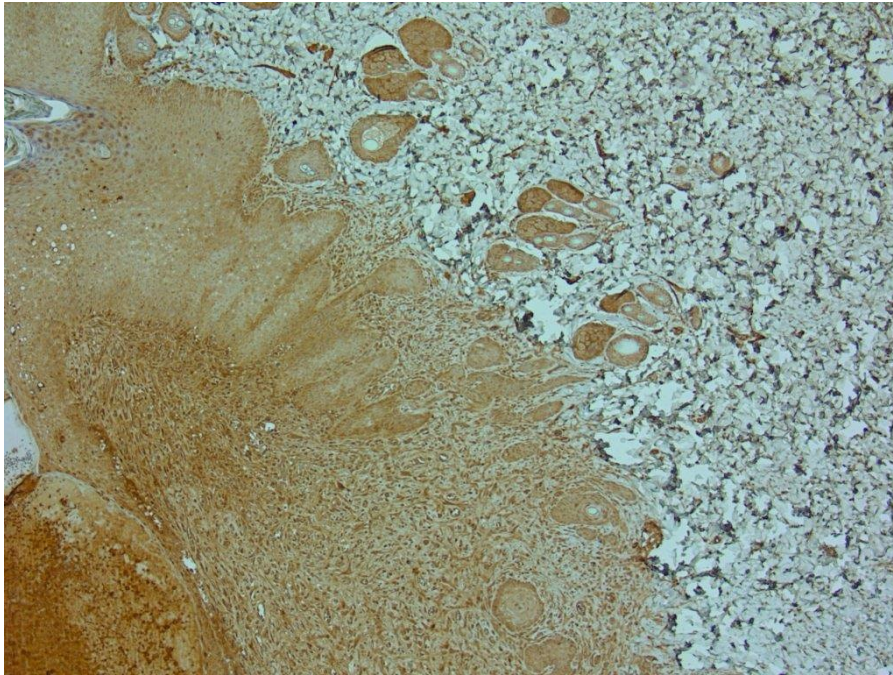
B
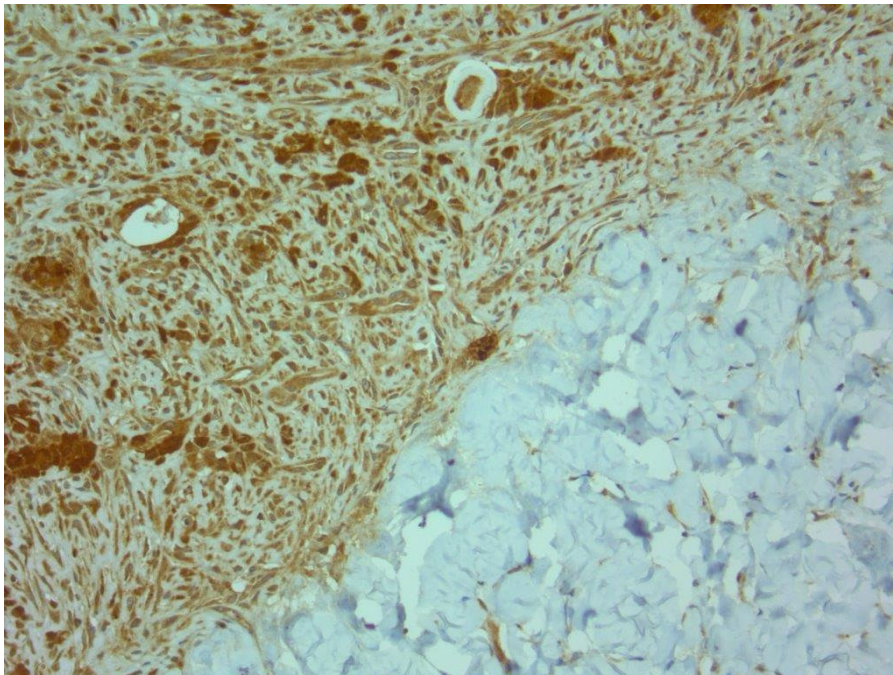
Figure 4.44 Immunohistochemistry for 11β-HSD-1 on representative skin sections. A) magnification 100X B) magnification 250X.

A
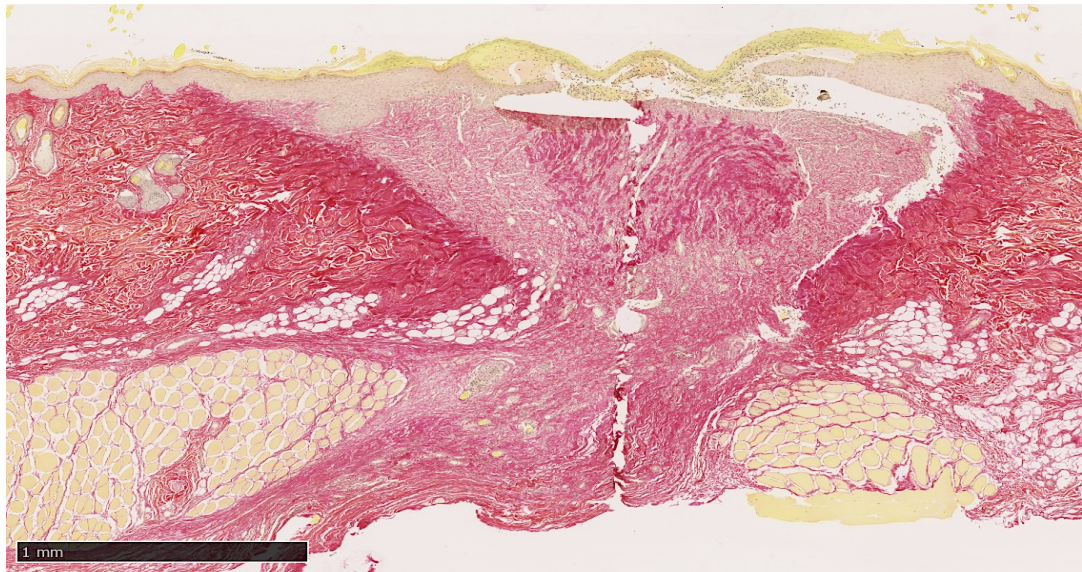
B
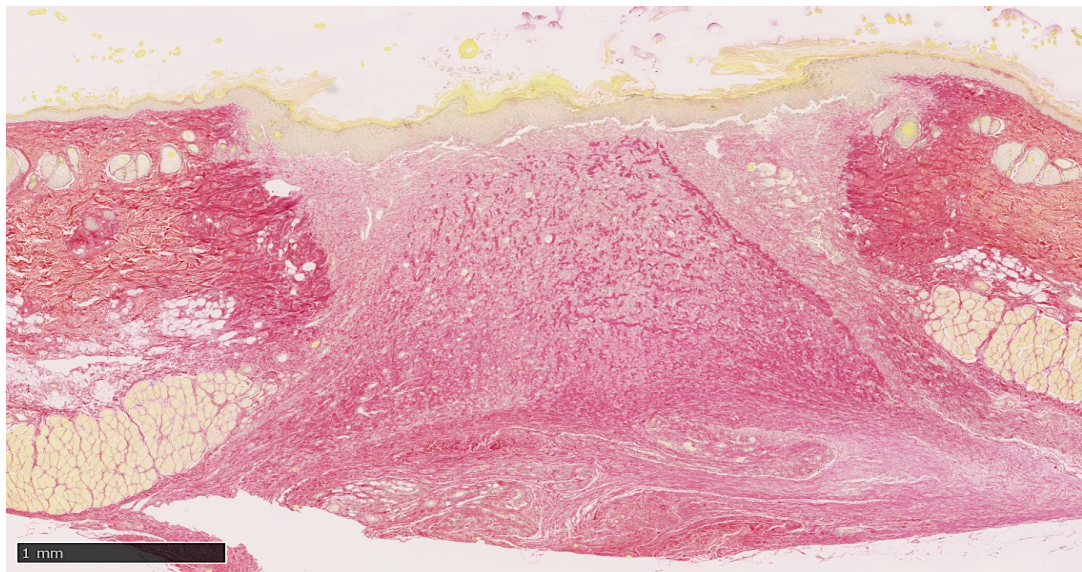
Figure 4.45 Immunohistochemistry for Picro-sirius red on representative skin sections. A) control vehicle treated, B) control drug treated, C) uraemic drug treated and D) uraemic vehicle treated (C & D overleaf). Wounds and surrounding skin retrieved from rats at time of culling at day 7 after systemic emodin or vehicle administration. Scale demonstrated on figure.

C

D
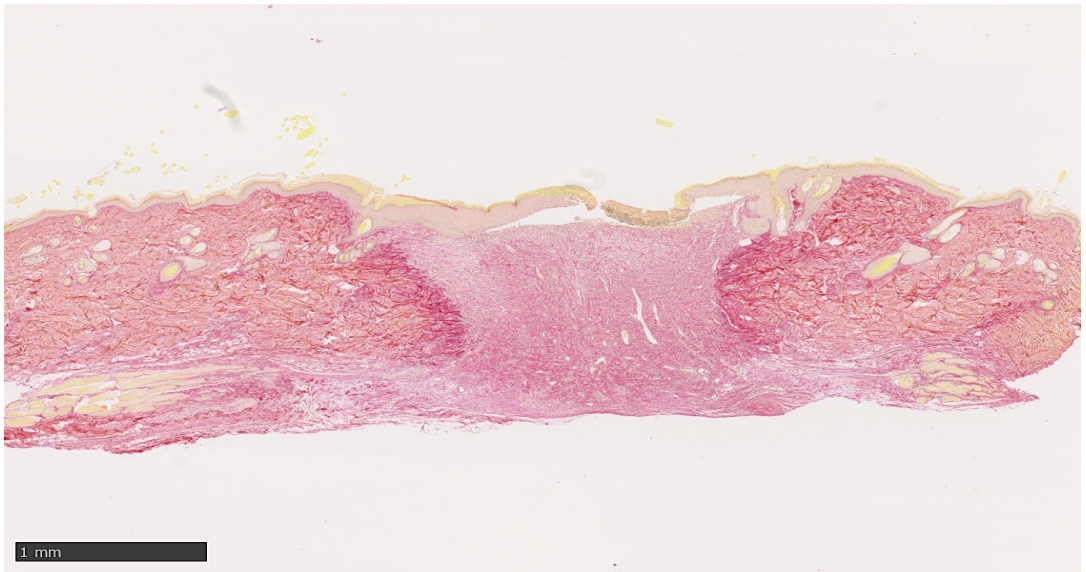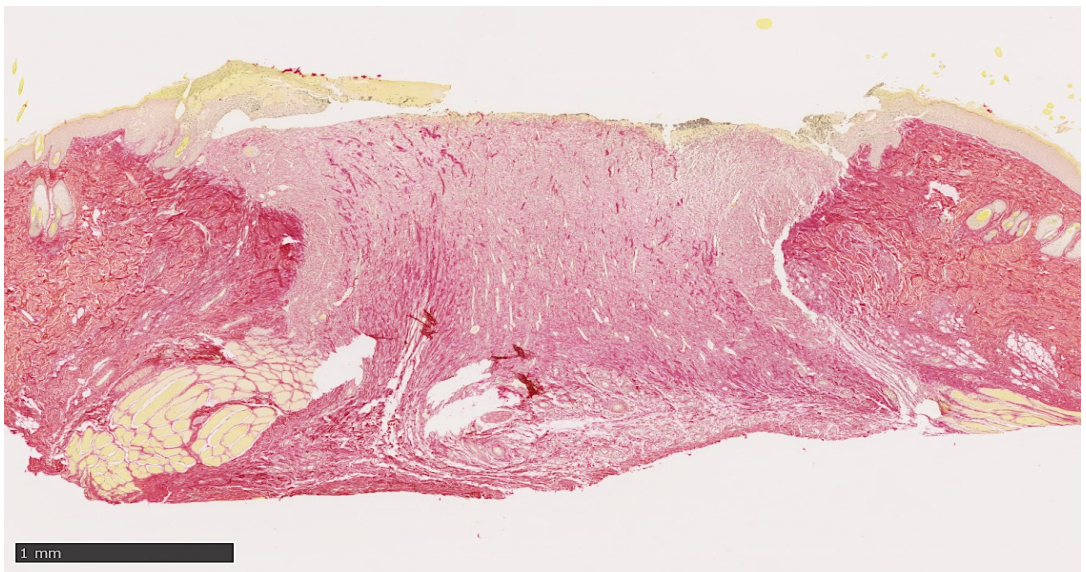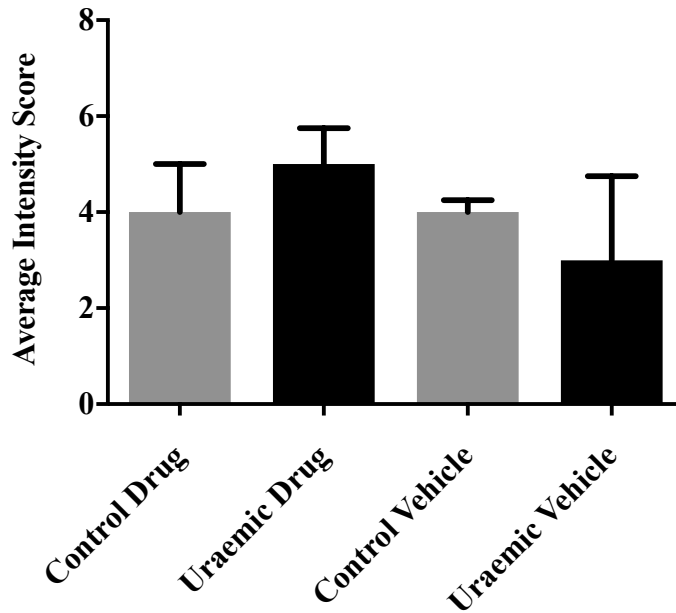
Figure 4.46 11β-HSD-1 intensity score. Intensity of immunohistochemical staining for 11β-HSD-1 on skin sections was assessed by a Consultant Histopathologist in a blinded fashion. No significance difference was reported between groups irrespective of whether systemic emodin or vehicle was administered. n = 12 wounds per group. Data represented as median + 95% CI, analysed by Kruskal Wallis with Dunn's multiple comparison test.

4.3 Discussion

11β-HSD-1 is a bidirectional enzyme. Although oxoreductase activity has previously been shown to predominate in intact cells such as fibroblasts (80) (converting 11-dehydrocorticosterone to corticosterone in rodents), the directionality is unstable and dependent on the availability of NADPH, which in turn is reliant on H6PDH presence in high enough concentrations in the ER lumen (80-82). The enzyme is under complex regulatory control by many factors such as GC and stress (70, 80) which could only be controlled for in a limited way in experiments of this kind (same culture media, dark conditions in an incubator set at 37°C). Although skin samples were snap frozen in liquid nitrogen upon retrieval and stored at -80°C until ready for use, samples had to be defrosted to remove subcutaneous fat and weigh prior to incubation. Every effort was made to keep the samples on ice as much as possible, however, the effect freeze-

thawing may have had on enzyme activity is unknown. Ideally, both potential products of 11β-HSD-1 activity (11-dehydrocorticosterone and corticosterone) would have been measured on the media samples to determine the ratio of oxoreductase to dehydrogenase activity present, although it would be difficult to remove 11β-HSD-2 activity from this equation (catalyzes corticosterone to 11-dehydrocorticosterone). The optimal method to measure 11β-HSD-1 activity would be using isotopically labelled cortisol (192) which was unavailable to my laboratory group during the study period.

Although an *ex vivo* model of wound healing has been previously described by Stojadinovic *et al.* (98, 193), as has the determination of steroid concentrations from cell culture media (55), a combination of the two methods as used in this study has seldom been employed. Corticosterone concentrations obtained from experiments were within the range detectable by the assay (0.1 - 25 ng/mL) (194), but the conditions of the experiment such as 24-hour period of incubation of skin in the culture medium, volume of media per skin sample, composition of media may not have been fully optimized to measure peak skin corticosterone concentrations.

Many difficulties were encountered in processing skin samples to obtain sufficient total protein for western blotting and good quality and quantity RNA for PCR reactions. Various methods of homogenisation were attempted including using different lysis buffers, a BeadBug™ microtube homogenizer (Sigma-Aldrich) with changeable sized microbeads, the Cryo-Cup Grinder consisting of a double-walled insulating cup within which a stainless-steel mortar is embedded and a pestle made of a non-heat conductive plastic (Stratech Scientific Ltd, Cambridgeshire, UK), the Silent Crusher S Homogenizer (Type 5F) (Heidolph, Essex, UK) and a Micro Cryo Crusher (Stratech Scientific Ltd). Ultimately, manual homogenization using a rough coated ceramic pestle and mortar prevailed as the most effective method of skin breakdown to a fine powder. Plentiful liquid nitrogen was required to keep the system cool throughout as well as perseverance and acceptance each sample would take time and considerable arm strength.

Western blotting is a useful method for determining the presence or absence of a protein of interest, however no information can be ascertained as to whether the protein detected is physiologically active. Additionally, preliminary experiments are needed to optimize protein concentrations used in electrophoresis as well as primary and secondary antibody concentrations used in the detection phase. Unfortunately, once these conditions had been optimized the manufacturer of the antibodies used (Santa Cruz Biotechnology) had its research license revoked under the Animal Welfare Act due to allegations of mistreatment of goats and rabbits. Although it was still possible to purchase these antibodies commercially from other sources until stocks were exhausted, I considered this ethically questionable. Antibodies from an alternative producer (Aviva Systems Biology) were hence obtained and optimized for use in all experiments.

When quantifying 11β-HSD-1 mRNA expression in skin samples after 7 days of emodin or vehicle administration, no significant differences were noted between the 4 treatment groups. It may be that this time point is too late to observe differences as Tiganescu et al. noted early differences (at day 2) when examining wound healing in mice (94). It is important to appreciate that our study design differed from their experiments in that the rodents they used were female, hairless mice. Additionally, control skin used was unwounded skin obtained from the lower dorsal region of the same animals in contrast to data presented in this chapter. If skin including the wounded area had been used for western blots and PCR reactions, different results may have been obtained. Unfortunately, PCR for 11β-HSD-2 mRNA was unsuccessful despite multiple attempts using 2 different TaqMan$^{®}$ probes for 11β-HSD-2. Tiganescu et al. found 11β-HSD-2 mRNA expression was negligible in mice (92), it is possible that the rat specific probes used here were not able to give consistent results for a similar reason. As discussed with regards to western blotting, mRNA expression of a protein that is a bidirectional enzyme, does not enlighten us as to physiologically active consequences and thus has limited value in isolation.

The results of the wound healing array should also be interpreted with caution due to small group sizes (n = 3). Skin homogenates were used as source of RNA for the arrays, yield of RNA was reasonably low and high C_T values were obtained. The

online data analysis site advises interpreting these figures with caution, although a greater or less than 2-fold change may have been recorded, they cannot be validated without a reasonable number of biological replicates (See Appendix 7.3, 7.4 and 7.5 for full list of up and downregulated genes with explanations of why caution is required). It would be interesting to compare arrays performed on serum samples for the same animals and to increase each group's sample size.

We aspired to measure granulation tissue areas from skin sections to quantify healing. However, it became evident when mounting and sectioning samples that incorporating the centre of the wound was not possible (on tissue retrieval wounds were bisected possibly disrupting granulation tissue that had formed). It was reportedly difficult to ensure sections were cut in a plane exactly parallel to this meaning the wound area would not be consistently represented across samples.

The results obtained from the experiments within this chapter do consistently demonstrate reduced wound healing in uraemic rats when compared to control animals at 7 days. This effect was independent of serum or skin corticosterone concentrations and cannot be solely attributed to weight loss associated with the uraemic state. With the administration of systemic emodin, by day 7 wound healing in uraemic animals was seen to improve to the same level as non-uraemic animals also receiving the drug. No significant differences were reported in either 11β-HSD-1 or 11β-HSD-2 mRNA or protein expression using the methods employed. This was as predicted, as enzyme inhibition would not necessarily cause protein synthesis to be upregulated.

A positive control for the *in vivo* experiments (a compound known to promote wound healing specifically in uraemia), to my knowledge is not currently available. This could have been useful to evaluate the size of effect of emodin against. The use of additional known 11β-HSD-1 inhibitors such as R0151 (93) was precluded by accessibility and cost, although this inhibitor like others is yet to be studied in CKD.

The shortfalls of this study include the inability to measure 11β-HSD-1 activity reliably by the more sensitive and reproducible radioactive isotope assay to establish

the role of 11β-HSD-1 in wound healing. Additionally, such an assay will help in teasing out emodin induced 11β-HSD-1 inhibition or other pleotropic effects in wound healing. Comparing the effects of other 11β-HSD-1 specific inhibitors (in development for dementia and hypertension) would further substantiate a putative role of 11β-HSD-1 in wound healing. For definitive evidence a skin specific 11β-HSD-1 KO could be utilized. However, experiments conducted thus far would need to be repeated in a mouse model to ensure consistent results were obtained prior to using a KO model. Interestingly, translation of this experimental research could be relatively simple (after ethical approval) as human skin is readily accessible intra-operatively.

CHAPTER 5

Final Discussion

In this thesis, I have found that both 11β-HSD-1 and 11β-HSD-2 are present in HEK and HDF cell lysates (detected by western blotting). In response to treatment with the uraemic toxins IS and PC in isolation, 11β-HSD-1 and 11β-HSD-2 continued to be expressed, with no differences seen when compared to cells with no toxin exposure. HEK and HDF cells treated with the selective 11β-HSD-1 inhibitor emodin, unsurprisingly continued to express 11β-HSD-1 and 11β-HSD-2, again with no differences noted when compared to untreated cells. I established an *in vitro* wound healing scratch assay with and without solitary uraemic toxin exposure but did not demonstrate significant differences in healing with IS, PC or emodin. Despite the ease and reproducibility of this model, it cannot be used in the uraemic setting as it is likely many potential uraemic toxins play a role in combination rather than in isolation. Additionally, monolayer cell cultures do not provide a true to life environment to study the complex cell-cell or cell-extracellular matrix interactions involved in wound healing.

I aimed to determine the activity of 11β-HSD-1 in skin in uraemia which proved to be challenging with the techniques available in our laboratory. An indirect method of measuring enzyme activity was employed which measured the product of 11β-HSD-1 activity (cortisol in human cells and corticosterone for rodent samples). *In vitro,* upon addition of IS, PC or emodin the concentration of cortisol produced by HDF cells was too low to be detected. In HEK cells, cortisol concentrations were quantifiable but no differences in production were determined in the simulated uraemic environment or when cells were treated with emodin.

My *in vivo* studies confirmed the presence of 11β-HSD-1 and 11β-HSD-2 in the skin of uraemic as well as non-uraemic control Wistar rats. I have consistently demonstrated that rats have delayed wound healing in experimental uraemia. As expected there was no difference in the expression of both isoforms of 11β-HSD by western blotting in skin homogenates. I detected 11β-HSD-1 mRNA in equivalent quantities in uraemic and control rats although technical difficulties were encountered when assessing 11β-HSD-2 mRNA expression. Immunohistochemical analysis by a Consultant Histopathologist blinded to treatment groups corroborated the presence of 11β-HSD-1 in fibroblasts, keratinocytes and endothelial cells in the skin of both

uraemic and control animals with no clear differences in enzyme expression noted. I established an ELISA technique to measure corticosterone concentrations using skin samples *ex vivo* to indirectly assess 11β-HSD-1 activity but unfortunately this was not sensitive enough to delineate small changes in corticosterone production. I did not have access to a hot lab using radioactive isotope techniques in my institute during my studies to reliably measure 11β-HSD-1 activity.

Despite these difficulties, I could demonstrate that the 11β-HSD-1 inhibitor emodin administered systemically can restore wound healing in experimental uraemia. Although I encountered problems in the practicalities of topical emodin use in rats, I consider it still has potential to be used via the topical route, either as a cream or as embedded dressings in the clinical setting.

The work described in this thesis is a small step in addressing a deficit in the published literature regarding the important but neglected field of wound healing in patients with established renal failure. Delayed wound healing is associated with significant morbidity and mortality in uraemic patients. There is an urgent need to find novel therapies to promote speedy wound healing and I believe the work presented here provides the foundation for avenues to be pursued in future.

To confirm a role for 11β-HSD-1 in wound healing in uraemia, methods that can directly measure the enzyme activity and directionality should be pursued. Tiganescu *et al.* did demonstrate acceleration of wound healing with an inhibitor of 11β-HSD-1 (RO151) as well as by using a 11β-HSD-1 global KO mouse (93). The use of an 11β-HSD-1 skin specific KO could be employed to help validate such results in a uraemic mouse model designed to study wound healing.

It would be interesting to explore the mechanism of action of emodin in the uraemic state further. Emodin has previously been shown to improve wound healing after topical administration in non-uraemic rats (107). The authors suggested a TGF-β1 mediated upregulation of Smad 2/Smad 3 and downregulation of Smad 7 related gene transcription could be involved. However, in the work presented here, healing in emodin treated uraemic animals improved to equal that of emodin treated non-

168

uraemic animals at day 7. Why the beneficial actions of emodin would seem to prefer uraemic conditions thus far remains unanswered.

To assist further studies in wound healing in end stage renal failure, the wound healing array utilised in these studies could be used as a starting point. By analysing the serum of uraemic animals versus non uraemic animals (with larger group sizes) to elucidate which genes are upregulated or down regulated, which phase of wound healing is affected and potential biological pathways implicated, the net would be cast wide in the search for key effectors. Comparison to arrays run with RNA derived from skin samples could assist in narrowing down the search to a tissue specific level. Subsequent experiments could then be planned to substantiate these findings.

The field could be further expanded by studying healing across the 5 stages of chronic kidney disease, as well as in patients treated with haemodialysis, peritoneal dialysis or renal transplantation. Diabetes mellitus is a leading cause of CKD in the UK. Many patients suffer considerable morbidity owing to the combined effects of their diabetes and renal failure. An important clinical manifestation of this is the poor wound healing seen in diabetic foot ulcers, often leading to devastating limb amputations. It would be valuable to design a diabetic uraemic wound healing model to study factors implicated in poor healing as well as to develop therapeutic agents that could be used in the clinical setting to overcome these. The beneficial effects of 11β-HSD-1 inhibition attenuating insulin resistance in addition to my observations of improved wound healing makes this pathway an ideal candidate for future translational research. I would recommend that human skin from uraemic and non uraemic donors with and without diabetes be used to study differences in 11β-HSD-1 activity with the subsequent administration of topical therapies to verify restoration of wound healing.

The current standard of care in renal transplant recipients and patients afflicted with autoimmune conditions with kidney involvement such as the ANCA-associated vasculitides and lupus nephritis has included large doses of systemic glucocorticoids which are associated with a multitude of complications including delayed wound healing. Morgan *et al.* demonstrated that the reactivation of GCs by 11β-HSD-1 in peripheral tissues (rather than circulating levels) is a key contributor to the Cushingoid

phenotype of GC excess in mice. Moreover, the side effects associated with GC excess such as glucose intolerance, hepatic steatosis, adiposity, hypertension, myopathy and dermal atrophy were ameliorated in global 11β-HSD-1 KO mice (41). Considering this information, 11β-HSD-1 inhibition, either topically or systemically to mitigate the side effects of exogenously administered steroids in skin and other organs could prove highly beneficial.

The work described in this thesis demonstrates some of the complexities of studying wound healing in renal impairment. Nonetheless, poor healing remains an important clinical issue with scope for intervention to minimise complications and reduce morbidity and mortality. Finding targets such as 11β-HSD-1 (inhibition of which would be safe as KO mice do not exhibit any adverse phenotype) that could be inhibited with inexpensive drugs would be greatly welcomed.

6. References

1.   Merrill J, Hampers C. Uremia. New England Journal of Medicine. 1970;282(17):953-61.

2.   Thomas R, Kanso A, Sedor JR. Chronic kidney disease and its complications. Prim Care. 2008;35(2):329-44, vii.

3.   Herzog CA, Asinger RW, Berger AK, Charytan DM, Diez J, Hart RG, et al. Cardiovascular disease in chronic kidney disease. A clinical update from Kidney Disease: Improving Global Outcomes (KDIGO). Kidney Int. 2011;80(6):572-86.

4.   Kooman JP, Broers NJ, Usvyat L, Thijssen S, van der Sande FM, Cornelis T, et al. Out of control: accelerated aging in uremia. Nephrol Dial Transplant. 2013;28(1):48-54.

5.   Carrero JJ, Stenvinkel P, Fellstrom B, Qureshi AR, Lamb K, Heimburger O, et al. Telomere attrition is associated with inflammation, low fetuin-A levels and high mortality in prevalent haemodialysis patients. J Intern Med. 2008;263(3):302-12.

6.   Rao M. Aging and Nephrology The Sun Sets. Indian Journal of Nephrology. 2005;15(Supp 2):S3-S6.

7.   Kato S, Chmielewski M, Honda H, Pecoits-Filho R, Matsuo S, Yuzawa Y, et al. Aspects of immune dysfunction in end-stage renal disease. Clin J Am Soc Nephrol. 2008;3(5):1526-33.

8.   White WE, Yaqoob MM, Harwood SM. Aging and uremia: Is there cellular and molecular crossover? World J Nephrol. 2015;4(1):19-30.

9.   Kumar PJ, Clark ML. Kumar & Clark's clinical medicine. 8th ed. ed. Edinburgh: Saunders/Elsevier; 2012.

10.   Mescher A. Junqueira's Basic Histology: Text and Atlas, 12th Edition : Text and Atlas: Text and Atlas: Mcgraw-hill; 2009.

11.   Gawkrodger DJ. Dermatology : an illustrated colour text. 3rd ed. ed. Edinburgh: Churchill Livingstone; 2002.

12.   Braverman IM. The cutaneous microcirculation: ultrastructure and microanatomical organization. Microcirculation. 1997;4(3):329-40.

13.   Ngo MA, Sinitsyna NN, Qin Q, Rice RH. Oxygen-dependent differentiation of human keratinocytes. J Invest Dermatol. 2007;127(2):354-61.

14.   Eckert RL, Rorke EA. Molecular biology of keratinocyte differentiation. Environ Health Perspect. 1989;80:109-16.

15.   Elias PM. Stratum corneum defensive functions: an integrated view. J Invest Dermatol. 2005;125(2):183-200.

16.   Proksch E, Brandner JM, Jensen JM. The skin: an indispensable barrier. Exp Dermatol. 2008;17(12):1063-72.

17.   Gilchrest BA, Rowe JW, Mihm MC, Jr. Clinical and histological skin changes in chronic renal failure: evidence for a dialysis-resistant, transplant-responsive microangiopathy. Lancet. 1980;2(8207):1271-5.

18.   Lupi O, Rezende L, Zangrando M, Sessim M, Silveira CB, Sepulcri MAS, et al. Manifestações cutâneas na doença renal terminal. Anais Brasileiros de Dermatologia. 2011;86:319-26.

19.   Lewis S, Raj D, Guzman NJ. Renal failure: implications of chronic kidney disease in the management of the diabetic foot. Semin Vasc Surg. 2012;25(2):82-8.

20.   Avermaete A, Altmeyer P, Bacharach-Buhles M. Skin changes in dialysis patients: a review. Nephrol Dial Transplant. 2001;16(12):2293-6.

21.   Abdelbaqi-Salhab M, Shalhub S, Morgan MB. A current review of the cutaneous manifestations of renal disease. J Cutan Pathol. 2003;30(9):527-38.

22.   Escolar G, Diaz-Ricart M, Cases A. Uremic platelet dysfunction: past and present. Curr Hematol Rep. 2005;4(5):359-67.

23.   Horowitz HI, Cohen BD, Martinez P, Papayoanou MF. Defective ADP-induced platelet factor 3 activation in uremia. Blood. 1967;30(3):331-40.

24.   Noris M, Remuzzi G. Uremic bleeding: closing the circle after 30 years of controversies? Blood. 1999;94(8):2569-74.

25.   Brandenburg VM, Cozzolino M, Ketteler M. Calciphylaxis: a still unmet challenge. J Nephrol. 2011;24(2):142-8.

26.   Nigwekar SU, Wolf M, Sterns RH, Hix JK. Calciphylaxis from nonuremic causes: a systematic review. Clin J Am Soc Nephrol. 2008;3(4):1139-43.

27.   Essary LR, Wick MR. Cutaneous calciphylaxis. An underrecognized clinicopathologic entity. Am J Clin Pathol. 2000;113(2):280-7.

28.   Nigwekar SU, Kroshinsky D, Nazarian RM, Goverman J, Malhotra R, Jackson VA, et al. Calciphylaxis: risk factors, diagnosis, and treatment. Am J Kidney Dis. 2015;66(1):133-46.

29.   Mazhar AR, Johnson RJ, Gillen D, Stivelman JC, Ryan MJ, Davis CL, et al. Risk factors and mortality associated with calciphylaxis in end-stage renal disease. Kidney Int. 2001;60(1):324-32.

30.   Agarwal R, Brunelli SM, Williams K, Mitchell MD, Feldman HI, Umscheid CA. Gadolinium-based contrast agents and nephrogenic systemic fibrosis: a systematic review and meta-analysis. Nephrol Dial Transplant. 2009;24(3):856-63.

31.   Wagner B, Drel V, Gorin Y. Pathophysiology of gadolinium-associated systemic fibrosis. Am J Physiol Renal Physiol. 2016;311(1):F1-F11.

32.   Nainani N, Panesar M. Nephrogenic systemic fibrosis. Am J Nephrol. 2009;29(1):1-9.

33.   Maroz N, Simman R. Wound Healing in Patients With Impaired Kidney Function. J Am Coll Clin Wound Spec. 2013;5(1):2-7.

34.   Schwartz IF, Iaina A. Uraemic pruritus. Nephrol Dial Transplant. 1999;14(4):834-9.

35.   Wikstrom B, Gellert R, Ladefoged SD, Danda Y, Akai M, Ide K, et al. Kappa-opioid system in uremic pruritus: multicenter, randomized, double-blind, placebo-controlled clinical studies. J Am Soc Nephrol. 2005;16(12):3742-7.

36.   Odou P, Azar R, Luyckx M, Brunet C, Dine T. A hypothesis for endogenous opioid peptides in uraemic pruritus: role of enkephalin. Nephrol Dial Transplant. 2001;16(9):1953-4.

37.   Robinson-Bostom L, DiGiovanna JJ. Cutaneous manifestations of end-stage renal disease. J Am Acad Dermatol. 2000;43(6):975-86;quiz 87-90.

38.   Seth AK, De la Garza M, Fang RC, Hong SJ, Galiano RD. Excisional wound healing is delayed in a murine model of chronic kidney disease. PLoS One. 2013;8(3):e59979.

39.   Brewster UC. Dermatological disease in patients with CKD. Am J Kidney Dis. 2008;51(2):331-44.

40.   Gathercole LL, Lavery GG, Morgan SA, Cooper MS, Sinclair AJ, Tomlinson JW, et al. 11β-Hydroxysteroid Dehydrogenase 1: Translational and Therapeutic Aspects. Endocrine Reviews. 2013;34(4):525-55.

41.   Morgan SA, McCabe EL, Gathercole LL, Hassan-Smith ZK, Larner DP, Bujalska IJ, et al. 11beta-HSD1 is the major regulator of the tissue-specific effects of circulating glucocorticoid excess. Proc Natl Acad Sci U S A. 2014;111(24):E2482-91.

42.   Slominski A, Zbytek B, Nikolakis G, Manna PR, Skobowiat C, Zmijewski M, et al. Steroidogenesis in the skin: implications for local immune functions. J Steroid Biochem Mol Biol. 2013;137:107-23.

43.   Slominski AT, Manna PR, Tuckey RC. Cutaneous glucocorticosteroidogenesis: securing local homeostasis and the skin integrity. Exp Dermatol. 2014;23(6):369-74.

44.   Buhaescu I, Izzedine H. Mevalonate pathway: a review of clinical and therapeutical implications. Clin Biochem. 2007;40(9-10):575-84.

45.   Shepherd J. Who should receive a statin these days? Lessons from recent clinical trials. J Intern Med. 2006;260(4):305-19.

46.   Farsaei S, Khalili H, Farboud ES. Potential role of statins on wound healing: review of the literature. Int Wound J. 2012;9(3):238-47.

47.   Fitzmaurice GJ, McWilliams B, Nolke L, Redmond JM, McGuinness JG, O'Donnell ME. Do statins have a role in the promotion of postoperative wound healing in cardiac surgical patients? Ann Thorac Surg. 2014;98(2):756-64.

48.   Bitto A, Minutoli L, Altavilla D, Polito F, Fiumara T, Marini H, et al. Simvastatin enhances VEGF production and ameliorates impaired wound healing in experimental diabetes. Pharmacol Res. 2008;57(2):159-69.

49.   Rego AC, Araujo Filho I, Damasceno BP, Egito ES, Silveira IA, Brandao-Neto J, et al. Simvastatin improves the healing of infected skin wounds of rats. Acta Cir Bras. 2007;22 Suppl 1:57-63.

50.   Das S, Schapira M, Tomic-Canic M, Goyanka R, Cardozo T, Samuels HH. Farnesyl pyrophosphate is a novel transcriptional activator for a subset of nuclear hormone receptors. Mol Endocrinol. 2007;21(11):2672-86.

51.   Vukelic S, Stojadinovic O, Pastar I, Vouthounis C, Krzyzanowska A, Das S, et al. Farnesyl pyrophosphate inhibits epithelialization and wound healing through the glucocorticoid receptor. J Biol Chem. 2010;285(3):1980-8.

52.   Anuka E, Gal M, Stocco DM, Orly J. Expression and roles of steroidogenic acute regulatory (StAR) protein in 'non-classical', extra-adrenal and extra-gonadal cells and tissues. Mol Cell Endocrinol. 2013;371(1-2):47-61.

53.   Stocco DM, Clark BJ. Regulation of the acute production of steroids in steroidogenic cells. Endocr Rev. 1996;17(3):221-44.

54.   Slominski A, Ermak G, Mihm M. ACTH receptor, CYP11A1, CYP17 and CYP21A2 genes are expressed in skin. J Clin Endocrinol Metab. 1996;81(7):2746-9.

55.   Hannen RF, Michael AE, Jaulim A, Bhogal R, Burrin JM, Philpott MP. Steroid synthesis by primary human keratinocytes; implications for skin disease. Biochem Biophys Res Commun. 2011;404(1):62-7.

56.   Thiboutot D, Jabara S, McAllister JM, Sivarajah A, Gilliland K, Cong Z, et al. Human skin is a steroidogenic tissue: steroidogenic enzymes and cofactors are expressed in epidermis, normal sebocytes, and an immortalized sebocyte cell line (SEB-1). J Invest Dermatol. 2003;120(6):905-14.

57.   Cirillo N, Prime SS. Keratinocytes synthesize and activate cortisol. J Cell Biochem. 2011;112(6):1499-505.

58.   Terao M, Itoi S, Murota H, Katayama I. Expression profiles of cortisol-inactivating enzyme, 11beta-hydroxysteroid dehydrogenase-2, in human epidermal tumors and its role in keratinocyte proliferation. Exp Dermatol. 2013;22(2):98-101.

59.   Slominski A, Wortsman J, Luger T, Paus R, Solomon S. Corticotropin releasing hormone and proopiomelanocortin involvement in the cutaneous response to stress. Physiol Rev. 2000;80(3):979-1020.

60.   Slominski A, Zbytek B, Semak I, Sweatman T, Wortsman J. CRH stimulates POMC activity and corticosterone production in dermal fibroblasts. J Neuroimmunol. 2005;162(1-2):97-102.

61.   Slominski A, Zbytek B, Szczesniewski A, Wortsman J. Cultured human dermal fibroblasts do produce cortisol. J Invest Dermatol. 2006;126(5):1177-8.

62.   Hammami MM, Siiteri PK. Regulation of 11 beta-hydroxysteroid dehydrogenase activity in human skin fibroblasts: enzymatic modulation of glucocorticoid action. J Clin Endocrinol Metab. 1991;73(2):326-34.

63.   Itoi S, Terao M, Murota H, Katayama I. 11beta-Hydroxysteroid dehydrogenase 1 contributes to the pro-inflammatory response of keratinocytes. Biochem Biophys Res Commun. 2013;440(2):265-70.

64.   Skobowiat C, Slominski AT. UVB Activates Hypothalamic-Pituitary-Adrenal Axis in C57BL/6 Mice. J Invest Dermatol. 2015;135(6):1638-48.

65.   Slominski A, Zbytek B, Szczesniewski A, Semak I, Kaminski J, Sweatman T, et al. CRH stimulation of corticosteroids production in melanocytes is mediated by ACTH. Am J Physiol Endocrinol Metab. 2005;288(4):E701-6.

66.   Slominski A, Zbytek B, Zmijewski M, Slominski RM, Kauser S, Wortsman J, et al. Corticotropin releasing hormone and the skin. Front Biosci. 2006;11:2230-48.

67.   Slominski A, Wortsman J, Tuckey RC, Paus R. Differential expression of HPA axis homolog in the skin. Mol Cell Endocrinol. 2007;265-266:143-9.

68.   Lu NZ, Cidlowski JA. Translational regulatory mechanisms generate N-terminal glucocorticoid receptor isoforms with unique transcriptional target genes. Mol Cell. 2005;18(3):331-42.

69.   Oakley RH, Jewell CM, Yudt MR, Bofetiado DM, Cidlowski JA. The dominant negative activity of the human glucocorticoid receptor beta isoform. Specificity and mechanisms of action. J Biol Chem. 1999;274(39):27857-66.

70.   Tomlinson JW, Stewart PM. Cortisol metabolism and the role of 11beta-hydroxysteroid dehydrogenase. Best Pract Res Clin Endocrinol Metab. 2001;15(1):61-78.

71.   Monder C. Characterization and biological significance of corticosteroid 11 beta-dehydrogenase, the oxidizing component of 11 beta-hydroxysteroid dehydrogenase. Ann N Y Acad Sci. 1990;595:26-39.

72.   Ricketts ML, Verhaeg JM, Bujalska I, Howie AJ, Rainey WE, Stewart PM. Immunohistochemical localization of type 1 11beta-hydroxysteroid dehydrogenase in human tissues. J Clin Endocrinol Metab. 1998;83(4):1325-35.

73.   Hennebert O, Chalbot S, Alran S, Morfin R. Dehydroepiandrosterone 7alpha-hydroxylation in human tissues: possible interference with type 1 11beta-

hydroxysteroid dehydrogenase-mediated processes. J Steroid Biochem Mol Biol. 2007;104(3-5):326-33.

74.   White CI, Jansen MA, McGregor K, Mylonas KJ, Richardson RV, Thomson A, et al. Cardiomyocyte and Vascular Smooth Muscle-Independent 11beta-Hydroxysteroid Dehydrogenase 1 Amplifies Infarct Expansion, Hypertrophy, and the Development of Heart Failure After Myocardial Infarction in Male Mice. Endocrinology. 2016;157(1):346-57.

75.   Sheppard KE, Autelitano DJ. 11Beta-hydroxysteroid dehydrogenase 1 transforms 11-dehydrocorticosterone into transcriptionally active glucocorticoid in neonatal rat heart. Endocrinology. 2002;143(1):198-204.

76.   Cooper MS, Walker EA, Bland R, Fraser WD, Hewison M, Stewart PM. Expression and functional consequences of 11beta-hydroxysteroid dehydrogenase activity in human bone. Bone. 2000;27(3):375-81.

77.   Sun K, Yang K, Challis JR. Differential expression of 11 beta-hydroxysteroid dehydrogenase types 1 and 2 in human placenta and fetal membranes. J Clin Endocrinol Metab. 1997;82(1):300-5.

78.   Chapman K, Holmes M, Seckl J. 11beta-hydroxysteroid dehydrogenases: intracellular gate-keepers of tissue glucocorticoid action. Physiol Rev. 2013;93(3):1139-206.

79.   Odermatt A, Arnold P, Stauffer A, Frey BM, Frey FJ. The N-terminal anchor sequences of 11beta-hydroxysteroid dehydrogenases determine their orientation in the endoplasmic reticulum membrane. J Biol Chem. 1999;274(40):28762-70.

80.   Tomlinson JW, Walker EA, Bujalska IJ, Draper N, Lavery GG, Cooper MS, et al. 11beta-hydroxysteroid dehydrogenase type 1: a tissue-specific regulator of glucocorticoid response. Endocr Rev. 2004;25(5):831-66.

81.   Lakshmi V, Monder C. Purification and characterization of the corticosteroid 11 beta-dehydrogenase component of the rat liver 11 beta-hydroxysteroid dehydrogenase complex. Endocrinology. 1988;123(5):2390-8.

82.   Draper N, Walker EA, Bujalska IJ, Tomlinson JW, Chalder SM, Arlt W, et al. Mutations in the genes encoding 11beta-hydroxysteroid dehydrogenase type 1 and hexose-6-phosphate dehydrogenase interact to cause cortisone reductase deficiency. Nat Genet. 2003;34(4):434-9.

83.   Lavery GG, Walker EA, Tiganescu A, Ride JP, Shackleton CH, Tomlinson JW, et al. Steroid biomarkers and genetic studies reveal inactivating mutations in hexose-6-phosphate dehydrogenase in patients with cortisone reductase deficiency. J Clin Endocrinol Metab. 2008;93(10):3827-32.

84.   Abrahams L, Semjonous NM, Guest P, Zielinska A, Hughes B, Lavery GG, et al. Biomarkers of hypothalamic-pituitary-adrenal axis activity in mice lacking 11beta-HSD1 and H6PDH. J Endocrinol. 2012;214(3):367-72.

85.   Draper N, Stewart PM. 11beta-hydroxysteroid dehydrogenase and the pre-receptor regulation of corticosteroid hormone action. J Endocrinol. 2005;186(2):251-71.

86.   Stewart PM, Whorwood CB, Mason JI. Type 2 11 beta-hydroxysteroid dehydrogenase in foetal and adult life. J Steroid Biochem Mol Biol. 1995;55(5-6):465-71.

87.   Odermatt A, Arnold P, Frey FJ. The intracellular localization of the mineralocorticoid receptor is regulated by 11beta-hydroxysteroid dehydrogenase type 2. J Biol Chem. 2001;276(30):28484-92.

88.   Stewart PM, Mason JI. Cortisol to cortisone: glucocorticoid to mineralocorticoid. Steroids. 1995;60(1):143-6.

89.   Chapagain A, Caton PW, Kieswich J, Andrikopoulos P, Nayuni N, Long JH, et al. Elevated hepatic 11beta-hydroxysteroid dehydrogenase type 1 induces insulin resistance in uremia. Proc Natl Acad Sci U S A. 2014;111(10):3817-22.

90.   N'Gankam V, Uehlinger D, Dick B, Frey BM, Frey FJ. Increased cortisol metabolites and reduced activity of 11beta-hydroxysteroid dehydrogenase in patients on hemodialysis. Kidney Int. 2002;61(5):1859-66.

91.   Andersson AK, Atkinson SE, Khanolkar-Young S, Chaduvula M, Jain S, Suneetha L, et al. Alteration of the cortisol-cortisone shuttle in leprosy type 1 reactions in leprosy patients in Hyderabad, India. Immunol Lett. 2007;109(1):72-5.

92.   Tiganescu A, Walker EA, Hardy RS, Mayes AE, Stewart PM. Localization, age- and site-dependent expression, and regulation of 11beta-hydroxysteroid dehydrogenase type 1 in skin. J Invest Dermatol. 2011;131(1):30-6.

93.   Tiganescu A, Tahrani AA, Morgan SA, Otranto M, Desmouliere A, Abrahams L, et al. 11beta-Hydroxysteroid dehydrogenase blockade prevents age-induced skin structure and function defects. J Clin Invest. 2013;123(7):3051-60.

94.   Tiganescu A, Hupe M, Uchida Y, Mauro T, Elias PM, Holleran WM. Increased glucocorticoid activation during mouse skin wound healing. J Endocrinol. 2014;221(1):51-61.

95.   Lee SE, Kim JM, Jeong MK, Zouboulis CC, Lee SH. 11beta-hydroxysteroid dehydrogenase type 1 is expressed in human sebaceous glands and regulates glucocorticoid-induced lipid synthesis and toll-like receptor 2 expression in SZ95 sebocytes. Br J Dermatol. 2013;168(1):47-55.

96.   Skobowiat C, Sayre RM, Dowdy JC, Slominski AT. Ultraviolet radiation regulates cortisol activity in a waveband-dependent manner in human skin ex vivo. Br J Dermatol. 2013;168(3):595-601.

97.   Tiganescu A, Hupe M, Jiang YJ, Celli A, Uchida Y, Mauro TM, et al. UVB induces epidermal 11β-hydroxysteroid dehydrogenase type 1 activityin vivo. Experimental Dermatology. 2015;24(5):370-6.

98.   Vukelic S, Stojadinovic O, Pastar I, Rabach M, Krzyzanowska A, Lebrun E, et al. Cortisol synthesis in epidermis is induced by IL-1 and tissue injury. J Biol Chem. 2011;286(12):10265-75.

99.   Courtney R, Stewart PM, Toh M, Ndongo MN, Calle RA, Hirshberg B. Modulation of 11beta-hydroxysteroid dehydrogenase (11betaHSD) activity biomarkers and pharmacokinetics of PF-00915275, a selective 11betaHSD1 inhibitor. J Clin Endocrinol Metab. 2008;93(2):550-6.

100.   Heise T, Morrow L, Hompesch M, Haring HU, Kapitza C, Abt M, et al. Safety, efficacy and weight effect of two 11beta-HSD1 inhibitors in metformin-treated patients with type 2 diabetes. Diabetes Obes Metab. 2014;16(11):1070-7.

101.   Scott JS, Goldberg FW, Turnbull AV. Medicinal chemistry of inhibitors of 11beta-hydroxysteroid dehydrogenase type 1 (11beta-HSD1). J Med Chem. 2014;57(11):4466-86.

102.   Terao M, Tani M, Itoi S, Yoshimura T, Hamasaki T, Murota H, et al. 11beta-hydroxysteroid dehydrogenase 1 specific inhibitor increased dermal collagen content and promotes fibroblast proliferation. PLoS One. 2014;9(3):e93051.

103.   Tice CM, Zhao W, Xu Z, Cacatian ST, Simpson RD, Ye YJ, et al. Spirocyclic ureas: orally bioavailable 11 beta-HSD1 inhibitors identified by computer-aided drug design. Bioorg Med Chem Lett. 2010;20(3):881-6.

104.   Su X, Vicker N, Potter BV. Inhibitors of 11beta-hydroxysteroid dehydrogenase type 1. Prog Med Chem. 2008;46:29-130.

105.   Shen CY, Jiang JG, Yang L, Wang DW, Zhu W. Anti-ageing active ingredients from herbs and nutraceuticals used in traditional Chinese medicine: pharmacological mechanisms and implications for drug discovery. Br J Pharmacol. 2016.

106.   Dong X, Fu J, Yin X, Cao S, Li X, Lin L, et al. Emodin: A Review of its Pharmacology, Toxicity and Pharmacokinetics. Phytother Res. 2016;30(8):1207-18.

107.   Tang T, Yin L, Yang J, Shan G. Emodin, an anthraquinone derivative from Rheum officinale Baill, enhances cutaneous wound healing in rats. Eur J Pharmacol. 2007;567(3):177-85.

108.   Radha KS, Madhyastha HK, Nakajima Y, Omura S, Maruyama M. Emodin upregulates urokinase plasminogen activator, plasminogen activator inhibitor-1 and promotes wound healing in human fibroblasts. Vascul Pharmacol. 2008;48(4-6):184-90.

109.   Feng Y, Huang SL, Dou W, Zhang S, Chen JH, Shen Y, et al. Emodin, a natural product, selectively inhibits 11beta-hydroxysteroid dehydrogenase type 1 and ameliorates metabolic disorder in diet-induced obese mice. Br J Pharmacol. 2010;161(1):113-26.

110.   Eming SA, Krieg T, Davidson JM. Inflammation in wound repair: molecular and cellular mechanisms. J Invest Dermatol. 2007;127(3):514-25.

111.   Sen CK, Gordillo GM, Roy S, Kirsner R, Lambert L, Hunt TK, et al. Human skin wounds: a major and snowballing threat to public health and the economy. Wound Repair Regen. 2009;17(6):763-71.

112.   Baum CL, Arpey CJ. Normal cutaneous wound healing: clinical correlation with cellular and molecular events. Dermatol Surg. 2005;31(6):674-86; discussion 86.

113.   Velnar T, Bailey T, Smrkolj V. The wound healing process: an overview of the cellular and molecular mechanisms. J Int Med Res. 2009;37(5):1528-42.

114.   Rasche H. Haemostasis and thrombosis: an overview. European Heart Journal Supplements. 2001;3(suppl_Q):Q3-Q7.

115.   Jurk K, Kehrel BE. Platelets: physiology and biochemistry. Semin Thromb Hemost. 2005;31(4):381-92.

116.   Janis JE, Harrison B. Wound healing: part I. Basic science. Plast Reconstr Surg. 2014;133(2):199e-207e.

117.   Pastar I, Nusbaum AG, Gil J, Patel SB, Chen J, Valdes J, et al. Interactions of methicillin resistant Staphylococcus aureus USA300 and Pseudomonas aeruginosa in polymicrobial wound infection. PLoS One. 2013;8(2):e56846.

118.   Midwood KS, Williams LV, Schwarzbauer JE. Tissue repair and the dynamics of the extracellular matrix. Int J Biochem Cell Biol. 2004;36(6):1031-7.

119.   Martin P, Leibovich SJ. Inflammatory cells during wound repair: the good, the bad and the ugly. Trends Cell Biol. 2005;15(11):599-607.

120.   Demidova-Rice TN, Durham JT, Herman IM. Wound Healing Angiogenesis: Innovations and Challenges in Acute and Chronic Wound Healing. Adv Wound Care (New Rochelle). 2012;1(1):17-22.

121.   Ziello JE, Jovin IS, Huang Y. Hypoxia-Inducible Factor (HIF)-1 regulatory pathway and its potential for therapeutic intervention in malignancy and ischemia. Yale J Biol Med. 2007;80(2):51-60.

122.   Bergers G, Song S. The role of pericytes in blood-vessel formation and maintenance. Neuro Oncol. 2005;7(4):452-64.

123.   Grinnell F. Fibroblasts, myofibroblasts, and wound contraction. J Cell Biol. 1994;124(4):401-4.

124.   Santoro MM, Gaudino G. Cellular and molecular facets of keratinocyte reepithelization during wound healing. Exp Cell Res. 2005;304(1):274-86.

125.   Lenselink EA. Role of fibronectin in normal wound healing. Int Wound J. 2015;12(3):313-6.

126.   Van Doren SR. Matrix metalloproteinase interactions with collagen and elastin. Matrix Biol. 2015;44-46:224-31.

127.   Nayman J. Effect of renal failure on wound healing in dogs. Response to hemodialysis following uremia induced by uranium nitrate. Ann Surg. 1966;164(2):227-35.

128.   McDermott FT, Nayman J, De Boer WG. The effect of acute renal failure upon wound healing: histological and autoradiographic studies in the mouse. Ann Surg. 1968;168(1):142-6.

129.   Dou L, Bertrand E, Cerini C, Faure V, Sampol J, Vanholder R, et al. The uremic solutes p-cresol and indoxyl sulfate inhibit endothelial proliferation and wound repair. Kidney Int. 2004;65(2):442-51.

130.   Brummer P, Kasanen A. Serum indican and urinary indican excretion in achlorhydria. Acta Med Scand. 1955;152(2):123-8.

131.   Evenepoel P, Meijers BK, Bammens BR, Verbeke K. Uremic toxins originating from colonic microbial metabolism. Kidney Int Suppl. 2009(114):S12-9.

132.   Schreiner GE, Maher JF. Uremia: Biochemistry, Pathogenesis and Treatment. Academic Medicine. 1962;37(4):408.

133.   Leong SC, Sirich TL. Indoxyl Sulfate-Review of Toxicity and Therapeutic Strategies. Toxins (Basel). 2016;8(12).

134.   Eloot S, Schneditz D, Cornelis T, Van Biesen W, Glorieux G, Dhondt A, et al. Protein-Bound Uremic Toxin Profiling as a Tool to Optimize Hemodialysis. PLoS One. 2016;11(1):e0147159.

135.   Deguchi T, Ohtsuki S, Otagiri M, Takanaga H, Asaba H, Mori S, et al. Major role of organic anion transporter 3 in the transport of indoxyl sulfate in the kidney. Kidney Int. 2002;61(5):1760-8.

136.   Wikoff WR, Nagle MA, Kouznetsova VL, Tsigelny IF, Nigam SK. Untargeted metabolomics identifies enterobiome metabolites and putative uremic toxins as substrates of organic anion transporter 1 (Oat1). J Proteome Res. 2011;10(6):2842-51.

137.   Vanholder R, De Smet R, Lesaffer G. p-cresol: a toxin revealing many neglected but relevant aspects of uraemic toxicity. Nephrol Dial Transplant. 1999;14(12):2813-5.

138.   Vanholder R, De Smet R, Lameire N. Protein-bound uremic solutes: the forgotten toxins. Kidney Int Suppl. 2001;78:S266-70.

139.   Keweloh H, Diefenbach R, Rehm H-J. Increase of phenol tolerance of Escherichia coli by alterations of the fatty acid composition of the membrane lipids. Archives of Microbiology. 1991;157(1):49-53.

140.   Elliott AA, Elliott JR. Voltage-dependent inhibition of RCK1 K+ channels by phenol, p-cresol, and benzyl alcohol. Mol Pharmacol. 1997;51(3):475-83.

141.   Wratten ML, Tetta C, De Smet R, Neri R, Sereni L, Camussi G, et al. Uremic Ultrafiltrate Inhibits Platelet-Activating Factor Synthesis. Blood Purification. 1999;17:134-41.

142.   Goto S, Yoshiya K, Kita T, Fujii H, Fukagawa M. Uremic toxins and oral adsorbents. Ther Apher Dial. 2011;15(2):132-4.

143.   Mitra M, Ho LD, Coller HA. An In Vitro Model of Cellular Quiescence in Primary Human Dermal Fibroblasts. Methods Mol Biol. 2018;1686:27-47.

144.   Yu YS, Sun XS, Jiang HN, Han Y, Zhao CB, Tan JH. Studies of the cell cycle of in vitro cultured skin fibroblasts in goats: work in progress. Theriogenology. 2003;59(5-6):1277-89.

145.   Yokozawa T ZP, D, Oura H, Koizumi F,. Animal Model of Adenine-Induced Chronic Renal Failure in Rats. Nephron. 1986;44(3):230-4.

146.   Yokozawa T, Oura H, Koizumi F. 2,8-Dihydroxyadenine urolithiasis induced by dietary adenine in rats. Nihon Jinzo Gakkai Shi. 1985;27(3):371-8.

147.   Okada H KY, Yawata T, Uyama H, Ozono S, Motomiya Y, Hirao Y. Reversibility of adenine-induced renal failure in rats. Clinical Experimental Nephrology. 1999;3:82-8.

148.   Byrne CJ, McCafferty K, Kieswich J, Harwood S, Andrikopoulos P, Raftery M, et al. Ischemic conditioning protects the uremic heart in a rodent model of myocardial infarction. Circulation. 2012;125(10):1256-65.

149.   Garrido P, Reis F, Costa E, Teixeira-Lemos E, Parada B, Alves R, et al. Characterization of a rat model of moderate chronic renal failure--focus on hematological, biochemical, and cardio-renal profiles. Ren Fail. 2009;31(9):833-42.

150.   ThermoFisher. How TaqMan Assays Work 2019 [Available from: https://www.thermofisher.com/uk/en/home/life-science/pcr/real-time-pcr/real-time-pcr-learning-center/real-time-pcr-basics/how-taqman-assays-work.html.

151.   Qiagen. Qiagen RT2 QC PCR Array 2018 [cited 2018. Available from: https://www.qiagen.com/gb/shop/pcr/primer-sets/rt2-profiler-pcr-arrays/?catno=PARN-999Z - orderinginformation.

152.   Schmittgen TD, Livak KJ. Analyzing real-time PCR data by the comparative C(T) method. Nat Protoc. 2008;3(6):1101-8.

153.   Slominski A, Gomez-Sanchez CE, Foecking MF, Wortsman J. Active steroidogenesis in the normal rat skin. Biochim Biophys Acta. 2000;1474(1):1-4.

154.   Slominski A, Wortsman J. Neuroendocrinology of the skin. Endocr Rev. 2000;21(5):457-87.

155. Anand S, Johansen KL, Kurella Tamura M. Aging and chronic kidney disease: the impact on physical function and cognition. J Gerontol A Biol Sci Med Sci. 2014;69(3):315-22.

156. Liang CC, Park AY, Guan JL. In vitro scratch assay: a convenient and inexpensive method for analysis of cell migration in vitro. Nat Protoc. 2007;2(2):329-33.

157. Jonkman JE, Cathcart JA, Xu F, Bartolini ME, Amon JE, Stevens KM, et al. An introduction to the wound healing assay using live-cell microscopy. Cell Adh Migr. 2014;8(5):440-51.

158. Grada A, Otero-Vinas M, Prieto-Castrillo F, Obagi Z, Falanga V. Research Techniques Made Simple: Analysis of Collective Cell Migration Using the Wound Healing Assay. J Invest Dermatol. 2017;137(2):e11-e6.

159. Sponsel HT, Breckon R, Hammond W, Anderson RJ. Mechanisms of recovery from mechanical injury of renal tubular epithelial cells. Am J Physiol. 1994;267(2 Pt 2):F257-64.

160. Thurston LM, Abayasekara DR, Michael AE. 11beta-Hydroxysteroid dehydrogenase expression and activities in bovine granulosa cells and corpora lutea implicate corticosteroids in bovine ovarian physiology. J Endocrinol. 2007;193(2):299-310.

161. Huang KT, Chen YH, Walker AM. Inaccuracies in MTS assays: major distorting effects of medium, serum albumin, and fatty acids. Biotechniques. 2004;37(3):406, 8, 10-2.

162. Hardy RS, Filer A, Cooper MS, Parsonage G, Raza K, Hardie DL, et al. Differential expression, function and response to inflammatory stimuli of 11beta-hydroxysteroid dehydrogenase type 1 in human fibroblasts: a mechanism for tissue-specific regulation of inflammation. Arthritis Res Ther. 2006;8(4):R108.

163. Ishii T, Masuzaki H, Tanaka T, Arai N, Yasue S, Kobayashi N, et al. Augmentation of 11β-hydroxysteroid dehydrogenase type 1 in LPS-activated J774.1 macrophages - Role of 11β-HSD1 in pro-inflammatory properties in macrophages. FEBS Letters. 2007;581(3):349-54.

164. Sigma-Aldrich. LDH Cytotoxic Assay [Available from: https://www.sigmaaldrich.com/content/dam/sigma-aldrich/docs/Roche/Bulletin/1/11644793001bul.pdf.

165. van Tonder A, Joubert AM, Cromarty AD. Limitations of the 3-(4,5-dimethylthiazol-2-yl)-2,5-diphenyl-2H-tetrazolium bromide (MTT) assay when compared to three commonly used cell enumeration assays. BMC Res Notes. 2015;8:47.

166. Vistica DT, Skehan P, Scudiero D, Monks A, Pittman A, Boyd MR. Tetrazolium-based assays for cellular viability: a critical examination of selected parameters affecting formazan production. Cancer Res. 1991;51(10):2515-20.

167.	Sliwka L, Wiktorska K, Suchocki P, Milczarek M, Mielczarek S, Lubelska K, et al. The Comparison of MTT and CVS Assays for the Assessment of Anticancer Agent Interactions. PLoS One. 2016;11(5):e0155772.

168.	Promega. CellTiter96 (R) AQueous One Solution Cell Proliferation Assay 2019 [Available from: https://www.promega.co.uk/products/cell-health-assays/cell-viability-and-cytotoxicity-assays/celltiter-96-aqueous-one-solution-cell-proliferation-assay-_mts_/?catNum=G3582.

169.	Vanholder R, De Smet R. Pathophysiologic effects of uremic retention solutes. J Am Soc Nephrol. 1999;10(8):1815-23.

170.	Merrill JP, Hampers CL. Uremia; progress in pathophysiology and treatment. New York,: Grune & Stratton; 1971. 115 p. p.

171.	Madison KC. Barrier function of the skin: "la raison d'etre" of the epidermis. J Invest Dermatol. 2003;121(2):231-41.

172.	Yue DK, McLennan S, Marsh M, Mai YW, Spaliviero J, Delbridge L, et al. Effects of experimental diabetes, uremia, and malnutrition on wound healing. Diabetes. 1987;36(3):295-9.

173.	Stewart PM, Wallace AM, Atherden SM, Shearing CH, Edwards CR. Mineralocorticoid activity of carbenoxolone: contrasting effects of carbenoxolone and liquorice on 11 beta-hydroxysteroid dehydrogenase activity in man. Clin Sci (Lond). 1990;78(1):49-54.

174.	Connors BW. Tales of a dirty drug: carbenoxolone, gap junctions, and seizures. Epilepsy Curr. 2012;12(2):66-8.

175.	Aldrich S. Sample Purification and Quality Assessment 2019 [Available from: https://www.sigmaaldrich.com/technical-documents/articles/biology/sample-purification-and-quality-assessment.html.

176.	Koivisto L, Heino J, Hakkinen L, Larjava H. Integrins in Wound Healing. Adv Wound Care (New Rochelle). 2014;3(12):762-83.

177.	De Luca M, Pellegrini G, Zambruno G, Marchisio PC. Role of integrins in cell adhesion and polarity in normal keratinocytes and human skin pathologies. J Dermatol. 1994;21(11):821-8.

178.	Larjava H, Salo T, Haapasalmi K, Kramer RH, Heino J. Expression of integrins and basement membrane components by wound keratinocytes. J Clin Invest. 1993;92(3):1425-35.

179.	Bunemann E, Hoff NP, Buhren BA, Wiesner U, Meller S, Bolke E, et al. Chemokine ligand-receptor interactions critically regulate cutaneous wound healing. Eur J Med Res. 2018;23(1):4.

180.   Tsou PS, Rabquer BJ, Ohara RA, Stinson WA, Campbell PL, Amin MA, et al. Scleroderma dermal microvascular endothelial cells exhibit defective response to pro-angiogenic chemokines. Rheumatology (Oxford). 2016;55(4):745-54.

181.   Abreu-Velez AM, Howard MS. Collagen IV in Normal Skin and in Pathological Processes. N Am J Med Sci. 2012;4(1):1-8.

182.   Sudhakar A, Nyberg P, Keshamouni VG, Mannam AP, Li J, Sugimoto H, et al. Human alpha1 type IV collagen NC1 domain exhibits distinct antiangiogenic activity mediated by alpha1beta1 integrin. J Clin Invest. 2005;115(10):2801-10.

183.   Turner AW, Nikpay M, Silva A, Lau P, Martinuk A, Linseman TA, et al. Functional interaction between COL4A1/COL4A2 and SMAD3 risk loci for coronary artery disease. Atherosclerosis. 2015;242(2):543-52.

184.   Alberts B. Molecular biology of the cell. 4th ed. New York: Garland Science; 2002. xxxiv, 1548 p. p.

185.   Reddy S, Andl T, Bagasra A, Lu MM, Epstein DJ, Morrisey EE, et al. Characterization of Wnt gene expression in developing and postnatal hair follicles and identification of Wnt5a as a target of Sonic hedgehog in hair follicle morphogenesis. Mech Dev. 2001;107(1-2):69-82.

186.   Masckauchan TN, Agalliu D, Vorontchikhina M, Ahn A, Parmalee NL, Li CM, et al. Wnt5a signaling induces proliferation and survival of endothelial cells in vitro and expression of MMP-1 and Tie-2. Mol Biol Cell. 2006;17(12):5163-72.

187.   Montesinos MC, Desai-Merchant A, Cronstein BN. Promotion of Wound Healing by an Agonist of Adenosine A2A Receptor Is Dependent on Tissue Plasminogen Activator. Inflammation. 2015;38(6):2036-41.

188.   Schafer BM, Maier K, Eickhoff U, Todd RF, Kramer MD. Plasminogen activation in healing human wounds. Am J Pathol. 1994;144(6):1269-80.

189.   Shen Y, Guo Y, Mikus P, Sulniute R, Wilczynska M, Ny T, et al. Plasminogen is a key proinflammatory regulator that accelerates the healing of acute and diabetic wounds. Blood. 2012;119(24):5879-87.

190.   Romer J, Bugge TH, Pyke C, Lund LR, Flick MJ, Degen JL, et al. Impaired wound healing in mice with a disrupted plasminogen gene. Nat Med. 1996;2(3):287-92.

191.   Sulniute R, Shen Y, Guo YZ, Fallah M, Ahlskog N, Ny L, et al. Plasminogen is a critical regulator of cutaneous wound healing. Thromb Haemost. 2016;115(5):1001-9.

192.   Andrew R, Smith K, Jones GC, Walker BR. Distinguishing the activities of 11beta-hydroxysteroid dehydrogenases in vivo using isotopically labeled cortisol. J Clin Endocrinol Metab. 2002;87(1):277-85.

193.   Stojadinovic O, Tomic-Canic M. Human ex vivo wound healing model. Methods Mol Biol. 2013;1037:255-64.

194.   R&D. Corticosterone Parameter Assay Kit 2019 [Available from: https://www.rndsystems.com/products/corticosterone-parameter-assay-kit_kge009_-product-datasheets.

7. Appendices

7.1 Copyright Permission

7.2 Gene Table from RT² Profiler PCR Array- Rotor Disc 100 Format

Position	UniGene	GenBank	Symbol	Description
A01	Rn.195319	NM_031004	Acta2	Smooth muscle alpha-actin
A02	Rn.3114	NM_019183	Actc1	Actin, alpha, cardiac muscle 1
A03	Rn.161953	NM_053546	Angpt1	Angiopoietin 1
A04	Rn.137780	NM_001105822	Ccl12	Chemokine (C-C motif) ligand 12
A05	Rn.26815	NM_001007612	Ccl7	Chemokine (C-C motif) ligand 7
A06	Rn.44218	NM_053353	Cd40lg	CD40 ligand
A07	Rn.1303	NM_031334	Cdh1	Cadherin 1
A08	Rn.99441	NM_001130548	Col14a1	Collagen, type XIV, alpha 1
A09	Rn.2953	NM_053304	Col1a1	Collagen, type I, alpha 1
A10	Rn.107239	NM_053356	Col1a2	Collagen, type I, alpha 2
A11	Rn.3247	NM_032085	Col3a1	Collagen, type III, alpha 1
A12	Rn.53801	NM_001135009	Col4a1	Collagen, type IV, alpha 1
B01	Rn.121139	NM_001135759	Col4a3	Collagen, type IV, alpha 3
B02	Rn.117	NM_134452	Col5a1	Collagen, type V, alpha 1
B03	Rn.2875	NM_053488	Col5a2	Collagen, type V, alpha 2
B04	Rn.38654	NM_021760	Col5a3	Collagen, type V, alpha 3
B05	Rn.44285	XM_340799	Csf2	Colony stimulating factor 2 (granulocyte-macrophage)
B06	Rn.53973	NM_017104	Csf3	Colony stimulating factor 3 (granulocyte)
B07	Rn.17145	NM_022266	Ctgf	Connective tissue growth factor
B08	Rn.112601	NM_053357	Ctnnb1	Catenin (cadherin associated protein), beta 1
B09	Rn.103332	NM_001106041	Ctsg	Cathepsin G
B10	Rn.5598	NM_031560	Ctsk	Cathepsin K
B11	Rn.1294	NM_013156	Ctsl1	Cathepsin L1
B12	Rn.10907	NM_030845	Cxcl1	Chemokine (C-X-C motif) ligand 1 (melanoma growth stimulating activity, alpha)
C01	Rn.13664	NM_182952	Cxcl11	Chemokine (C-X-C motif) ligand 11
C02	Rn.10525	NM_138522	Cxcl3	Chemokine (C-X-C motif) ligand 3
C03	Rn.44449	NM_022214	Cxcl5	Chemokine (C-X-C motif) ligand 5
C04	Rn.6075	NM_012842	Egf	Epidermal growth factor
C05	Rn.37227	NM_031507	Egfr	Epidermal growth factor receptor
C06	Rn.42925	NM_021698	F13a1	Coagulation factor XIII, A1 polypeptide
C07	Rn.9980	NM_013057	F3	Coagulation factor III (thromboplastin, tissue factor)
C08	Rn.98846	NM_001008724	Fga	Fibrinogen alpha chain
C09	Rn.44439	NM_012951	Fgf10	Fibroblast growth factor 10
C10	Rn.31808	NM_019305	Fgf2	Fibroblast growth factor 2
C11	Rn.98842	NM_022182	Fgf7	Fibroblast growth factor 7
C12	Rn.10148	NM_012945	Hbegf	Heparin-binding EGF-like growth factor
D01	Rn.10468	NM_017017	Hgf	Hepatocyte growth factor
D02	Rn.10795	NM_138880	Ifng	Interferon gamma
D03	Rn.6282	NM_178866	Igf1	Insulin-like growth factor 1
D04	Rn.9868	NM_012854	Il10	Interleukin 10
D05	Rn.9869	NM_031512	Il1b	Interleukin 1 beta
D06	Rn.9871	NM_053836	Il2	Interleukin 2
D07	Rn.108255	NM_201270	Il4	Interleukin 4
D08	Rn.9873	NM_012589	Il6	Interleukin 6
D09	Rn.12138	NM_001008725	Il6st	Interleukin 6 signal transducer
D10	Rn.91044	NM_030994	Itga1	Integrin, alpha 1
D11	Rn.83597	XM_345156	Itga2	Integrin, alpha 2
D12	Rn.154664	NM_001108292	Itga3	Integrin, alpha 3
E01	Rn.12704	NM_001107737	Itga4	Integrin, alpha 4
E02	Rn.100796	NM_001108118	Itga5	Integrin, alpha 5 (fibronectin receptor, alpha polypeptide)
E03	Rn.161799	XM_215984	Itga6	Integrin, alpha 6
E04	Rn.23339	NM_001106549	Itgav	Integrin, alpha V
E05	Rn.25733	NM_017022	Itgb1	Integrin, beta 1
E06	Rn.162202	NM_153720	Itgb3	Integrin, beta 3
E07	Rn.16988	NM_147139	Itgb5	Integrin, beta 5
E08	Rn.19828	NM_001004263	Itgb6	Integrin, beta 6
E09	Rn.34914	NM_053842	Mapk1	Mitogen activated protein kinase 1

Position	UniGene	GenBank	Symbol	Description
E10	Rn.2592	NM_017347	Mapk3	Mitogen activated protein kinase 3
E11	Rn.2661	NM_031051	Mif	Macrophage migration inhibitory factor
E12	Rn.79007	NM_001134530	Mmp1a	Matrix metallopeptidase 1a (interstitial collagenase)
F01	Rn.6422	NM_031054	Mmp2	Matrix metallopeptidase 2
F02	Rn.10282	NM_012864	Mmp7	Matrix metallopeptidase 7
F03	Rn.10209	NM_031055	Mmp9	Matrix metallopeptidase 9
F04	Rn.10999	NM_012801	Pdgfa	Platelet-derived growth factor alpha polypeptide
F05	Rn.107102	NM_013151	Plat	Plasminogen activator, tissue
F06	Rn.6064	NM_013085	Plau	Plasminogen activator, urokinase
F07	Rn.82711	NM_017350	Plaur	Plasminogen activator, urokinase receptor
F08	Rn.20178	NM_053491	Plg	Plasminogen
F09	Rn.22158	NM_031606	Pten	Phosphatase and tensin homolog
F10	Rn.44369	NM_017232	Ptgs2	Prostaglandin-endoperoxide synthase 2
F11	Rn.29157	NM_134366	Rac1	Ras-related C3 botulinum toxin substrate 1
F12	Rn.107401	NM_057132	Rhoa	Ras homolog gene family, member A
G01	Rn.29367	NM_012620	Serpine1	Serpin peptidase inhibitor, clade E (nexin, plasminogen activator inhibitor type 1), member 1
G02	Rn.10247	NM_012747	Stat3	Signal transducer and activator of transcription 3
G03	Rn.34397	NM_031549	Tagln	Transgelin
G04	Rn.9952	NM_012671	Tgfa	Transforming growth factor alpha
G05	Rn.40136	NM_021578	Tgfb1	Transforming growth factor, beta 1
G06	Rn.9953	NM_017256	Tgfbr3	Transforming growth factor, beta receptor III
G07	Rn.25754	NM_053819	Timp1	TIMP metallopeptidase inhibitor 1
G08	Rn.2275	NM_012675	Tnf	Tumor necrosis factor (TNF superfamily, member 2)
G09	Rn.1923	NM_031836	Vegfa	Vascular endothelial growth factor A
G10	Rn.87493	NM_019156	Vtn	Vitronectin
G11	Rn.63486	NM_031716	Wisp1	WNT1 inducible signaling pathway protein 1
G12	Rn.48749	NM_022631	Wnt5a	Wingless-type MMTV integration site family, member 5A
H01	Rn.94978	NM_031144	Actb	Actin, beta
H02	Rn.1868	NM_012512	B2m	Beta-2 microglobulin
H03	Rn.47	NM_012583	Hprt1	Hypoxanthine phosphoribosyltransferase 1
H04	Rn.107896	NM_017025	Ldha	Lactate dehydrogenase A
H05	Rn.973	NM_001007604	Rplp1	Ribosomal protein, large, P1
H06	N/A	U26919	RGDC	Rat Genomic DNA Contamination
H07	N/A	SA_00104	RTC	Reverse Transcription Control
H08	N/A	SA_00104	RTC	Reverse Transcription Control
H09	N/A	SA_00104	RTC	Reverse Transcription Control
H10	N/A	SA_00103	PPC	Positive PCR Control
H11	N/A	SA_00103	PPC	Positive PCR Control
H12	N/A	SA_00103	PPC	Positive PCR Control

7.3 Control Drug versus Control Vehicle Array Gene Expression

Position	Gene Symbol	Fold Regulation	Comments
E03	Itga6	56.46	B
G01	Serpine1	56.20	B
E06	Itgb3	28.43	B
C02	Cxcl3	17.78	
F06	Plau	11.36	B
A12	Col4a1	11.07	
G10	Vtn	9.98	B
G12	Wnt5a	8.55	
F01	Mmp2	5.58	B
E01	Itga4	4.96	B
B02	Col5a1	4.91	B
F07	Plaur	4.86	B
F08	Plg	4.42	B
C12	Hbegf	3.94	B
D09	Il6st	3.38	B
B09	Ctsg	3.29	B
D05	Il1b	3.11	B
G05	Tgfb1	2.92	B
A08	Col14a1	2.86	B
B04	Col5a3	2.46	B
A09	Col1a1	2.46	A
A01	Acta2	2.39	A
B10	Ctsk	2.31	B
G03	Tagln	2.28	A
C05	Egfr	2.26	B
A06	Cd40lg	2.26	B
H01	Actb	2.20	
G04	Tgfa	2.13	B
C10	Fgf2	2.05	B

Position	Gene Symbol	Fold Regulation	Comments
F02	Mmp7	-6.43	B
H06	RGDC	-4.73	B
C06	F13a1	-4.54	B
C03	Cxcl6	-4.41	B
D01	Hgf	-3.25	B
A04	Ccl12	-2.89	B
D07	Il4	-2.84	B
C08	Fga	-2.31	B
H10	PPC	-2.26	
H12	PPC	-2.19	
H11	PPC	-2.13	
G11	Wisp1	-2.05	C
A05	Ccl7	-2.05	C
B06	Csf3	-2.05	C
B05	Csf2	-2.05	C
D06	Il2	-2.05	C
C04	Egf	-2.02	B

7.4 Uraemic Drug versus Uraemic Vehicle Array Gene Expression

Position	Gene Symbol	Fold Regulation	Comments
D04	Il10	25.70	B
F07	Plaur	14.03	B
C08	Fga	9.56	B
F08	Plg	9.54	B
E12	Mmp1	8.34	B
E06	Itgb3	8.08	B
A05	Ccl7	8.06	B
F03	Mmp9	7.47	B
G10	Vtn	7.40	B
F06	Plau	5.62	B
C12	Hbegf	5.37	B
C10	Fgf2	4.28	B
G12	Wnt5a	4.17	B
A09	Col1a1	3.72	B
C03	Cxcl6	3.50	B
B01	Col4a3	3.43	B
E01	Itga4	3.40	B
F01	Mmp2	3.23	B
D07	Il4	2.47	C
F02	Mmp7	2.47	C
A04	Ccl12	2.47	C
D08	Il6	2.47	C
A06	Cd40lg	2.47	C
D06	Il2	2.47	C
C09	Fgf10	2.47	C
B06	Csf3	2.47	C
B09	Ctsg	2.47	C
B05	Csf2	2.47	C
B04	Col5a3	2.47	C
G08	Tnf	2.47	C
D01	Hgf	2.47	C
F10	Ptgs2	2.33	B
H11	PPC	2.24	
D02	Ifng	2.24	B
H10	PPC	2.20	
B10	Ctsk	2.17	B
H12	PPC	2.14	
A02	Actc1	2.02	B

Position	Gene Symbol	Fold Regulation	Comments
F05	Plat	-37.87	
G07	Timp1	-11.98	B
A12	Col4a1	-9.32	B
G01	Serpine1	-6.71	B
F04	Pdgfa	-5.98	B
D11	Itga2	-5.38	B
A07	Cdh1	-4.70	B
G06	Tgfbr3	-4.48	B
C02	Cxcl3	-4.41	B
E02	Itga5	-4.24	
D05	Il1b	-4.10	B
E04	Itgav	-3.77	B
B02	Col5a1	-2.85	B
E08	Itgb6	-2.75	B
D03	Igf1	-2.58	B
G03	Tagln	-2.00	B

7.5 Uraemic Vehicle versus Control Vehicle Array Gene Expression

Position	Gene Symbol	Fold Regulation	Comments
E03	Itga6	21.20	B
G01	Serpine1	16.41	B
C02	Cxcl3	10.77	B
D05	Il1b	5.23	B
B02	Col5a1	4.68	B
A12	Col4a1	4.47	B
E02	Itga5	4.21	
E01	Itga4	3.91	B
A03	Angpt1	3.71	B
C04	Egf	3.55	B
C11	Fgf7	2.80	B
F07	Plaur	2.54	B
G11	Wisp1	2.39	B

Position	Gene Symbol	Fold Regulation	Comments
C06	F13a1	-21.86	B
B04	Col5a3	-11.58	B
D12	Itga3	-6.98	B
G12	Wnt5a	-4.65	B
C08	Fga	-4.13	B
A09	Col1a1	-3.77	B
A04	Ccl12	-3.54	B
B10	Ctsk	-3.34	B
G08	Tnf	-3.30	B
D08	Il6	-3.26	B
F02	Mmp7	-3.17	B
C10	Fgf2	-2.82	B
H06	RGDC	-2.67	B
D01	Hgf	-2.62	B

7.6 Wound Healing Array Key

A: This gene's average threshold cycle is relatively high (> 30) in either the control or the test sample, and is reasonably low in the other sample (< 30). These data mean that the gene's expression is relatively low in one sample and reasonably detected in the other sample suggesting that the actual fold-change value is at least as large as the calculated and reported fold-change result. This fold-change result may also have greater variations if p value > 0.05; therefore, it is important to have a sufficient number of biological replicates to validate the result for this gene.

B: This gene's average threshold cycle is relatively high (> 30), meaning that its relative expression level is low, in both control and test samples, and the p-value for the fold-change is either unavailable or relatively high (p > 0.05). This fold-change result may also have greater variations; therefore, it is important to have a sufficient number of biological replicates to validate the result for this gene.

C: This gene's average threshold cycle is either not determined or greater than the defined cut-off (default 35), in both samples meaning that its expression was undetected, making this fold-change result erroneous and un-interpretable.